Investigation of chemically substituted cobalt ferrite for high magnetostriction based sensor and actuator applications

Naresh Ranvah

School of Engineering

Cardiff University

A thesis submitted for the award of the degree of

Doctor of Philosophy

September 2010

ProQuest LLC
789 East Eisenhower Parkway
P.O. Box 1346
Ann Arbor, MI 48106-1346

Declaration

This work has not previously been accepted in substance for any degree and is not concurrently submitted in candidature for any degree.

Signed: .....Naresh Ranvah..... (candidate) Date: .....04/10/2010.....

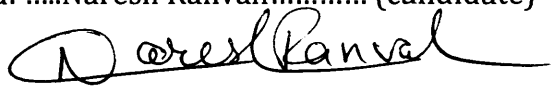

Statement 1

This thesis is being submitted in partial fulfilment of requirements for the degree of PhD.

Signed: .....Naresh Ranvah..... (candidate) Date: .....04/10/2010.....

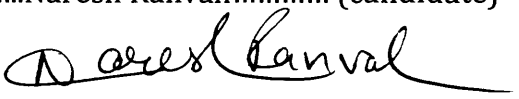

Statement 2

This thesis is the result of my own independent work/investigation, except where otherwise stated. Other sources are acknowledged by explicit references.

Signed: .....Naresh Ranvah..... (candidate) Date: .....04/10/2010.....

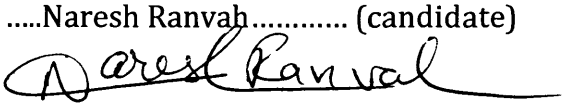

Statement 3

I hereby give consent for my thesis, if accepted, to be available for photocopying and for internal library loan, and for the title and summary to be made available to outside organisations.

Signed: .....Naresh Ranvah..... (candidate) Date: .....04/10/2010.....

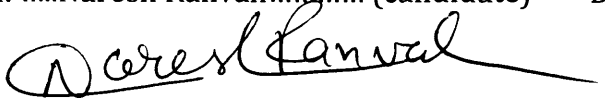

Acknowledgement

During the course of this project many people have extended their support to me and have enabled me to successfully complete this study. I would like to express my sincere appreciation for my academic supervisor Prof. D. C. Jiles who has mentored me and guided me with his accomplished knowledge of the subject of magnetics. He has done this despite his busy schedule and workload. I would like to thank my second supervisor Dr. P. I. Williams who has guided me with his subject knowledge and helped me maintain the standard of my research.

I would also like to thank Dr. Yevgen Melikhov for constantly mentoring me and helping me with measurements and analysis. Dr. John Synder has been of special help in analysing my results. Prof. Moses always asked me important questions and ensured that my research was conclusive. I would like to express my appreciation for Ikenna who was a co-researcher on the project and helped me to take this project to completion. He was not only helpful in providing me with samples and stimulating discussions, but also taught me a few lessons about life.

I would also like to thank other staff and students at Wolfson Magnetics who helped me to better my research methods and provided me to learn from them. Dr. Ravi Hadimani has been a witness to majority of my research and has helped me through my struggles. Esai, Rafal, Lukasz, Steven, Szymon, and Arun have helped me with my research and have made my stay enjoyable. In the end, I would like to thank my parents, my sister, my brother, and my friend Iti, who

have all been pillars of support and have led me to the conclusion of this study. I thank my grand parents who have been role models for me and the rest of my family which have provided me with the best chance to grow into a good human being in this world.

Abstract

There has been a recent interest in high magnetostriction materials for magnetostriction based stress/torque sensor and actuator applications. Several materials have been investigated with this aim, including Tefenol ($Tb_{0.3}Dy_{0.7}Fe_2$), $SmFe_2$, and Galfanol ($Fe_{80}Ga_{20}$). However, these materials have several drawbacks for stress sesnor and actuator applications. Among these are low sensitivity to magnetic field or stress, low chemical stability, high costs and lack of mechanical strength.

In recent years, cobalt ferrite has emerged as a candidate material for magnetostrictive stress/torque sensor and actuator applications. Cobalt ferrite has a relatively high magnetostriction ($\lambda \cong 200$ ppm), high sensitivity ($d\lambda/dH \cong 200$ ppm), is chemically stable and mechanically robust. However, the magnetoelastic properties of pure cobalt ferrite ($CoFe_2O_4$), relevant for magnetostrictive sensor and actuator applications, can be improved by chemical substitution. The properties of cobalt ferrite and cobalt ferrite based materials depend heavily on the site occupancy of the different ions in its cubic spinel lattice. Previously, the substitution of M^{3+} (M = Mn, Cr) in place of some of Fe^{3+} has shown to improve magnetostrictive sensitivity. This can be attributed to reduced anisotropy caused by magnetic dilution resulting from substitution Fe^{3+} with less magnetic ions. However, the maximum magnetostriction, which is an indicator of the range of a magnetostrictive sensor/actuator device, reduced in these cases.

In the present study, it was aimed to use the site preference of dopant ions to tailor the magnetoelastic properties of cobalt ferrite. It was hypothesised that a dopant ion with strong tetrahedral-site preference will result in more favourable properties for magnetostrictive sensor and actuator applications. Three different substitutions were tried.

Gallium substituted cobalt ferrite ($CoGa_xFe_{2-x}O_4$ with x = 0.0, 0.2, 0.4, 0.6, & 0.8) was investigated. The maximum magnetization at near zero Kelvin temperatures increased for low amounts of gallium substitution. This agrees with the Mössbauer investigation of the material which points towards Ga^{3+} ions substituting into A-sites initially. The strain sensitivity increased for low values of gallium content, however, the maximum magnetostriction decreased.

Germanium cobalt co-substituted cobalt ferrite ($Co_{1+x}Ge_xFe_{2-2x}O_4$ with x = 0.0, 0.1, 0.2, 0.3, 0.4, & 0.6) was expected to give better properties because of a strong tetrahedral-site preference. The maximum magnetostriction and strain sensitivity were observed to be higher than for cobalt ferrite, for low amounts of Germanium substitution.

Aluminium substitution was observed to indicate towards a weak tetrahedral site preference for aluminium. This resulted in lesser maximum magnetisation at near zero Kelvin temperatures, in comparison to cobalt ferrite.

AC measurements of B-H properties were made and it was observed that the coercivity of cobalt ferrite did not change significantly in the 10 - 100 Hz range.

This could be because of the non-conducting nature of cobalt ferrite, which prevents formation of any eddy currents, a dominant source of frequency dependent loss in conducting materials.

Chemical substitution has been observed to be effective in tailoring properties of cobalt ferrite. In the present work, methods and understanding have been proposed to improve properties of cobalt ferrite using chemical substitution.

Table of Contents

List of symbols and abbreviations

$E_{exchange}$	Exchange Energy
J	Exchange coupling coefficient
S_i	i^{th} Spin
E_a	Anisotropy Energy
K_{un}	n^{th} order uniaxial anisotropy constants
α_i	Direction cosines of magnetisation vector with respect to crystal axis
K_i	i^{th} order anisotropy constants in a cubic lattice
λ	Magnetostriction
H	Magnetic field
σ	Stress
B	Magnetic induction
μ_0	Permeability of free space
l	Length
V	Volume
c_{ij}	Elastic modulus for cubic lattice
e_{ij}	Strain Tensor for cubic lattice
B_i	Magnetoelastic coupling constant
E_{magel}	Magnetoelastic energy of a crystal
λ_{100}	Magnetostriction constant in the [100] direction in a cubic lattice
λ_{111}	Magnetostriction constant in the [111] direction in a cubic lattice

λ_s	Saturation magnetostriction
δ	Inversion factor in a spinel lattice
I_{mag}	Current required to magnetise
MPMS	Magnetic Property Measurement System
RSO	Reciprocating Sample Option
W	Work
N_d	Demagnetising factor
LAS	Law of Approach to Saturation
M	Magnetisation
M_s	Saturation magnetisation
τ_a	Rotational torque caused by anisotropy
T_H	Rotational torque caused by applied field
κ	Forced anisotropy constant
H_{an}	Anisotropy field
R	Resistance
ε	Strain
F_G	Gauge factor for a strain gauge
EDS	Energy Dispersive X-ray Spectroscopy
T_c	Curie Temperature
G_I	Voltage to Current Gain for a power amplifier
AC	Alternating Current
H_c	Coercive field

Chapter 1. Introduction

There has been a continual interest in the properties of magnetic materials for sensor and actuator applications. The diverse choice of magnetic materials with interesting properties has enabled their application in a range of applications (Lenz, 1990, Lenz & Edelstein, 2006, TatuoKinmatu & Tatuo, 1929). Over the last 30 years, there has been a growing interest in magnetostrictive magnetic materials with the aim of non-contact detection of torque/stress (Jiles & Lo, 2003, Pasquale, 2003, Paulsen *et al.*, 2003, Garshelis, 1992). These sensors have applications in automotive steering systems, power trains, etc (Garshelis, 1992). The non-contact nature of these sensors provides design solutions in cases where direct electrical contact is difficult.

Early studies on materials for these applications focussed on rare earth containing compounds and alloys with giant magnetostriction (Pinkerton *et al.*, 1997, Clark, 1980). These materials however were brittle, expensive, and chemically reactive. Moreover, although these materials had high magnetostriction, a high field is required to produce these strains because of their low magnetostrictive strain sensitivity to field ($d\lambda/dH$, where λ is the magnetostriction and H is the magnetic field). These materials were also conductors, which produced eddy currents, and were hence less suitable for applications with AC magnetic field environments (Chen *et al.*, 1999, Liang *et al.*, 2007).

Ceramic cobalt ferrite based materials have emerged as candidates for non-contact torque/stress sensor/actuator applications. These materials overcome some of the drawbacks of the rare-earth based compounds (Chen et al., 1999). There has been an active investigation in the area of improving magnetoelastic properties of these cobalt ferrite based materials, which are critical to their potential as materials for torque/stress sensor/actuator applications. Cobalt ferrite composites with other compounds have been investigated in the past. Altering properties by varying processing techniques is also an important area of investigation.

In recent years, chemical substitution has emerged as a useful mechanism of tailoring specific properties of cobalt ferrite. Early investigations into the substitution of silicon in place of iron in cobalt ferrite had shown chemical substitution to be effective in reducing the Curie temperature of cobalt ferrite. This in turn was an indicator of reduction in room temperature hysteresis (Shinde *et al.*, 1998). However, when this substitution was further investigated in Iowa State University, the silicon substituted cobalt ferrite usually ended up being two phase because of the chemical stability of silicon dioxide and the resulting material was brittle (Paulsen et al., 2003). It was then decided to substitute other elements into cobalt ferrite in place of iron. Manganese and chromium substitution showed to cause a reduction in Curie temperature and anisotropy, and an increase in the strain derivative. However, both these substitutions led to a reduction in magnitude of the maximum magnetostriction. Both these substituted ions had a B-site preference (Melikhov *et al.*, 2006a, Melikhov *et al.*, 2006b).

This study focuses on investigating the effects of chemical substitution on tailoring the properties of cobalt ferrite that are critical to the performance of the resulting material in torque/stress sensor/actuator applications. It was decided to investigate substitutions that have an A-site preference and try to increase both maximum magnetostriction and the strain derivative.

Chapter 2 provides a background to the issues and theories that are central to this study. It details the evolution of related science through research in the past. A theoretical background of the important magnetic and magnetoelastic properties of materials of interest is given. Cobalt ferrite's spinel structure is described briefly with a focus on the effect of site occupancy on the magnetoelastic properties. The manner in which the ions from the tetrahedral and octahedral sites interact is described. A more dedicated explanation of the spinel structure in cobalt ferrite is then provided. A brief summary of previous studies focussing on improving the properties of cobalt ferrite is also given. The merits of the various methods employed to alter properties of cobalt ferrite based materials are discussed.

Chapter 3 describes the experimental methodology used in this study. A brief description is given for the ceramic processing technique used to prepare the samples for this study. This is followed by a description of the techniques used to measure the temperature dependence of the maximum magnetisation and magnetic hysteresis loops. A comparison is given between the different methods that can be used to determine the magnetic anisotropy in magnetic materials. An argument is provided for why the technique chosen in this study, fitting high field regions of magnetic hysteresis loops to the Law of Approach to Saturation,

is suitable for cobalt ferrite based materials. A discussion is presented which elucidates the issues associated with using this method at low temperatures where the internal anisotropy field in the materials of interest is of a comparable magnitude to the highest applied field available in the experiment. The chapter ends with a description of the strain gauge assisted technique used to measure the magnetostriction of the samples and the methods used to standardise these curves.

Chapter 4 presents a discussion of the effect of chemical substitution on properties of cobalt ferrite by performing an analysis based on experimental results obtained in this study. The chapter is divided into three sections which describe the effect of individual substitutions (gallium, germanium/cobalt, and aluminium) in cobalt ferrite. First the site preference of substituted cations is discussed. This is followed by a description of the effect of chemical substitution on Curie temperature of the material. The temperature dependence of maximum magnetic moment is then described. An analysis is presented for how site occupancy of different ions alters the maximum magnetisation at near zero Kelvin temperatures. The effect of chemical substitution on the magnetic hysteresis loops at different temperatures between 10 and 400 K is described. The temperature dependence of coercivity for substituted materials is discussed. This is followed by a detailed description of the anisotropy calculations and results for temperature dependence of first order magnetocrystalline anisotropy constant of substituted cobalt ferrite. The magnetostriction curves for substituted samples are shown at four different temperatures between 250 and 400 K. A comparison of the maximum magnetostriction and the maximum strain

derivative in the linear region for samples with different amounts of substitution is presented. A summary of findings is provided at the end of the chapter to highlight the important results obtained from the study.

Chapter 5 describes the AC magnetic hysteresis loop measurements on pure cobalt ferrite. A description of the design considerations for the measurement system is followed by the schematics and an exact description of the hardware and software used. A description of the challenges faced in making the measurement instrumentation is presented. This is followed by a description of the procedure for standardising the results and ensuring their repeatability. The results are presented and are compared against earlier work. The results are also discussed in light of their importance to the use of cobalt ferrite based materials in applications with AC magnetic field conditions.

Chapter 6 describes the important conclusions of this thesis. Research areas proposed for possible future work are also discussed.

Appendix I discusses the magnetic properties of a germanium/cobalt substituted sample which has majority germanium/cobalt in comparison to iron. The properties of this material are a departure from the trends observed for other materials.

Appendix II contains the exact drawings of the parts used in design of AC magnetic property system. The design was preformed with careful consideration for measurement challenges and criterion. These drawings have been provided so that future researchers can replicate the process and use it as a starting point in their research.

Appendix III contains the publications that were an outcome of this study.

1.01 Bibliography

Chen, Y, Snyder, JE, Schwichtenberg, CR, Callum, KW, Jiles, DC. 1999. Metal-bonded Co-ferrite composites for magnetostrictive torque sensor applications. *Magnetics, IEEE Transactions on* **35:** 3652.

Clark, AE 1980. *Ferromagnetic Materials* Amsterdam: North-Holland.

Garshelis, IJ. 1992. A torque transducer utilizing a circularly polarized ring. *Magnetics, IEEE Transactions on* **28:** 2202-2204.

Jiles, DC, Lo, CCH. 2003. The role of new materials in the development of magnetic sensors and actuators. *Sensors and Actuators A: Physical* on **106**: 3-7.

Lenz, J, Edelstein, AS. 2006. Magnetic Sensors and Their Applications. *IEEE SENSORS JOURNAL* **6:** 631-649.

Lenz, JE. 1990. A review of magnetic sensors. *Proceedings of the IEEE* **78:** 973-989.

Liang, S, Ravi, BG, Sampath, S, Gambino, RJ. 2007. Atmospheric Plasma Sprayed Cobalt Ferrite Coatings for Magnetostrictive Sensor Applications. *Magnetics, IEEE Transactions on* **43:** 2391-2393.

Melikhov, Y, Snyder, JE, Jiles, DC, Ring, AP, Paulsen, JA, Lo, CCH, Dennis, KW. 2006a. Temperature dependence of magnetic anisotropy in Mn-substituted cobalt ferrite. *JOURNAL OF APPLIED PHYSICS* **99:** 08R102.

Melikhov, Y, Snyder, JE, Lo, CCH, Matlage, PN, Song, SH, Dennis, KW, Jiles, DC. 2006b. The Effect of Cr-Substitution on the Magnetic Anisotropy and Its Temperature Dependence in Cr-Substituted Cobalt Ferrite. *Magnetics, IEEE Transactions on* **42:** 2861-2863.

Pasquale, M. 2003. Mechanical sensors and actuators. *Sensors and Actuators A: Physical* **106:** 142-148.

Paulsen, JA, Snyder, JE, Ring, AP, Lieb, JS, Lo, CCH, Jiles, DC. 2003. Study of the Curie Temperature of Cobalt Ferrite Based Composites for Stress Sensor Applications. *IEEE TRANSACTIONS ON MAGNETICS* **39:** 3316-3318.

Pinkerton, FE, Capehart, TW, Herbst, JF, Brewer, EG, Murphy, CB. 1997. Magnetostrictive SmFe2/metal composites. *Applied Physics Letters* **70:** 2601-2603.

Tatuo, K, Kinmatu, S, Tatuo, K. 1929. Application of the Inverse Wiedemann Effect to Torque Measurements and to Torque Variation Recordings. *Report of Aeronautical Research Institute, Tokyo Imperial University* **4:** 425-445.

Chapter 2. Background

2.01 Introduction

Interest in magnetic materials for sensor purposes extends as far back as late 1920s (Tatuo et al. 1929). A large variety of magnetic sensors have been developed over the years delivering engineering solutions for complex problems (Lenz and Edelstein 2006; Lenz 1990). Among these sensors and actuators is a class of magnetostriction based torque/stress sensors and actuators. In recent years, there has been an active interest in application of magnetostrictive materials for use in non-contact detection of torque & torsional stress in automotive steering systems and power trains (Garshelis 1992; Jiles and Lo 2003; Pasquale 2003; Pasquale et al. 2002; Paulsen et al. 2003). This study investigates the development and application of cobalt ferrite based materials for torque/stress sensor and actuator purposes.

2.02 Properties of magnetic materials

In this section, some basic properties of magnetic materials that are central to this study will be discussed.

2.02.1 Magnetocrystalline Anisotropy

The dependence of internal energy on direction of spontaneous magnetisation with respect to a certain reference direction is called *magnetic anisotropy*. The energy associated with this phenomenon is called *magnetic anisotropy energy*.

This is usually expressed in J/m^3. If this dependence is caused by crystal structure, then it is called *magnetocrystalline anisotropy.*

The origins of magnetocrystalline anisotropy energy are complicated. There was a prevalent thought that the magnetic anisotropy energy is either a macroscale manifestation of the exchange coupling or it is a result of dipole moment interactions within the lattice (Kittel 1949). The following discussion examines each of these claims and provides rebuttal to these arguments.

The exchange energy of a spin system can be written as (Heisenberg 1928)

Equation 2-1 $$E_{\text{exchange}} = -2J\sum_{i\neq j} S_i \cdot S_j$$

where E_{exchange} is the exchange energy, J is the exchange coupling coefficient, and S_i *and* S_j are spins of electrons that are coupled by exchange. However, exchange coupling cannot explain magnetic anisotropy because its analytical expression does not contain any term that accounts for the angle of spins with respect to the crystal axis. In other words, if the entire spin system within a crystal lattice were rotated with respect to the crystal axis, the exchange contributions would not change, whereas the anisotropy energy would change with such a rotation.

The magnetic moment interaction between electrons leads to values of anisotropy energy, which are much smaller than those observed (Kittel 1949). The magnetic dipole interaction contribution to anisotropy is zero for an unstrained crystal. Even in a deformed crystal these values are about 10^3 times less than what is observed in practice, for example in the case of iron and nickel crystals. Another reason why magnetic dipole interaction alone cannot explain

the anisotropy energy is the change in the sign of the anisotropy with change in the temperature. Anisotropy energy is very sensitive to temperature and this cannot be explained by dipole moment interaction inside crystals.

A widely accepted explanation of the origin of the anisotropy energy was given by Van Vleck (Vleck 1947). A version of this explanation provided by Kittle is presented below:

"The spin interacts with the orbit by means of the spin-orbit coupling and the orbital motion in turn interacts with the crystal structure by means of the electrostatic field and overlapping wave functions associated with neighbouring atoms in the lattice." – (Kittel 1949)

The simplest case of anisotropy is uniaxial anisotropy. For example, in an hexagonal cobalt crystal, the stable direction of spontaneous magnetisation is along the *c*-axis of the crystal, with symmetry along both directions on the *c*-axis. Therefore, the anisotropy energy of a magnetisation vector can be written as (Chikazumi 1997):

Equation 2-2 $$E_a = K_{u1}\sin^2\theta + K_{u2}\sin^4\theta + K_{u3}\sin^6\theta + K_{u4}\sin^6\theta\cos 6\phi$$

where E_a is the anisotropy energy, θ is the angle between the magnetisation vector and the *c*-axis, K_{un} are the n^{th} order anisotropy constants for a uniaxial anisotropy system, and ϕ is the azimuthal angle of the magnetisation vector in the plane perpendicular to the easy axis. If K_{un} are positive then the minimum anisotropy energy state occurs at θ=0° or 180°, i.e. when the moments are aligned to the easy axis. In this case, the *c*-axis is the *easy axis*. If K_{un} are negative then the minimum energy state corresponds to θ=90°,i.e. when the moments are

aligned in the plane perpendicular to *c*-axis. In this case, the plane perpendicular to the *c*-axis is the easy plane.

In cubic crystals, the anisotropy energy can be expressed in terms of the direction cosines of the magnetisation vector with respect to the three edges of the cube. Due to cubic symmetry, several directions in the cube will yield the same anisotropy energy; an example of which is shown in Figure 2-1.

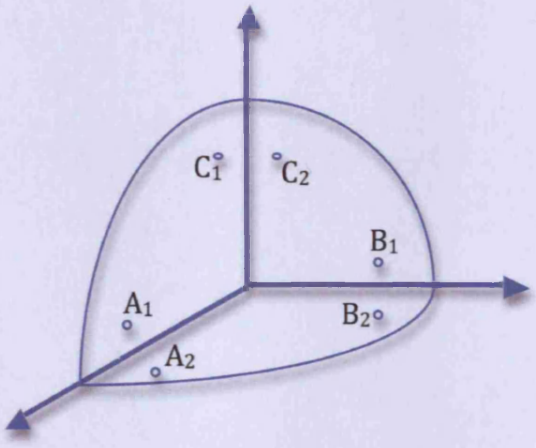

Figure 2-1: The directions A_1, A_2, B_1, B_2, C_1, & C_2, all have the same anisotropy energy due to cubic symmetry.

Taking cubic symmetry into consideration, the anisotropy energy of cubic crystals can be written as (Kittel 1949):

Equation 2-3 $$E_a = K_1\left(\alpha_1^2\alpha_2^2 + \alpha_2^2\alpha_3^2 + \alpha_3^2\alpha_1^2\right) + K_2\left(\alpha_1^2\alpha_2^2\alpha_3^2\right) + \ldots$$

where α_i (i = 1,2,3) are the directions cosines of the magnetisation vector with respect to the three crystal directions along the cube edges, i.e. [100], [010], and [001], and K_i are the i^{th} order anisotropy constants. If the magnetisation is along the [100] direction, then $\alpha_1 = 1$, $\alpha_2 = \alpha_3 = 0$, i.e. $E_a = 0$. For [111], $\alpha_1 = \alpha_2 = \alpha_3 = 1/\sqrt{3}$, such that

Equation 2-4 $$E_a = \frac{1}{3}K_1 + \frac{1}{27}K_2 + \ldots$$

Therefore, if $K_2 = 0$ (i.e. neglecting higher order terms) and $K_1 > 0$, then the minimum energy occurs at magnetisation being aligned to the [100] axis. In such cases, the easy axis is along the [100] direction. Because of cubic symmetry, [010] and [001] are also the easy axes in this case. If $K_2 = 0$ and $K_1 < 0$, then the [111] directions are the easy axes. The energy distribution associated with the description above is show in Figure 2-2.

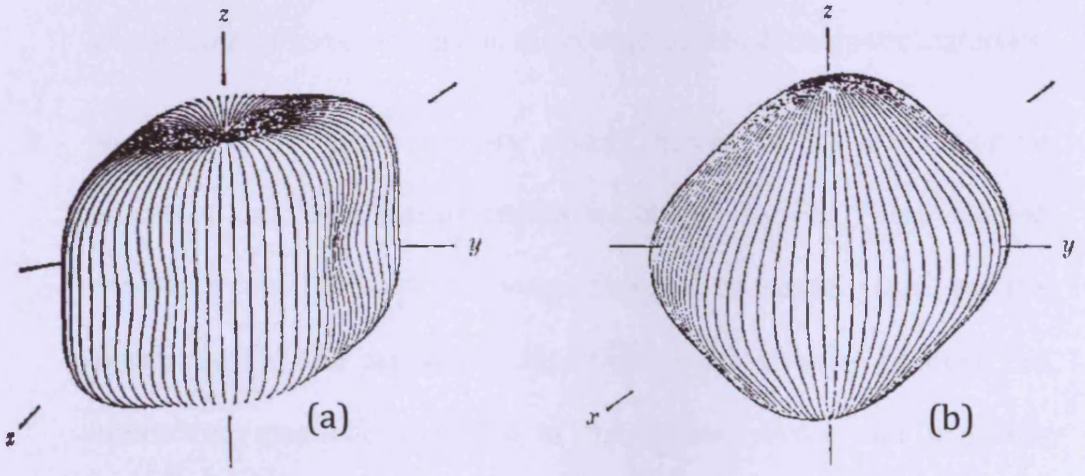

Figure 2-2: Polar diagram of the cubic lattice's anisotropy energy for (a) $K_1 > 0$ and $K_2 = 0$, (b) $K_1 < 0$ and $K_2 = 0$. (Chikazumi 1997)

There can be further complicated cases where $K_2 \neq 0$, or where $K_1 = 0$. The case that is of interest to us is that of the magnetocrystalline anisotropy in cobalt ferrite lattice. This will be discussed in 2.05.1.

2.02.2 Magnetostriction

Magnetostriction is defined as the change in the dimensions of a magnetic material as a result of change in its magnetisation. The change in magnetisation

can be caused by any of the following stimuli: change in applied magnetic field, change in temperature, or change in applied stress.

Magnetostriction is usually described in ppm (parts per million) dimensionless units for most materials. Although it is of such a small order of magnitude (in the range of $10^{-6} - 10^{-2}$ ppm), it is one of the most important secondary magnetic effects. The motivation for studying magnetostriction comes from three areas of investigation (Lee 1955):

1. Study of magnetostriction can help us understand the mechanisms by which internal forces act inside the crystal lattices of magnetic materials.

2. Magnetostrictive processes are closely related to the magnetisation processes and these two processes are indeed coupled. These coupled processes are defined as *magnetoelastic processes.* Due to the dependence of the magnetic interaction on the distance between the interacting magnetic particles in the lattice, elastic and magnetic materials exhibit magnetoelastic phenomena (Lacheisserie 1993). The dependence of the dimensions and the elastic properties (strain) of materials on its magnetic state is described by *direct magnetoelastic processes.* The opposite effect, the dependence of the magnetic state on the elastic properties and strain, are classified as *inverse magnetoelastic phenomenon.*

3. There is a huge scope for magnetoelastic applications that can exploit, direct magnetoelastic processes for actuation purposes and inverse magnetoelastic processes for sensor purposes.

Joule first observed magnetostriction as an increase in the length of an iron bar along the direction of the applied field (Joule 1842). Other direct and inverse magnetoelastic effects were later observed in several different forms (Lee 1955). Among these were:

- **Guillemin effect:** A bar of ferromagnetic material that is bent tends to straighten when an external magnetic field is applied (Guillemin 1846).
- **Wiedemann effect:** When a ferromagnetic rod, clamped at one end, is subjected to a circular magnetic field by passing current through its longitudinal axis and a longitudinal magnetic field is applied to it at the same time, it experiences a torsional force that results in it twisting at the free end (Wiedemann 1883).
- **Associated inverse effects like the Villari effect:** The magnetisation of a ferromagnetic material changes on application of a tensile/compressive stress (Villari 1865).

The direct and inverse magnetoelastic phenomena are related by the following equation based on the le Chatelier's principle (Bozorth 1951):

Equation 2-5 $$\left(\frac{d\lambda}{dH}\right)_{\sigma} = \mu_0 \left(\frac{dB}{d\sigma}\right)_{H},$$

where $\lambda = \delta l/l$ is the magnetostriction, H is the magnetic field, σ is the stress, and B is the magnetic induction.

Magnetostriction can be classified into two main types:

- **Longitudinal Magnetostriction**: measured as $\frac{\delta l}{l}$.

- **Volume Magnetostriction**: measured as $\frac{\delta V}{V}$.

It has been understood that longitudinal magnetostriction, also known as Joule magnetostriction, comes from the alignment of the domains along the easy axis and the rotation of these domains, under the action of a magnetic field, from the easy axis towards the applied field direction. At very high fields though, the domain magnetisation itself increases, generating a volume magnetostriction primarily, and the increase in longitudinal magnetostriction during this process is less dominant (Lee 1955). An example of a typical magnetostriction curve is given in Figure 2-3.

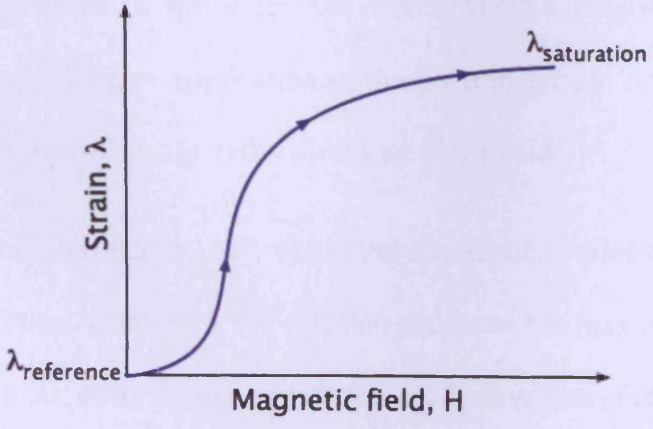

Figure 2-3 An example of a typical magnetostriction curve for a ferromagnetic material.

All ferromagnetic materials develop a magnetostrictive strain below their Curie temperature. The strain developed in a ferromagnetic material, in its

demagnetised state, is called spontaneous magnetisation, $\lambda_{spontaneous}$. This strain is attributed to domain formation. However, as seen in Figure 2-3, the strain at $H = 0$ is called $\lambda_{reference}$ because $H = 0$ does not imply a demagnetised state for a ferromagnetic material.

It must be noted that Figure 2-3 illustrates the magnetic field – magnetostrictive strain dependence for a material with a *positive magnetostriction*, i.e. a material in which the change in length of the specimen along the direction of applied magnetic field is positive. Most ferrites, among many other materials exhibit *negative magnetostriction*, i.e. the material experiences compression along the direction of the applied magnetic field. The magnetostrictive strain of a ferromagnetic material changes as the applied field is increased, saturating at higher fields to a value λ_s (saturation magnetostriction).

The crystalline axis of a ferromagnetic material, inside a domain, is spontaneously strained in the direction of the domain magnetisation. When these domains rotate, upon application of the field, the strain tensors line up to produce a higher overall strain in the direction of the field.

It should be mentioned that a 180° rotation of the domains does not produce any net magnetostriction, whereas a 90° rotation produces the maximum increase in magnetostriction. All other angles of rotation produce values of magnetostriction in between zero and maximum.

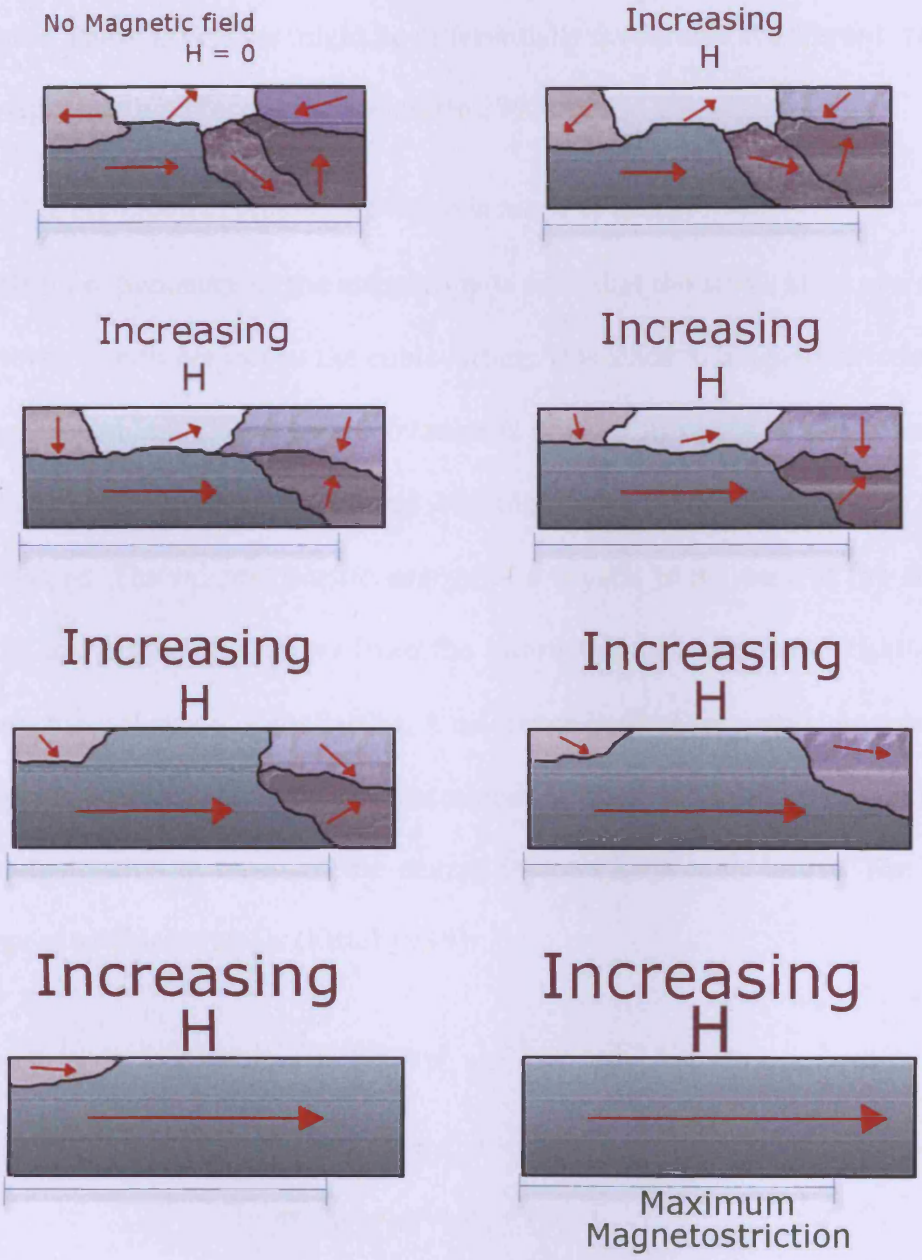

Figure 2-4 An illustration of how magnetostrictive strain changes with applied field due to rotation of domains. Strain tensors from individual domains line up to create a larger overall strain.

Figure 2-4 shows the change in magnetostrictive strain caused by domain processes. This diagram does not take account of the fact that different energies

are associated with the 180° rotation of the domains and 90° rotation of domains. These processes might be differentially favourable at different stages of the magnetisation process (Lacheisserie 1993).

2.02.2.1 Description of magnetostriction in terms of energy

The strain dependence of the anisotropy is such that the stable state of a crystal is deformed with respect to the cubic lattice. This leads to magnetostriction. The energy dependence of magnetostriction is treated in terms of the changes in magnetoelastic energy of the crystal with the change in the magnetisation and its dimensions. The *magnetoelastic energy* of a crystal is the part of the internal energy of a crystal that arises from the interaction between magnetisation and the mechanical strain of the lattice. A reference level of zero magnetocrystalline energy is defined for an unconstrained lattice. All further discussion of magnetostriction in terms of the energy is done for a cubic lattice. The elastic energy of a cubic crystal is (Kittel 1949):

Equation 2-6

$$\begin{aligned} E_{el} = & \frac{1}{2}c_{11}\left(e_{xx}^2 + e_{yy}^2 + e_{zz}^2\right) \\ & + \frac{1}{2}c_{44}\left(e_{xy}^2 + e_{yz}^2 + e_{zx}^2\right) \\ & + c_{12}\left(e_{yy}e_{zz} + e_{zz}e_{xx} + e_{xx}e_{yy}\right) \end{aligned}$$

where E_{el} is the elastic energy, the c_{ij} terms are the elastic moduli and the e_{ij} terms are the strain tensors for the cubic lattice.

As described in Equation 2-, the anisotropy energy of an unstrained cubic lattice, to the first order is:

Equation 2-a $$E_a = K\left(\alpha_1^2\alpha_2^2 + \alpha_2^2\alpha_3^2 + \alpha_3^2\alpha_1^2\right)$$

where α_i are the direction cosines of the magnetisation vector with respect to the cubic axis and K is the first order cubic anisotropy constant.

The Taylor series expansion of the anisotropy energy in terms of the strain tensors is:

Equation 2-7 $$E_a = \left(E_a\right)_0 + \sum_{i \geq j}\left(\frac{\partial E_a}{\partial e_{ij}}\right)_0 e_{ij} + \ldots$$

where $\left(E_a\right)_0$ is the anisotropy of the unconstrained lattice as defined in equation Equation 2-a. From symmetry considerations we arrive at(Kittel 1949),:

Equation 2-b

$$\begin{aligned}
\frac{\partial E_a}{\partial e_{xx}} &= B_1\alpha_1^2; \\
\frac{\partial E_a}{\partial e_{yy}} &= B_1\alpha_2^2; \\
\frac{\partial E_a}{\partial e_{zz}} &= B_1\alpha_3^2; \\
\frac{\partial E_a}{\partial e_{xy}} &= B_2\alpha_1\alpha_2; \\
\frac{\partial E_a}{\partial e_{yz}} &= B_2\alpha_2\alpha_3; \\
\frac{\partial E_a}{\partial e_{zx}} &= B_2\alpha_3\alpha_1;
\end{aligned}$$

where B_1 and B_2 are the *magnetoelastic coupling constants*, values of which depend on the strength of interactions in the solid. Therefore, the part of the total internal energy that depends on the direction of magnetisation and the crystal strain is:

Equation 2-8

$$\begin{aligned} E_{magel} &= K\left(\alpha_1^2\alpha_2^2 + \alpha_2^2\alpha_3^2 + \alpha_3^2\alpha_1^2\right) \\ &+B_1\left(\alpha_1^2 e_{xx} + \alpha_2^2 e_{yy} + \alpha_3^2 e_{zz}\right) \\ &+B_2\left(\alpha_1\alpha_2 e_{xy} + \alpha_2\alpha_3 e_{yz} + \alpha_3\alpha_1 e_{zx}\right) \\ &+\frac{1}{2}c_{11}\left(e_{xx}^2 + e_{yy}^2 + e_{zz}^2\right) \\ &+\frac{1}{2}c_{44}\left(e_{xy}^2 + e_{yz}^2 + e_{zx}^2\right) \\ &+c_{12}\left(e_{xx}e_{yy} + e_{yy}e_{zz} + e_{zz}e_{xx}\right) \end{aligned}$$

where E_{magel} is the magnetoelastic energy of the crystal.

Minimising the energy with respect to the strain tensors we get:

Equation 2-9

$$\begin{aligned} \frac{\partial E_{magel}}{\partial e_{xx}} &= B_1\alpha_1^2 + c_{11}e_{xx} + c_{12}\left(e_{yy} + e_{zz}\right) = 0, \\ \frac{\partial E_{magel}}{\partial e_{yy}} &= B_1\alpha_2^2 + c_{11}e_{yy} + c_{12}\left(e_{zz} + e_{xx}\right) = 0, \\ \frac{\partial E_{magel}}{\partial e_{zz}} &= B_1\alpha_3^2 + c_{11}e_{zz} + c_{12}\left(e_{zz} + e_{xx}\right) = 0, \\ \frac{\partial E_{magel}}{\partial e_{xy}} &= B_2\alpha_1\alpha_2 + c_{44}e_{xy} = 0, \\ \frac{\partial E_{magel}}{\partial e_{yz}} &= B_2\alpha_2\alpha_3 + c_{44}e_{yz} = 0, \\ \frac{\partial E_{magel}}{\partial e_{zx}} &= B_2\alpha_3\alpha_1 + c_{44}e_{zx} = 0, \end{aligned}$$

The solutions to which are (Chikazumi 1997):

Equation 2-10

$$e_{ii} = B_1\frac{c_{12} - \alpha_i^2\left(c_{11} + 2c_{12}\right)}{\left(c_{11} - c_{12}\right)\left(c_{11} + 2c_{12}\right)}$$

&

Equation 2-11 $e_{ij} = -B_2 \frac{\alpha_i \alpha_j}{c_{44}}; \qquad (i \neq j).$

A more widely known description of the equilibrium strain in cubic crystals, expressed in terms of directional magnetostriction constants is (Chikazumi 1997):

Equation 2-12
$$\lambda = \frac{\delta l}{l}$$
$$= \frac{3}{2}\lambda_{100}\left(\alpha_1^2\beta_1^2 + \alpha_2^2\beta_2^2 + \alpha_3^2\beta_3^2 - \frac{1}{3}\right) + 3\lambda_{111}\left(\alpha_1\alpha_2\beta_1\beta_2 + \alpha_2\alpha_3\beta_2\beta_3 + \alpha_3\alpha_1\beta_3\beta_1\right)$$

where magnetostriction constants λ_{100} and λ_{111} are the saturation magnetostriction strain along the crystal direction [100] & [111] respectively. λ_{100} and λ_{111} can be measured using single crystal samples, hence making this formulation very useful. The magnetostriction constants λ_{100} and λ_{111} can also be described in terms of the elastic constants and the magnetoelastic coupling constants as (Chikazumi 1997):

Equation 2-13 &
$$\lambda_{100} = -\frac{2}{3}\frac{B_1}{c_{11} - c_{12}}$$
$$\lambda_{111} = -\frac{1}{3}\frac{B_2}{c_{44}}$$

A similar calculation for randomly oriented polycrystalline cubic materials is complicated by the presence of individual grains. The mean magnetisation in each grain is influenced by the presence of other grains and the crystal directions in each grain are different from those of its neighbours (Vladimirsky 1943).

The saturation magnetostriction of randomly oriented cubic polycrystalline materials can however be described in terms of the magnetostriction constants as (Akulov 1930):

Equation 2-14 $\lambda_s = \frac{2}{5}\lambda_{100} + \frac{3}{5}\lambda_{111}$.

The above equation has been derived with the assumption that the stress is distributed uniformly across the material.

2.03 Cubic Spinels

As discussed before, the properties of magnetic materials are highly influenced by their crystal structure. Among the many crystal structures in which magnetic materials appear, cubic spinel ferrites are of most interest to this study.

Spinel ferrites have the general formula $MO{\cdot}Fe_2O_3$ (also written as MFe_2O_4), where M is one or more of the following divalent ions – Mn, Fe, Co, Ni, Cu, Zn, Mg, etc.

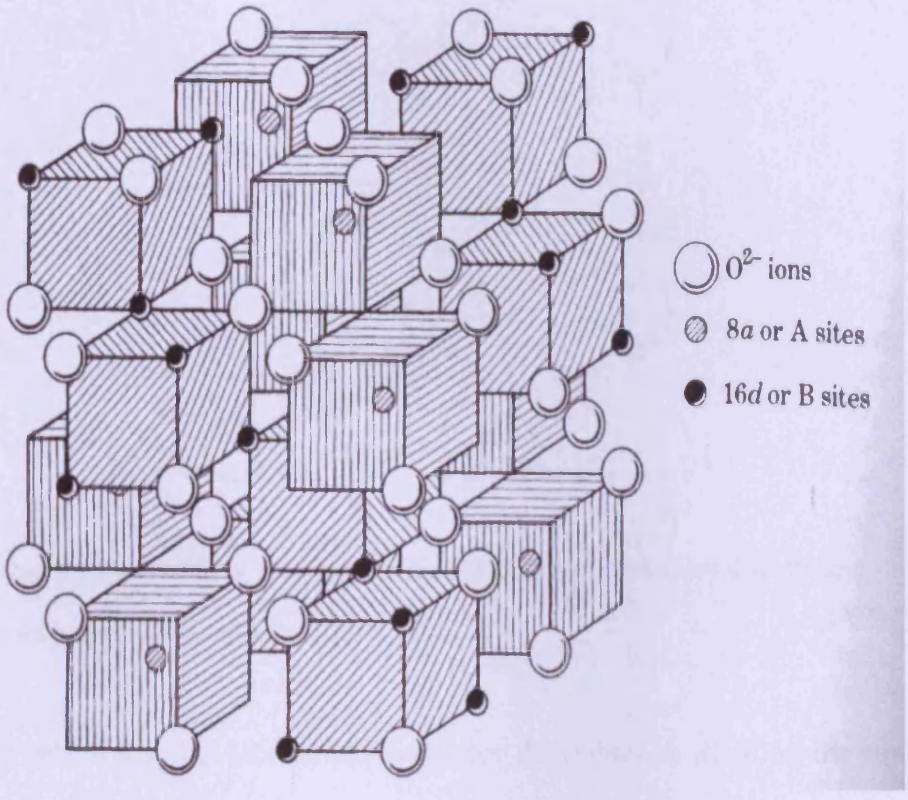

Figure 2-5 An illustration of the spinel lattice (Chikazumi 1997)

The crystal structure of spinels is shown in Figure 2-5. A unit cell of spinel ferrite contains 32 O^{2-} ions, 24 metal ions, therefore, a total of 56 ions. In the neutral valence state, there is not much difference between the radius of an oxygen atom and that of the metal ions. However, negatively charged oxygen ions are much bigger than the positively charges metal ions. Therefore O^{2-} ions occupy the majority of the lattice making up a face centred cubic (FCC) lattice. The metal ions occupy the interstitial spaces in this FCC lattice. Such an arrangement of ions is called a spinel lattice. There are two kinds of interstitial sites in a spinel lattice – tetrahedral (A-sites, surrounded by 4 oxygen atoms forming a tetrahedron) and octahedral (B-sites, surrounded by 6 oxygen atoms forming a octahedron), shown in Figure 2-6.

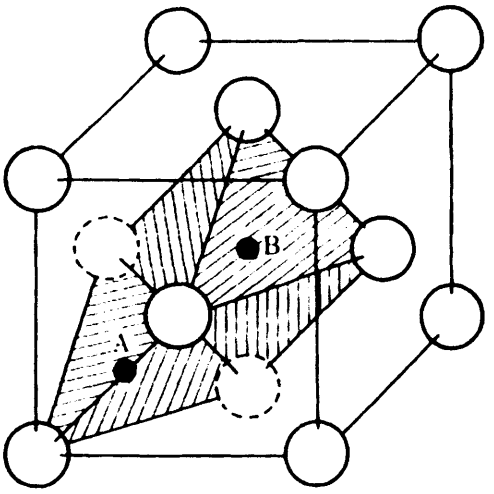

Figure 2-6 An illustration of showing the 4 neighbours of a tetrahedral A-site and the six neighbours of the octahedral B-site (Chikazumi 1997).

The unit cell of a spinel lattice can be better described by dividing the unit cell into eight equal octants, each with an edge size $a/2$, where a is the lattice parameter. The oxygen ions are distributed in the same way in all the cells. The face centred cubic lattice of oxygen atoms has an edge size of $a/2$, as shown in Figure 2-7.

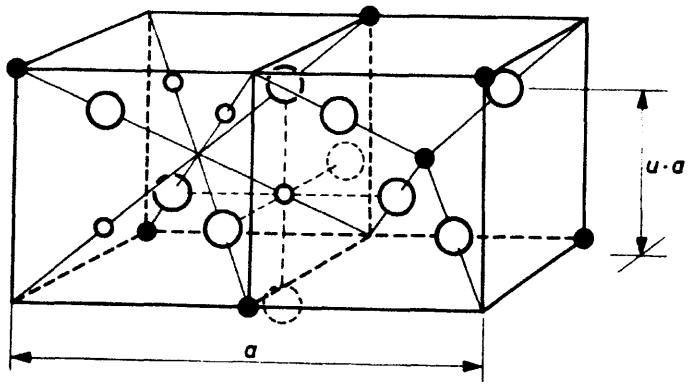

Figure 2-7 The octants inside a spinel structure, where *a* is the unit cell size. The term $u \bullet a$ describes the lattice distortion as defined with the help of the *u*-parameter. Oxygen atoms are the big hollow spheres. The small filled spheres are the A-sites (tetrahedral) and the small hollow spheres are the B-sites (octahedral). The oxygen atoms form an f.c.c. like lattice with an edge size of $a/2$ (Smit and Wijn 1959).

Each unit cell contains 8 A-sites and 16 B-sites. Since the ratio of O^{2-} ions, bonded to A and B-sites, is 2:3, the occupation of A-sites by M^{2+} ions and B-sites by Fe^{3+} ions would lead to charge neutrality. Such a lattice configuration with all B-sites being occupied by Fe^{3+} ions and A-sites being occupied by M^{2+} ions is called a *normal spinel.* Among the initial studies, like those done on $MgAl_2O_4$, it was thought that, because of this charge neutrality, all spinels are normal spinels (Smit and Wijn 1959). However, it was later shown that a several ferrites, cobalt ferrite included, occur in the inverse spinel structure despite the charge neutrality condition being violated (Barth and Posnjak 1932). An *inverse spinel* is a lattice configuration in which A-sites are occupied by half of the Fe^{3+}, and the B-sites are occupied by the remaining half of Fe^{3+} and the M^{2+} ions. Most ferrites though are somewhere between a normal spinel and an inverse spinel and are

called *mixed spinels*. Table 2-1 shows the magnetic properties of some common ferrites:

Table 2-1 Magnetic and physical properties of some ferrites MFe_2O_4 (Chikazumi 1997). M_{mol} is the moment of a molecule; saturation magnetic induction is represented as B_s, and r.t. denotes room temperature.

M	Density ($kg.m^{-3}$)	Lattice const. a (Å)	Resistivity ($\Omega.m$)	M_{mol} at 0 K (μ_B)	B_s r.t. (T)	T_c (K)	u-parameter
Zn	5330	8.44	1	–	–	–	0.385
Mn	5000	8.51	10^2	4.55	0.50	300	0.385
Fe	5240	8.39	4×10^{-5}	4.1	0.60	585	0.379
Co	5290	8.38	10^5	3.94	0.53	520	0.381
Ni	5380	8.34	10^7	2.3	0.34	585	–
Cu (quenched)	5420	8.37	10^3	2.3	–	455	0.380
Cu (slow cool)	5350	c:8.70 a:8.22	–	1.3	0.17	–	–
Mg	4520	8.36	10^5	1.1	0.15	440	0.381
Li	4750	8.33	1	2.6	0.39	670	0.382
γ-Fe_2O_3	–	8.34	–	2.3	–	575	–

2.03.1 Properties of spinels

Superexchange interactions: In an M_1-O-M_2 configuration, as is seen in ferrite spinels, the exchange interactions between M_1-M_2 are weak due to the presence of O^{2-} ion in between any two metal ions. A stronger coupling in these lattices happens through the *superexchange interactions* which propagates through the O^{2-} ion (Anderson 1950, 1959; Kramers 1934). The electronic configuration of O^{2-} ion is $1s^2\ 2s^2\ 2p^6$. The $2p$ orbital of O^{2-} ions stretches towards the $3d$ orbitals of the M_1 and M_2 ions as shown in Figure 2-8.

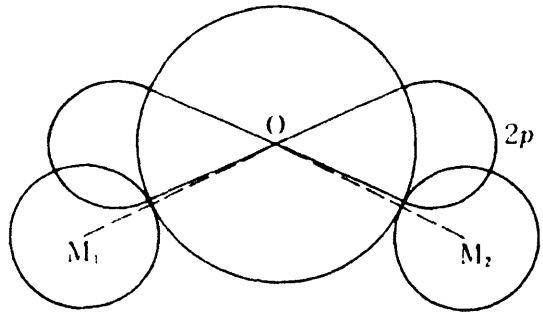

Figure 2-8 Orbital overlap between oxygen and metal ions in a spinel lattice. Shown here is the orbital overlap in an M_1-O-M_2 bond in a spinel ferrite (Chikazumi 1997).

If an electron from the 2*p* orbital gets transferred to the 3*d* orbital of, lets say, M_2, then it happens with the criterion of the spin preservation being maintained. This extra electron in the 3*d* orbital is added such that it has a spin opposite to the net spin of the 3*d* orbital, as dictated by Hund's rule. The net spin of the 2*p* orbit must now be anti-parallel to the spin of the transferred electron because of the Pauli's exclusion principle. The exchange interaction with the other metal ion M_2 is therefore negative. This superexchange interaction makes the spins of M_1 and M_2 anti-parallel to each other. This superexchange interaction is strongest when the angle M_1-O-M_2 is 180°. The interaction becomes weaker as this angle reduces and becomes positive if the angle reduces to a value less than 90° (Anderson 1950).

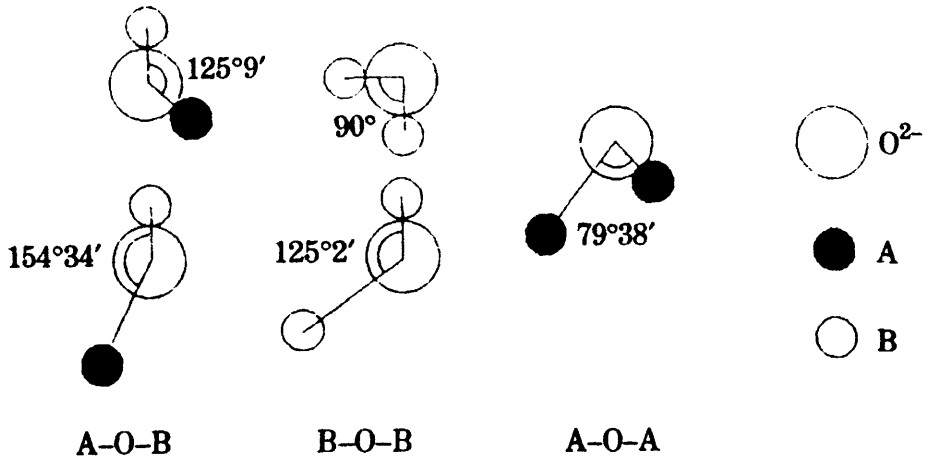

Figure 2-9 Various possible superexchange interactions in a spinel lattice (Chikazumi 1997).

Figure 2-9 shows the angles between the various M_1-O-M_2 pairs that exist in the crystal structure of ferrites, namely A-O-A, B-O-B, and A-O-B. In general, it is observed that the A-O-B angle is closest to 180° and is the strongest coupling, anti-parallel in nature (Chikazumi 1997). The B-O-B and A-O-A angles are smaller and the coupling is weaker. A dominant A-O-B coupling leads to the *Néel collinear arrangement* (Néel 1948). If we assume such a collinear arrangement of spins, it is easier to calculate the net magnetic moment of each formula unit of spinel ferrites.

The magnetic arrangement of different ions in a normal spinel is written as:

Equation 2-17 $$\left(\overrightarrow{M^{2+}}\right)_A O.\left(\overleftarrow{Fe^{3+}}\overrightarrow{Fe^{3+}}\right)_B O_3$$

The moment contribution of Fe^{3+} ($3d^5$) is $5\mu_B$. The contribution of M^{2+} is $n\,\mu_B$, where n is the number of free spins in the electronic structure of M^{2+} ions. Therefore, the net magnetic moment, per formula unit for a normal spinel is:

Equation 2-18
$$m_{\text{normal}} = \{(5+5)-n\}\mu_B = (10-n)\mu_B$$

The magnetic arrangement of the different ions in the inverse spinel lattice can be written as:

Equation 2-19 $\left(\overrightarrow{Fe^{3+}}\right)_A O.\left(\overrightarrow{M^{2+}}\overrightarrow{Fe^{3+}}\right)_B O_3$

Thus the net moment of an inverse spinel lattice is M_B-M_A, where M_A and M_B are the moments on site A and B respectively.

In an inverse spinel, the net moment per formula unit would thus be:

Equation 2-20
$$m_{\text{inverse}} = \{(5+n)-5\}\mu_B = n\mu_B$$

The spins of Fe^{3+} ions in the A and B-sites cancel each other in an inverse spinel lattice. The same calculation can be done for mixed spinel. The ionic distribution in lattice sites of a mixed spinel can be described as:

Equation 2-21 $\left(\overrightarrow{M_{\delta}^{2+}}\overrightarrow{Fe^{3+}}_{1-\delta}\right)_A O.\left(\overrightarrow{M_{1-\delta}^{2+}}\overrightarrow{Fe^{3+}}_{1+\delta}\right)_B O_3$

where δ is known as the inversion factor. In a mixed spinel with an *inversion factor* of δ, the ratio M^{2+} ions are in the A-sites to those in B-sites is $\delta/(1-\delta)$. The net magnetic moment per formula unit is:

Equation 2-22

$$\begin{aligned} m_{\text{mixed}} &= \delta m_{\text{normal}} + (1-\delta) m_{\text{inverse}} \\ &= \delta(10-n)\mu_B + (1-\delta)(n)\mu_B \\ &= \left((10-2n)\delta + n\right)\mu_B \end{aligned}$$

However, the real measured values of net magnetic moment may differ from the calculation shown above. This is because of the presence of orbital magnetic moments, which are still unquenched by the crystalline field. For example, the net magnetic moment of the inverse spinel lattice of cobalt ferrite is $3.94\mu_B$. The prediction from the equation would be $3\mu_B$, as the moment contribution of a Co^{2+} ion is $3\mu_B$ (Chikazumi 1997).

The inversion ratio δ can vary for the same chemical composition. It depends on the processing route, wherein the parameters affecting it include processing temperatures, cooling rates, etc (Smit and Wijn 1959).

It was demonstrated that many other spin structures existed in spinel ferrites in cases where the assumption of a dominant A-O-B anti-parallel coupling was invalid (Brabers 1995). If, the negative B-O-B interaction is comparable to the negative A-O-B interaction, i.e. if exchange integral $|J_{AB}| < 3/2\ |J_{BB}|\ m_B/m_A$, the B-lattice splits into two sub-lattices with their magnetisations at an angle to each other and the resultant moment being anti-parallel with m_A. Such a triangular configuration of moments in A & B sites is called the Yafet-Kittel triangular configuration (Yafet and Kittel 1952).

2.04 Materials for magnetostrictive stress/torque sensor and actuator applications

The properties of a magnetic material that are of particular importance in stress/torque sensor and actuator applications are:

- Hysteresis - the lesser is the hysteresis, the higher is the reversible magnetostriction in the material, which is a desirable property. Reducing Curie temperature has shown to reduce the hysteresis at temperatures below Curie temperature. Therefore, reducing Curie temperature can be used a metric of reducing hysteresis at temperatures below it.

- Magnetostriction (λ) - the higher the magnetostriction in the linear region of the magnetostriction curve, as shown in Figure 2-10, the higher would be the range of operation of devices based on it

- Sensitivity of magnetostriction to applied field or strain derivative ($d\lambda/dH$) - The higher the strain derivative, the more responsive will be the material to any applied stimulus.

The strain derivative of the material which is an important factor that decides the sensitivity of the material in its application as an actuator, also determines how sensitive the material would be in a stress/torque sensor operation. The relationship between strain derivative and sensitivity of its magnetic induction to applied stress is described as (Bozorth 1951)

2-23 $$\left(\frac{dB}{d\sigma}\right)_{\lambda} = \left(\frac{d\lambda}{dH}\right)_{\sigma}.$$

The above equation, based on the Le Chatelier principle (only applicable under reversible conditions) illustrates that a material that would be sensitive in sensor capability ($dB/d\sigma$) would also be sensitive in actuation capability ($d\lambda/dH$).

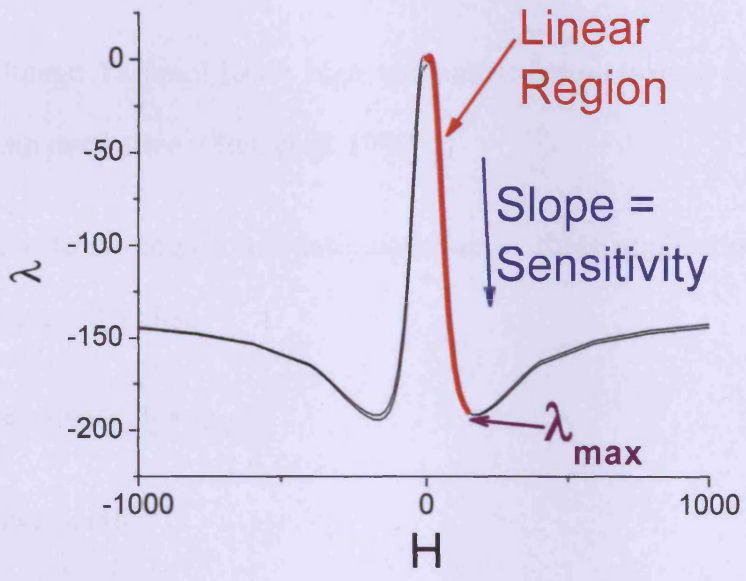

Figure 2-10 The linear region of magnetostriction curve for a material with a negative magnetostriction.

Previous investigations into materials for magnetostrictive stress/torque sensors and actuators focussed on rare earth materials with high magnetostriction. Among these were Terfenol ($Tb_{0.3}Dy_{0.7}Fe_2$) (Clark 1980) and $SmFe_2$ (Pinkerton et al. 1997), which have a high magnetostriction in the range (1000-3000) ppm. However, these materials has several drawbacks:

- Terfenol was brittle and did not have good mechanical properties (Chen et al. 1999; Corcolle et al. 2008; Liang et al. 2007; Lo et al. 2005)
- Large eddy current losses occur at high frequencies in these materials (Liang et al. 2007)
- Rare earth containing materials are expensive and thus not cost-effective for many applications (Chen et al. 1999; Corcolle et al. 2008; Liang et al. 2007; Lo et al. 2005)
- Although Terfenol has a high magnetostriction, it does not have a high strain derivative (Chen et al. 1999).

The solution to finding a candidate material for these applications then lies in finding a material which:

- is mechanically robust
- is an insulator
- is relatively inexpensive
- has high strain derivative

The importance of a high strain derivative can be judged from its impact on the power required to magnetise the material. Figure 2-11 shows the comparison of two hypothetical materials with different magnetostriction characteristics. If the two materials were used in torque/stress sensor/actuator applications, their maximum magnetostriction would determine the range of operation of the device. For example, Material-1, as shown in Figure 2-12, would have a higher

range of operation in the device. Material-1 would also achieve its maximum magnetostriction at a lower magnetic field value, i.e. it has a higher strain derivative. For comparison's sake, if Material-1 were to be benchmarked against Material-2, then, to achieve the same magnetostriction λ_2, a magnetic field H_1 would need to be applied to Material-1. Material-2 develops the same magnetostriction at a field value $H_{2,max}$. The currents needed to magnetise these two samples would be in the ratio:

Equation 2-24
$$\left[\frac{I_{mag1}}{I_{mag2}} \propto \frac{H_1}{H_{2,max}}\right]_{\lambda=\lambda_2},$$

where I_{mag1} and I_{mag2} are the currents needed to produce fields H_1 and $H_{2,max}$ respectively. Since, because of larger strain derivative in Material-1, $H_1 < H_{2,max}$, and thus $I_{mag1} < I_{mag2}$.

In this comparison, Material-1 has a higher range of operation and also requires less current to magnetise it to achieve the same magnetostriction as the maximum magnetostriction of Material-2.

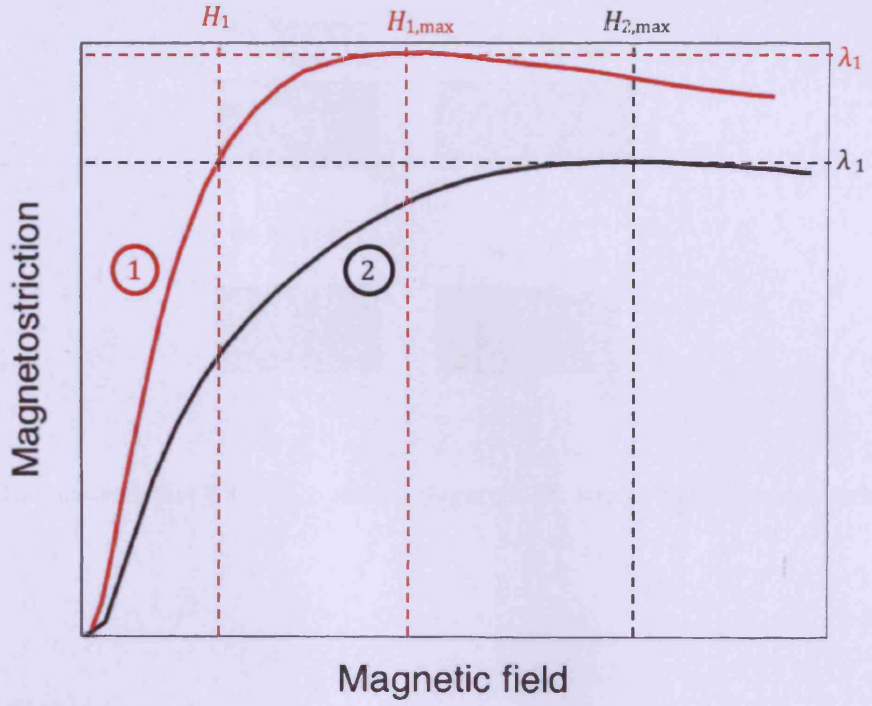

Figure 2-11 A comparison of the magnetostriction of two hypothetical materials: Material-1 (red curve) and Material-2 (black curve). The maximum magnetostriction for materials 1 & 2 are marked as λ_1 and λ_2 respectively. $H_{1,max}$ is the field at which Material-1 reaches its maximum magnetostriction and $H_{2,max}$ is the corresponding field for Material-2. H_1 is the field at which Material-1 reaches the maximum magnetostriction of Material-2.

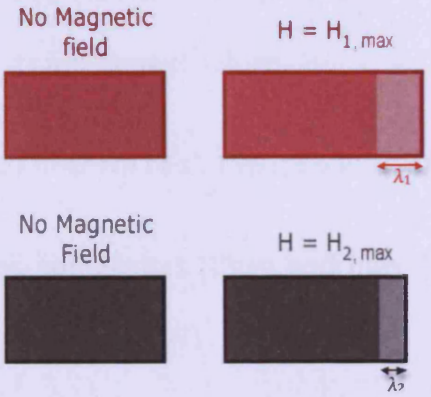

Figure 2-12 Illustrates that Material-1, show in **Figure 2-11**, attains higher magnetostriction than Material-1.

2.05 Cobalt Ferrite

By the 1990s, cobalt ferrite based materials had emerged as candidate materials for torque/stress sensor and actuator applications (Chen et al. 1999). Polycrystalline cobalt ferrite composites have reasonably high magnetostriction (~200 ppm), high strain derivative (~10^{-9} A^{-1}.m), is chemically robust, electrical insulator, and relatively inexpensive. The strain derivative for cobalt ferrite is an order of magnitude higher than Terfenol based composites, as shown in Figure 2-13. The sensitivity of surface field to torque in metal bonded cobalt ferrite was measured to be 64 A/m per N-m (Chen and Jiles 2000; Chen et al. 1999), in comparison to the 19 A/m per N-m for iron, nickel and cobalt alloy (Chen et al. 2001).

However, properties of pure cobalt ferrite could be further enhanced to make it more suitable for to the needs of a torque/stress sensor and actuator

applications. Enhancing magnetoelastic properties of cobalt ferrite has been pursued by several routes as mentioned below:

- Magnetic Annealing (Bozorth et al. 1955; Lo et al. 2005)
- Cobalt Ferrite based composites (Chen and Jiles 2000; Chen et al. 2001; Chen et al. 2000; Chen et al. 1999)
- Chemical Substitution (Lee et al. 2007; Lo et al. 2006; Matlage et al. 2005; Melikhov et al. 2006a; Melikhov et al. 2006b)

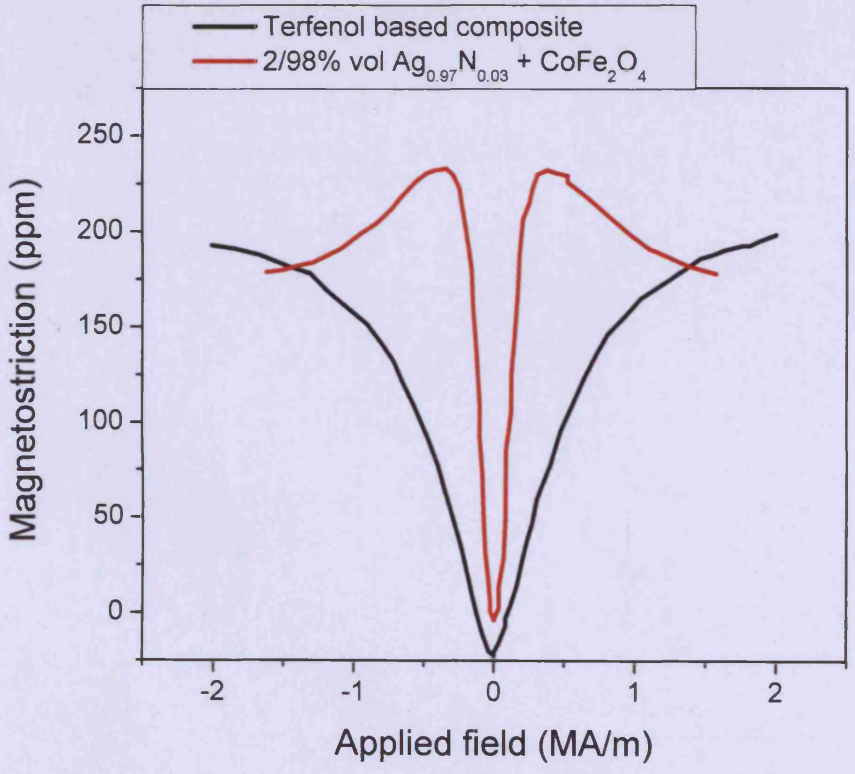

Figure 2-13 Comparison between strain derivative of metal bonded cobalt ferrite and Terfenol composites (Chen et al. 1999).

2.05.1 Properties of cobalt ferrite

The magnetoelastic properties of cobalt ferrite are dominated by its spin structure, which in turn is affected by site occupancy of the various ions in the lattice. Determination of precise spin structure of cobalt ferrite has been hampered by its very high anisotropy at low temperatures, which makes it difficult to saturate the magnetisation, even at fields as high as 5 T (Brabers 1995). Pure cobalt ferrite has been known to have a Néel type collinear arrangement of spins (Brabers 1995; Guillot et al. 1988). For polycrystalline cobalt ferrite, it was also found that, in samples with a large amount of Co in the A–sites (i.e. a lower degree of inversion), the long range spin structure can be interrupted by local canted spins, where the moments are neither parallel non-antiparallel to each other, but are at an angle between 90° and 180° (Teillet et al. 1993).ß

The magnetostriction coefficients for crystalline cobalt ferrite were measured to be λ_{100} = -590 ppm & λ_{111} = -120 ppm (Bozorth 1951). However, the saturation magnetostriction of polycrystalline cobalt ferrite was determined to be −225 ppm. The first order cubic anisotropy constant was measured to be between $1.1 \times 10^5 - 3.8 \times 10^5$ J-m^{-3}, with variations caused by differences in chemical substitution and processing techniques. It was also concluded that:

- A small amount of chemical substitution can lead to change in the sign of the anisotropy and magnetostriction in ferrites. An illustration of how changing of signs of the anisotropy and magnetostriction coefficients can lead to change in the λ-H curves is shown in Figure 2-14. Table 2-2 lists

the various combinations of K_1, λ_{100}, and λ_{111} that lead to the different shapes of magnetostriction curve.

- A high anisotropy leads to a lower strain derivative principally because it requires a higher magnetic field to change the magnetisation.

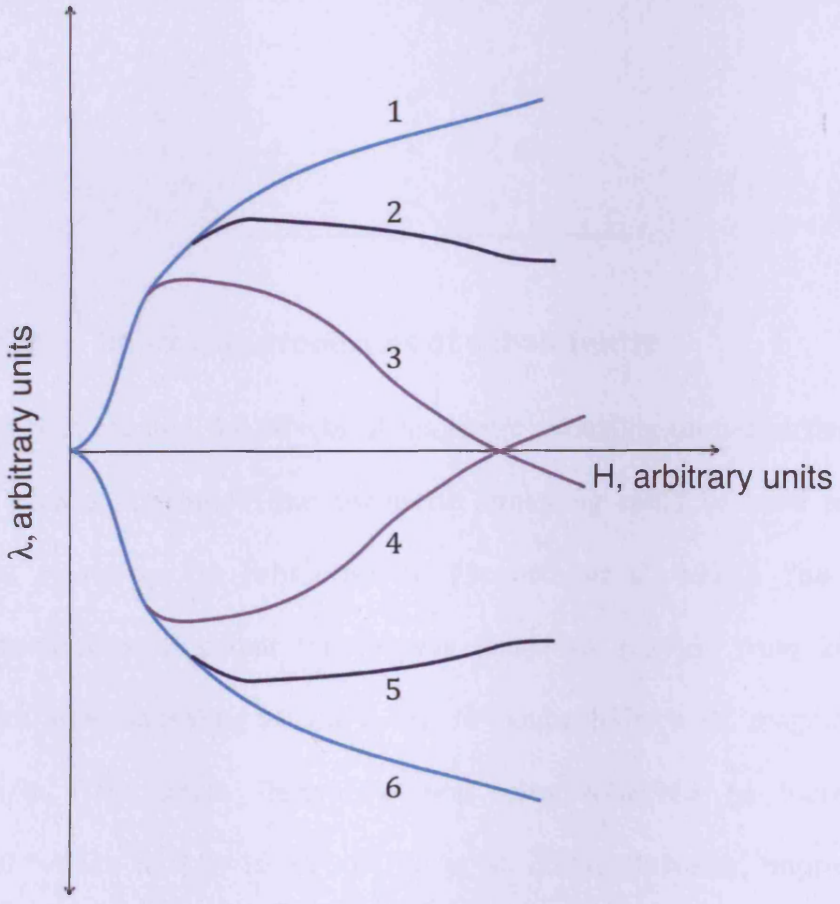

Figure 2-14 Various types of magnetostriction curves expected through different combinations of K_1, λ_{100}, and λ_{111}, as shown in **Table** 3-2 (Bozorth et al. 1955). The numbers of each curve corresponds to the shapes described in Table 3-2.

Table 2-2 Combinations of K_1, λ_{100}, and λ_{111} that lead to different shapes of magnetostriction curves as shown in **Figure 2-14** (Bozorth et al. 1955).

K_1	λ_{100}	λ_{111}	Curve Type
+	+	+	1
+	+	−	2, 4
+	−	+	3, 5
+	−	−	6
−	+	+	1
−	+	−	3, 5
−	−	+	2, 4
−	−	−	6

2.05.2 Improving properties of cobalt ferrite

Bozorth first studied the effects of magnetic annealing on properties of cobalt ferrite. It was concluded that magnetic annealing could be used to induce a uniaxial anisotropy in cobalt ferrite (Bozorth et al. 1955). The maximum magnetostriction of cobalt ferrite was found to increase from 200 ppm to 250 ppm after annealing at 300 K for 36 hours under a DC magnetic field of 318 kA/m. The strain derivative was also observed to increase from 1.5×10^{-9} $A^{-1}.m$ to 3.9×10^{-9} $A^{-1}.m$ (Lo et al. 2005). However, improvement of properties achieved by magnetic annealing degrades with time and heat (Lo et al. 2005).

Chemical substitution has been tried in various forms to enhance the properties of cobalt ferrite. Early investigations focussed on the effect of substitution of various M^{2+} ions in place of some of Co^{2+} in cobalt ferrite (Smit and Wijn 1959). However, to improve the magnetoelastic properties of cobalt ferrite for

stress/torque sensor and actuator applications, another substitution route was preferred to substituting M^{2+} ions in place of Co^{2+}. Substitution of non-magnetic ions for some of Fe^{3+} was preferred to reduce the anisotropy and hence increase the sensitivity. However, it was also observed that such a substitution led to the reduction of the maximum magnetostriction amplitude which was disadvantageous.

Metal bonded cobalt ferrite also shows magnetomechanical hysteresis. This hysteresis can be reduced by chemical substitution (Paulsen et al. 2003). It was observed that the magnetomechanical hysteresis of metal bonded cobalt ferrite became negligibly small at temperatures above 60 °C (Chen et al. 2000). The co-substitution of Co^{2+}/Si^{4+} for some of Fe^{2+} in cobalt ferrite was seen to reduce the magnetomechanical hysteresis. This reduction of magnetomechanical hysteresis was correlated with the reduction of the Curie temperature of $Co_{1+x}Si_xFe_{2-2x}O_4$ with increasing x. However, in the case of Co^{2+}/Si^{4+} co-substitution, it was also observed that it was difficult to obtain single-phase material because of the high chemical stability of SiO_2.

The substitution of Mn^{3+} in place of some of Fe^{3+} was also seen to reduce the Curie temperature of the cobalt ferrite, as shown in Figure 2-15. It can be seen that, although the Curie temperature T_c keeps decreasing with the addition of Mn^{3+}, the maximum magnetostriction also decreases with the addition of Mn^{3+}. The change in Curie temperature with substitution of Mn^{3+} was seen to be linearly dependent on manganese content (x). The maximum magnetostriction of material with the lowest Mn^{3+} composition ($x = 0.2$) is lower than the pure cobalt ferrite. Any further addition of Mn^{3+} ($x \geq 0.2$) resulted in further reduction

of the maximum magnetostriction. The saturation magnetostriction was also seen to reduce with Mn^{3+} substitution and this might be correlated to the reduction in maximum magnetostriction. The first order cubic anisotropy constant K_1 was also seen to reduce with increasing manganese content at all temperatures in the 10 – 400 K range (Melikhov et al. 2006a). The strain derivative was seen to increase for small amounts of Mn^{3+} substitution at room temperature (Lo 2007).

The substitution of Cr^{3+} in place of some of the Fe^{3+} in cobalt ferrite was seen to reduce the Curie temperature at a faster rate (Lee et al. 2007). However, the maximum magnetostriction was also seen to reduce at a faster rate for chromium substitution in comparison with that of manganese substitution. The strain derivative was also seen to increase for small amounts of chromium substitution.

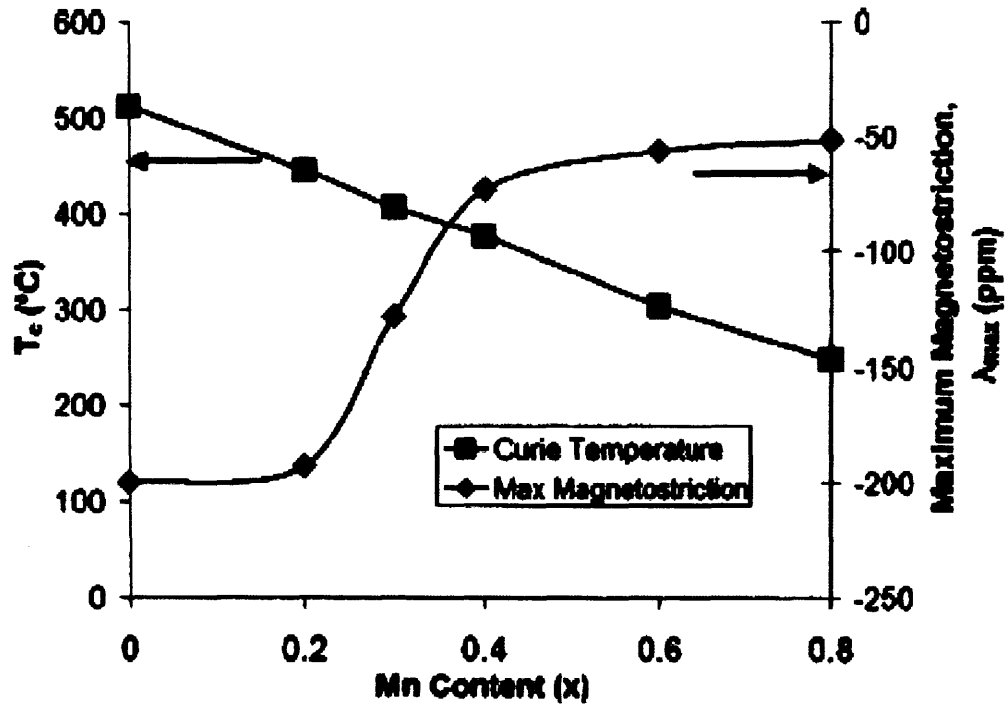

Figure 2-15 The variation of the Curie temperature T_c and maximum magnetostriction λ_{max} with manganese content in $CoMn_xFe_{2-x}O_4$ (Paulsen et al. 2005).

Both manganese and chromium substitutions have B-site preference. This study investigates the effect of chemical substitution into A-sites on the properties of cobalt ferrite with the aim of improving both strain derivative and maximum magnetostriction. Further chapters include the description of research done in this study.

2.06 Bibliography

Akulov, N. S. 1930. Über die Anwendungen des Gesetzes ferromagnetischer Anisotropie zur Berechnung der Eigenschaften polykristallinischen Eisens. *Z. Phys.* 66(7-8), pp. 533-542.

Anderson, P. W. 1950. Antiferromagnetism. Theory of Superexchange Interaction. *Physical Review* 79(2), p. 350.

Anderson, P. W. 1959. New Approach to the Theory of Superexchange Interactions. *Physical Review* 115(1), p. 2.

Barth, T. F. W. and Posnjak, E. 1932. Spinel Structure: with and without Variate Atom Equipoints. *Zs. f. Kristallographie* 82, pp. 325-341.

Bozorth, R. M. 1951. *Ferromagnetism*. Princeton, New Jersey: D. Van Nostrand Company, Inc.

Bozorth, R. M. et al. 1955. Anisotropy and Magnetostriction of Some Ferrites. *Phys. Rev.* 99(6), pp. 1788--1798.

Brabers, V. A. M. 1995. Progress in Spinel Ferrites Research. *Handbook of Magnetic Materials*. Amsterdam: Elsevier Science B. V.

Chen, Y. and Jiles, D. C. 2000. The Magnetomechanical Effect Under Torsional Stress in a Cobalt Ferrite Composite. *IEEE TRANSACTIONS ON MAGNETICS* 36(5), pp. 3244-3247.

Chen, Y. et al. 2001. Magnetomechanical effects under torsional strain in iron, cobalt and nickel. *Journal of Magnetism and Magnetic Materials* 236(1-2), pp. 131-138.

Chen, Y. et al. 2000. Temperature dependence of the magnetomechanical effect in metal-bonded cobalt ferrite composites under torsional strain. *J. Appl. Phys* 87(9), pp. 5798-5800.

Chen, Y. et al. 1999. Metal-bonded Co-ferrite composites for magnetostrictive torque sensor applications. *Magnetics, IEEE Transactions on* 35(5), p. 3652.

Chikazumi, S. 1997. *Physics of Ferromagnetism*. Second ed. Great Clarendon Street, Oxford, OX2 6DP: Oxford University Press.

Clark, A. E. 1980. *Ferromagnetic Materials*. Amsterdam: North-Holland.

Corcolle, R. et al. 2008. Optimal Design of Magnetostrictive Composites: An Analytical Approach. *Magnetics, IEEE Transactions on* 44(1), pp. 17-23.

Garshelis, I. J. 1992. A torque transducer utilizing a circularly polarized ring. *Magnetics, IEEE Transactions on* 28(5), pp. 2202-2204.

Guillemin, A. 1846. *C. R. Acad. Sci, Paris* 22.

Guillot, M. et al. 1988. High magnetic field magnetization study in cadmium-cobalt ferrite single crystals. *Zeitschrift für Physik B Condensed Matter* 71(2), pp. 193-197.

Heisenberg, W. 1928. Theory of Ferromagnetism. *Zeitschrift für Physik A Hadrons and Nuclei* 49(9-10), pp. 619-636.

Jiles, D. C. and Lo, C. C. H. eds. 2003. *The role of new materials in the development of magnetic sensors and actuators*. September. Sensors and Actuators A: Physical.

Joule, J. P. 1842. On a new class of magnetic forces. *Sturgeons Annals of Electricity* 8.

Kittel, C. 1949. Physical Theory of Ferromagnetic domains. *Reviews of Modern Physics* 21(4), pp. 541-583.

Kramers, H. A. 1934. L'interaction Entre les Atomes Magnetogenes dans un Cristal Paramagnetique. *Physica* 1(1-6), pp. 182-192.

Lacheisserie, E. d. T. d. 1993. *Magnetostriction: Theory and Applications of Magnetoelasticity*. Boca Rotan, Florida: CRC Press Inc.

Lee, E. W. 1955. Magnetostriction and Magnetomechanical Effects. *Rep. Prog. Phys.* 18, pp. 184-229.

Lee, S. J. et al. 2007. Magnetic and magnetoelastic properties of Cr-substituted cobalt ferrite. *Journal of Applied Physics* 102(7), p. 073910.

Lenz, J. and Edelstein, A. S. 2006. Magnetic Sensors and Their Applications. *IEEE SENSORS JOURNAL* 6(3), pp. 631-649.

Lenz, J. E. 1990. A review of magnetic sensors. *Proceedings of the IEEE* 78(6), pp. 973-989.

Liang, S. et al. 2007. Atmospheric Plasma Sprayed Cobalt Ferrite Coatings for Magnetostrictive Sensor Applications. *Magnetics, IEEE Transactions on* 43(6), pp. 2391-2393.

Lo, C. C. H. 2007. Compositional Dependence of the Magnetomechanical Effect in Substituted Cobalt Ferrite for Magnetoelastic Stress Sensors. *Magnetics, IEEE Transactions on* 43(6), pp. 2367-2369.

Lo, C. C. H. et al. 2006. Magnetoelastic and Magnetic Properties of Chromium substituted Cobalt Ferrite.

Lo, C. C. H. et al. 2005. Improvement of Magnetomechancial Properties of Cobalt Ferrite by Magnetic Annealing. *IEEE TRANSACTIONS ON MAGNETICS* 41(10), pp. 3676-3678.

Matlage, P. N. et al. 2005. *Non-contact Magnetoelastic Stress Sensor Based on Substituted Cobalt Ferrite*. San Jose, California: 50th Annual Conference on Magnetism and Magnetic Materials.

Melikhov, Y. et al. 2006a. Temperature dependence of magnetic anisotropy in Mn-substituted cobalt ferrite. *JOURNAL OF APPLIED PHYSICS* 99, p. 08R102.

Melikhov, Y. et al. 2006b. The Effect of Cr-Substitution on the Magnetic Anisotropy and Its Temperature Dependence in Cr-Substituted Cobalt Ferrite. *Magnetics, IEEE Transactions on* 42(10), pp. 2861-2863.

Néel, L. 1948. Propriétés magnétiques des ferrites - ferrimagnétisme et antiferromagnétisme. *ANNALES DE PHYSIQUE* 3.

Pasquale, M. 2003. Mechanical sensors and actuators. *Sensors and Actuators A: Physical* 106(1-3), pp. 142-148.

Pasquale, M. et al. 2002. Stress sensing with Co based ferrite composites. *Journal of Magnetism and Magnetic Materials* 242-245(Part 2), pp. 1460-1463.

Paulsen, J. A. et al. 2005. Manganese-substituted cobalt ferrite magnetostrictive materials for magnetic stress sensor applications. *Journal of Applied Physics* 97, p. 044502.

Paulsen, J. A. et al. 2003. Study of the Curie Temperature of Cobalt Ferrite Based Composites for Stress Sensor Applications. *IEEE Transactions on Magnetics* 39(5), pp. 3316-3318.

Pinkerton, F. E. et al. 1997. Magnetostrictive SmFe2/metal composites. *Applied Physics Letters* 70(19), pp. 2601-2603.

Smit, J. and Wijn, H. J. 1959. *Ferrites*. N. V. Philips' Gloeilampenfabrieken, Eindhoven, Holland.

Tatuo, K. et al. 1929. Application of the Inverse Wiedemann Effect to Torque Measurements and to Torque Variation Recordings. *Report of Aeronautical Research Institute, Tokyo Imperial University* 4(52), pp. 425-445.

Teillet, J. et al. 1993. Magnetic structure of CoFe2O4. *Journal of Magnetism and Magnetic Materials* 123(1-2), pp. 93-96.

Villari, E. 1865. Change of magnetization by tension and by electric current. *Ann. Phys. Chem* 126.

Vladimirsky, K. V. 1943. *C. R. Acad. Sci, U.R.S.S* 41.

Vleck, J. H. V. 1947. Quelques aspects de la théorie du magnétisme. *Ann. IH Poincare* 10, pp. 57-190.

Wiedemann, W. 1883. *Lehre von der Elektrizität* 3, p. 680.

Yafet, Y. and Kittel, C. 1952. Antiferromagnetic Arrangements in Ferrites. *Physical Review* 87(2), p. 290.

Chapter 3. Experimental Methodology

3.01 Introduction

As discussed in Chapter 1, a few magnetic properties of cobalt ferrite were identified to be important for investigating its efficacy as a material for stress/torque sensor and actuator application. Careful consideration was given to the manner in which these properties could be measured. Experiments were planned, executed and analysed to ensure that most reliable scientific data and analysis can be contributed to the subject knowledge through this work. This chapter describes the experimental methods and calculation techniques used to collect data and produce the results presented in this thesis. All measurement methods were chosen and planned in consultation with academic supervisors. All measurements and analysis performed by other researchers have been duly credited where appropriate.

3.02 Samples Preparation

All samples were prepared by standard powder ceramic techniques designed by Song (Song, 2007). Gallium and germanium/cobalt substituted samples were prepared by Song at Iowa State University and aluminium substituted samples were prepared by Nlebedim at Cardiff University. High purity oxide powders were mixed in stoichiometric ratios and then calcined at 1000 °C for 24 hours. The resulting sample was then ball milled, the powder pressed into cylindrical samples and further sintered for 24 hours at 1350 °C. The samples were cooled in air for 12 hours. The samples thus prepared were found to be randomly

oriented polycrystalline samples. SEM micrographs were analysed by Song and Nlebedim for samples prepared by them that all samples used in the study are single phase materials.

3.03 Maximum magnetisation vs. Temperature

The maximum magnetisation vs temperature was measured using a Quantum Design Magnetic Property Measurement System (MPMS) (Quantum Design 2010). The MPMS, shown in Figure 3-1 is a Superconducting Quantum Interference Device (SQUID) magnetometer. Quantum Design's MPMS uses liquid helium to bring the primary coils to the superconducting state such that a high current can be sent through them in order to produce high magnetic fields. The maximum magnetisation was defined as the magnetisation at a constant magnetic field of $\mu_0 H = 5$ T. Measurements were taken for all the samples between a temperature range of 10 – 400 K, in steps of 4 K.

Figure 3-1 The Magnetic Property Measurement System used for measurement of saturation magnetisation and magnetisation loops at different temperatures. Courtesy Dr. Hadimani (Cardiff University).

3.03.1 Measurement and related issues

Since, the MPMS measures the magnetic moment of the sample, the magnetisation was determined by calculating the volume of the sample. The samples weighed between 2 – 5 mg. The mass of the sample was determined with a precision of ±0.1 mg. The density of cobalt ferrite used for the calculations was 5314 kg/m^3. Although the samples used were small in size (all dimensions < 2 mm), the demagnetising effect was not expected to be dominant at high fields and thus was not compensated for. The samples were secured at the centre of a non-magnetic plastic straw supplied by Quantum Design, as shown in Figure 3-2, and it was ensured that the sample does not move during the measurement.

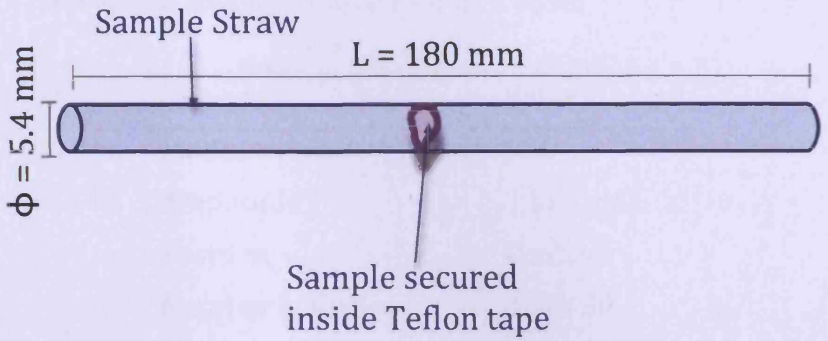

Figure 3-2 An illustration of how the sample was mounted inside the sample straw provided by Quantum Design.

The MPMS was used in *Reciprocating Sample Option* (RSO) mode to perform quicker measurements. The measurement parameters used are shown in Table 3-1. Since the RSO option involves vibrating the sample using a servo meter, a software sample-centring algorithm was used to centre the sample between the squid coils after every few measurements. It was thus ensured that the sample remained in the same position throughout the measurement, as shown in Figure 3-3. The rate of change of temperature was fixed at 2 K/min. The sample was stabilised within 0.05 K of target temperature for at least 1 minute before taking the measurement. This procedure was undertaken to ensure thermal stability during the measurements.

Table 3-1 A list of options used in RSO measurements in MPMS

Option	Value
Mode	RSO
Amplitude	1 to 5 cm
Position	Centre
Number of Cycles	15 to 30
Scans per measurement	2 to 4
Frequency	0.5 to 2 Hz
Auto Tracking	On

3.04 Magnetic hysteresis loops at different temperatures

Magnetic hysteresis loops were measured inside a Quantum Design MPMS equipment at each of the following temperatures – 10 K, 50 K, 100 K, 150 K, ..., 400 K. Major loops were measured between a magnetic field range of $\mu_0 H$ = ±5 T.

3.04.1 Measurement and related issues

The samples were mounted in a manner similar to that described in Section 3.03.1. The calculation of the magnetisation from the magnetic moment data was also similar. The temperature was changed at a rate of 10 K/min between any two M-H loop measurements at different selected temperatures. Before the measurement, the sample was allowed to stabilise to within ±0.05 K of the target temperature for 5 minutes. After which, the temperature was maintained in the ±0.05 K range of the target temperature. The options used in RSO measurements were the same as those listed in Table 3-1. The superconducting magnet in MPMS was used in the "Hysteresis" mode to enable faster changing of the magnetic field. Coercive field data was extracted from

these measured loops.

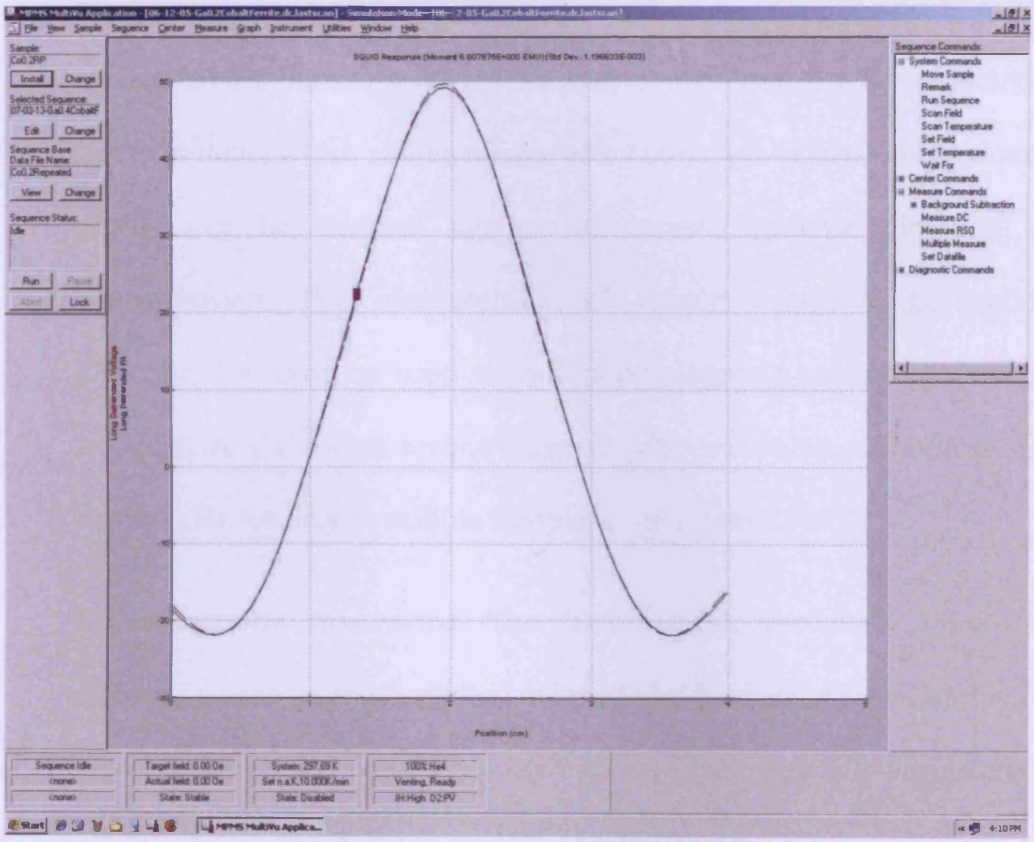

Figure 3-3 The sample was centred at 2 cm using an amplitude of 4 cm. The last scan of the voltage across the coil concludes that the sample has remained at the centre throughout the measurement.

3.05 Calculation of Magnetocrystalline Anisotropy

Several ways of determining magnetocrystalline anisotropy were considered for randomly oriented, chemically substituted, polycrystalline cobalt ferrite. Below is a discussion of these methods:

- **Torque Magnetometry:** To measure anisotropy by method of torque magnetometry, a fine elastic string between the poles of a rotatable electromagnet suspends the sample. When a magnetic field is applied, the

sample supported by a frictionless bearing, rotates to align its internal magnetisation with the applied magnetic field between the poles of the electromagnet. Subsequently, as the magnet is rotated, the torque exerted by the sample, which can be measured by the angle of twist of the elastic string, can be profiled against the crystallographic direction of magnetisation. The measurement of torque versus magnetisation direction can then be used to calculated magnetic anisotropy energy. Although very accurate, torque magnetometry was ruled out because it is not suitable for polycrystalline samples (Chikazumi, 1997).

- **Ferromagnetic resonance:** The ferromagnetic resonance frequency depends on the external applied magnetic field, which exerts a torque on a precessing spin system. Since the internal anisotropy field also exerts a torque on the internal spin system, the resonance frequency depends on the direction of spin system with respect to the easy axis directions. This underlying principle is used to calculate magnetic anisotropy from ferromagnetic resonance method. However, since the measurements needed to be performed on bulk samples, using ferromagnetic resonance to determine magnetocrystalline anisotropy was ruled out because it measures local anisotropies and not bulk (Chikazumi, 1997).

- **Calculating Anisotropy energy using M-H curve:** Anisotropy energy per unit volume can be calculated as shown in Figure 3-4. The associated formulation for work done, which is equal to the anisotropy energy per unit volume is (Cullity & Graham, 2009):

Equation 3-1 $W = \int_0^M \mu_0 H dM$,

where W is the work done in Jm^{-3}. However, the demagnetisation correction can significantly alter the regions of the curve that give a dominant contribution to the area calculation in this method. A demagnetisation correction can be done in the following manner:

Equation 3-2 $H_{internal} = H_{measured} - N_d M_{measured}$

where N_d is the demagnetisation factor.

However, since the samples used in the experiment were of small dimensions, an estimation of the demagnetisation correction factors could not be done very accurately. An illustration of how significantly demagnetisation correction can change the region of the M-H curve used in anisotropy calculations, using this method, is given in Figure 3-5.

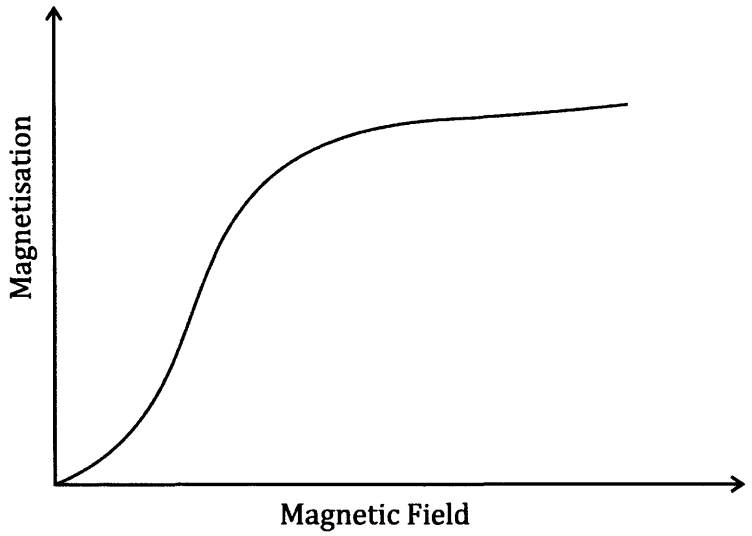

Figure 3-4 The area under the M-H curve, integrated with respect to the magnetisation axis gives the anisotropy energy per unit volume. The work done can be calculated as described in **Equation 3-**.

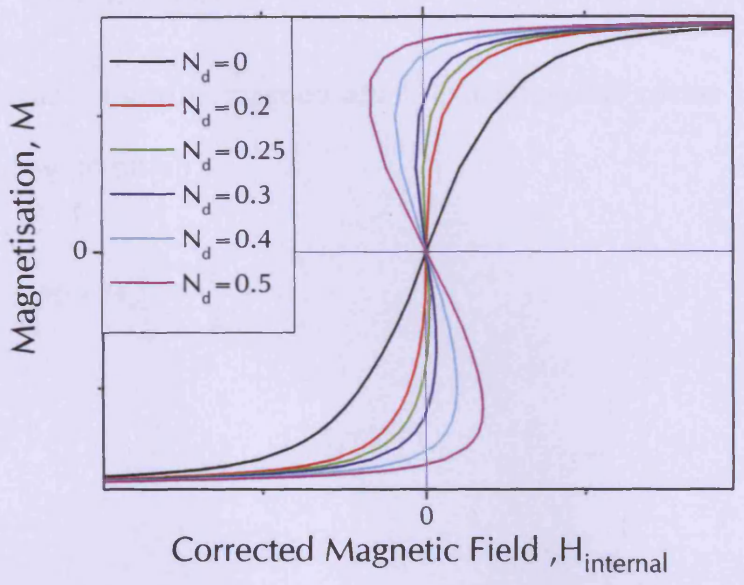

Figure 3-5 Calculation of the corrected magnetic field done as according to **Equation 3-**. Different demagnetisation factors N_d lead to different shapes of the curve and would thus lead to different values of the anisotropy energy calculated by integrating the curve with respect to the Magnetisation axis. Inaccurate estimation of N_d can lead to large errors in the anisotropy calculations in this method.

Another method that circumvents the issues encountered by the methods described above is described in the next section.

3.05.1 Law of Approach to Saturation (LAS)

In the high field regions of the magnetisation curve, nearly all the moments are saturated and aligned to a direction close to the applied magnetic field. A change of the field in this region does not result in any domain displacement processes. The dominant process in this region is the rotation of the domain magnetisations against local anisotropy towards the direction of the applied field. If the angle between magnetisation and direction of the field is θ, then the component of magnetisation in direction of the field can be written as:

Equation 3-3 $M = M_s \cos(\theta)$

where M_s is the saturation magnetisation. Expanding the cosine term, we can express the magnetisation as:

Equation 3-4 $M = M_s\left(1 - \frac{\theta^2}{2} + \cdots\right)$.

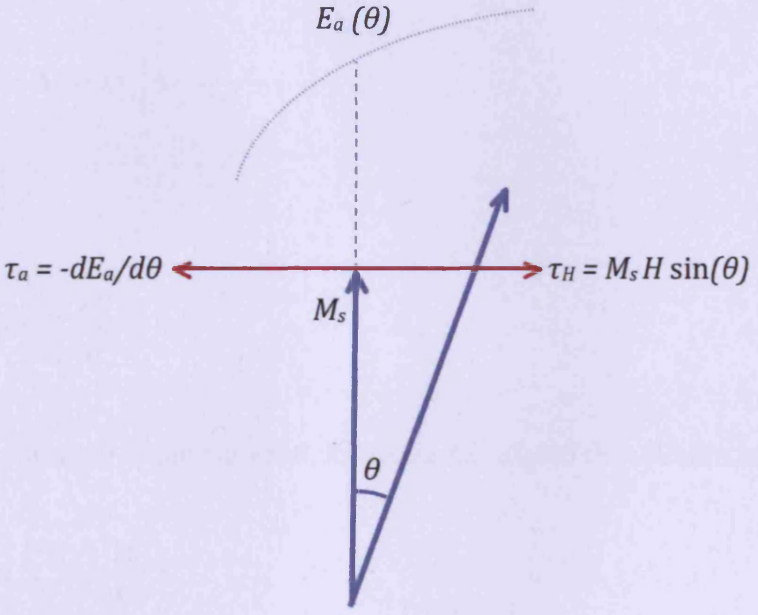

Figure 3-6 Rotation of the magnetisation against the magnetic anisotropy. The rotational torques caused by anisotropy and applied field are shown as τ_a and τ_H respectively (Chikazumi, 1997).

Figure 3-6 shows the two counterbalancing rotational torques exerted on the magnetisation vector by the applied field and the anisotropy. For counterbalancing torques we know that (Chikazumi, 1997):

Equation 3-5 $M_s H \sin\theta = -\frac{dE_a}{d\theta}$.

For small values of θ, $\sin\theta = \theta$. Therefore,

Equation 3-6 $$\theta = -\frac{(dE_a / d\theta)_{\theta \to 0}}{M_s H} = \frac{C}{M_s}\frac{1}{H},$$

where

Equation 3-7 $$C = -\frac{\partial E_a}{\partial \theta}_{\theta \to 0}.$$

Substituting Equation 3- in Equation 3-, we have:

Equation 3-8 $$M = M_s\left(1 - \frac{b}{H^2} - \cdots\right)$$

where

Equation 3-9 $$b = \frac{1}{2}\frac{C^2}{M_s^2}.$$

For a polycrystalline cubic material, it can be calculated that (Chikazumi, 1997):

Equation 3-10 $$\overline{C^2} = \frac{16}{105}K_1,$$

where $\overline{C^2}$ is the average value of C^2 for a polycrystalline cubic material and K_1 is the first order cubic anisotropy coefficient. Therefore, we obtain:

Equation 3-11
$$b = \frac{8}{105}\frac{K_1^2}{M_s^2}$$
$$\Rightarrow K_1 = \sqrt{\frac{105}{8}}bM_s.$$

A description of magnetisation processes in the approach to saturation at high fields is:

Equation 3-12 $$M = M_s\left(1-\frac{a}{H}-\frac{b}{H^2}+\cdots\right)+\kappa H,$$

where the term a/H describes the pinning term which is not very dominant at high field values, b/H^2 term describes the effect of anisotropy, and κ is the forced magnetisation constant which described the linear increase of magnetisation at very high fields. Equation 3- describes the Law of Approach to Saturation (LAS).

3.05.2 Calculation of Anisotropy using Law of Approach to Saturation

The Law of Approach to Saturation (LAS) can be used in conjunction with the measured M-H loops to calculate the anisotropy constants in polycrystalline cubic materials. M-H curve data was obtained using the procedure described in Section 3.04. The measurements were made at 10 K, 50 K, 100 K, 150 K, ..., 400 K.

It was assumed that, after the closing of the loop at high fields, all irreversible magnetisation processes were complete. The high field regions then represent the processes of rotation against anisotropy, and at higher temperatures, also forced magnetisation. According to the LAS, the effect of these processes on magnetisation, for $H >> H_c$, can be modelled as:

Equation 3-13 $$M = M_s\left(1-\frac{b}{H^2}\right)+\kappa H.$$

The above equation ignores the pinning term because the irreversible processes are assumed to be absent at these field values, as described earlier. Data from the high field regions of the M-H curve can be fitted to the LA equation (Equation 3-)

to calculate M_s, b, & κ. These parameters can then be used to determine the first order cubic anisotropy coefficient K_1 for randomly oriented polycrystalline materials using Equation 3-.

High field regions were defined as shown in Table 3-3. Two different high field regions were defined in different temperature ranges because of different values of anisotropy at different temperatures. At lower temperatures, the anisotropy of cobalt ferrite based materials was high, thereby preventing the rotational processes at the applied magnetic fields levels below 2.5 T and thus preventing the complete approach to saturation. Similar fitting criteria has also been used in the past for estimation of the anisotropy constants in cobalt ferrite based materials (Melikhov *et al.*, 2006b, Melikhov *et al.*, 2006a).

Table 3-3 Definition of high field region used for anisotropy calculations using the Law of Approach to Saturation. The maximum field in all cases was $\mu_0 H \leq 5$ T.

Temperature Range	High field Region
Above 150 K	$\mu_0 H \geq 1$ T
150 K and below	$\mu_0 H \geq 2.5$ T

The magnetisation vs magnetic field data for these high field regions was obtained by averaging the four high field regions in the major loop. The fitting was done using Levenberg-Marquardt Algorithm for non-linear curve fitting (Origin Labs, 2010). An example of fitting is shown in Figure 3-7.

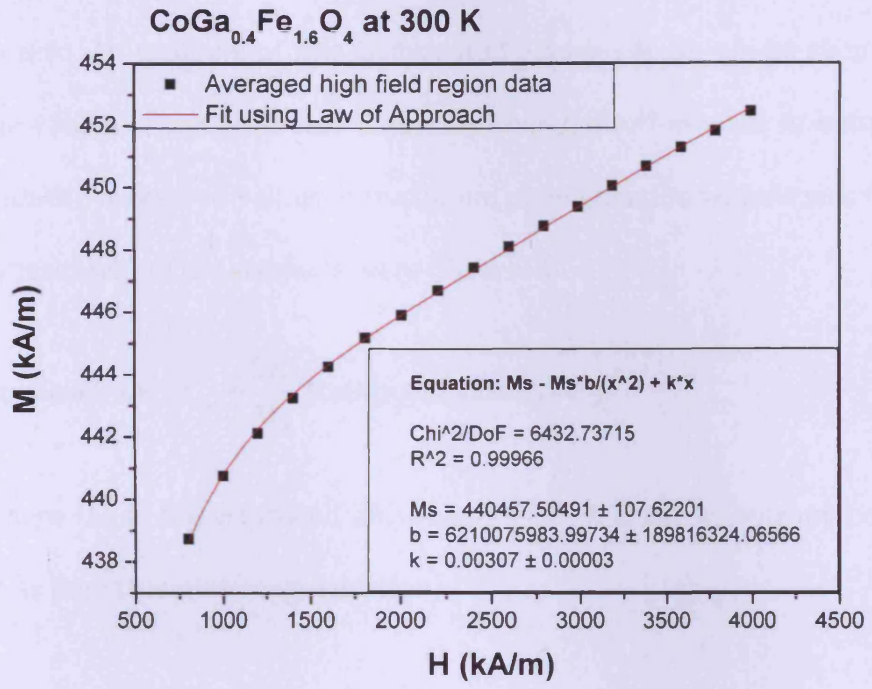

Figure 3-7 An example of fitting high field regions of M-H data to the Law of Approach using the Levenberg-Marquardt Algorithm.

For certain samples, at low temperatures, it was found that the calculated value of the forced magnetisation constant κ, increased with decreasing temperature, which was an artefact (Melikhov et al., 2006a, Melikhov et al., 2006b). In such cases, the estimated anisotropy field calculated using Equation 3- was higher than the maximum applied magnetic field of $\mu_0 H = 5$ T. This indicated that the anisotropy field dominated over forced magnetisation in these cases. The forced magnetisation constant κ was assumed to be negligible in these cases and experimental data was refitted to the Law of Approach with $\kappa = 0$. M_s and b were the only fitting parameters in these cases. The values of the saturation magnetisation calculated after forcing κ to zero in places where the artefact was observed were in better agreement with the measured values of the maximum

magnetisation (at $\mu_0 H$ = 5 T), in comparison to values obtained without forcing κ to zero. An example of this is shown in Figure 3-8. As can be seen in the figure, the values of the predicted saturation magnetisation were in better agreement with the measured values of maximum magnetisation when κ was forced to zero in cases where the artefacts were observed.

Equation 3-14 $H_{an} = \frac{2K}{M_s}$ **(Cullity & Graham, 2009),**

where H_{an} is the estimated anisotropy field, K is the anisotropy coefficient, and M_S is the saturation magnetisation.

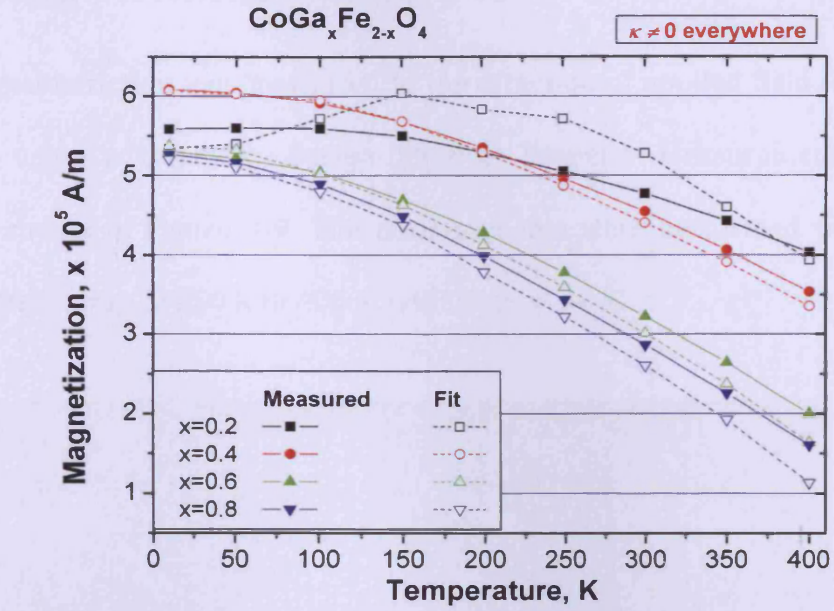

(a)

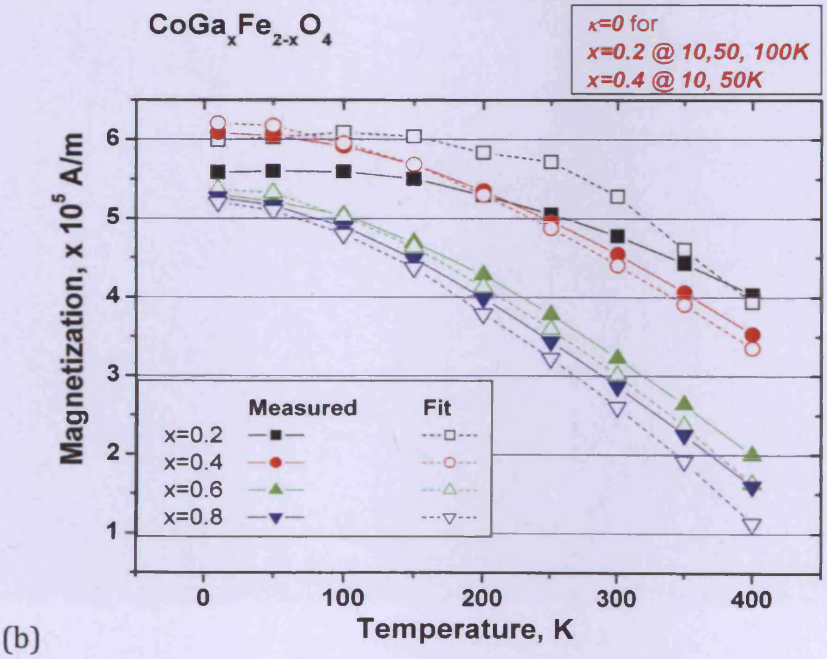

(b)

Figure 3-8 Comparison of values of saturation magnetisation obtained after fitting high field region data of *M-H* curves to the Law of Approach to Saturation with the purpose of obtaining values of the anisotropy coefficients at different temperatures with two methods: (a) $\kappa = 0$ in cases where its values increased with decreasing temperatures, (b) $\kappa \neq 0$ even in cases where its value increased with decreasing temperature.

3.06 Magnetostriction Measurement

The magnetostriction was measured in the direction of applied field for all the samples using a Quantum Design Physical Property Measurement System (PPMS), shown in Figure 3-9. The measurements were performed within the temperature range of 250 K to 400 K, with steps of 50 K.

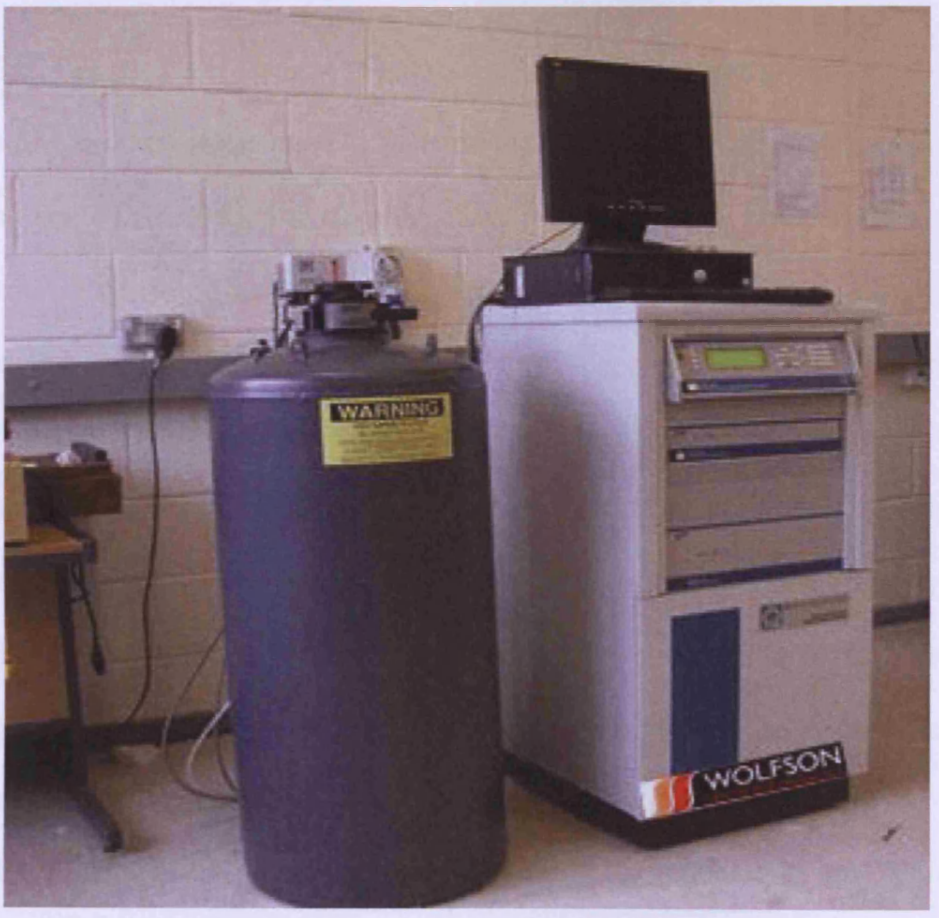

Figure 3-9 The Physical Property Measurement System (PPMS) used to make magnetostriction measurements.

The samples were cut from cylindrical bulk material with 1 cm diameter and height in the range of 0.5 – 1.5 cm. The samples were cut using a diamond saw,

rotating at 80 RPM. As the samples were ceramic, a low RPM needed to be maintained in order to prevent the occurrence and propagation of cracks. It was observed that cracks can introduce significant errors in the magnetostriction measurements and hence only samples without cracks were used for the measurements.

3.06.1 Strain gauge setup

The magnetostriction was measured by mounting strain gauges on the sample and measuring the change in resistance of the strain gauge on application of the magnetic field. Since the measurement was done in the presence of a magnetic field, a non-inductive strain gauge was acquired from Vishay Micro-measurements. The WK-06-031 CF-350 strain gauge was chosen from the Vishay Catalogue because of its temperature range of 4 – 565 K, which covered the temperature range of the measurement. The strain gauge was bonded to the sample using M-Bond 610 adhesive, also acquired from Vishay Micro-measurements. The adhesive was also chosen to ensure reliable experimentation throughout the range of temperatures within which the experiments were conducted. Operating over a range of temperatures, there was a need to eliminate the possibility of thermal expansion dominating the strain gauge output. The chosen strain gauge was made of K-alloy, which has self-temperature-compensation (Vishay Mircomeasurements, 2007).

3.06.2 Wheatstone-Bridge configuration

A half Wheatstone bridge configuration was used to ensure the accuracy of the measurements. A schematic diagram of the bridge is given in Figure 3-10. A

350 Ω strain gauge, described in Section 3.06.1, was bonded to the sample. A similar strain gauge was mounted on a dummy sample made of copper that does not experience any magnetostriction. The bridge resistors R_1 and R_2 were also of the same value as the strain gauge resistance – 350 Ω. Using the setup provided in PPMS, the bridge was powered using a constant current source.

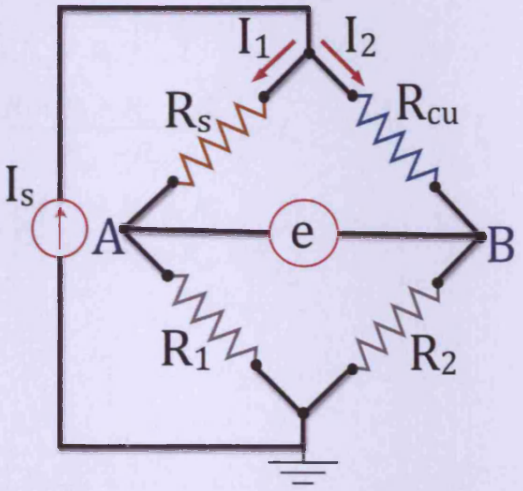

Figure 3-10 A schematic diagram of the Wheatstone bridge used to measure magnetostriction. R_s is the resistance of the strain gauge on the sample, R_{cu} is the resistance of the strain gauge on the dummy sample made of copper R_1 and R_2 are the bridge resistors which complete the bridge. I_s is the current source, I_1 and I_2 are the currents in the branches R_s-R_1 and R_{cu}-R_2 respectively, and e is the voltage measured between the two legs of the strain gauge bridge.

Because there was no current flow in the branch A-B, as shown in Figure 3-10, branches R_s-R_1 and R_{cu}-R_2 can be considered to be in parallel. Since the voltage across R_s-R_1 and R_{cu}-R_2 has to be same, the relation between branch currents I_1 and I_2 can be described as:

Equation 3-15 $I_1(R_s + R_1) = I_2(R_{cu} + R_2)$

The sum of branch currents is equal to the source current. Therefore,

Equation 3-16 $I_1 + I_2 = I_s$.

From the above two equations, we have:

$$I_1 + I_1\left(\frac{R_s + R_1}{R_{cu} + R_2}\right) = I_s$$

Equation 3-17
$$\Rightarrow I_1\left(\frac{R_s + R_1 + R_{cu} + R_2}{R_{cu} + R_2}\right) = I_s$$

$$\Rightarrow I_1 = I_s\left(\frac{R_{cu} + R_2}{R_s + R_1 + R_{cu} + R_2}\right)$$

and similarly

Equation 3-18 $I_2 = I_s\left(\frac{R_s + R_1}{R_s + R_1 + R_{cu} + R_2}\right)$.

Voltages at nodes A and B can be written as:

Equation 3-19
$$V_A = I_1 R_1$$
$$= I_s\left(\frac{R_{cu} + R_2}{R_s + R_1 + R_{cu} + R_2}\right)R_1$$

and

Equation 3-20
$$V_B = I_2 R_2$$
$$= I_s\left(\frac{R_s + R_1}{R_s + R_1 + R_{cu} + R_2}\right)R_2.$$

Therefore, the bridge voltage *e*, which is the voltage between the nodes A and B, can be written as:

$$
\begin{aligned}
e &= V_B - V_A \\
&= I_s\left(\frac{R_s + R_1}{R_s + R_1 + R_{cu} + R_2}\right)R_2 - I_s\left(\frac{R_{cu} + R_2}{R_s + R_1 + R_{cu} + R_2}\right)R_1 \\
&= I_s\frac{R_2(R_s + R_1) - R_1(R_{cu} + R_2)}{R_s + R_1 + R_{cu} + R_2} \\
&= I_s\frac{R_2R_s - R_1R_{cu} + R_2R_1 - R_1R_2}{R_s + R_1 + R_{cu} + R_2} \\
&= I_s\frac{R_2R_s - R_1R_{cu}}{R_s + R_1 + R_{cu} + R_2}
\end{aligned}
$$

Equation 3-21

The resistance of the precision resistors R_1 and R_2, which complete the bridge from outside the PPMS, were not affected by the temperature and magnetic field conditions at which the measurements were made. Therefore, the resistance of these two resistors can be described as:

$$R_1 = R + \Delta R_1 \quad \text{and} \quad R_2 = R + \Delta R_2$$

Equation 3-22

where $R = 350\,\Omega$ and ΔR_1 and ΔR_2 are constants dependent on the ambient temperature.

The resistance of the strain gauge on the sample will change with temperature inside the sample chamber of PPMS and with the applied magnetic field. Therefore,

$$R_s = R + \Delta R_\lambda + \Delta R_{T,s},$$

Equation 3-23

where ΔR_λ and $\Delta R_{T,s}$ are change in resistance of the strain gauge caused by the magnetostriction of the sample and the thermal expansion of the sample because of the temperature inside the PPMS's sample chamber.

The resistance of the strain gauge on the copper dummy sample can similarly be described as:

Equation 3-24 $R_{cu} = R + \Delta R_{T,cu}$.

The bridge voltage can then be written as:

Equation 3-25 $$e = I_s \frac{(R+\Delta R_2)(R+\Delta R_\lambda + \Delta R_{T,s}) - (R+\Delta R_1)(R+\Delta R_{T,cu})}{4R + \Delta R_1 + \Delta R_2 + \Delta R_\lambda + \Delta R_{T,s} + \Delta R_{T,cu}}$$

Expanding the numerator we have

Equation 3-26
$$\begin{aligned} \text{Numerator} &= R^2 + R(\Delta R_\lambda + \Delta R_{T,s} + \Delta R_2) + (\Delta R_2 \Delta R_\lambda + \Delta R_2 \Delta R_{T,s}) - \\ &\quad R^2 - R(\Delta R_{T,cu} + \Delta R_1) - (\Delta R_1 \Delta R_{T,cu}) \\ &= R(\Delta R_\lambda + \Delta R_{T,s} + \Delta R_2 - \Delta R_{T,cu} - \Delta R_1) + \\ &\quad (\Delta R_2 \Delta R_\lambda + \Delta R_2 \Delta R_{T,s} - \Delta R_1 \Delta R_{T,cu}) \end{aligned}$$

Since all the $\Delta R_x << 1$, the $\Delta R_x \Delta R_y$ terms (ΔR_x and ΔR_y are representative of a generalised ΔR in the above equation) are smaller than the rest of the numerator by several orders of magnitude. Similarly, the ΔR_x terms in the denominator of Equation 3- are much smaller than the R term. Ignoring these terms we get

Equation 3-27
$$\begin{aligned} e &= I_s \frac{R(\Delta R_\lambda + \Delta R_{T,s} + \Delta R_2 - \Delta R_{T,cu} - \Delta R_1)}{4R} \\ &= I_s \frac{(\Delta R_\lambda + \Delta R_{T,s} + \Delta R_2 - \Delta R_{T,cu} - \Delta R_1)}{4} \end{aligned}$$

Since, during the measurement of any magnetostriction curve, the temperature was constant, only ΔR_λ changes with applied magnetic field and all the other terms in Equation 3- introduce a temperature dependent offset. Since, offsets were removed from all the magnetostriction curves, as described in the next section, the magnetic field dependence of e can be described as:

Equation 3-28 $$e = I_s \frac{\Delta R_\lambda}{4}.$$

3.06.3 PPMS configuration

The samples and the dummy copper samples with the strain gauge were mounted onto PPMS pucks supplied by Quantum Design. The connections of the sample onto the puck were made as shown in Figure 3-11. A photographic representation of the entire assembly is shown in Figure 3-12. The current shown in Figure 3-10 was sourced from the PPMS. The measurement parameters used to configure the PPMS are given in Table 3-4.

Table 3-4 Bridge setup for measurement of magnetostriction using a channel on the puck.

Bridge Parameters	Value
Source Current (I_s)	1000 μA
Maximum Voltage	90 mV
Maximum Power	1000 μW

Since the PPMS was designed to measure magnetoresistance, its output is a resistance which is related to the Wheatstone bridge parameters as

Equation 3-29 $$R_{PPMS} = \frac{e}{I_s},$$

where R_{PPMS} is the resistance output of the PPMS. Given Equation 3- and Equation 3-, it can be said that:

Equation 3-30 $\Delta R_{\lambda} = 4R_{\text{PPMS}}$.

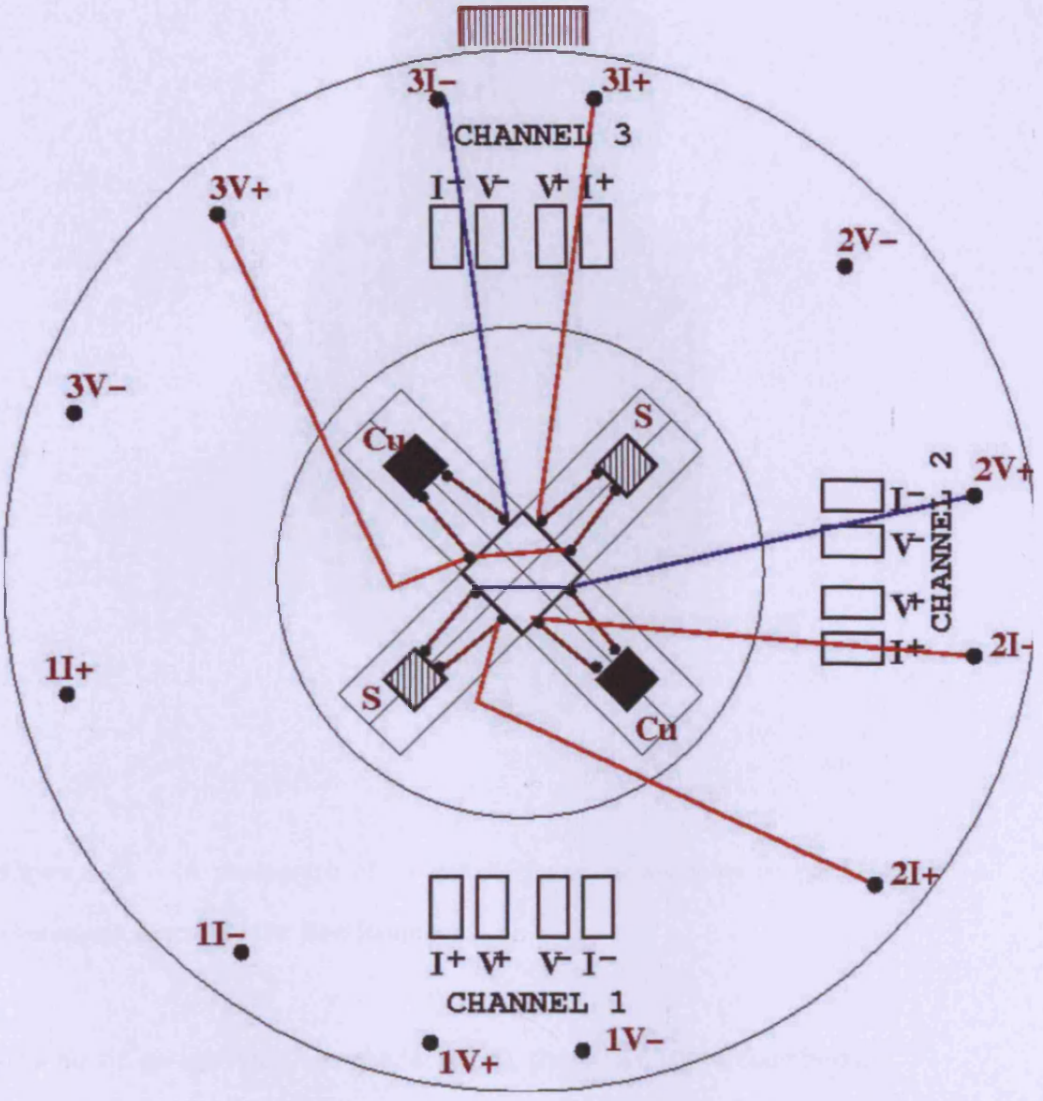

Figure 3-11 The layout of electrical connections of the measurement sample and the dummy sample strain gauges to the PPMS puck. The setup was designed to perform experiments on two samples at the same time. One sample and its accompanying copper dummy sample were connected to the precision resistors outside through connections on Channel-2. Channel-3 was used to measure the magnetostriction on the other sample.

Figure 3-12 A photograph of the sample mounting assembly on the PPMS puck. Photograph courtesy of Dr. Ravi Hadimani.

For a strain gauge with a gauge factor F_G, the strain was described as

Equation 3-31 $$\varepsilon = \frac{\Delta R}{R}\frac{1}{F_G},$$

where ε is the strain developed in the strain gauge. Therefore, in terms of the PPMS output,

Equation 3-32 $$\lambda = \varepsilon = \frac{4R_{\text{PPMS}}}{R}\frac{1}{F_G},$$

where λ is the magnetostrictive strain caused by the applied field.

As mentioned in Section 3.06.2, the magnetostrictive strain measured had offsets because of temperature dependent effects. An example of such a strain is shown in Figure 3-13.

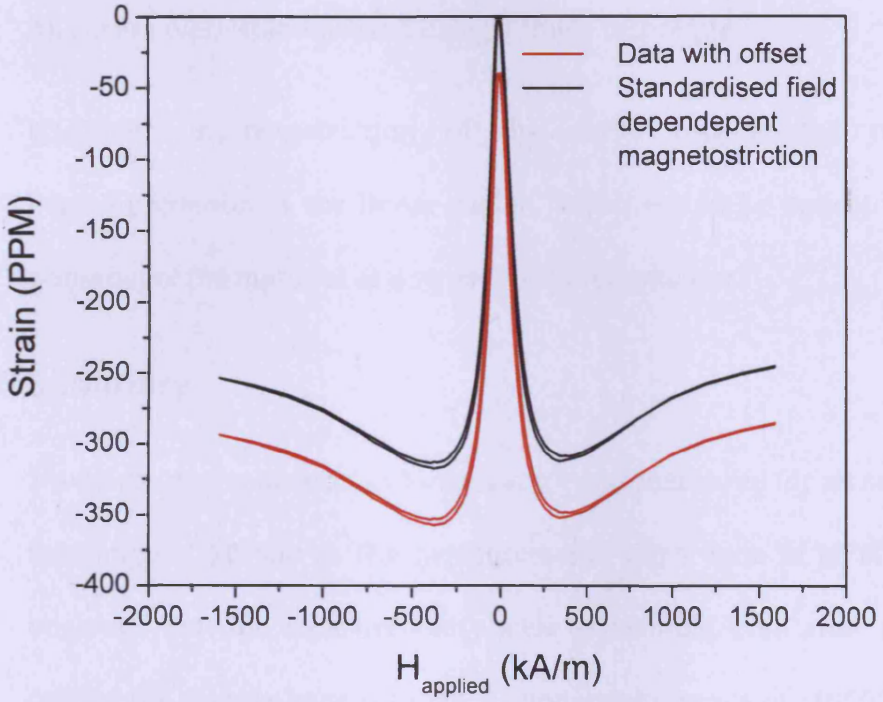

Figure 3-13 An example of the offset in measured magnetostriction data which was removed to standardise the magnetostriction curves.

Since the temperature was constant during any one measurement, all these temperature dependent effects were eliminated by defining the zero magnetostriction as follows:

- If the slope of the magnetostriction is negative, then the curve is shifted such that the whole λ-H curve lies in the region $\lambda \in [0, -\infty)$, thus fixing the top most point of the curve as $\lambda = 0$.

- If the slope of the magnetostriction is positive, then the curve is shifted such that the whole λ-H curve lies in the region $\lambda \in [0, \infty)$, thus fixing the lowest point of the curve as $\lambda = 0$.

Defining zero magnetostriction in this way served two purposes:

- All curves were standardised using a single technique
- Maximum magnetostriction of the curve became the maximum magnetostriction in the linear region, which would be indicative of the potential of the material as a stress sensor or actuator.

3.07 Summary

- Maximum magnetisation vs temperature was measured for all samples in the range of 10-400 K. The measurements were done in MPMS. It was observed that the measurements were repeatable even after a year of cycling the sample once through a temperature range of 10-400 K and a field range of $\mu_0 H$ = [-5 T, 5 T]. This indicated that the magnetic properties of the samples do not change significantly over time if subjected to temperatures below 400 K and magnetic fields below 5 T.
- Magnetisation loops were measured at 9 temperatures between 10-400 K within the field range of $\mu_0 H$ = [-5 T, 5 T]. The measured hysteresis loops were then analysed to determine the temperature variation of coercivity and anisotropy.
- Magnetostriction was measured using a strain gauge setup inside a Quantum Design PPMS equipment. Additional hardware was designed

and built by this researcher to enable PPMS in making magnetostriction measurements.

- The results of the experiments described in this chapter are discussed in the following chapter. A careful choice of experimental methodology has been instrumental to obtaining reliable scientific data used to analyse the effect of chemical substitution on properties of cobalt ferrite over a range of temperatures.

3.08 Bibliography

Bozorth, RM, Tilden, EF, Williams, AJ. 1955. Anisotropy and Magnetostriction of Some Ferrites. *Phys. Rev.* **99:** 1788--1798.

Chikazumi, S 1997. *Physics of Ferromagnetism* Great Clarendon Street, Oxford, OX2 6DP: Oxford University Press.

Cullity, BD, Graham, CD 2009. *Introduction to Magnetic Materials*: John Willey & Sons.

Melikhov, Y, Snyder, JE, Jiles, DC, Ring, AP, Paulsen, JA, Lo, CCH, Dennis, KW. 2006a. Temperature dependence of magnetic anisotropy in Mn-substituted cobalt ferrite. *JOURNAL OF APPLIED PHYSICS* **99:** 08R102.

Melikhov, Y, Snyder, JE, Lo, CCH, Matlage, PN, Song, SH, Dennis, KW, Jiles, DC. 2006b. The Effect of Cr-Substitution on the Magnetic Anisotropy and Its Temperature Dependence in Cr-Substituted Cobalt Ferrite. *Magnetics, IEEE Transactions on* **42:** 2861-2863.

Origin Labs. 2010. Nonlinear Curve Fitting Using Levenberg-Marquardt Algorithm (http://www.originlab.com/index.aspx?go=Products/Origin/DataAnalysis/CurveFitting/NonlinearFitting&pid=1189)

Quantum Design. 2010. Quantum Design, Inc. - Products - Magnetic Property Measurement System MPMS® - MPMS-XL - MPMS EverCool (http://www.qdusa.com/products/mpms.html)

Song, SH. 2007. Magnetic and magnetoelastic properties of M-substituted cobalt ferrites (M=Mn, Cr, Ga, Ge). Iowa State University, Ames, Iowa.

Vishay Micromeasurements. 2007. Strain Gauge Selection: Criteria Procedures, Recommendations. *Tech Note TN-505-4.* Vishay Micro Measurements.

Chapter 4. Effect of Chemical Substitution on Properties of Cobalt Ferrite

4.01 Introduction

As discussed in Chapter 2, cobalt ferrite has emerged as a candidate material for magnetostrictive stress/torque sensor and actuator applications (Paulsen *et al.*, 2003, Paulsen *et al.*, 2005, Lo *et al.*, 2006, Melikhov *et al.*, 2006a, Melikhov *et al.*, 2006b, Song *et al.*, 2007, Lee *et al.*, 2007, Chen *et al.*, 1999, Chen & Jiles, 2000, Chen *et al.*, 2000, Chen *et al.*, 2001). It has also been observed that the magnetoelastic properties of cobalt ferrite can be improved by chemical substitution. As discussed earlier, the previously studied substitutions of manganese and chromium had a B-site preference and although they led to an increase in strain derivative, the maximum magnetostriction decreased in all cases.

This chapter deals with the investigation of chemical substitution to improve the properties of cobalt ferrite.

In the current study, three different substitutions in cobalt ferrite ($CoFe_2O_4$) were studied:

- **Gallium Substitution:** Substitution of some of Fe^{3+} by Ga^{3+} ions. The resulting stoichiometry is $CoGa_xFe_{2-x}O_4$.

- **Germanium Substitution:** Co-substitution of some pairs of Fe^{3+}-Fe^{3+} ions by Co^{2+}/Ge^{4+} pairs. The resulting stoichiometry is $Co_{1+x}Ge_xFe_{2-2x}O_4$.

- **Aluminium Substitution:** Substitution of some of Fe^{3+} by Al^{3+} ions. The resulting stoichiometry is $CoAl_xFe_{2-x}O_4$.

The substitutions were undertaken with these aims:

- Replacing A-site Fe^{3+} ions with non-magnetic or less magnetic ions, such that the net moment per formula unit increases.

- Displacing Co^{2+} ions to B-sites to achieve higher magnetostriction.

- Increasing the strain derivative by reducing the anisotropy

4.02 Gallium Substitution

A series of gallium-substituted samples of cobalt ferrite was made using standard powder ceramic techniques, described in Chapter 2, by Song of Iowa State University. Samples with composition $CoGa_xFe_{2-x}O_4$ were made with x=0, 0.2, 0.4, 0.6, & 0.8. The actual compositions of the samples were determined by Song using Energy Dispersive X-ray Spectroscopy (EDS), and are show in Table 4-1. The actual compositions were found to be close to the target compositions.

Data for pure cobalt ferrite ($CoGa_xFe_{2-x}O_4$) were obtained from Song (Song, 2007).

Table 4-1 Comparison of actual and target composition for $CoGa_xFe_{2-x}O_4$ (Song, 2007).

Target Composition	Composition determined by EDS		
	Co	Fe	Ga
$CoFe_2O_4$	0.95	2.05	—
$CoGa_{0.2}Fe_{1.8}O_4$	1.00	1.81	0.19
$CoGa_{0.4}Fe_{1.6}O_4$	1.04	1.55	0.41
$CoGa_{0.6}Fe_{1.4}O_4$	0.98	1.33	0.69
$CoGa_{0.8}Fe_{1.2}O_4$	1.04	1.15	0.81

4.02.1 Site Preference of Gallium

Several studies have investigated the site preference of Ga^{3+} ions in the cubic spinel lattice. $Ga_xFe_{1-x}NiCrO_4$ prepared by ceramic methods was tested for site preference of the various ions (Kulkarni & et al., 1985) and it was concluded that Ga^{3+} ions have an A-site (tetrahedral) preference. Investigation of the crystal structure of $MgAl_{2-x}Ga_xO_4$ also mentions an A-site preference for Ga^{3+} ions (Ito *et al.*, 2000). The site preference of gallium cations in $MnGa_xFe_{2-x}O_4$ was determined by Mössbauer measurements in the presence of a magnetic field at low temperatures (Mahmoud *et al.*, 2001). It was found that Ga^{3+} has an A-site preference and distributes randomly in A-sites. $MnFe_2O_4$ was found to be in a state of partial inversion, where 20% of Fe^{3+} occupies A-sites. It was found that Ga^{3+} substitutes for Fe^{3+} in A-sites leading to a lowering of the A-site absorption peaks.

However, these studies did not establish the strength of the Ga^{3+} ion's A-site preference in cobalt ferrite. Investigation of site preference of ions in $CoGa_xFe_{2-x}O_4$ ($x = 0$, 0.2, 0.4, 0.6, & 0.8) was performed with the help of

Mössbauer measurements (Krieble et al., 2008). Two different hyperfine sextets indicated the presence of two different kinds of Fe^{3+} ions in two different lattice locations, in A-sites and B-sites. This confirmed a mixed spinel structure for gallium substituted cobalt ferrite. Line spacing, which is indicative of magnetic hyperfine field at Fe^{3+} nuclei and is related to the exchange coupling, was observed to reduce with increased gallium substitution. The strength of the hyperfine field was seen to reduce faster for B-sites than for A-sites with increased gallium substitution, as is visible in Figure 4-1. The distribution width of the hyperfine field increased faster for B-sites in comparison to A-sites with increasing gallium substitution (shown in Figure 4-2). Both these phenomena were more prominent for Ga^{3+} substitution in comparison to those of Mn^{3+} and Cr^{3+} substitution. It was concluded that for lower amounts of substitution ($x = 0.2$ & 0.4), Ga^{3+} substitutes into A-sites, which results in a reduction of the B-site hyperfine field and an increase in distribution width of B-sites. This happens because B-site Fe^{3+} ions are superexchange coupled to A-site ions and the introduction of Ga^{3+} in A-sites leads to the magnetic dilution of the A-sites.

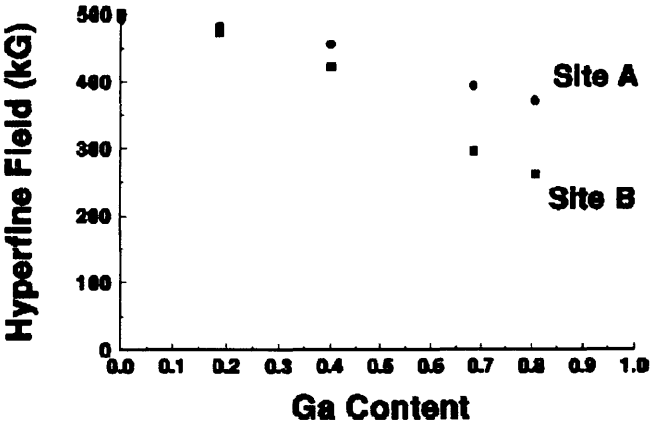

Figure 4-1 Variation of the strength of the hyperfine field as a function of the Ga content (x) in $CoGa_xFe_{2-x}O_4$ (Krieble et al., 2008).

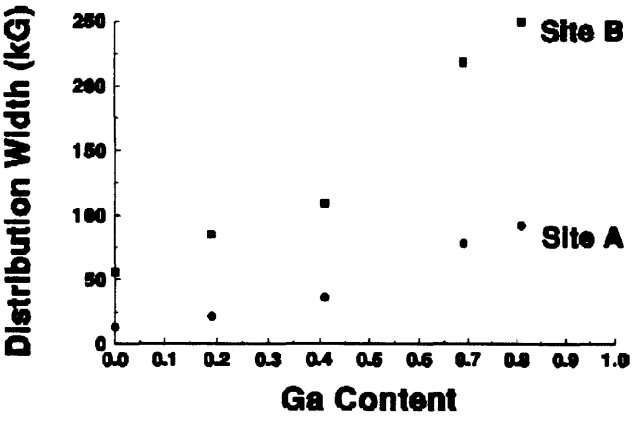

Figure 4-2 Variation of the distribution width with gallium content (x) in $CoGa_xFe_{2-x}O_4$ (Krieble *et al.*, 2008).

4.02.2 Curie temperature of gallium substituted cobalt ferrite

The Curie temperature (T_c) for gallium substituted cobalt ferrite, measured by Song, was observed to decrease with increased gallium content as had been noticed with other cations also (Song et al., 2007). The Curie temperature was measured by taking the samples from paramagnetic state (above their Curie

temperature), to a ferromagnetic state (below the Curie temperature) in presence of a low field (8000 A/m). Gallium substitution caused magnetic dilution and reduces the super exchange interaction, which in turn reduces the Curie temperature. It was observed that Curie temperature reduced linearly with increasing gallium content.

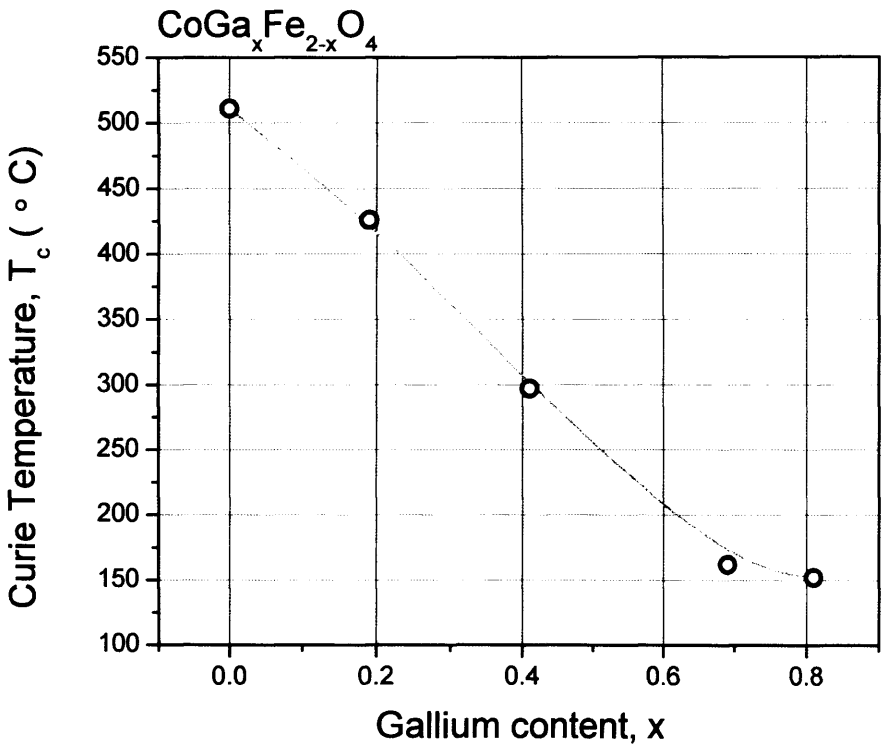

Figure 4-3 Variation of the Curie temperature of gallium-substituted cobalt ferrite (Song et al., 2007). The symbols (data points) show the actual experimental data.

A reduction in Curie temperature is desirable for sensor/actuator application as it indicates lesser hysteresis at any given temperature.

4.02.3 Maximum Magnetisation vs Temperature for gallium substituted cobalt ferrite

The maximum magnetisation (at constant $\mu_0 H = 5$ T) vs temperature was measured for all the samples in the temperature range of 10 K and 400 K. The observed trends are shown in Figure 4-4.

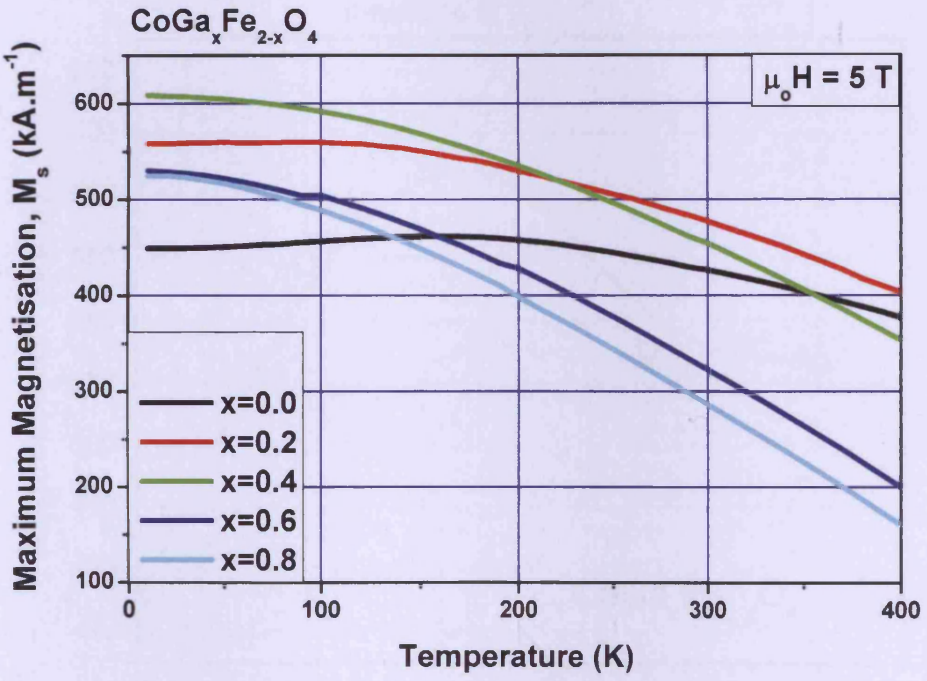

Figure 4-4 Variation of the maximum magnetisation of $CoGa_xFe_{2-x}O_4$ with temperature.

The maximum magnetisation increased monotonically with decreasing temperature for all samples between 400 – 160 K. Below 160 K, it increased slowly with decreasing temperatures for most of the samples. However, it decreased slowly with decreasing temperature for $CoFe_2O_4$ below 160 K and for $CoGa_{0.2}Fe_{1.8}O_4$ below 100 K. This apparent decrease can be explained by the presence of a high anisotropy field at low temperature in these two cases, which

prevented a complete approach to saturation at the maximum applied field of $\mu_0 H$ = 5 T. Evidence supporting high anisotropy fields for these cases can be seen in Figure 4-19. Saturation magnetisation at low temperatures (eg. 10 K), shown in Figure 4-5, is correlated with the net moment of a formula unit of the compound, defined in Equation 2-22.

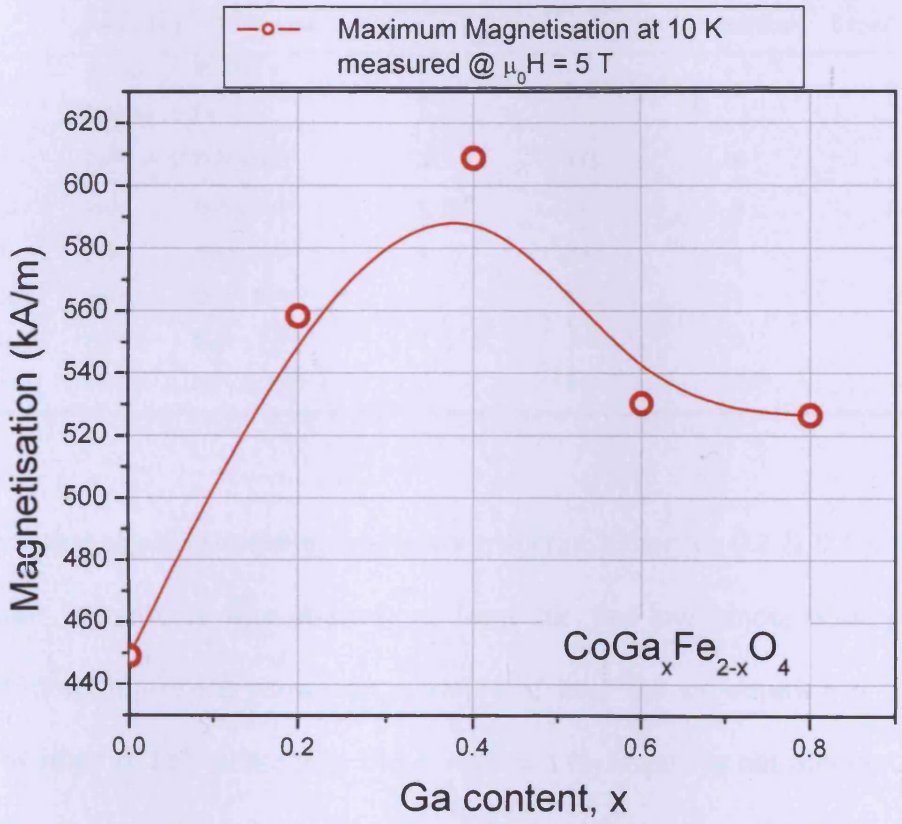

Figure 4-5 Near Zero Kelvin moment of gallium substituted cobalt ferrite.

The net moment per molecule for a ferrite is the subtraction of the A-site moment from the B-site moment because of the anti-parallel coupling of A & B-sites. Table 4-2 shows the calculated net moment of several ferrites at

zero degrees K. The theoretical values given in the table are calculated with an assumption of a certain degree of inversion of the spinel lattice in these ferrites.

Table 4-2 Experimental and theoretical values of saturation magnetisation of simple ferrites with spinel structure in Bohr Magnetons at 0 °K (Smit & Wijn, 1959).

Ferrite	Postulated ion distribution		Magnetic moment of A-site ions	Magnetic moment of B-site ions	Magnetic moment per molecule of $MeFe_2O_4$	
	A-site ions	B-site ions			Theoretical	Experimental
$MnFe_2O_4$	$Fe^{3+}_{0.2}$ + $Mn^{2+}_{0.8}$	$Mn^{2+}_{0.2}$ + $Fe^{3+}_{0.8}$	5	5+5	5	4.6
Fe_3O_4	Fe^{3+}	Fe^{2+}+ Fe^{3+}	5	4+5	4	4.1
$CoFe_2O_4$	Fe^{3+}	Co^{2+}+ Fe^{3+}	5	3+5	3	3.7
$NiFe_2O_4$	Fe^{3+}	Ni^{2+}+ Fe^{3+}	5	2+5	2	2.3
$CuFe_2O_4$	Fe^{3+}	Cu^{2+}+ Fe^{3+}	5	1+5	1	1.3
$MgFe_2O_4$	Fe^{3+}	Mg^{2+}+ Fe^{3+}	5	0+5	0	1.1
$Li_{0.5}Fe_{2.5}O_4$	Fe^{3+}	$Li^{1+}_{0.5}$+ $Fe^{3+}_{1.5}$	5	0+7.5	2.5	2.6

The fact that the maximum magnetisation increases for x = 0.2 & 0.4 indicates that Ga^{3+} substitutes into A-sites, at least for the low amounts of gallium substitution. Figure 4-6 shows an example of how the substitution of Ga^{3+} in place of some of Fe^{3+} present in the A-sites can increase the net moment. Since the net moment per formula unit is a result of net B-site moment minus the net A-site moment. The B-site moment is the bigger moment owing to twice the number of B-sites in comparison to A-sites. Therefore, the substitution of Ga^{3+} (with less magnetic moment contribution) into A-sites in place of Fe^{3+} (with higher magnetic moment contribution), increased the net magnetic moment per formula unit.

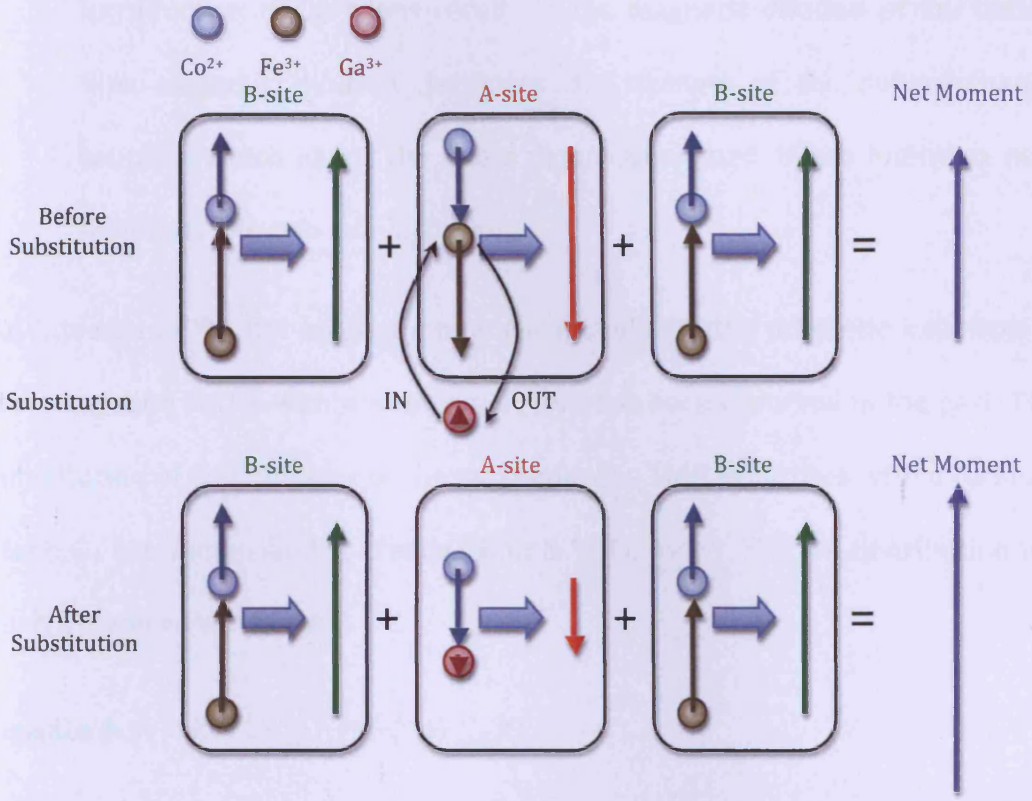

Figure 4-6 An illustration of how the chemical substitution can affect the net moment inside the cobalt ferrite lattice. A-site moments are coupled anti-parallel to the B-site moments. A random allocation of ions in the cobalt ferrite lattice is shown before substitution. As can be seen, Fe^{3+} has the highest moment contribution, followed by Co^{2+}. Ga^{3+} ion has no magnetic moment. The illustration is a simplistic representation of how the substitution of a non-magnetic ion can increase the net moment in an inverse spinel structure where B-sites are twice in number as A-sites.

For samples with higher gallium content though, the maximum magnetisation at near zero Kelvin decreases again with increasing gallium content. This could be because of either of the two following reasons:

- Ga^{3+} ions start substituting into B-sites, reducing the B-site moments, leading to a reduction in the net moment.

- Introduction of Ga^{3+} ions results in the magnetic dilution of the lattice. This magnetic dilution decreases the strength of the superexchange coupling which keeps the B-site moments aligned. B-site moments may then split into two sub-lattices.

An increase in the net magnetic moment on substituting magnetic ions from a ferromagnetic lattice with non-magnetic ions has been observed in the past. The substitution of Zn^{2+} in place of the magnetic ions Me^{2+} in ferrites with a formula $MeFe_2O_4$ has shown similar trends (Smit & Wijn, 1959). The ion distribution for such a material would be:

Equation 4-1 $$\left(Zn_{\delta}^{2+}Fe_{1-\delta}^{3+}\right)_A\left(Me_{1-\delta}^{2+}Fe_{1+\delta}^{3+}\right)O_4$$

An addition of the non-magnetic Zn^{2+} ions in place of the magnetic Me^{2+} ions in A-sites reduced the A-site moment. Therefore addition of Zn^{2+} ions was expected to increase the net moment per molecule. However, the observed behaviour of substituted ferrites was different, as shown in Figure 4-8. Theoretically, the saturation moment for all the materials shown in Figure 4-8 should increase linearly and reach $m_{total} = 10\ \mu_B$ at $\delta = 1$. This theoretical prediction is shown as dashed lines. For small concentration of Zn^{2+}, the linear increase in molecular magnetic moment has been seen to agree with the theoretical prediction. The deviation of the experimental data from the measured data can be explained in terms of a split B-lattice. The substitution of non-magnetic ions in place of magnetic ions in A-sites leads to a weakened B-B coupling. At high levels of substitution, the A-site moments are not able to keep all the B-site moments aligned to each other. This may lead to a splitting of B-lattice as shown in Figure

4-7. The net B-site moment decreases because of this process, which leads to a reduction in the net moment.

It was observed that even at temperatures around 300 K, which would be close to the operating temperatures of any device designed with the material, the maximum magnetisation for compositions x = 0.2 & x = 0.4 was higher than that of pure cobalt ferrite.

It can also be observed that for compositions with higher amount of gallium, which had a lower Curie Temperature (T_c), the maximum magnetisation at room temperature (300 K) changed faster with any change in temperature. This can be attributed to the maximum magnetisation following a Brillouin function close to its Curie Temperature (Cullity & Graham, 2009). The closer the thermodynamic temperature is to the Curie Temperature, the faster the maximum magnetisation falls with small increases in temperature.

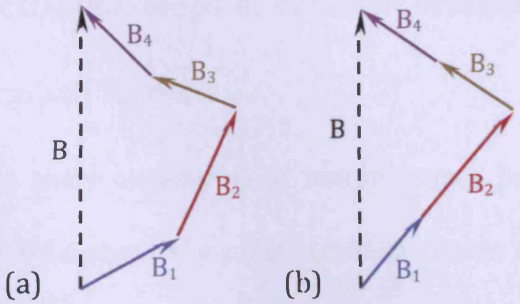

Figure 4-7 Splitting of the B-site lattice on reduction in the A-site moment. (a) B-lattice splits into 4 different sub-lattices. (b) B-lattice splits into pairs of two parallel sub lattices. The net B-site moment is the vector addition of all the B-site moments and is hence smaller than when all the B-site moments are aligned parallel.

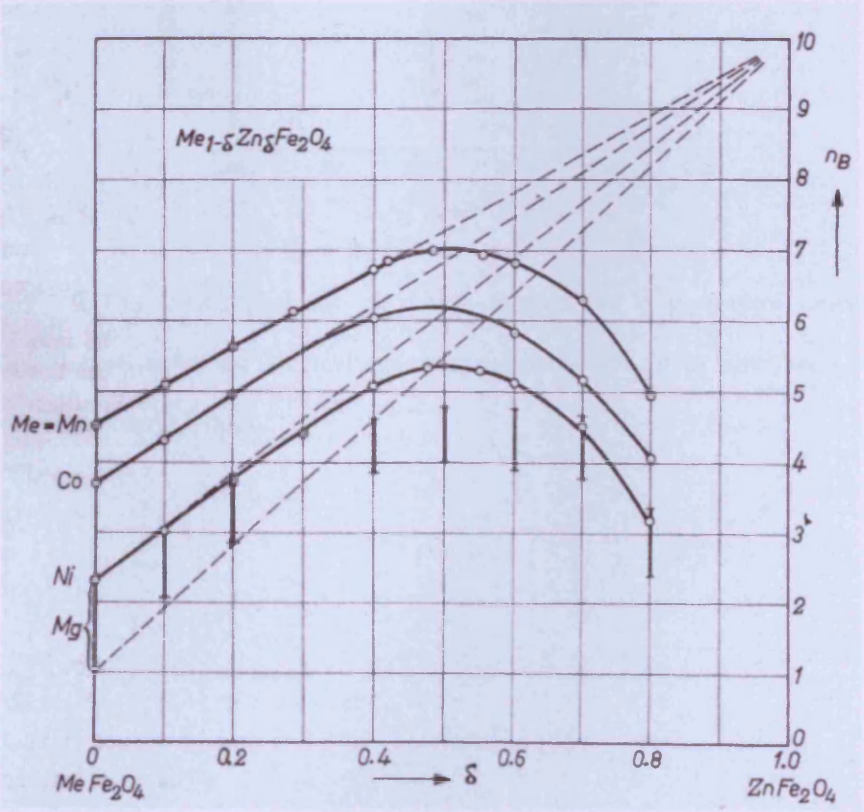

Figure 4-8 The saturation moment in Bohr Magnetons at 0 °K for various mixed crystal series with increasing Zn content. For manganese-zinc ferrites, a region is indicated for the magnetisation which is related to the ion distribution in the lattice, i.e. the degree of inversion of its spinel lattice. (Smit & Wijn, 1959)

4.02.4 Magnetisation loops at different temperatures for gallium substituted cobalt ferrite

Magnetisation curves were measured at temperatures between 10 & 400 K. Figure 4-9 to Figure 4-12 show the magnetisation curves at temperatures (10, 50, 100, 150, ..., 400 K) for gallium content x = 0.2 to x = 0.8.

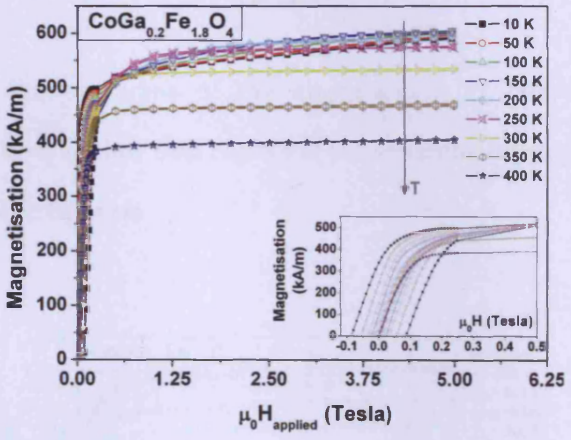

Figure 4-9 The first quadrant of magnetisation vs temperature curves for $CoGa_{0.2}Fe_{1.8}O_4$. Inset shows the low field regions of magnetisation curves which were used for calculation of the coercive field.

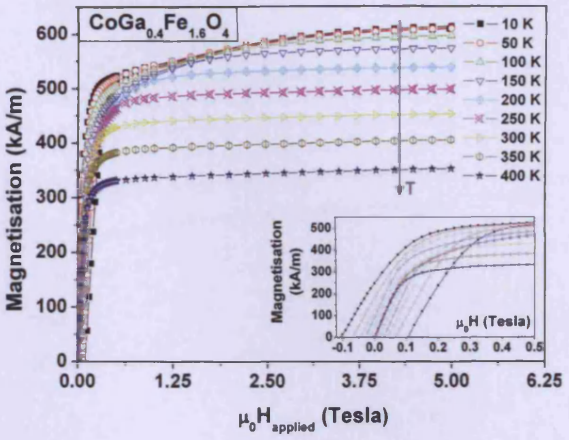

Figure 4-10 The first quadrant of the magnetisation vs temperature curves for $CoGa_{0.4}Fe_{1.6}O_4$. Inset shows the low field regions of magnetisation curves which were used for the calculation of the coercive field.

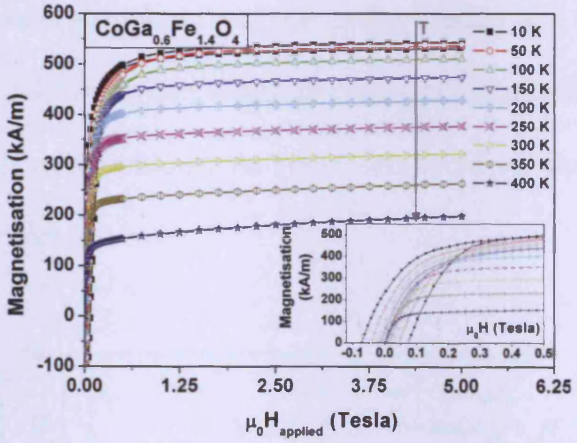

Figure 4-11 The first quadrant of the magnetisation vs temperature curves for $CoGa_{0.6}Fe_{1.4}O_4$. Inset shows the low field regions of magnetisation curves which were used for the calculation of the coercive field.

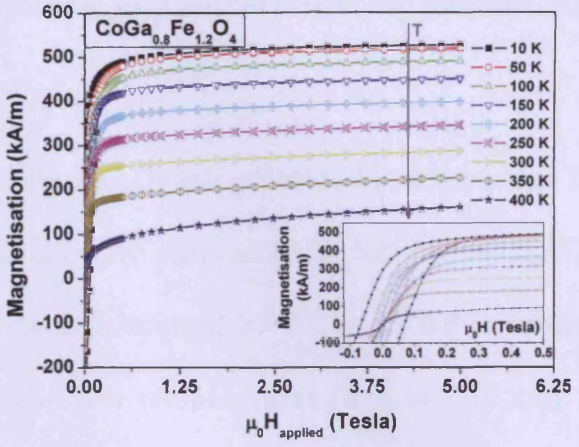

Figure 4-12 The first quadrant of the magnetisation vs temperature curves for $CoGa_{0.8}Fe_{1.2}O_4$. Inset shows the low field regions of magnetisation curves which were used for calculation of the coercive field.

The coercive field was calculated from the magnetisation and is shown in Figure 4-13. The coercive field was observed to decrease monotonically with increasing temperature for all compositions. At room temperature, the coercivity of all samples was below 5kA/m.

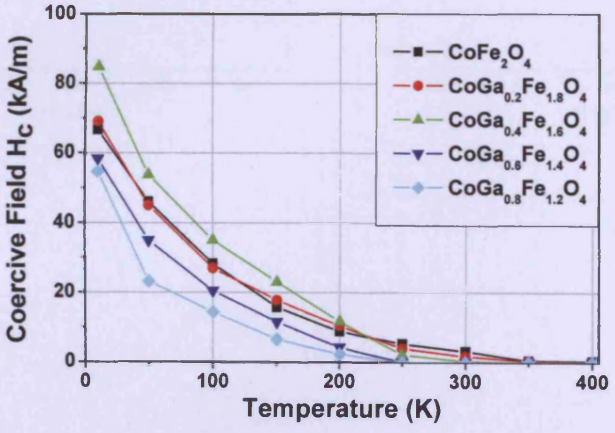

Figure 4-13 The variation of the coercive field of $CoGa_xFe_{2-x}O_4$ with temperature.

4.02.5 Anisotropy vs Temperature for gallium substituted cobalt ferrite

The anisotropy of $CoGa_xFe_{2-x}O_4$ was measured by fitting high field regions of the major loop to the Law of Approach to Saturation (LAS). The fitting for compositions with gallium content x = 0.2 to x = 0.8 is shown in Figure 4-14 - Figure 4-17. The fits at low temperatures (between 10 and 150 K), are not as good as the rest in cases where it was needed to use LAS with $\kappa = 0$ due to the presence of high anisotropy fields stronger than the applied field.

(a) (b)

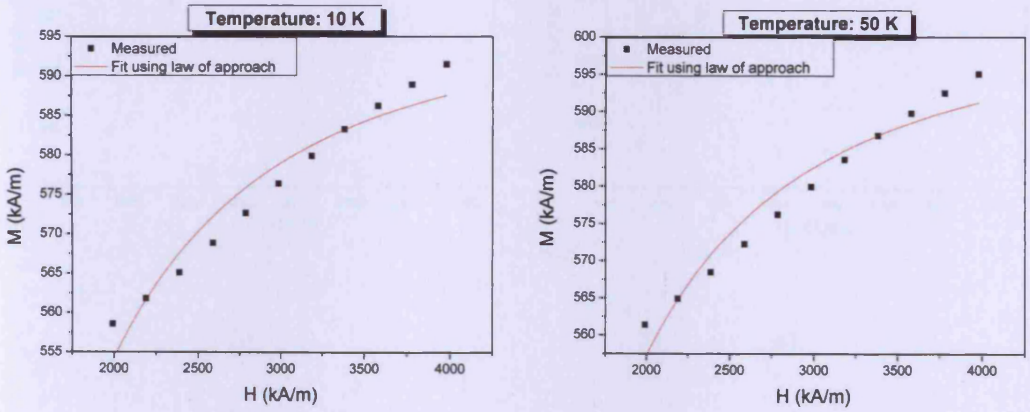

(c)

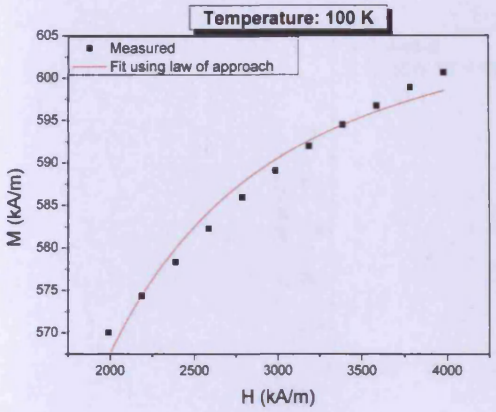
Temperature: 100 K
Measured
Fit using law of approach
M (kA/m)
H (kA/m)

(d)

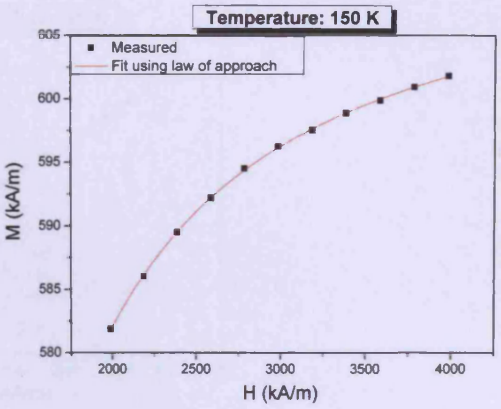
Temperature: 150 K
Measured
Fit using law of approach
M (kA/m)
H (kA/m)

(e)

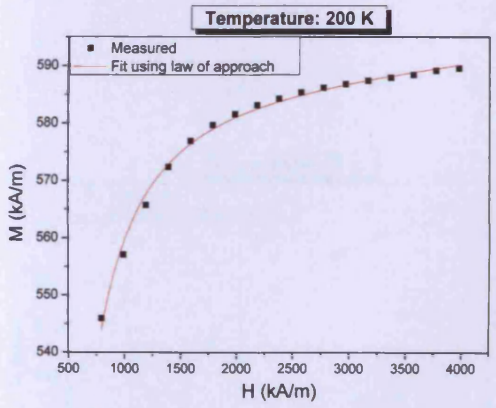
Temperature: 200 K
Measured
Fit using law of approach
M (kA/m)
H (kA/m)

(f)

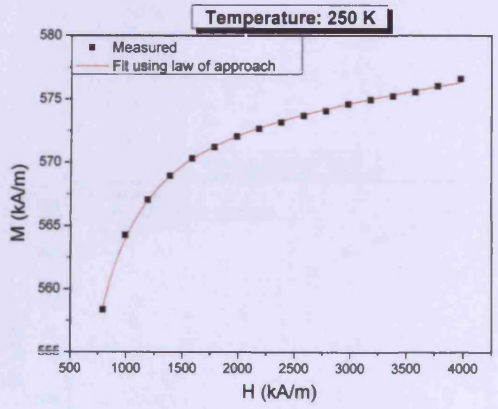
Temperature: 250 K
Measured
Fit using law of approach
M (kA/m)
H (kA/m)

(g)

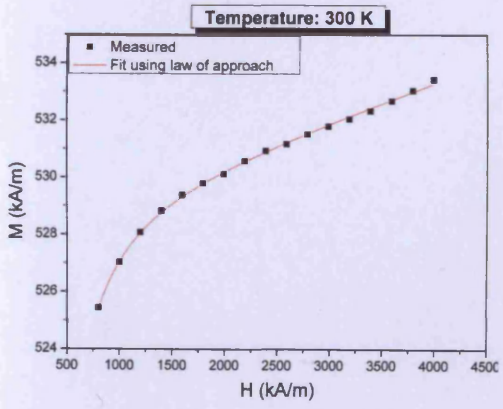
Temperature: 300 K
Measured
Fit using law of approach
M (kA/m)
H (kA/m)

(h)

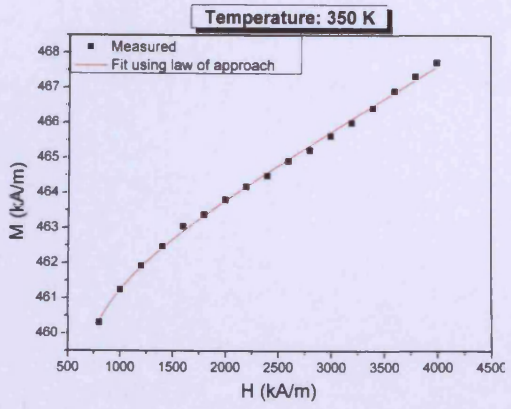
Temperature: 350 K
Measured
Fit using law of approach
M (kA/m)
H (kA/m)

(i)

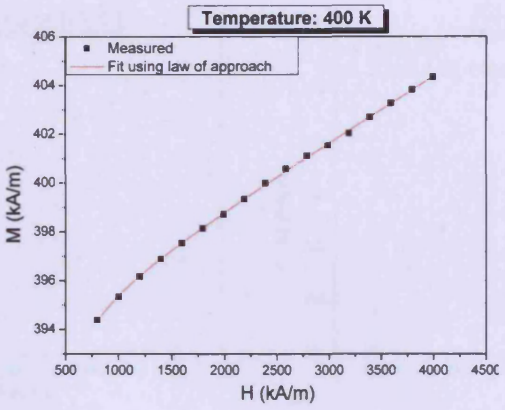

Figure 4-14 Fitting high field region M-H data for $CoGa_{0.2}Fe_{1.8}O_4$ at temperatures in the range 10 - 400 K.

(a) (b)

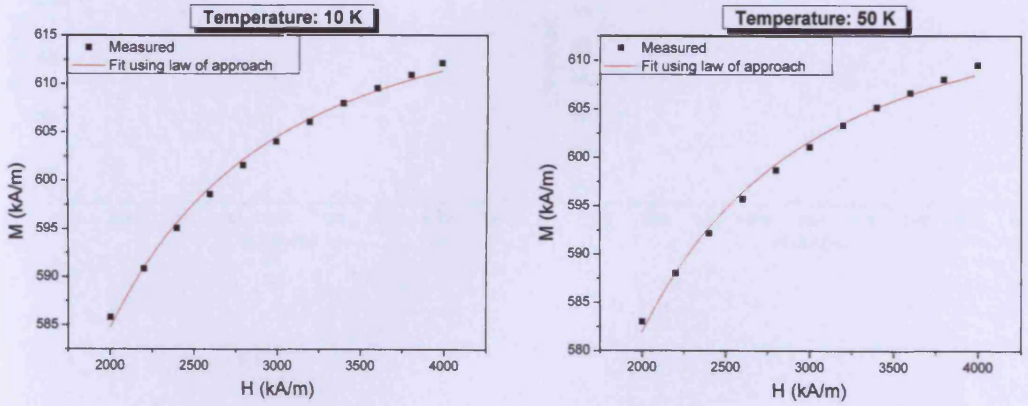

(c)

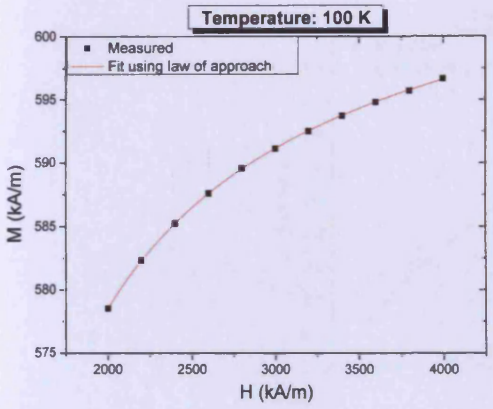
Temperature: 100 K
Measured
Fit using law of approach
M (kA/m)
H (kA/m)

(d)

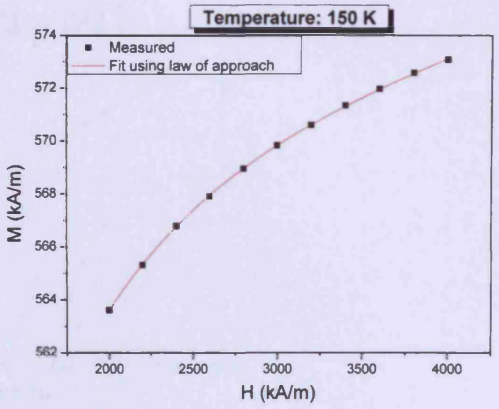
Temperature: 150 K
Measured
Fit using law of approach
M (kA/m)
H (kA/m)

(e)

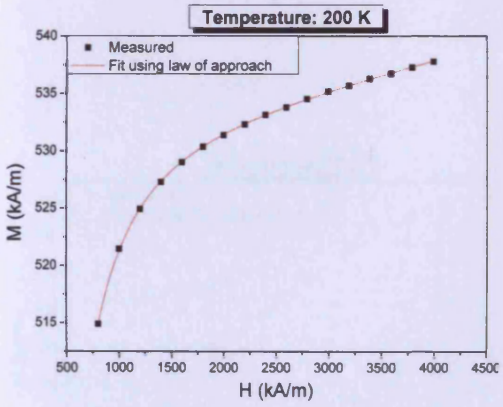
Temperature: 200 K
Measured
Fit using law of approach
M (kA/m)
H (kA/m)

(f)

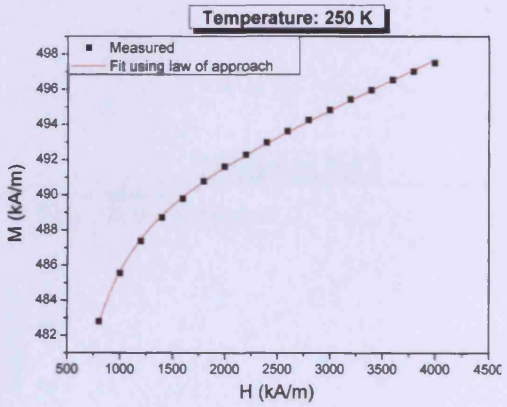
Temperature: 250 K
Measured
Fit using law of approach
M (kA/m)
H (kA/m)

(g)

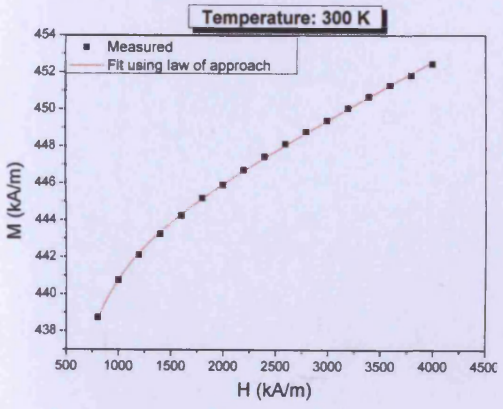
Temperature: 300 K
Measured
Fit using law of approach
M (kA/m)
H (kA/m)

(h)

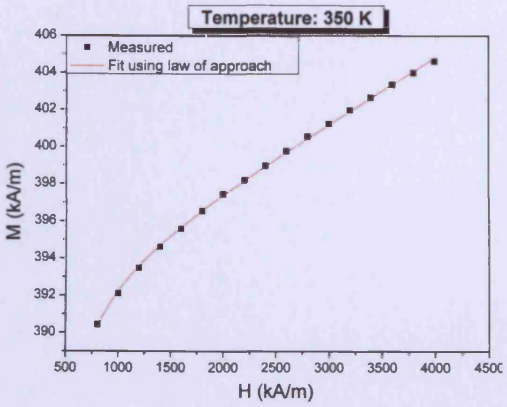
Temperature: 350 K
Measured
Fit using law of approach
M (kA/m)
H (kA/m)

(i)

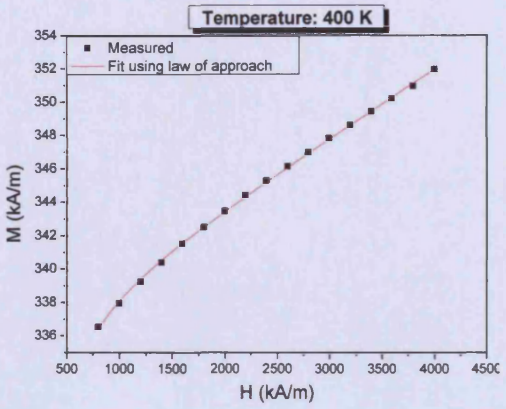

Figure 4-15 Fitting high field region M-H data for $CoGa_{0.4}Fe_{1.6}O_4$ at temperatures in the range 10 - 400 K.

(a) (b)

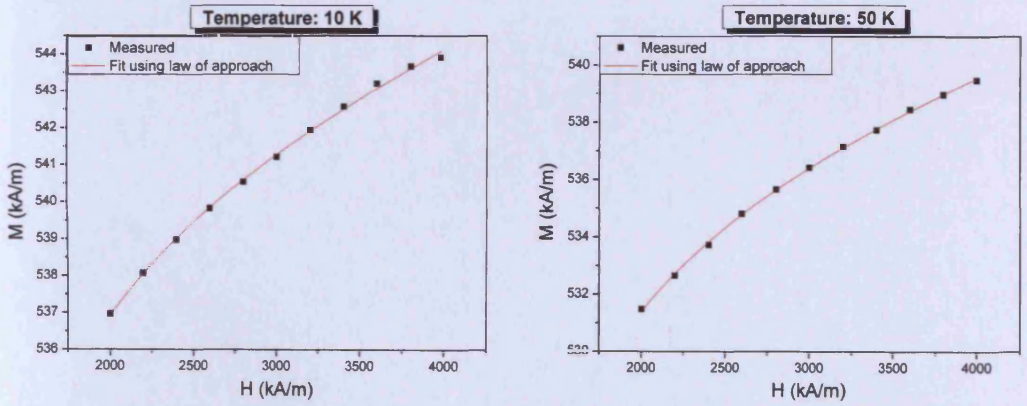

(c)

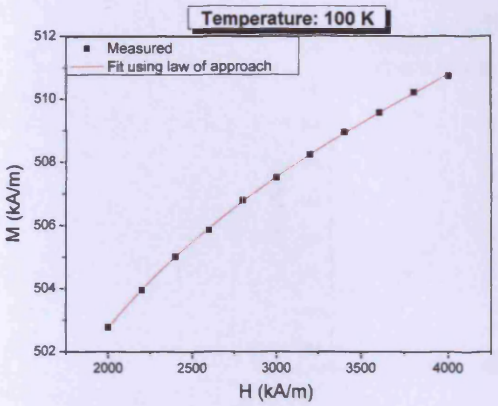
Temperature: 100 K
Measured
Fit using law of approach
M (kA/m)
H (kA/m)

(d)

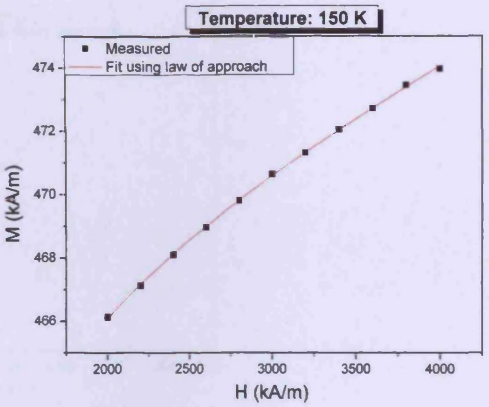
Temperature: 150 K
Measured
Fit using law of approach
M (kA/m)
H (kA/m)

(e)

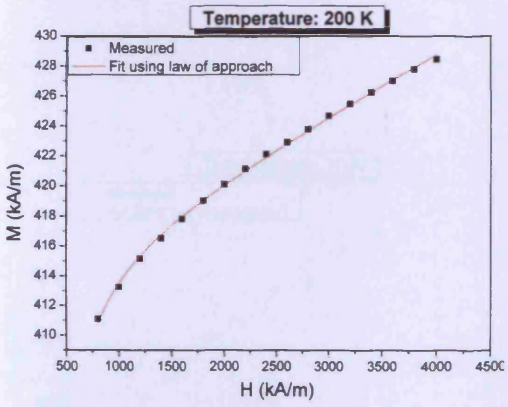
Temperature: 200 K
Measured
Fit using law of approach
M (kA/m)
H (kA/m)

(f)

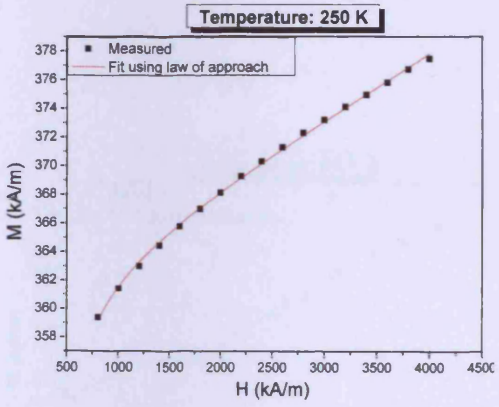
Temperature: 250 K
Measured
Fit using law of approach
M (kA/m)
H (kA/m)

(g)

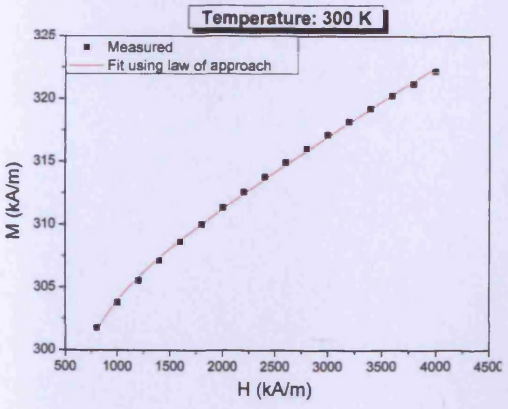
Temperature: 300 K
Measured
Fit using law of approach
M (kA/m)
H (kA/m)

(h)

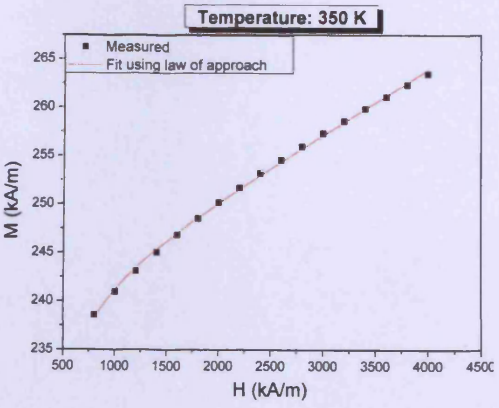
Temperature: 350 K
Measured
Fit using law of approach
M (kA/m)
H (kA/m)

(i)

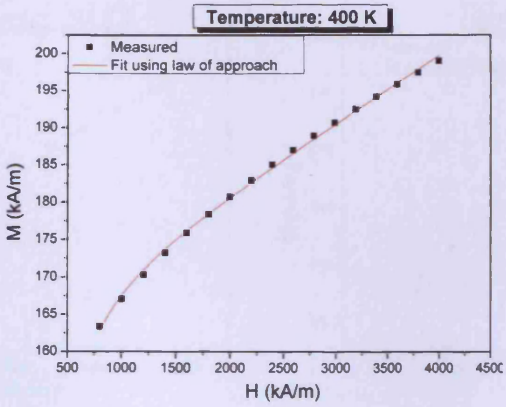

Figure 4-16 Fitting high field region M-H data for $CoGa_{0.6}Fe_{1.4}O_4$ at temperatures in the range 10 - 400 K.

(a) (b)

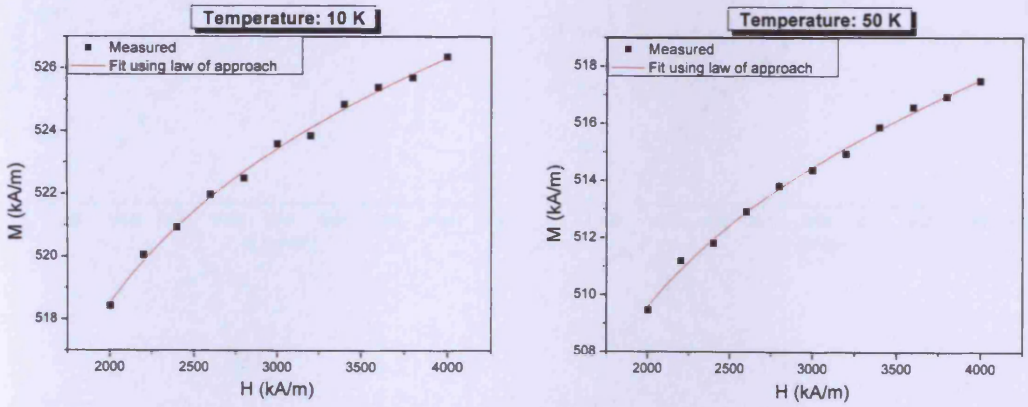

(c)

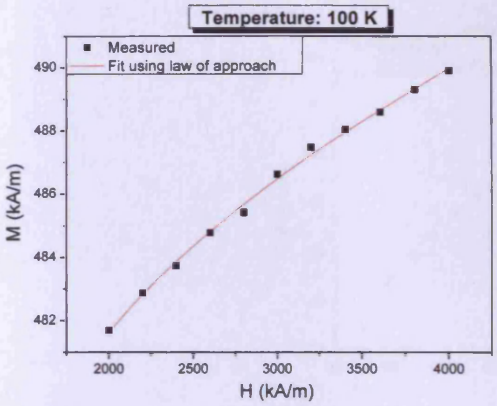
Temperature: 100 K
Measured
Fit using law of approach
M (kA/m)
H (kA/m)

(d)

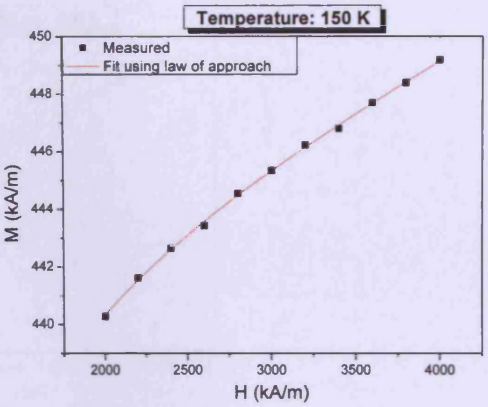
Temperature: 150 K
Measured
Fit using law of approach
M (kA/m)
H (kA/m)

(e)

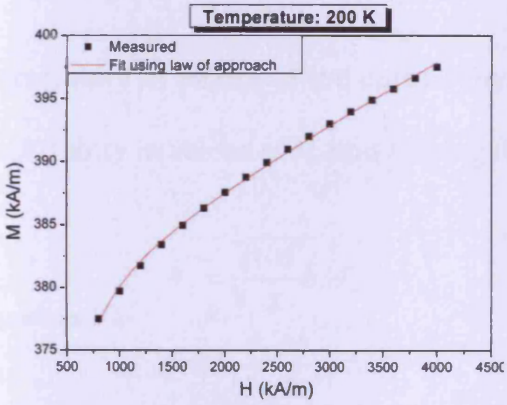
Temperature: 200 K
Measured
Fit using law of approach
M (kA/m)
H (kA/m)

(f)

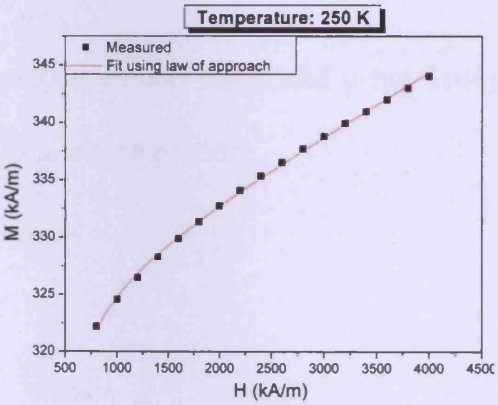
Temperature: 250 K
Measured
Fit using law of approach
M (kA/m)
H (kA/m)

(g)

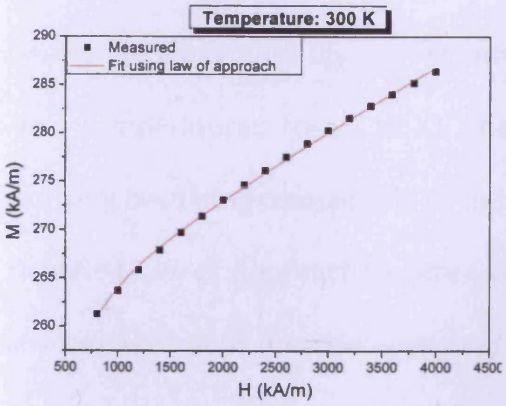
Temperature: 300 K
Measured
Fit using law of approach
M (kA/m)
H (kA/m)

(h)

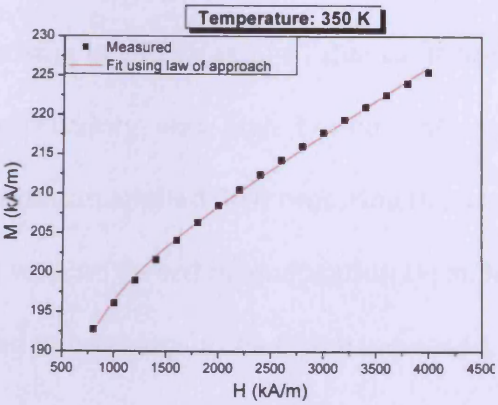
Temperature: 350 K
Measured
Fit using law of approach
M (kA/m)
H (kA/m)

(i)

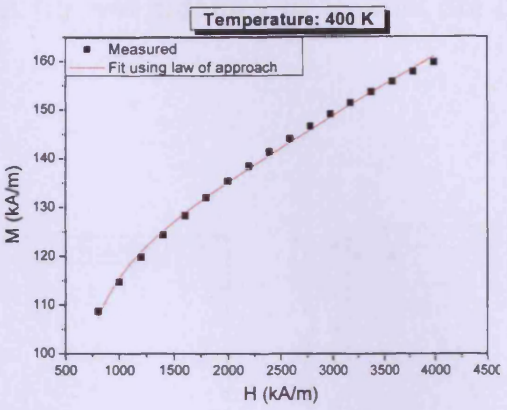

Figure 4-17 Fitting high field region M-H data for $CoGa_{0.8}Fe_{1.2}O_4$ at temperatures in the range 10 - 400 K.

Uncertainty in values of the anisotropy constant K_1 was calculated using fitting uncertainty in values of M_s and b using the following equation:

Equation 4-2

$$K_1 = \sqrt{\frac{105}{8}} bM_s$$
$$\therefore \Delta K_1 = \frac{\Delta b}{2} + \Delta M_s ,$$

where ΔK_1, Δb, and ΔM_s are the uncertainties in K_1, b, and M_s respectively. Figure 4-18 shows the temperature dependence of the anisotropy of $CoGa_xFe_{2-x}O_4$ along with the uncertainty arising in the value of K_1 due to fitting. At low temperatures (near 10 K), the uncertainty was high because of the anisotropy becoming comparable to the maximum applied field requiring the use of modified Law of Approach to Saturation with no forced magnetisation term. It was observed that as the anisotropy reduced uncertainty in the fitting increased.

Figure 4-19 shows the variation in temperature dependency of first order magnetocrystalline cubic anisotropy constant K_1 with the substitution of gallium

into cobalt ferrite. In data points calculated for cases where the forced magnetisation constant (κ) was assumed to be zero, are connected by dotted lines.

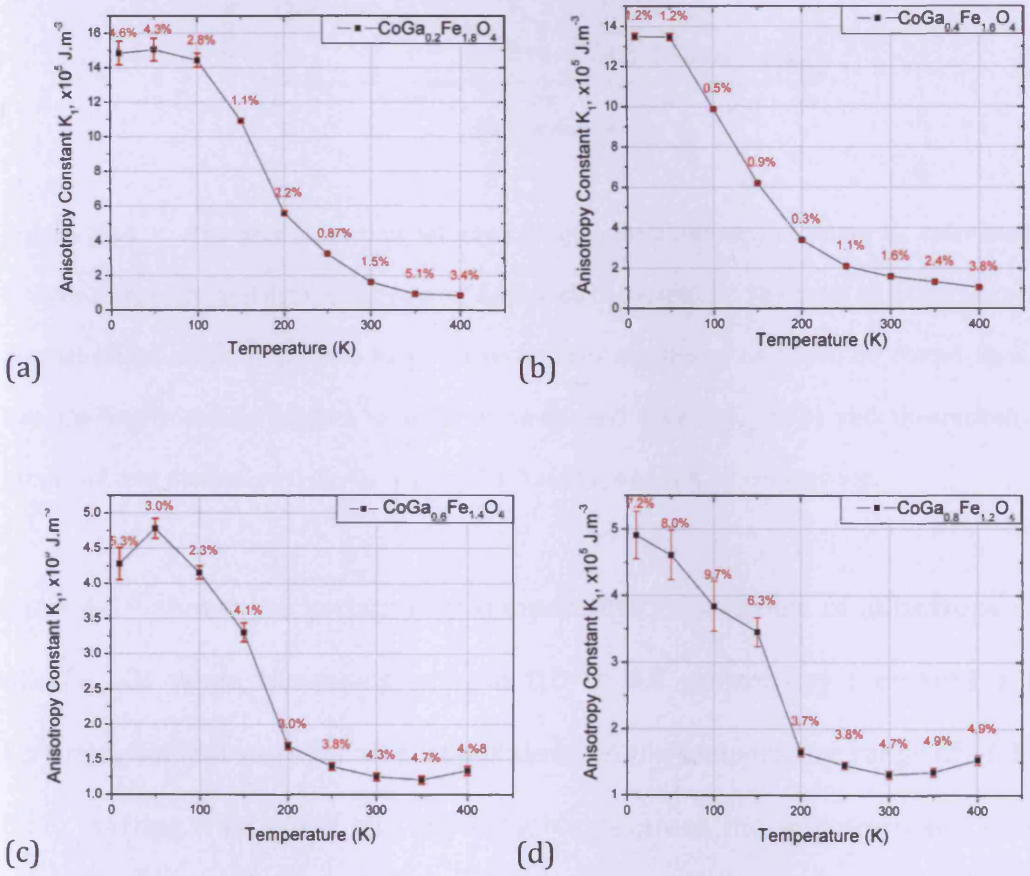

Figure 4-18 Variation of the first order magnetocrystalline anisotropy constant K_1 of gallium-substituted cobalt ferrite with temperature for compositions: (a) $CoGa_{0.2}Fe_{1.8}O_4$, (b) $CoGa_{0.4}Fe_{1.6}O_4$, (c) $CoGa_{0.6}Fe_{1.4}O_4$, and (d) $CoGa_{0.8}Fe_{1.2}O_4$. The error bars are shown for each point and the labels in red above each point indicate the estimated uncertainty (in percentage) for each point resulting from fitting high field regions of M-H loops to Law of Approach.

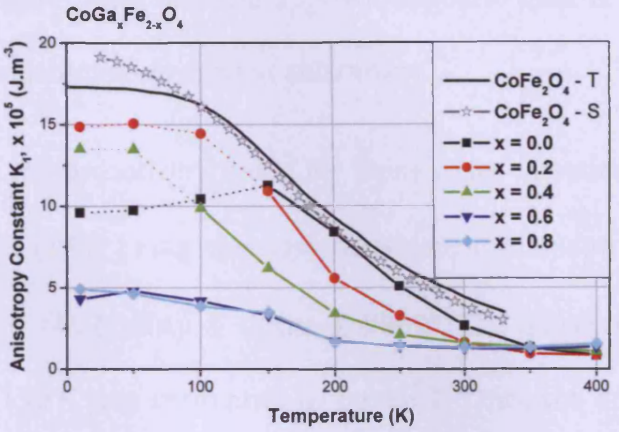

Figure 4-19 The first order magnetocrystalline cubic anisotropy constant K_1, calculated by fitting experimental data to the Law of Approach to saturation. The cases in which forced magnetisation constant (κ) was assumed to be zero are shown as joined by dotted lines. Experimentally measured data labelled as $CoFe_2O_4$–S (Shenker, 1957) and theoretically predicted data marked as $CoFe_2O_4$–T (Tachiki, 1960) are shown for comparison.

Figure 4-19 shows the variation of temperature dependence of anisotropy for $CoGa_xFe_{2-x}O_4$ when increasing x from 0.0 to 0.8. Anisotropy increased with decreasing temperature for all compositions, in the temperature range of 10 K – 400 K. Starting from 400 K and reducing temperature, the anisotropy increased slowly initially and increased with a steep slope below a particular temperature, as can be observed from Figure 4-19. The beginning of the steep rise occurred at progressively lower temperatures with increasing x. However, for samples with x = 0.0, 0.2, and 0.4, as the temperature was decreased, anisotropy was seen to peak at a temperature and then either decrease or level off. High anisotropy at low temperatures can prevent the maximum applied field ($\mu_0 H$ = 5 T) from being able to cause the rotation of moments away from the anisotropy field direction towards the applied field direction. This invalidates the assumption under which

the calculations were done that the applied magnetic field is enough to cause rotation of magnetic moments against anisotropy.

An estimation of the anisotropy fields for these cases supports the idea. For a cubic crystal with ⟨100⟩ being the easy direction, the anisotropy field can be written as $H_K = 2K_1/M_s$ (Cullity & Graham, 2009). The anisotropy field of pure cobalt ferrite at 150 K was estimated to be 4.8 T. Thus, the anisotropy field at lower temperatures is expected to be higher than the maximum applied magnetic field ($\mu_0 H = 5$ T). Similarly, the estimated anisotropy field for the sample with gallium content x = 0.2 was $\mu_0 H_K = 5.16$ T. In cases where anisotropy field prevents a complete approach to saturation, the results obtained by fitting M-H data to LAS are less accurate.

The LAS gives the absolute value of the cubic anisotropy coefficient K_1. The analytical expression for cubic anisotropy to the second order is the same for ⟨100⟩ or ⟨111⟩ easy directions. Pure cobalt ferrite has been reported to have the ⟨100⟩ easy-directions, with K_1 values that are positive and range from 2.1×10^5 to 3.9×10^5 J/m^3. Different values of the anisotropy field can be obtained in this range through a variation in the processing techniques, heat treatment and in the stoichiometry of the material (Smit & Wijn, 1959). The value of K_1 for pure cobalt ferrite at 300 K, in the present study, is 2.66×10^5 J/m^3. This is consistent with the results of Shenker and Tachiki (Tachiki, 1960, Shenker, 1957). Shenker had measured the magnetic anisotropy constant K_1 of crystalline pure cobalt ferrite by measuring the torque for varying directions of the applied field near the

direction of easy magnetisation. The K_1 measured by this method could be approximated by the empirical relationship

Equation 4-3 $K_1 = 19.6 \times 10^5 e^{-1.9 \times 10^{-5} T^2} \text{Jm}^{-3}$

where T is the temperature. The above equation was found to be applicable in the temperature range of 20 – 325 K. The value of K_1 at 300 K predicted by Equation 4- is 3.5×10^5 J/m^3. See Figure 4-19. Tachiki based his calculations on the assumption that cobalt ferrite is an inverse spinel. The anisotropy energy of Mn and Ni ferrite comes from the Fe^{3+} ions in the A & B sites. The anisotropy energy of magnetite comes from the Fe^{2+} ions in B-sites and Fe^{3+} ions in A-sites. However, the anisotropy energy of cobalt ferrite cannot be explained by the contribution of the Fe^{3+} ions, which is negligible in comparison to the value of the anisotropy energy observed at near zero Kelvin temperatures. Although the anisotropy energy due to the second order effect of the magnetic dipole interactions predicts the correct easy direction ⟨100⟩, the prediction of the magnitude of anisotropy energy is far from the observedvalues. It was thus concluded that the anisotropy energy of cobalt ferrite comes from Co^{2+} ions in B-sites.

The substitution of Ga^{3+} ions in place of Fe^{3+} ions causes magnetic dilution and reduces the superexchange interaction between Co^{2+} ions in the B-sites. This causes the anisotropy to decrease, as seen in Figure 4-19. This effect is largely responsible for the reduction in the anisotropy with the addition of low amounts of Ga^{3+}. For higher amounts of Ga^{3+} substitution, there can be two reasons for the reduction in anisotropy:

- Ga^{3+} ions start substituting into B-sites thus displacing Co^{2+} ions from B-sites. Since the presence of Co^{2+} ions in B-sites is responsible for the anisotropy, their displacement from the B-sites by non-magnetic Ga^{3+} ions causes a decrease in anisotropy.

- Introduction of Ga^{3+} ions causes a disruption in the super exchange interactions between B-sites. This causes the B lattice to split into two sub lattices as shown in Figure 4-7 with an average direction opposite to those of the moments in the A-site lattice.

4.02.6 Magnetostriction vs applied field for gallium substituted cobalt ferrite

The magnetostriction vs applied field characteristics were measured for all the samples and were standardised according to the procedures described in Chapter 3. Room temperature data for polycrystalline pure cobalt ferrite (x = 0.0 in $CoGa_xFe_{2-x}O_4$) have been obtained from Paulsen (Paulsen et al., 2005). Figure 4-20 – Figure 4-23 show the measured field induced magnetostriction and strain derivative measured at 250 K, 300 K, 350 K, and 400 K. It was observed that the magnetostriction curves for cobalt ferrite followed three different shapes, out of the four shown in Figure 4-24. Cobalt ferrite has two independent magnetostriction coefficients, λ_{100} and λ_{111}, along the two crystal directions ⟨100⟩ and ⟨111⟩ respectively. At room temperature (300 K), it is known that ⟨100⟩ is the easy direction and that λ_{100} is negative. Furthermore, the first order cubic anisotropy constant K_1 is positive for cobalt ferrite at all temperature, thus making ⟨100⟩ as the easy direction at all temperatures. ⟨111⟩

is the hard direction for cobalt ferrite and the magnetostriction contribution of this direction λ_{111} is positive. The polycrystalline saturation magnetostriction is given by

Equation 4-4 $$\lambda_s = \frac{2}{5}\lambda_{100} + \frac{3}{5}\lambda_{111}.$$

Bozorth measured the magnetostriction of crystalline cobalt ferrite along the easy and hard directions and results are shown in Figure 4-26. λ_{100} and λ_{111} are the saturation values of the field induced magnetostriction in the ⟨100⟩ and ⟨111⟩ directions respectively (Bozorth et al., 1955). Since at room temperature, $\lambda_{100} < 0$ and $|\lambda_{100}| > 3/2\ |\lambda_{111}|$, the saturation magnetostriction is negative.

The room temperature field induced magnetostriction of polycrystalline pure cobalt ferrite, shown in Figure 4-21, can be explained using the field induced magnetostriction in two crystal different directions. The net field induced magnetostriction is a sum of the magnetostriction contributions from λ_{100} and λ_{111} at the applied field values. At low field values, the field induced magnetostriction $\lambda(H)$, has a large negative slope because of a dominant negative magnetostriction contribution from λ_{100}. After the alignment of domain magnetisations along the easy axis, any further increase in the field causes the moments to rotate away from the easy axis towards the hard axis ⟨111⟩, which has a smaller positive magnetostriction contribution. This makes $\lambda(H)$ change with a positive slope with increase in the field after the alignment of domains along the easy axis. The variations and the contributions of the two magnetostriction coefficients towards the net field induced magnetostriction

have been discussed by Bozorth and co-workers, among others (Bozorth et al., 1955).

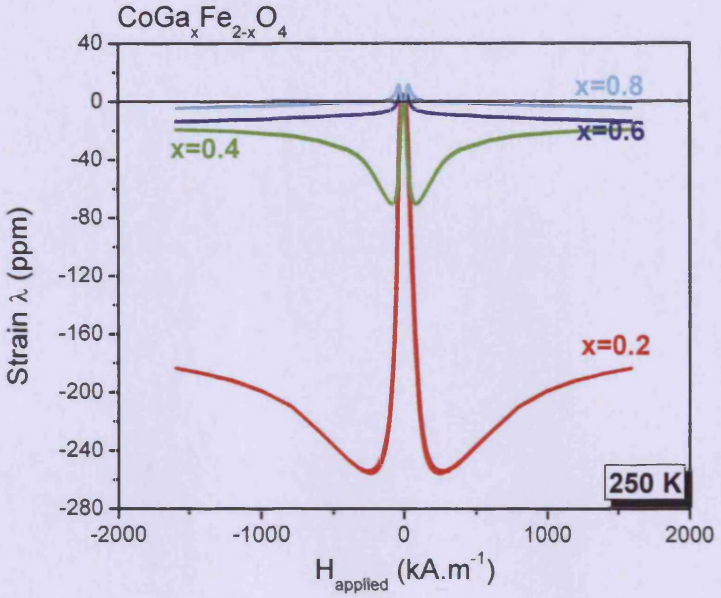

(a)

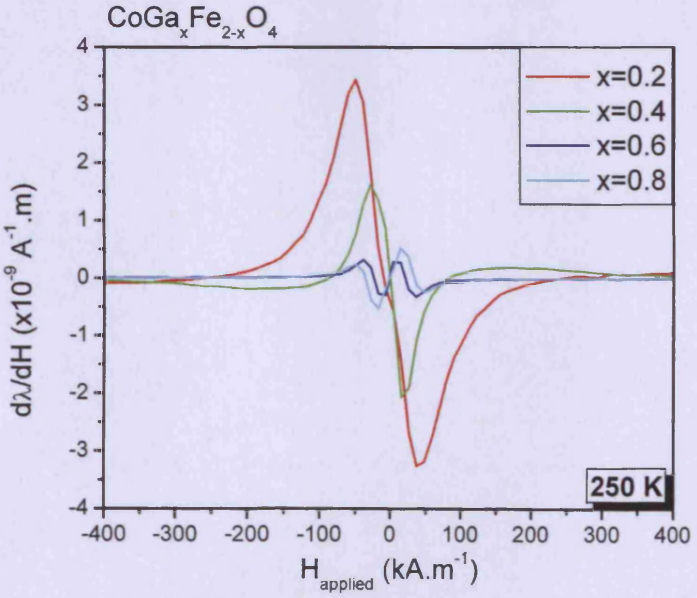

(b)

Figure 4-20 Magnetostrictive properties of gallium substituted cobalt ferrite at 250 K. (a) Field induced magnetostrictive strain (b) Strain derivative ($d\lambda/dH$)

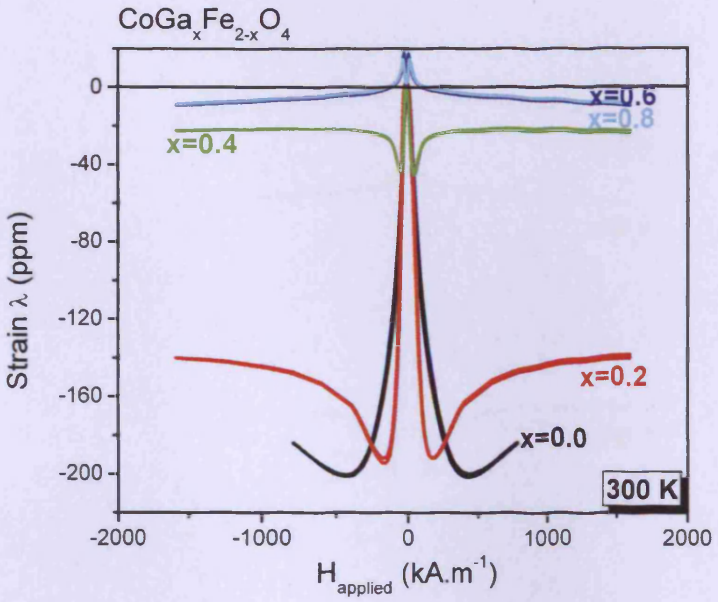

(a)

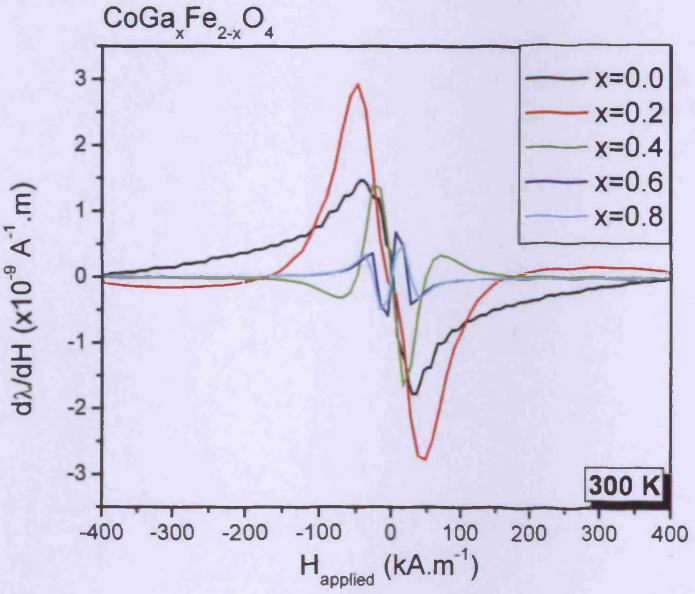

(b)

Figure 4-21 Magnetostrictive properties of gallium substituted cobalt ferrite at 300 K. (a) Field induced magnetostrictive strain (b) Strain derivative ($d\lambda/dH$)

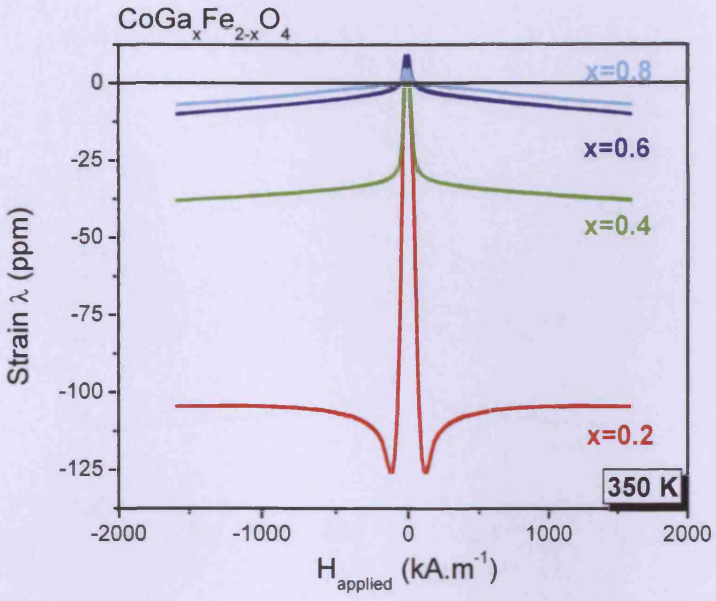

(a)

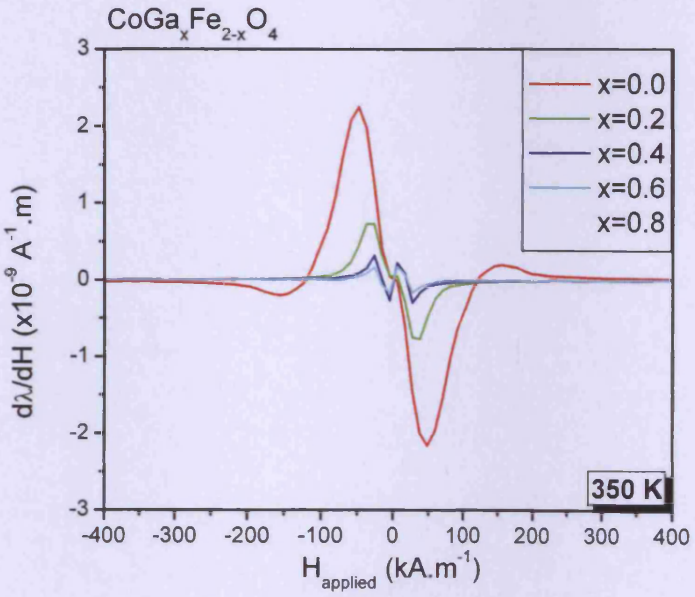

(b)

Figure 4-22 Magnetostrictive properties of gallium substituted cobalt ferrite at 350 K. (a) Field induced magnetostrictive strain (b) Strain derivative ($d\lambda/dH$)

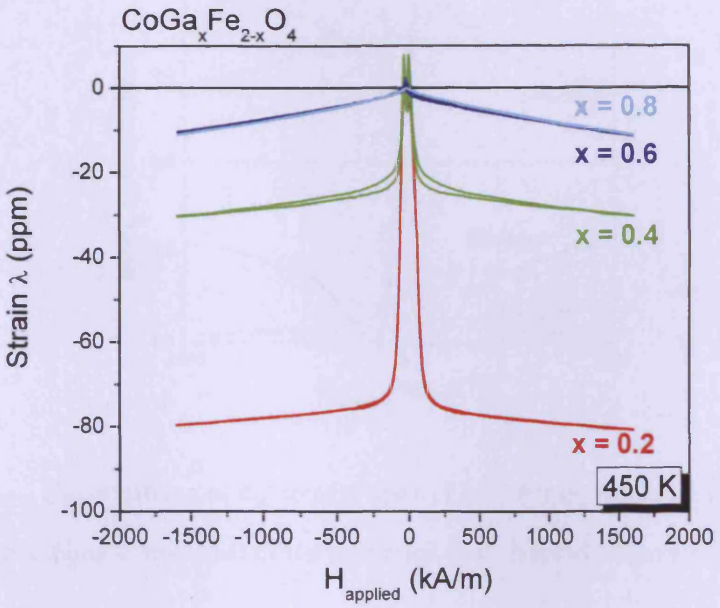

(a)

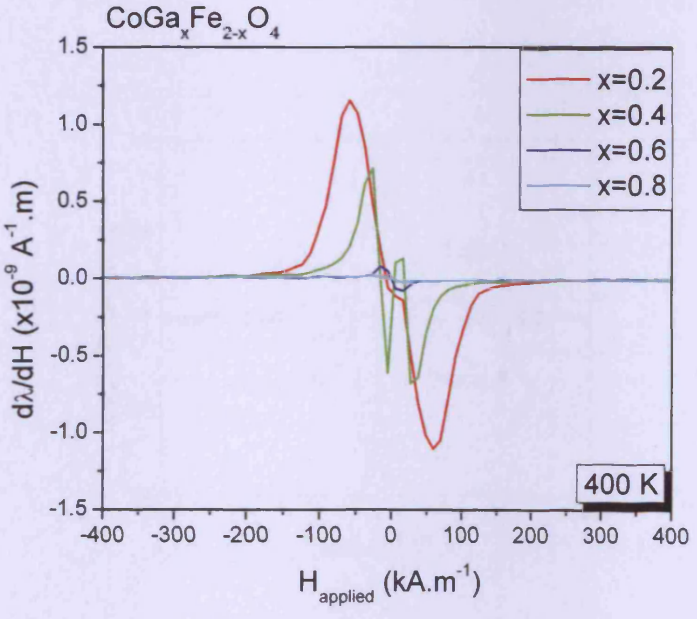

(b)

Figure 4-23 Magnetostrictive properties of gallium substituted cobalt ferrite at 400 K. (a) Field induced magnetostrictive strain (b) Strain derivative ($d\lambda/dH$)

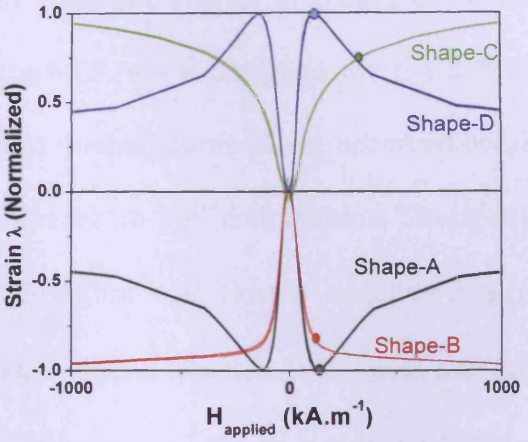

Figure 4-24 Classifications of different shapes of λ-H curves. The filled dots marked on each curve correspond to the value of the maximum field induced magnetostriction in linear region of the curve.

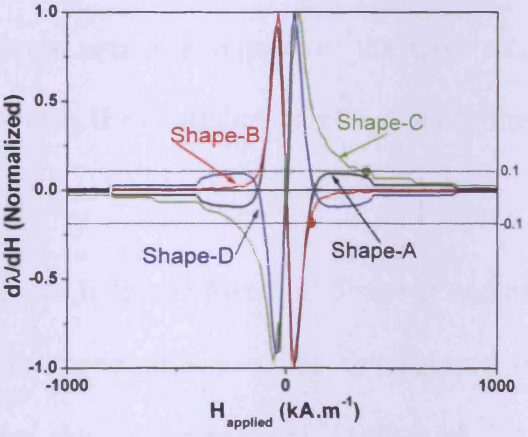

Figure 4-25 Classifications of the different shapes of $d\lambda/dH$ curves corresponding to the shapes of λ–H curves shown in **Figure 4-24**. The filled dots marked on each curve correspond to the value of the maximum field induced magnetostriction in the linear region of the curve. For Shape-B and Shape-C, the value of maximum field induced magnetostriction in the linear region was chosen as the point where $d\lambda/dH$ is 10% of $(d\lambda/dH)_{max}$ for that sample.

Three out of the four different shapes of magnetostriction curves, shown in Figure 4-24 and Figure 4-25, were observed for the different compositions of $CoGa_xFe_{2-x}O_4$ at different temperatures. These occurred because of changes in K_1, λ_{100} and λ_{111} with temperature and composition. Shape-A was observed when ⟨100⟩ was the easy direction and thus a negative λ_{100} made the dominant contribution to the field induced magnetostriction at low field values. The initial high negative slope continued until the alignment of the domains with the ⟨100⟩ direction. Any further increase in the field beyond this point resulted in λ_{111} making a positive slope contribution to the field induced magnetostriction. Figure 4-26 shows the effect of the contributions of the two magnetostriction coefficients in the case of crystalline pure cobalt ferrite (Bozorth et al., 1955).

Shape-B was observed for the cases where λ_{100}'s negative magnetostriction contribution to the strain was dominant over the λ_{111}'s contribution at all field values. At high field values, the contribution of λ_{111} was either negligible or small and negative.

Shape-C and Shape-D are inverted forms of Shape-B and Shape-A respectively. They are observed in cases where either the sign of the contributions of magnetostriction from the two directions ⟨100⟩ and ⟨111⟩ change or their relative magnitudes change. Similar variation in the shape of magnetostriction curves was observed in Ge/Co co-substituted cobalt ferrite (Ranvah *et al.*, 2008c).

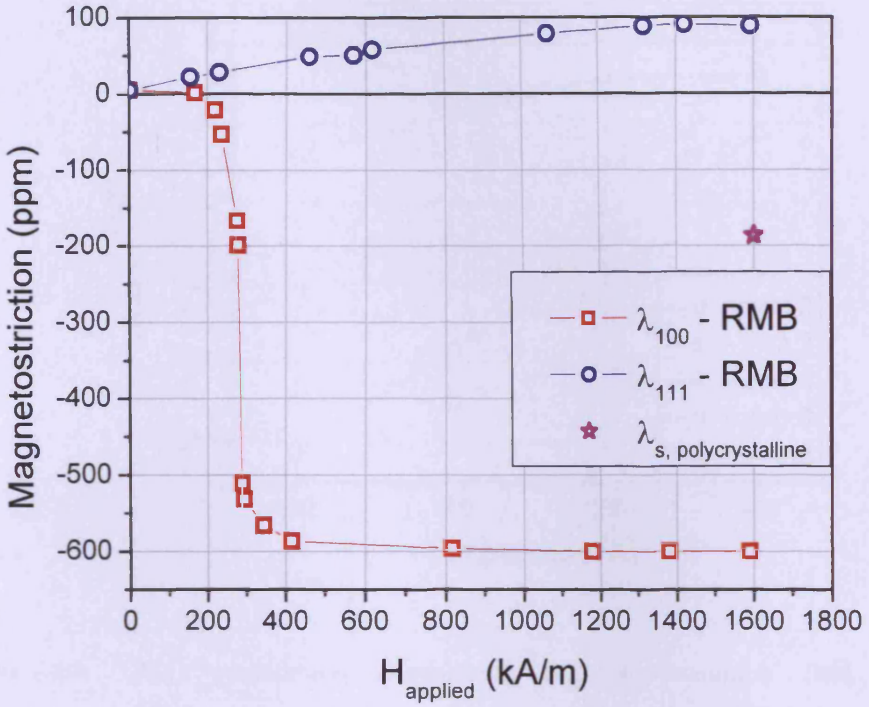

Figure 4-26 Magnetostriction of single crystal pure cobalt ferrite measured by Bozorth (BozorthTilden & Williams, 1955). λ_{100} – RMB denotes the field induced magnetostriction in the ⟨100⟩ direction, measured by Bozorth. λ_{111} – RMB denotes the field induced magnetostriction in the ⟨111⟩ direction, measured by Bozorth. The saturation magnetostriction for polycrystalline materials has been calculated using **Equation 4-**, using the saturation values of field induced magnetostriction in the ⟨100⟩ and ⟨111⟩ directions, which are the values of λ_{100} and λ_{111} respectively.

Figure 4-27 shows the temperature dependence of the maximum field induced magnetostriction in the linear region of the magnetostriction curves of gallium substituted cobalt ferrite. It can be observed that, depending on the shape of the curve, the maximum magnetostriction is either positive or negative.

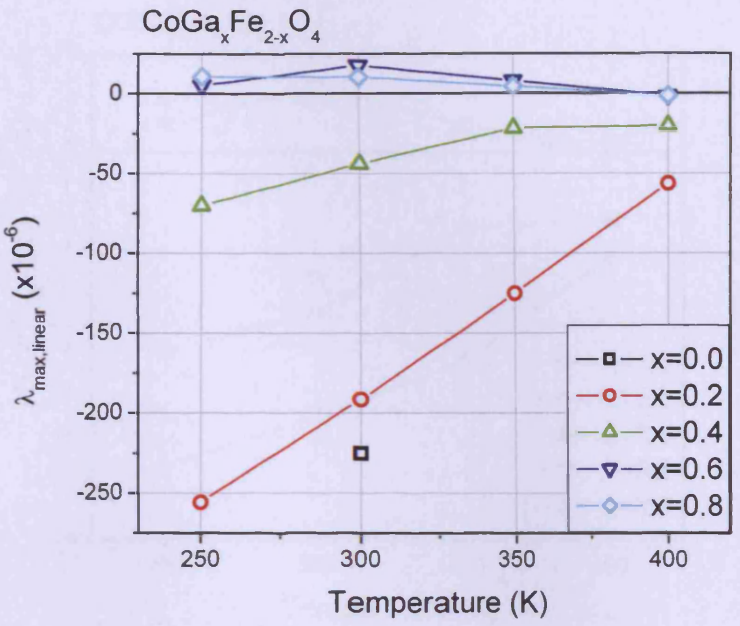

Figure 4-27 The temperature dependence of the maximum field induced magnetostriction in the linear region of magnetostriction curves for different compositions of gallium substituted cobalt ferrite.

Figure 4-28 shows the temperature dependence of the maximum value of the strain derivative in the linear region of the magnetostriction curve for different compositions of gallium substituted cobalt ferrite. It was observed that the maximum field induced magnetostriction in the linear regions decreased with increasing temperature. The same was also true for the maximum strain derivative in the linear region.

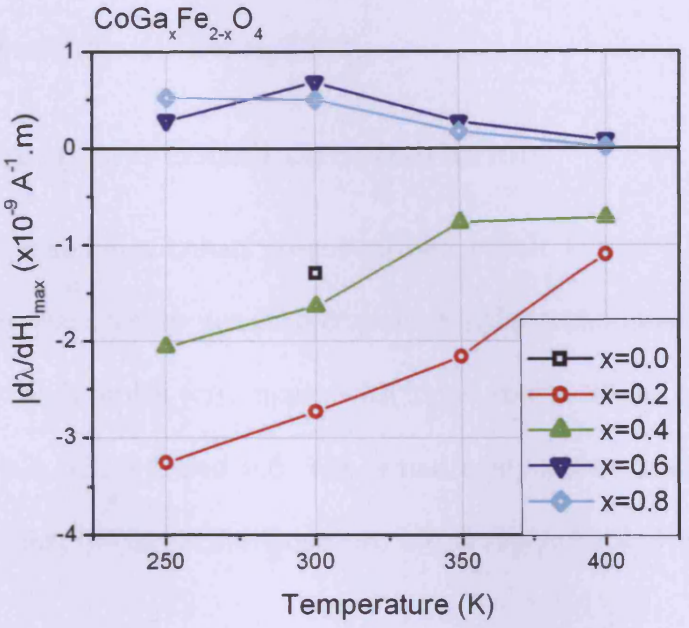

Figure 4-28 The temperature dependence of the maximum value of strain derivative in the linear region of the magnetostriction curves for different compositions of gallium substituted cobalt ferrite.

At room temperature, the maximum field induced magnetostriction in the linear region of the magnetostriction curve of pure cobalt ferrite ($\lambda_{max,linear\ region} = -225$ ppm) was more than that of any gallium substituted sample (Chen et al., 1999). The highest value was observed for $CoGa_{0.2}Fe_{1.8}O_4$, for which $\lambda_{max,linear\ region} = -192$ ppm (83% of the value observed for pure cobalt ferrite) at 300 K. However, the maximum strain derivative of $CoGa_{0.2}Fe_{1.8}O_4$ was 210% of the maximum strain derivative of pure cobalt ferrite. The strain derivative of $CoGa_{0.4}Fe_{1.6}O_4$ was also 130% that of cobalt ferrite. This increase in the strain derivative for small amounts of gallium substitution can be attributed to the lower anisotropy caused by the non-magnetic ions. Similar trends have

been observed in the case of the manganese (Paulsen et al., 2005) and the chromium substitution (Lee et al., 2007).

4.03 Germanium/Cobalt co-substitution

A series of germanium cobalt co-substituted cobalt ferrite ($Co_{1+x}Ge_xFe_{2-2x}O_4$) samples were prepared by standard ceramic powder techniques by Song of Iowa State University. Samples were made with target compositions corresponding to x = 0.0, 0.1, 0.2, 0.3, 0.4, and 0.6. The actual composition, measured by Song, compared against the target compositions are shown in Table 4-3.

Table 4-3 Comparison of the actual and the target composition for $Co_{1+x}Ge_xFe_{2-2x}O_4$ (Song, 2007).

Target Composition	Composition determined by EDS		
	Co	Fe	Ge
$CoFe_2O_4$	0.95	-	2.05
$Co_{1.1}Ge_{0.1}Fe_{1.8}O_4$	1.11	0.12	1.77
$Co_{1.2}Ge_{0.2}Fe_{1.6}O_4$	1.21	0.22	1.57
$Co_{1.3}Ga_{0.3}Fe_{1.4}O_4$	1.33	0.38	1.29
$Co_{1.4}Ga_{0.4}Fe_{1.2}O_4$	1.43	0.47	1.10
$Co_{1.6}Ga_{0.6}Fe_{0.8}O_4$	1.63	0.67	0.70

It was observed that the magnetic properties of $Co_{1.6}Ge_{0.6}Fe_{0.8}O_4$ were of a nature very different to those of other samples and could not be explained. Therefore, a brief description of the experimental observations for magnetic properties of $Co_{1.6}Ge_{0.6}Fe_{0.8}O_4$ is presented in the Appendix-I. However, there is an analysis presented for the magnetostrictive properties of the same sample. Magnetostrictive properties of $Co_{1.2}Ge_{0.2}Fe_{0.8}O_4$ could not be measured as the

samples available were cracked and thus the measurements could not be carried out with confidence in the results.

4.03.1 Site preference of ions in germanium cobalt co-substituted cobalt ferrite

The co-substitution of germanium/copper in place of some of the Fe^{3+} in copper ferrite has been tested for the site preference of the germanium in the spinel lattices (Al-Rawas et al., 2004). The site preference of the ions was determined by performing Mösbauer studies at 77 and 300 K. Germanium showed a very strong tetrahedral (A) site preference in the spinel lattice of copper ferrite as can be observed in distribution of the ions shown in Table 4-4.

Table 4-4 Derived cation distributions for $Cu_{1+x}Ge_xFe_{2-2x}O_4$ as determined from data obtained from Mössbauer studies (Al-Rawas *et al.*, 2004).

Target Composition	Distribution A-site in round brackets and B-site in square brackets
$CuFe_2O_4$	$(Cu_{0.08}Fe_{0.92})[Cu_{0.92}Fe_{1.08}]$
$Cu_{1.1}Ge_{0.1}Fe_{1.8}O_4$	$(Ge_{0.10}Fe_{0.90})[Cu_{1.10}Fe_{0.90}]$
$Cu_{1.2}Ga_{0.2}Fe_{1.6}O_4$	$(Ge_{0.20}Fe_{0.80})[Cu_{1.20}Fe_{0.80}]$
$Cu_{1.3}Ga_{0.3}Fe_{1.4}O_4$	$(Ge_{0.30}Fe_{0.70})[Cu_{1.30}Fe_{0.70}]$
$Cu_{1.4}Ga_{0.4}Fe_{0.2}O_4$	$(Ge_{0.40}Fe_{0.60})[Cu_{1.40}Fe_{0.60}]$

A study of the germanium/cobalt co-substituted cobalt ferrite which assumed 100% A-site occupancy for the Ge^{4+} ions hinted towards a weakening of A-B super exchange and splitting of the B-site site lattice in its spinel structure (Upadhyay, 1990).

4.03.2 Curie Temperature of germanium/cobalt co-substituted cobalt ferrite

Curie temperature of germanium/cobalt co-substituted cobalt ferrite was observed to reduce with increase in germanium concentration (Song, 2007), as can be seen in Figure 4-29.

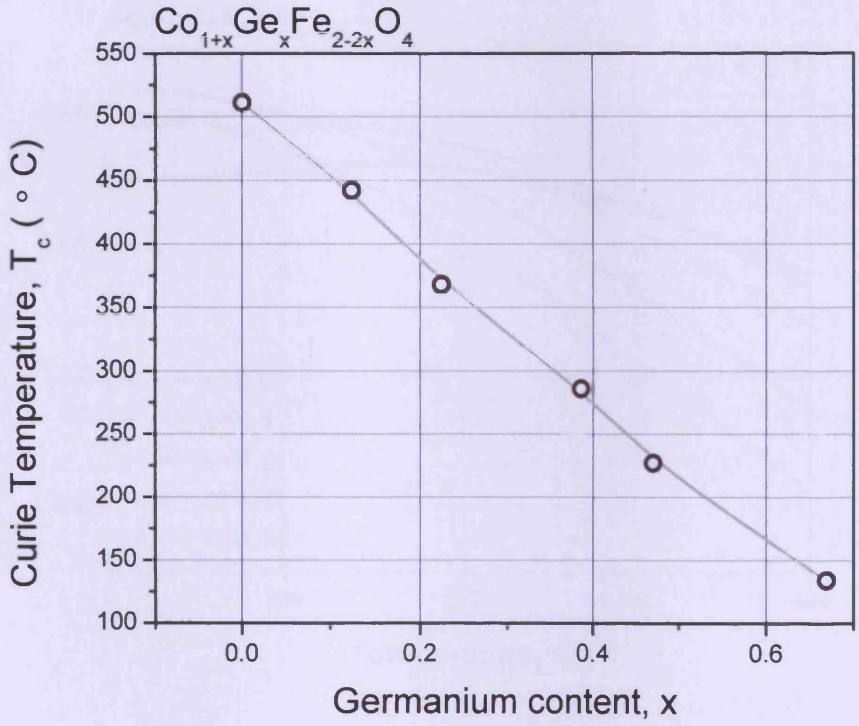

Figure 4-29 Variation of the Curie temperature (T_c) of germanium/cobalt co-substituted cobalt ferrite with germanium content.

The Curie temperature fell faster as a function of x for germanium substitution than for gallium substitution. In the case of Ge/Co co-substitution, the Curie temperature varied linearly with x, a repeat of trend observed in the case of Mn, Cr, and Ga substitution.

4.03.3 Maximum magnetisation vs Temperature for germanium cobalt co-substituted cobalt ferrite

The maximum magnetisation (at constant $\mu_0 H = 5$ T) was measured for all the samples in the range of 10 – 400 K. The trends observed for the maximum magnetisation in this temperature range are shown in Figure 4-30.

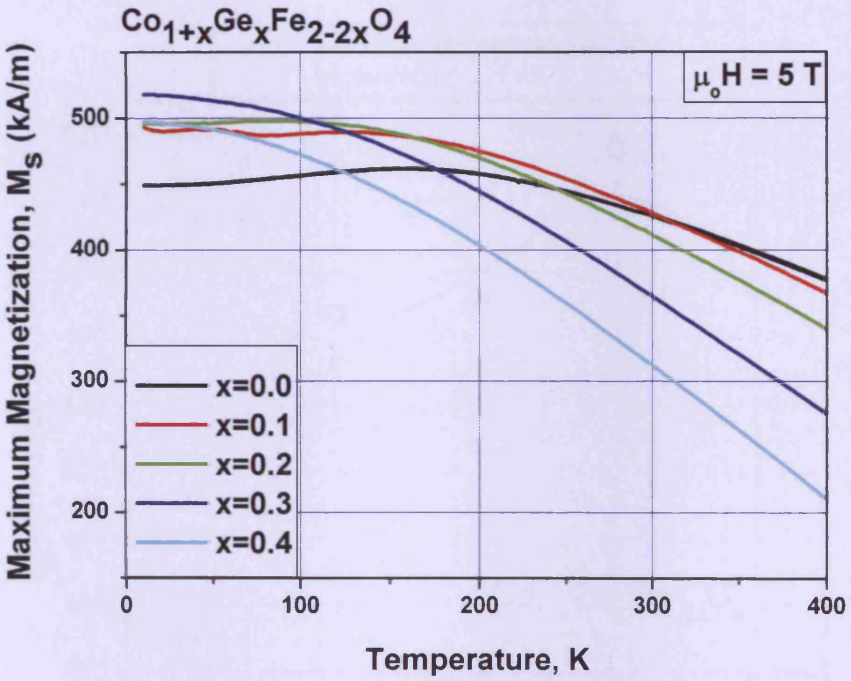

Figure 4-30 Variation of the maximum magnetisation of $Co_{1+x}Ge_xFe_{2-2x}O_4$ with

The maximum magnetisation increased with decreasing temperature in the range 400 -160 K. Below 160 K, it increased slowly for some compositions and decreased in the case of x = 0.0, 0.1, & 0.2. The maximum magnetisation peaked at 160 K for $CoFe_2O_4$, at 128 K for $Co_{1.1}Ge_{0.1}Fe_{1.8}O_4$, and at 78 K for $Co_{1.2}Ge_{0.2}Fe_{1.6}O_4$. This apparent decrease could be explained by the presence of anisotropy fields higher than $\mu_0 H = 5$ T in these cases. Since pure cobalt ferrite

has the highest anisotropy field and its anisotropy field crosses the $\mu_0 H = 5$ T barrier at a higher temperature, with the peak occuring at 160 K. Subsequently, increasing the germanium content, the temperature at which the anisotropy field crosses the $\mu_0 H = 5$ T barrier occurs at lower and lower values of the temperature. Similar trends were observed in the case of Mn (Melikhov et al., 2006a), Cr (Melikhov et al., 2006b), and Ga (Ranvah *et al.*, 2008b) substitution.

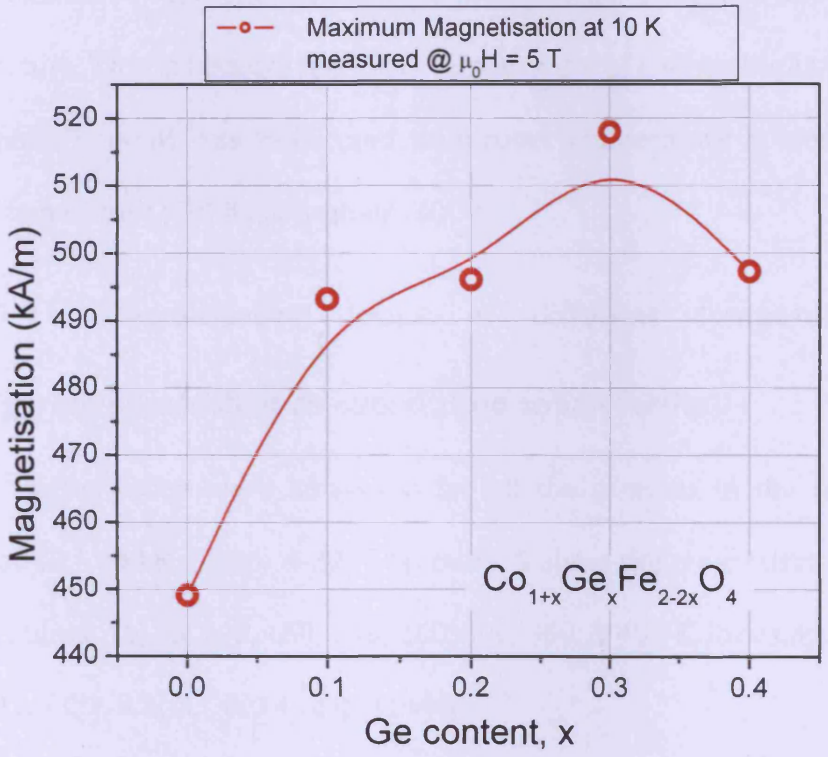

Figure 4-31 Near zero Kelvin moment of germanium/cobalt co-substituted cobalt ferrite.

Figure 4-31 shows the near zero Kelvin maximum magnetisation for germanium/cobalt co-substituted cobalt ferrite. As can be seen, the near zero Kelvin maximum magnetisation increases initially with increasing germanium content and decreases beyond a point. Although x = 0.3 seems like the peak in

the graph, the true peak might be to its left with a lower germanium content. This is because the high anisotropy for compositions with low germanium contents prevents a complete approach to saturation for these samples.

The maximum magnetisation of $Co_{1.1}Ge_{0.1}Fe_{1.8}O_4$ was observed to be higher than that of pure cobalt ferrite, even at room temperature as can be seen in Figure 4-30. It can also be seen that, at room temperature, the maximum magnetisation of compositions with higher germanium content falls faster with any increase in temperature. This is because the Curie temperature of compositions with higher germanium content was lower and thus room temperature is closer to their Curie temperature (Cullity & Graham, 2009).

4.03.4 Magnetisation loops at different temperatures for germanium/cobalt co-substituted cobalt ferrite

Magnetisation loops were measured for all the samples in the temperature range of 10 – 400 K. Figure 4-32 - Figure 4-35 show the magnetisation loops at temperatures: 10, 50, 100, 150, 200, 250, 300, 350, & 400 K, for samples with Ge-content x = 0.1, 0.2, 0.3, & 0.4 respectively.

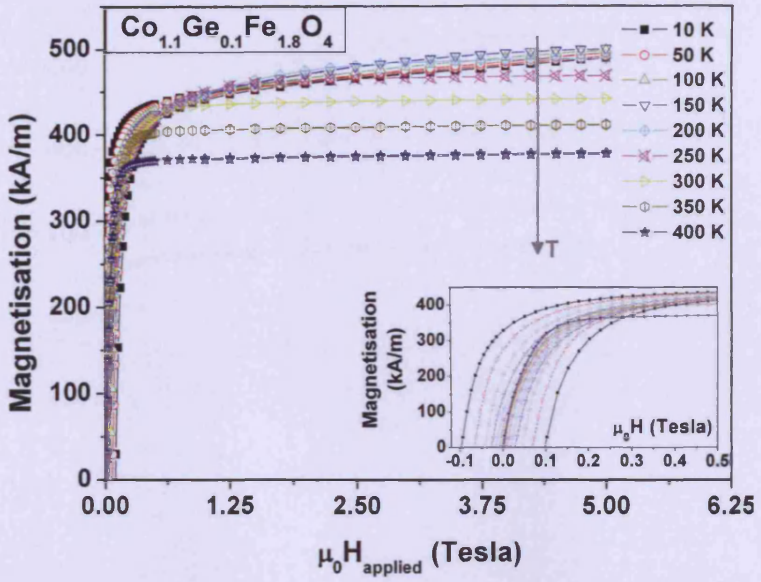

Figure 4-32 First quadrant of the magnetisation vs temperature curves for

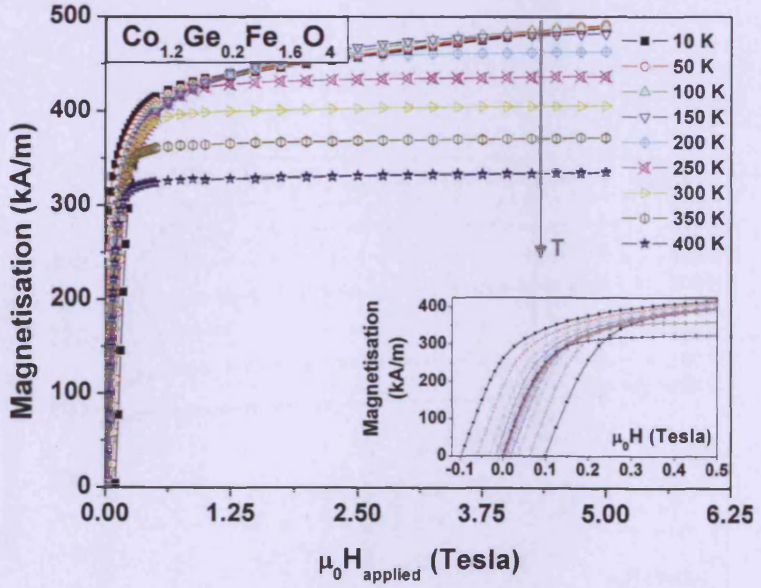

Figure 4-33 First quadrant of magnetisation vs temperature curves for $Co_{1.2}Ge_{0.2}Fe_{1.6}O_4$. Inset shows the low field regions of the magnetisation curves which were used for calculation of the coercive field.

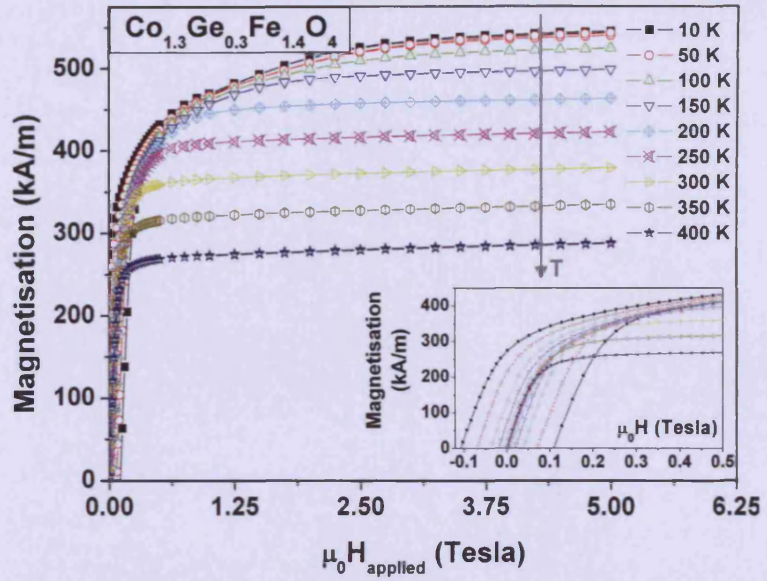

Figure 4-34 First quadrant of magnetisation vs temperature curves for $Co_{1.3}Ge_{0.3}Fe_{1.4}O_4$. Inset shows the low field regions of the magnetisation curves which were used for calculation of the coercive field.

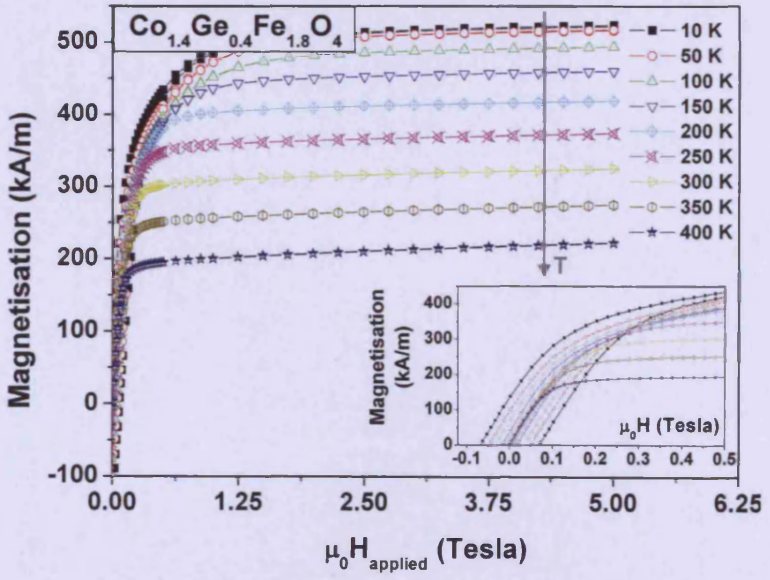

Figure 4-35 First quadrant of magnetisation vs temperature curves for $Co_{1.4}Ge_{0.4}Fe_{1.2}O_4$. Inset shows the low field regions of the magnetisation curves which were used for calculation of the coercive field.

The coercive field of the germanium/cobalt co-substituted cobalt ferrite was calculated using the magnetisation loops. Figure 4-36 shows the coercivity of germanium substituted cobalt ferrite. The coercivity was observed to decrease monotonically with increasing temperature in the range 10 – 400 K. At room temperature, the coercivity of all the samples was observed to be less than 7 kA/m.

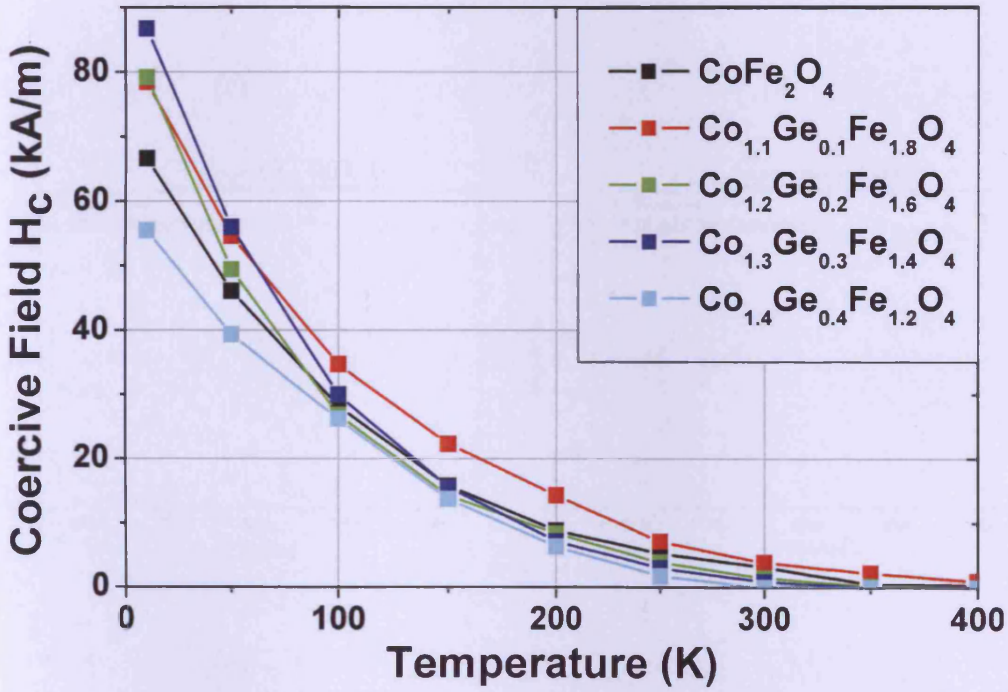

Figure 4-36 The variation of the coercive field of $Co_{1+x}Ge_xFe_{2-2x}O_4$ with temperature.

4.03.5 Anisotropy vs Temperature for germanium/cobalt co-substituted cobalt ferrite

The anisotropy of $Co_{1+x}Ge_xFe_{2-2x}O_4$ was measured by fitting the high field regions of the M-H loops to the Law of Approach to Saturation. The fitting for compositions from x = 0.1 to x = 0.4 is shown in Figure 4-37 - Figure 4-40.

(a)

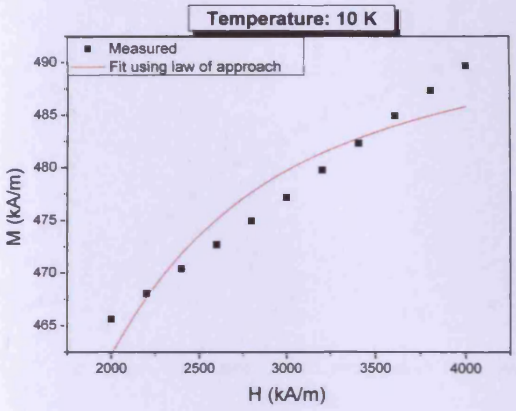
Temperature: 10 K
Measured
Fit using law of approach
M (kA/m)
H (kA/m)

(b)

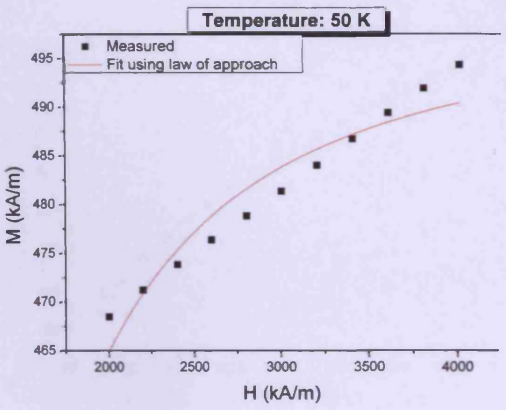
Temperature: 50 K
Measured
Fit using law of approach
M (kA/m)
H (kA/m)

(c)

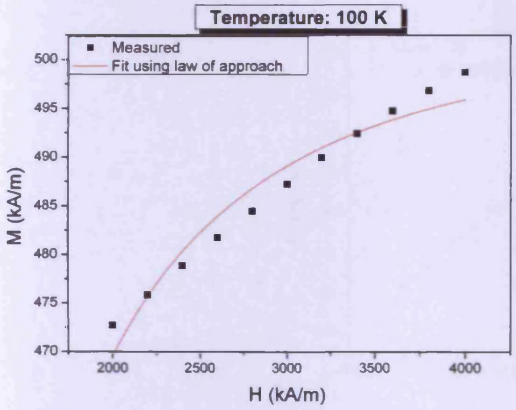
Temperature: 100 K
Measured
Fit using law of approach
M (kA/m)
H (kA/m)

(d)

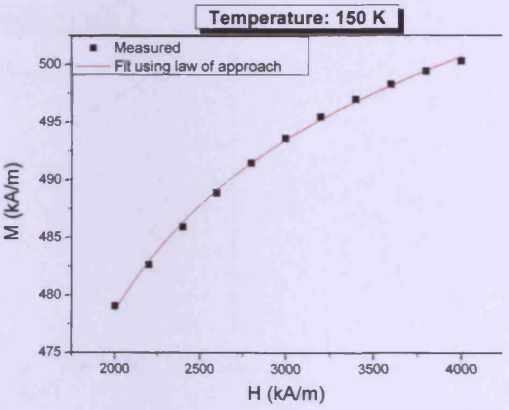
Temperature: 150 K
Measured
Fit using law of approach
M (kA/m)
H (kA/m)

(e)

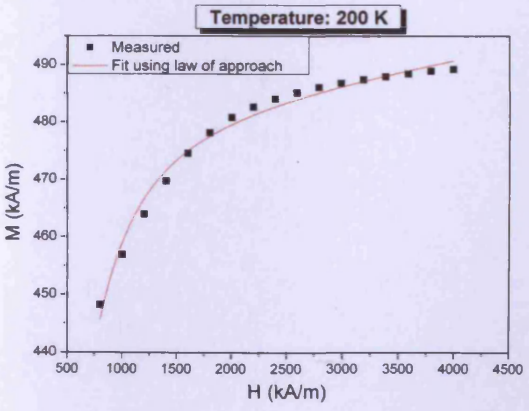
Temperature: 200 K
Measured
Fit using law of approach
M (kA/m)
H (kA/m)

(f)

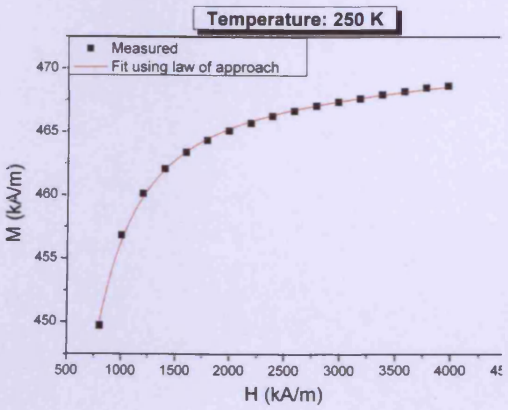
Temperature: 250 K
Measured
Fit using law of approach
M (kA/m)
H (kA/m)

(g) (h)

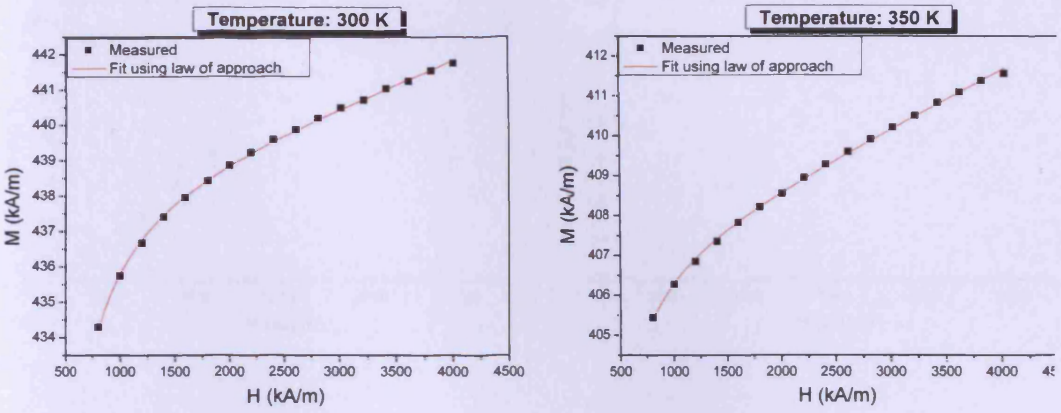

(i)

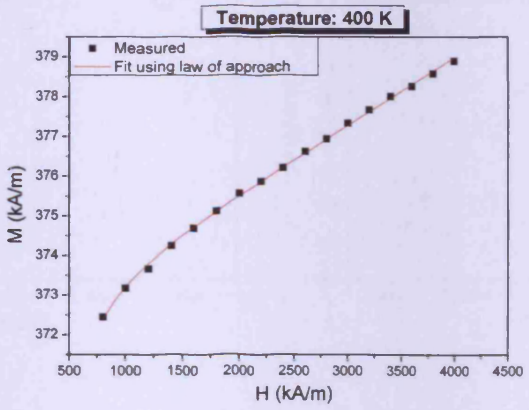

Figure 4-37 Fitting high field region M-H data for $Co_{1.1}Ge_{0.1}Fe_{1.8}O_4$ at temperatures in the range 10 - 400 K.

(a) (b)

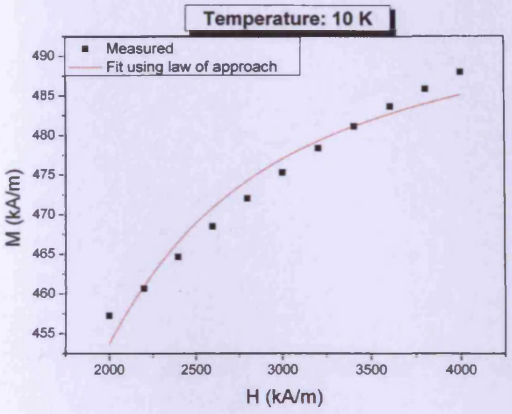
Temperature: 10 K
Measured
Fit using law of approach
M (kA/m)
H (kA/m)

(c)

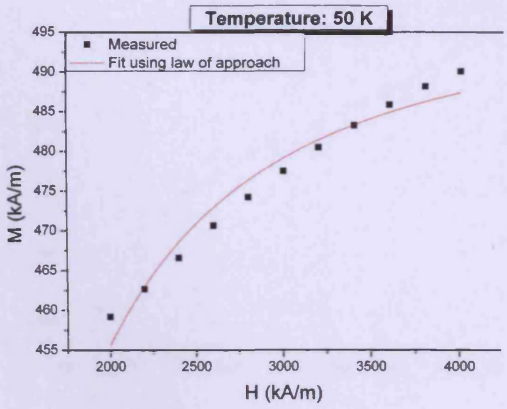
Temperature: 50 K
Measured
Fit using law of approach
M (kA/m)
H (kA/m)

(d)

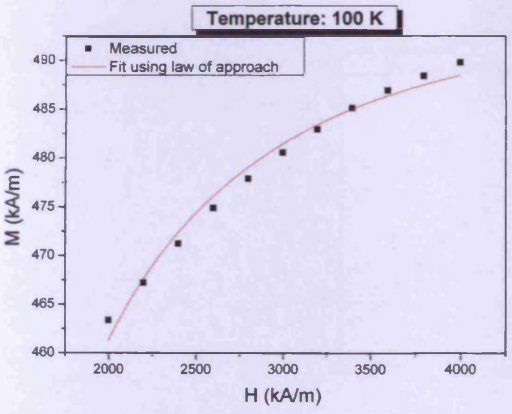
Temperature: 100 K
Measured
Fit using law of approach
M (kA/m)
H (kA/m)

(e)

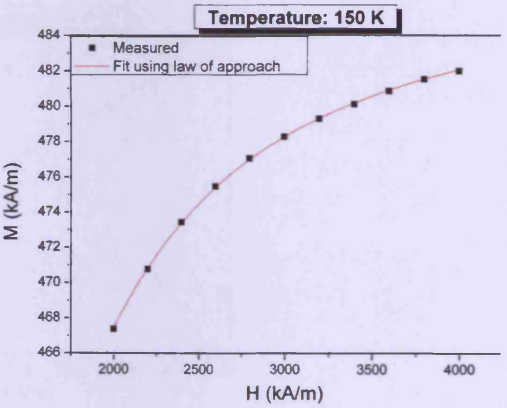
Temperature: 150 K
Measured
Fit using law of approach
M (kA/m)
H (kA/m)

(f)

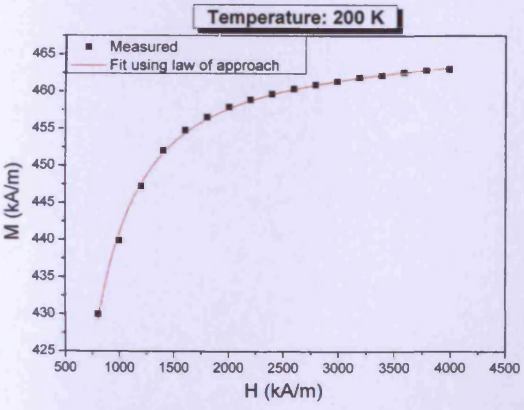
Temperature: 200 K
Measured
Fit using law of approach
M (kA/m)
H (kA/m)

(g)

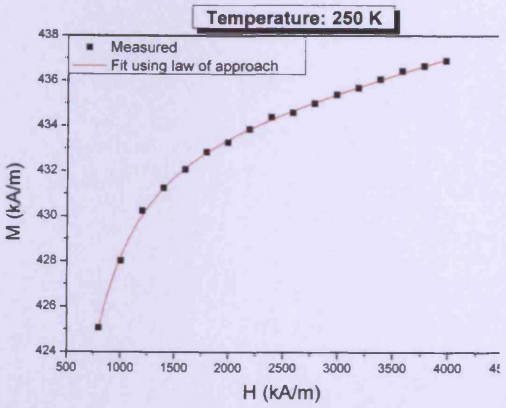
Temperature: 250 K
Measured
Fit using law of approach
M (kA/m)
H (kA/m)

(h)

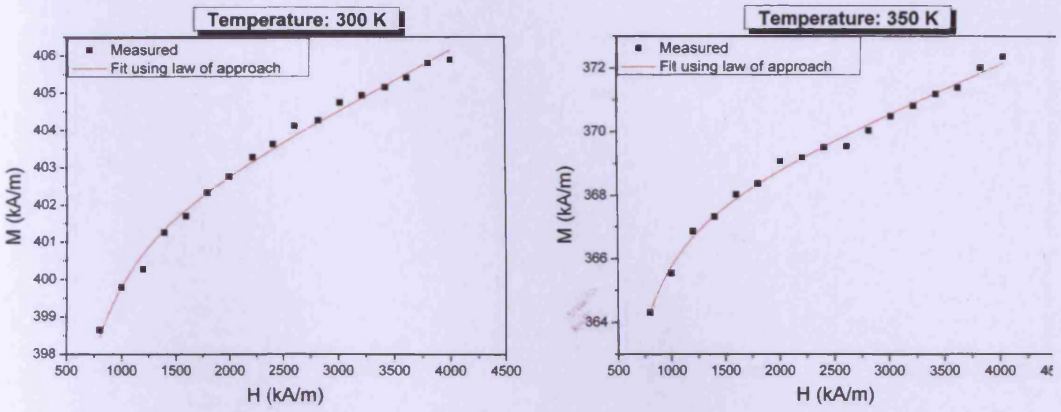

(i)

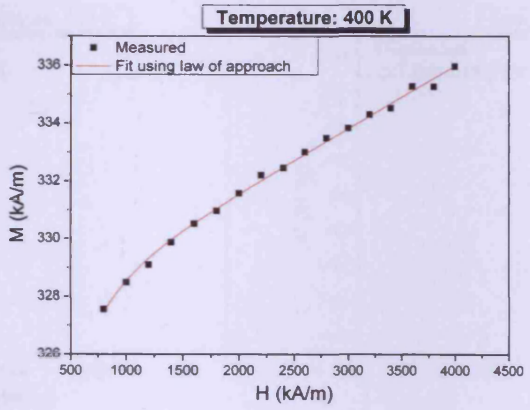

Figure 4-38 Fitting high field region M-H data for $Co_{1.2}Ge_{0.2}Fe_{1.6}O_4$ at temperatures in the range 10 - 400 K.

(a) (b)

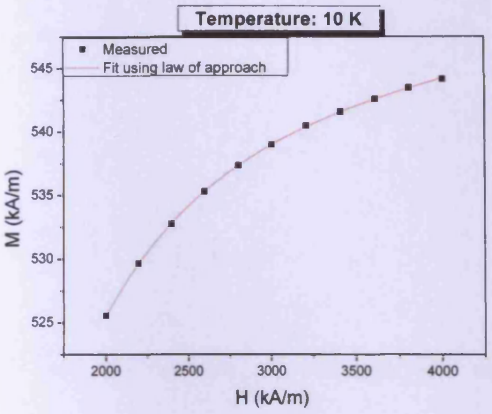
Temperature: 10 K
Measured
Fit using law of approach
M (kA/m)
H (kA/m)

(c)

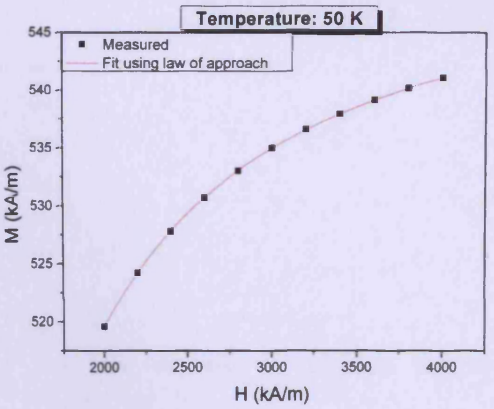
Temperature: 50 K
Measured
Fit using law of approach
M (kA/m)
H (kA/m)

(d)

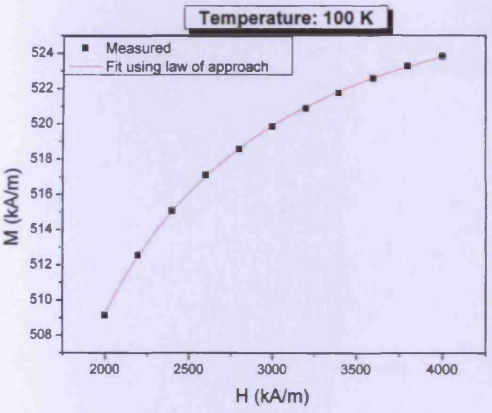
Temperature: 100 K
Measured
Fit using law of approach
M (kA/m)
H (kA/m)

(e)

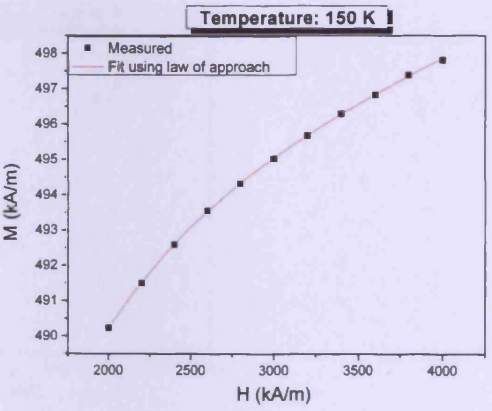
Temperature: 150 K
Measured
Fit using law of approach
M (kA/m)
H (kA/m)

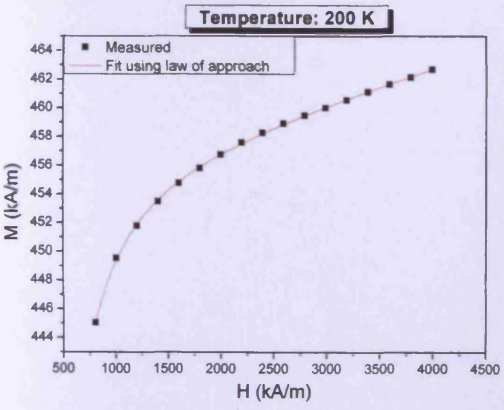
Temperature: 200 K
Measured
Fit using law of approach
M (kA/m)
H (kA/m)

(g)

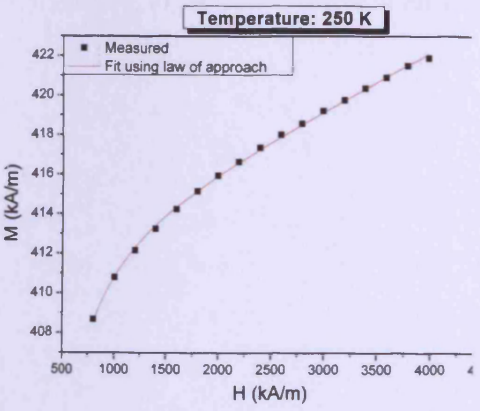
Temperature: 250 K
Measured
Fit using law of approach
M (kA/m)
H (kA/m)

(f)

(h)

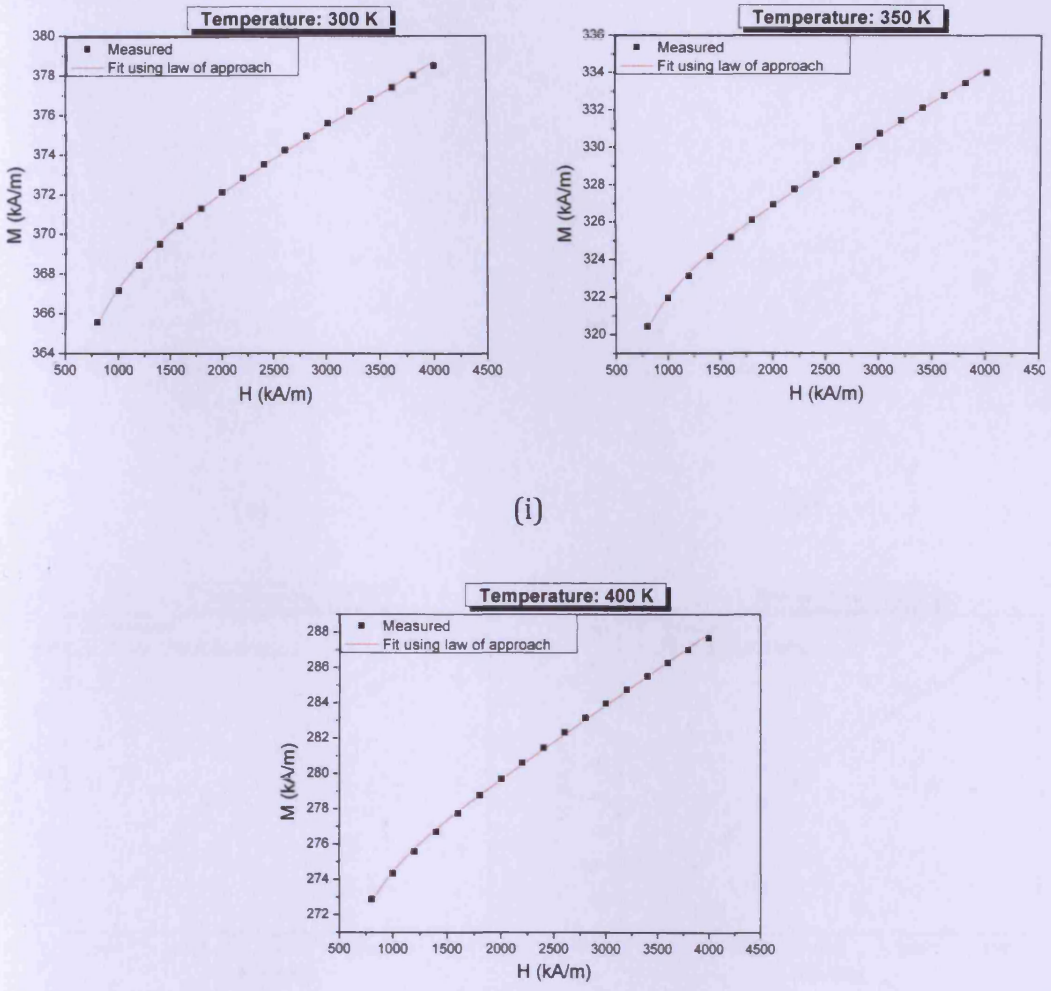

Figure 4-39 Fitting high field region M-H data for $Co_{1.3}Ge_{0.3}Fe_{1.4}O_4$ at temperatures in the range 10 - 400 K.

(a) (b)

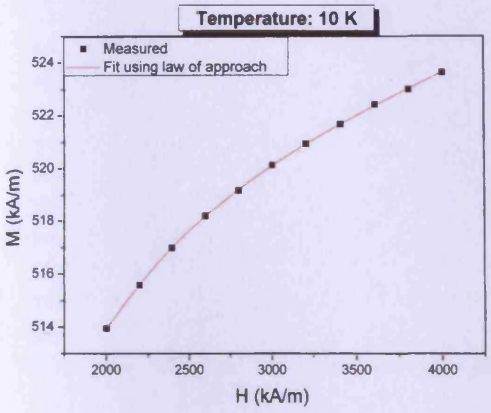
Temperature: 10 K
Measured
Fit using law of approach
M (kA/m)
H (kA/m)

(c)

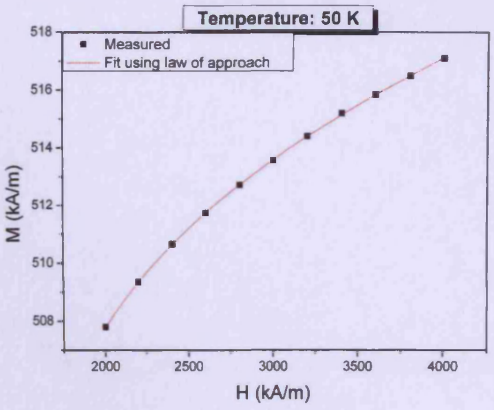
Temperature: 50 K
Measured
Fit using law of approach
M (kA/m)
H (kA/m)

(d)

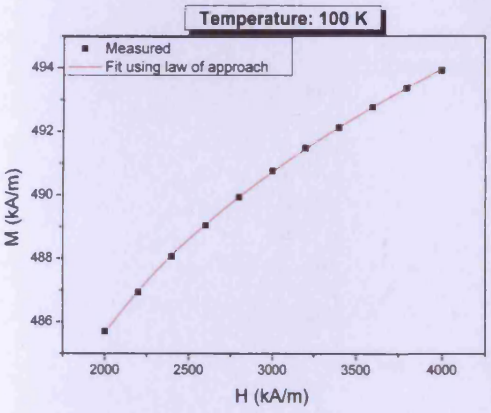
Temperature: 100 K
Measured
Fit using law of approach
M (kA/m)
H (kA/m)

(e)

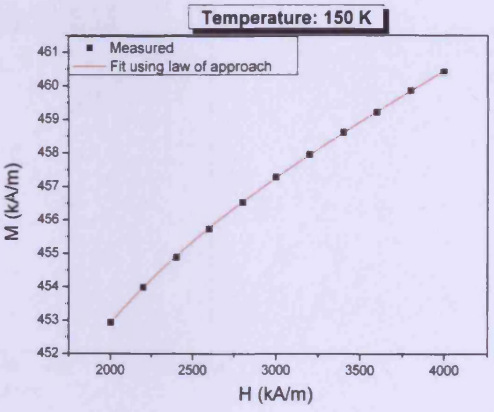
Temperature: 150 K
Measured
Fit using law of approach
M (kA/m)
H (kA/m)

(f)

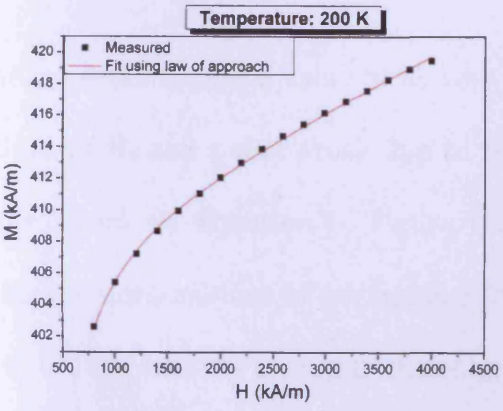
Temperature: 200 K
Measured
Fit using law of approach
M (kA/m)
H (kA/m)

(g)

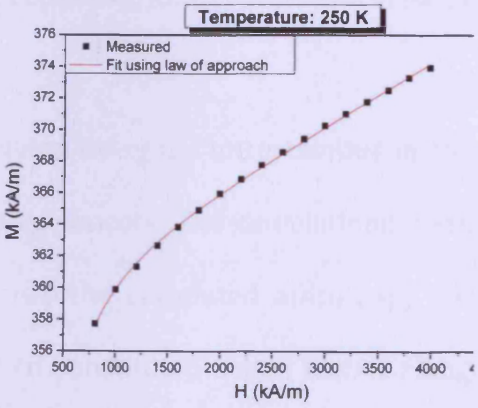
Temperature: 250 K
Measured
Fit using law of approach
M (kA/m)
H (kA/m)

(h)

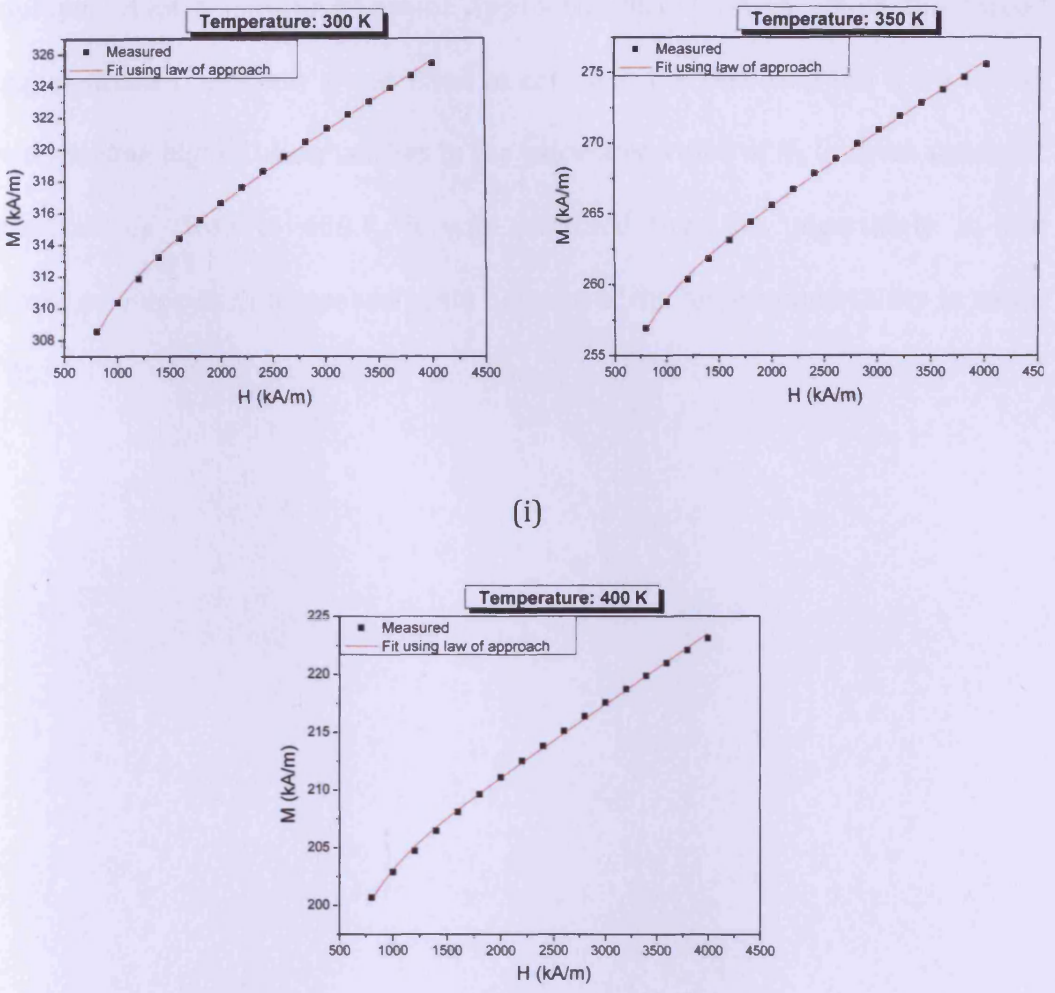

Figure 4-40 Fitting high field region M-H data for $Co_{1.4}Ge_{0.4}Fe_{1.2}O_4$ at temperatures in the range 10 - 400 K.

The uncertainty in the value of K_1 was calculated using the uncertainties in the values of M_s and κ that arose due to the fitting process. The calculations were done based on Equation 4-. Figure 4-41 shows the calculated anisotropy for different compositions of germanium/cobalt co-substituted cobalt ferrite along with the uncertainty arising in the value of K_1 due to the fitting. It was observed that in certain cases where anisotropy was high at low temperatures, the data did not represent a complete rotation of the magnetisation vectors from the anisotropic directions towards the field direction. This called for the

employment of a modified Law of Approach calculation in which the forced magnetisation coefficient κ was fixed to zero and the resulting fits were not as good, causing higher uncertainties in the calculated value of K_1 in these cases. At temperatures close to 400 K, it was observed that the uncertainty in the calculated value of K_1 increased again because of the higher uncertainty in value of M_S.

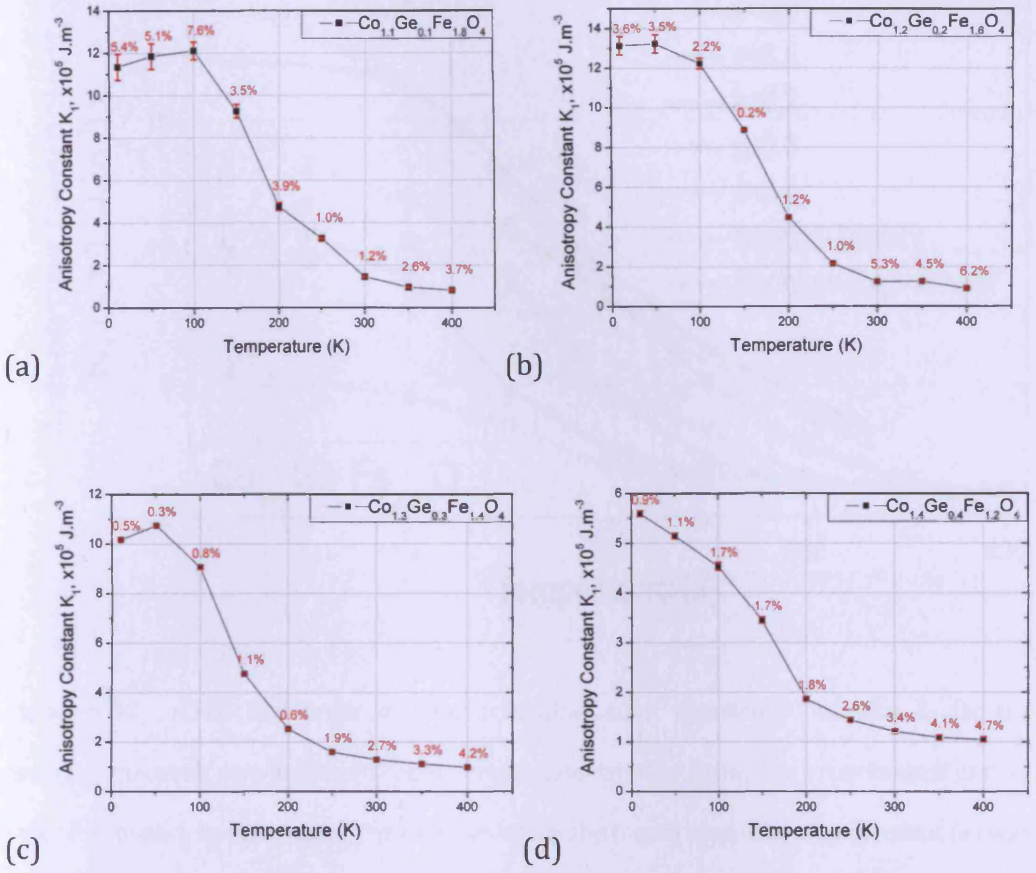

Figure 4-41 The variation of the first order magnetocrystalline anisotropy constant K_1 of germanium/cobalt co-substituted cobalt ferrite with temperature for compositions: (a) $Co_{1.1}Ge_{0.1}Fe_{1.8}O_4$, (b) $Co_{1.2}Ge_{0.2}Fe_{1.6}O_4$, (c) $Co_{1.3}Ge_{0.3}Fe_{1.4}O_4$, and (d) $Co_{1.4}Ge_{0.4}Fe_{1.2}O_4$. The error bars are shown for each point and the labels in red above each point indicate the estimated uncertainty (in percentage) for each point resulting from fitting the high field regions of the M-H loops to the Law of Approach.

Figure 4-42 shows the temperature dependence of the first order magnetocrystalline anisotropy constant K_1 (for randomly oriented polycrystalline cubic materials) with germanium/cobalt substitution. In cases where the calculation was done a forced magnetisation constant (κ) was fixed to zero, the data is shown on the graph connected by dotted lines.

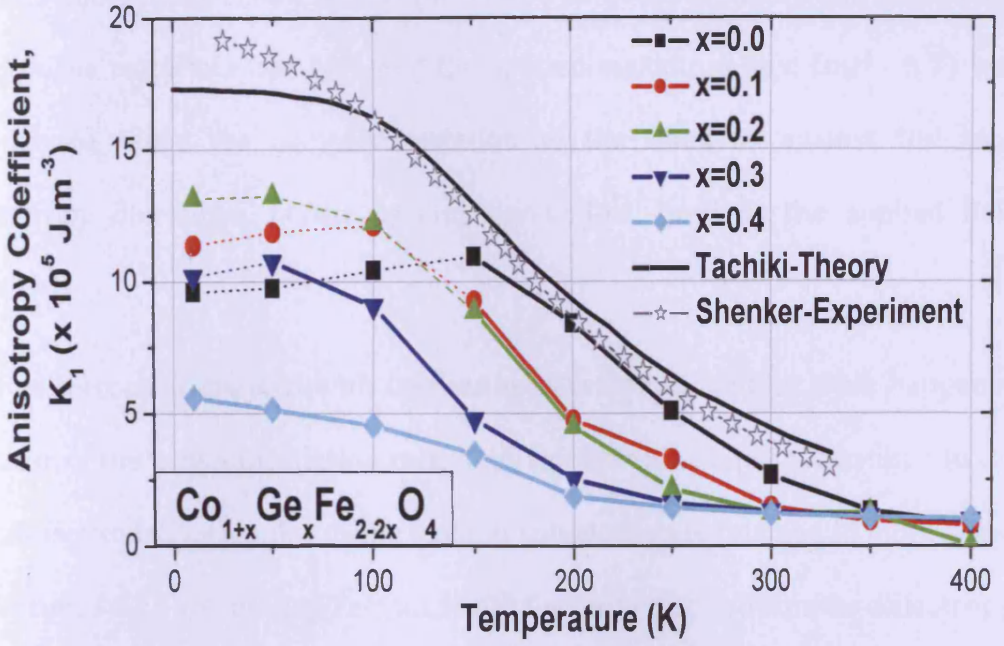

Figure 4-42 The first order magnetocrystalline cubic anisotropy constant K_1 for the germanium/cobalt co-substituted cobalt ferrite, calculated by fitting the experimental data to Law of Approach to saturation. The cases in which the forced magnetisation constant (κ) was assumed to be zero are shown as joined by dotted lines. The experimentally measured data labelled as Shenker-Experiment (Shenker, 1957) and theoretically predicted data marked as Tachiki-Theory (Tachiki, 1960) are shown for comparison.

The anisotropy increased with decreasing temperatures for all the compositions in the range 10 – 400 K. Starting from 400 K, the anisotropy increased slowly with decreasing temperatures until a temperature after which it increased steeply with any further reduction in temperature. The beginning of the steep slope occurred at progressively lower temperatures with increasing germanium content. For samples with germanium contents x = 0.0, 0.1, 0.2, and 0.3, the graph shows the anisotropy peaking at a certain temperature. This feature is an apparent artefact arising from the fact that the assumptions of the Law of Approach do not hold entirely for these calculations. As in the case of the

gallium-substituted cobalt ferrite (described in Section 4.02.5), the anisotropy field of the materials was high and the applied maximum field ($\mu_0 H$ = 5 T) was enough to cause the complete rotation of the domains against the local anisotropy directions, in the various crystallites, towards the applied field direction.

The anisotropy decreased with increasing germanium content. This happened because of the magnetic dilution caused by the introduction of germanium in the cobalt ferrite lattice similar to the gallium substitution (explained in more detail in Section 4.02.5). Replacing Fe^{3+} ions with Co^{2+} ions also reduces the anisotropy, although not as radically as in the case of substituting Ge^{4+} ions for Fe^{3+} ions.

4.03.6 Magnetostriction vs applied field for germanium/cobalt co-substituted cobalt ferrite

The magnetostriction vs the applied field characteristics were measured for all samples and were standardised according to the procedures described in Chapter 3. The room temperature data for polycrystalline pure cobalt ferrite has been obtained from Paulsen (Paulsen et al., 2005).

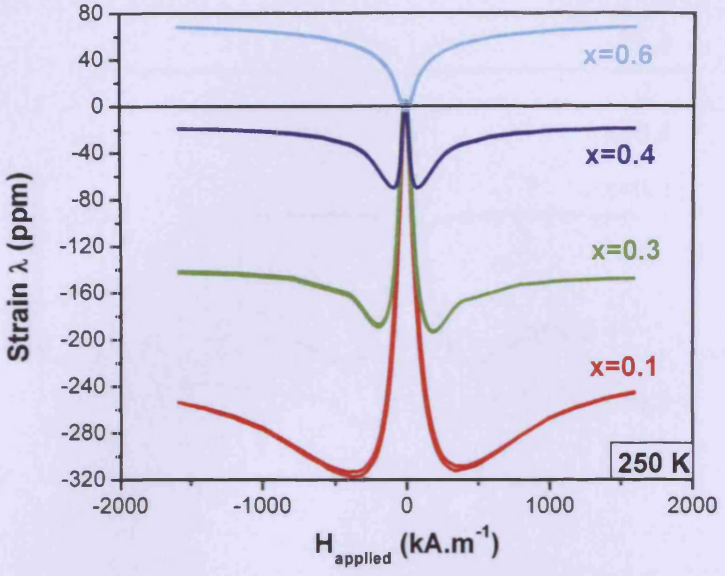

(a)

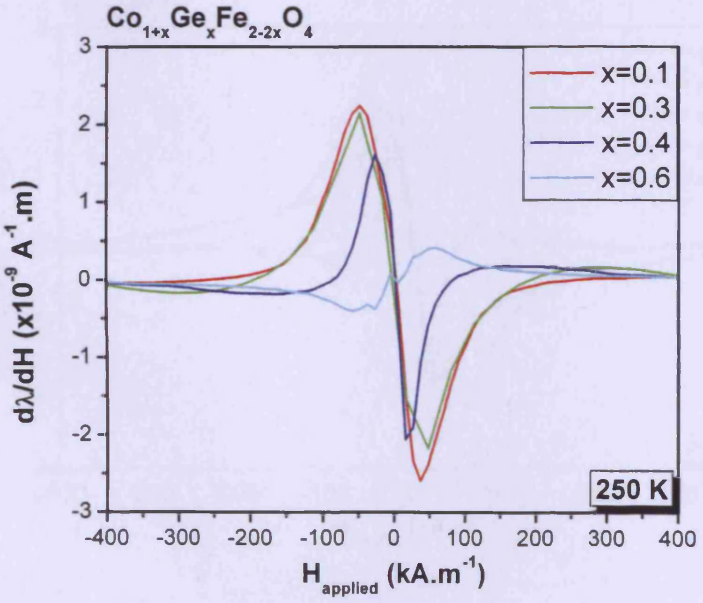

(b)

Figure 4-43 Magnetostrictive properties of germanium/cobalt co-substituted cobalt ferrite at 250 K. (a) Field induced magnetostrictive strain (b) Strain derivative

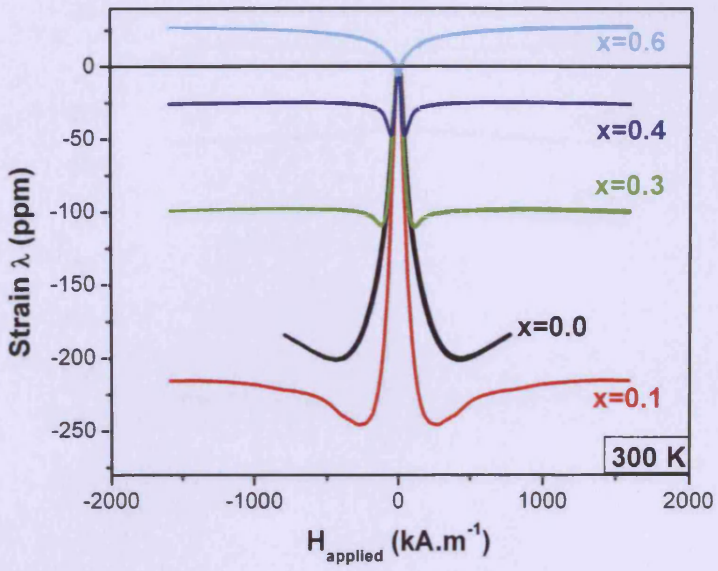

(a)

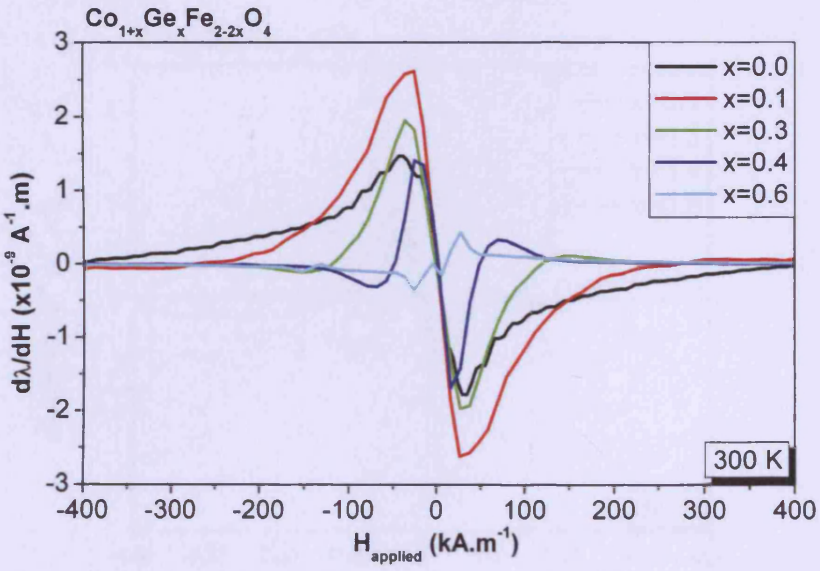

(b)

Figure 4-44 Magnetostrictive properties of germanium/cobalt co-substituted cobalt ferrite at 300 K. (a) Field induced magnetostrictive strain (b) Strain derivative

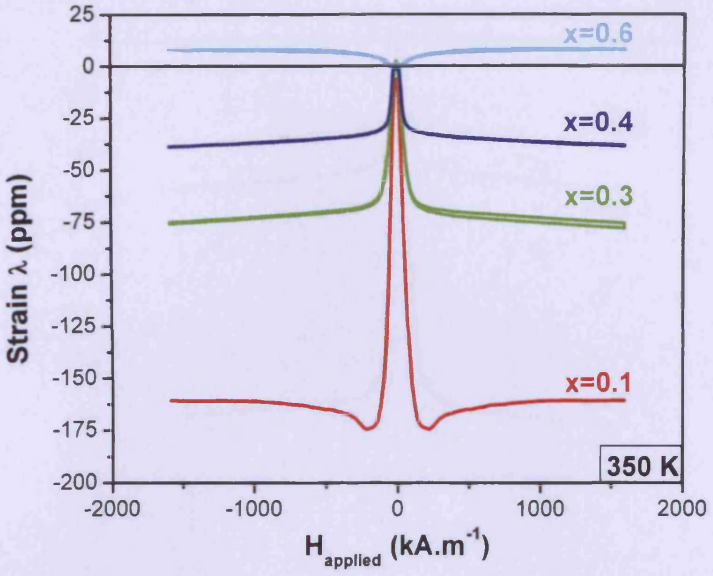

(a)

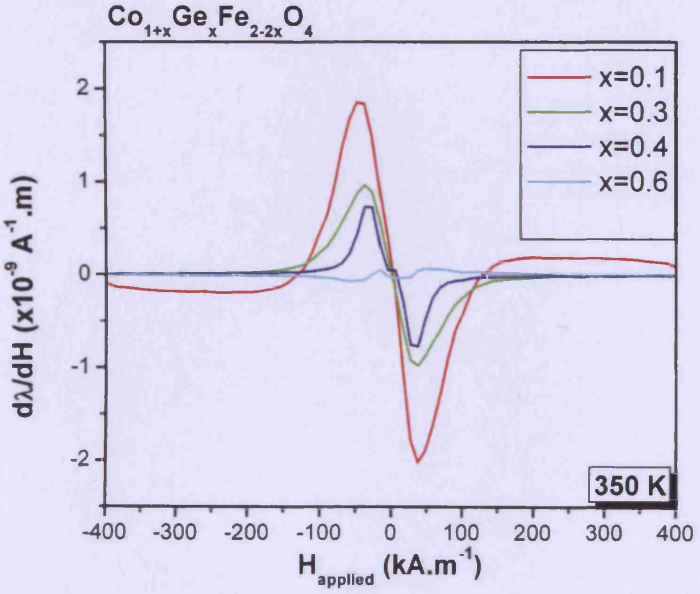

(b)

Figure 4-45 Magnetostrictive properties of germanium/cobalt co-substituted cobalt ferrite at 350 K. (a) Field induced magnetostrictive strain (b) Strain derivative

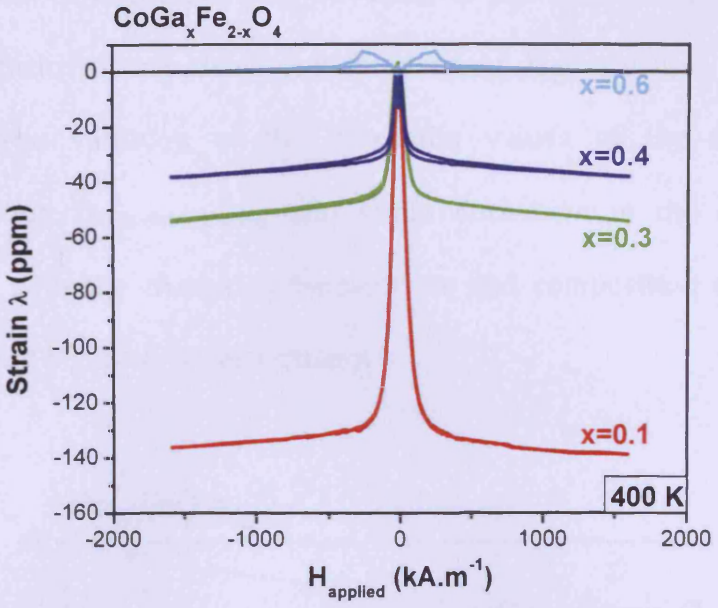

(a)

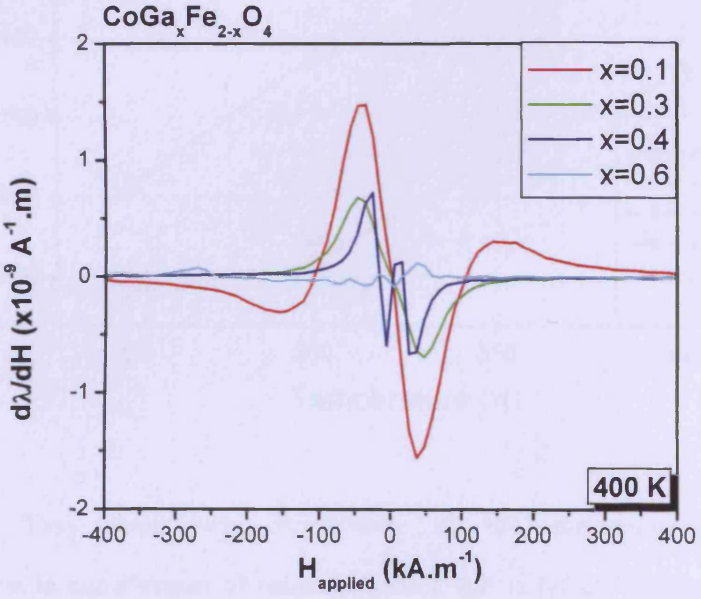

(b)

Figure 4-46 Magnetostrictive properties of germanium/cobalt co-substituted cobalt ferrite at 400 K. (a) Field induced magnetostrictive strain (b) Strain derivative

The magnetostriction curves were observed in all four different shapes shown in Figure 4-24 and Figure 4-25. The reason for the occurrence of these shapes is the

relative change in magnitude and direction of the contributions of the field induced magnetostrictive strain contributions of λ_{100} and λ_{111}, as explained previously. The variation of the maximum values of the field induced magnetostriction ($\lambda_{max,\ linear\ region}$) and strain derivative in the linear region ($(d\lambda/dH)_{max}$) with the change in temperature and composition are shown in Figure 4-47 and Figure 4-48 respectively.

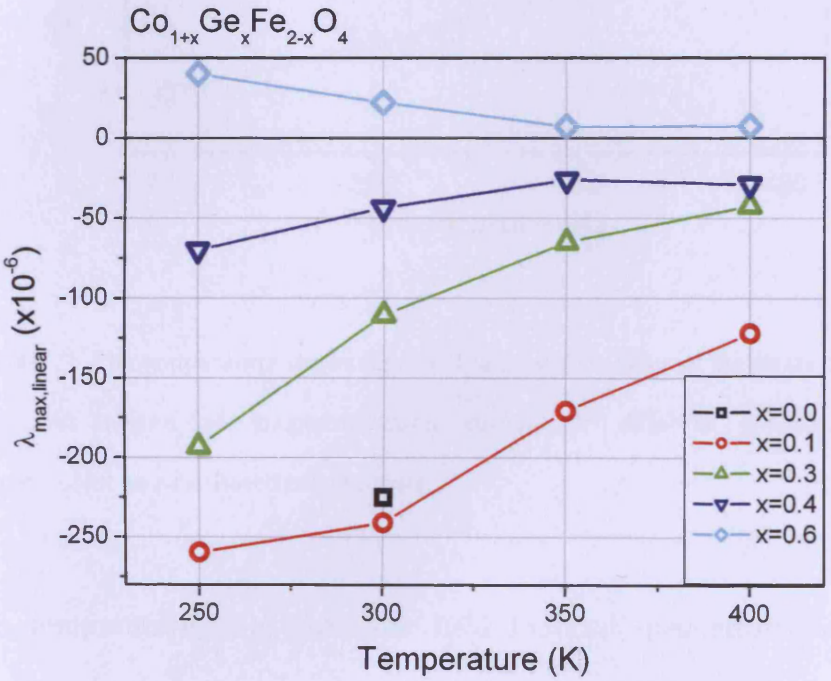

Figure 4-47 The temperature dependence of the maximum field induced magnetostriction in linear region of magnetostriction curves for different compositions of germanium/cobalt co- substituted cobalt ferrite.

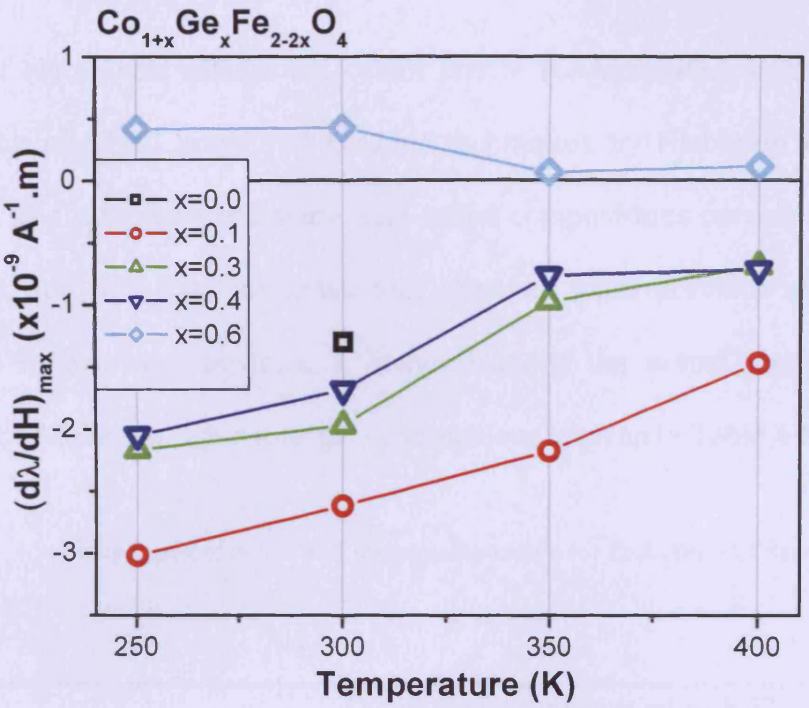

Figure 4-48 The temperature dependence of the maximum value of the strain derivative in the linear region of magnetostriction curves for different compositions of germanium/cobalt co-substituted cobalt ferrite.

At room temperature, the maximum field induced magnetostrictive strain ($\lambda_{max,\ linear\ region}$ = 241 ppm) for $Co_{1.1}Ge_{0.1}Fe_{1.8}O_4$ was higher than those of any chemically substituted cobalt ferrite investigated in this study and that of pure cobalt ferrite. It was equal to 107% of the maximum field induced magnetostrictive strain of pure cobalt ferrite at room temperature, which is the second highest. The maximum strain derivative of $Co_{1.1}Ge_{0.1}Fe_{1.8}O_4$ was also higher than that of pure cobalt ferrite (202%). The strain derivative of $Co_{1.1}Ge_{0.1}Fe_{1.8}O_4$ was 96% of the value for $CoGa_{0.2}Fe_{1.8}O_4$, but the $\lambda_{max,\ linear\ region}$ for $Co_{1.1}Ge_{0.1}Fe_{1.8}O_4$ was 126% of the value for $CoGa_{0.2}Fe_{1.8}O_4$.

4.04 Aluminium substitution

A series of aluminium substituted cobalt ferrite ($CoAl_xFe_{2-x}O_4$) samples were prepared by standard powdered ceramic techniques by Nlebedim of Cardiff University. The samples were made with target compositions corresponding to x = 0.1, 0.2, and 0.5. Data for x=0.0 was obtained from previous studies, as mentioned in previous sections. A comparison of the actual compositions, measured by Nlebedim, against target compositions is given in Table 4-5.

Table 4-5 Comparison of actual and target composition for $CoAl_xFe_{2-x}O_4$ (Ranvah *et al.*, 2009).

Target Composition	Composition determined by EDS		
	Co	Fe	Al
$CoFe_2O_4$	0.95	2.05	—
$CoAl_{0.1}Fe_{1.9}O_4$	1.03	1.89	0.08
$CoAl_{0.2}Fe_{1.8}O_4$	1.03	1.78	0.18
$CoAl_{0.5}Fe_{1.5}O_4$	1.03	1.48	0.49

4.04.1 Site preference of aluminium substituted cobalt ferrite

The site preference of Al^{3+} ions in the spinel lattice has been studied for aluminium substituted Mn-Ni-Zn ferrite ($Mn_{0.5}Ni_{0.1}Zn_{0.4}Al_xFe_{2-x}O_4$) prepared by ceramic methods (Sattar *et al.*, 2005). It was reported that aluminium does not have a strong preference for either of the A or B sites and distributes more or less randomly. This confirms the results on the site preference of aluminium in aluminium substituted copper ferrite, which is also an inverse spinel (Kulkarni *et al.*, 1996).

4.04.2 Curie temperature of aluminium substituted cobalt ferrite

The Curie temperature (T_c) for aluminium substituted cobalt ferrite, shown in Figure 4-49, has been observed to decrease linearly with increasing aluminium content (Nlebedim et al., 2010). Similar trends have been observed for other substitutions in cobalt ferrite (Ranvah et al., 2008b, Ranvah *et al.*, 2008a, Paulsen et al., 2005, Lee et al., 2007).

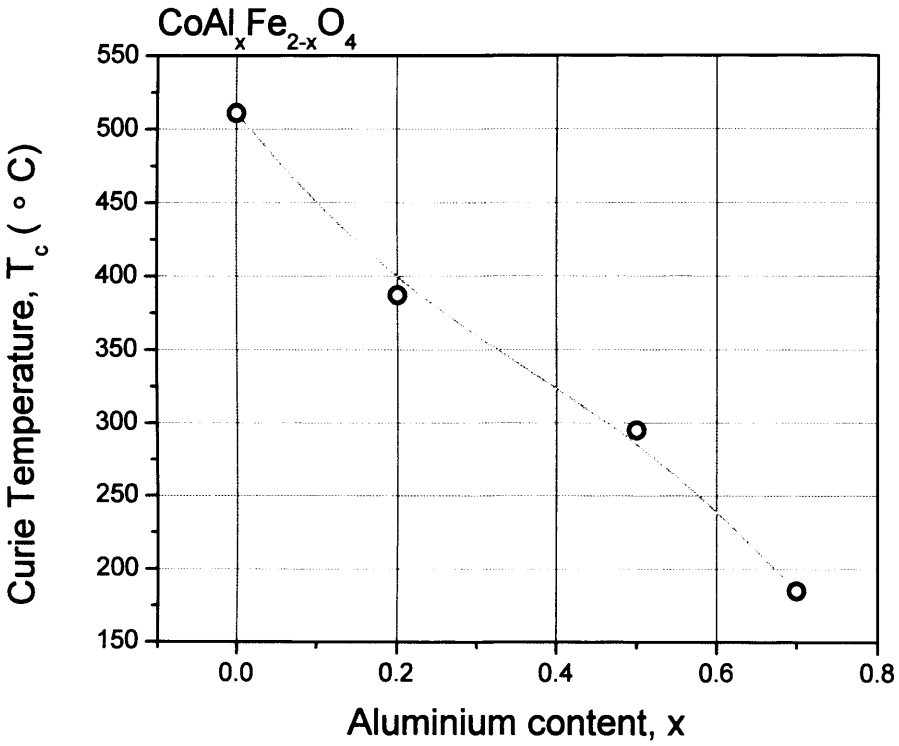

Figure 4-49 Variation of the Curie temperature of aluminium-substituted cobalt ferrite (Nlebedim *et al.*, 2010). The markers show the actual experimental data.

4.04.3 Maximum Magnetisation vs Temperature for aluminium substituted cobalt ferrite

The variation of the maximum magnetisation with temperature at constant field ($\mu_0 H = 5$ T) was measured in the temperature range of 10 – 400 K for all the samples.

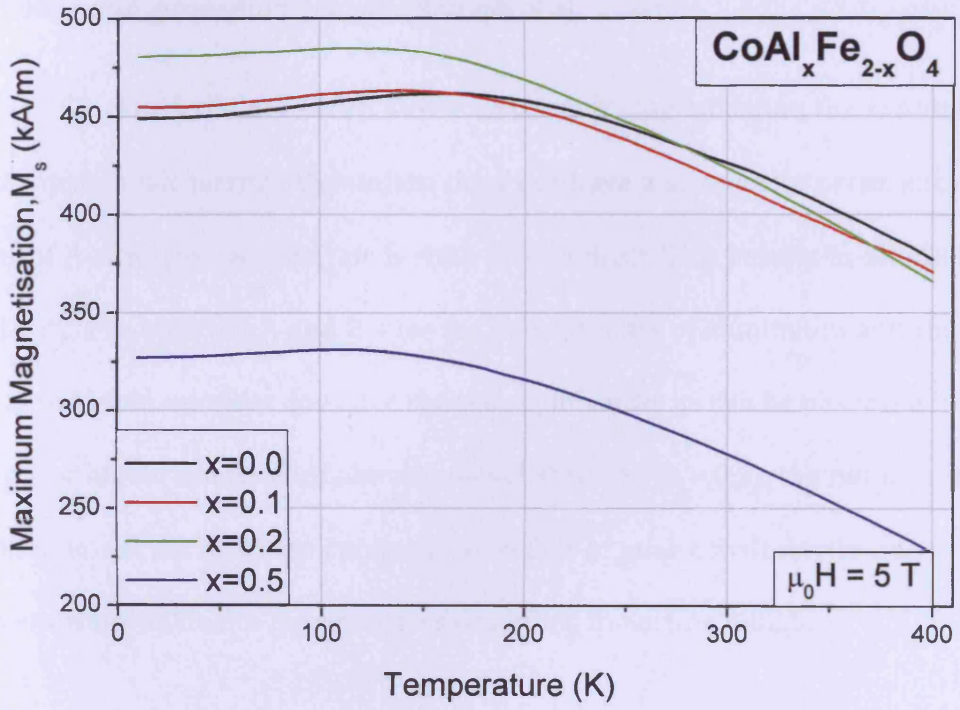

Figure 4-50 Variation of the maximum magnetisation of $CoAl_xFe_{2-x}O_4$ with temperature.

The trends recorded for maximum magnetisation are shown in Figure 4-50. The maximum magnetisation increased monotonically for all compositions as the temperature decreased from 400 to 160 K. Below 160 K, the maximum magnetisation either increased slowly or decreased slowly with decreasing temperature. The maximum magnetisation peaked at 160 K for $CoFe_2O_4$, at 140 K for $CoAl_{0.1}Fe_{1.9}O_4$, at 110 K for $CoAl_{0.2}Fe_{1.8}O_4$, and at 100 K for $CoAl_{0.1}Fe_{1.9}O_4$. This

apparent decrease in the maximum magnetisation with decreasing temperature can be explained by the presence of a high anisotropy field, which prevents complete rotation of the domain magnetisations from their local anisotropy directions towards the applied field direction. Similar trends have been observed in the case of the substitution of some of iron in cobalt ferrite with manganese (Melikhov et al., 2006a), chromium (Melikhov et al., 2006b), gallium (Ranvah et al., 2008a), and germanium/cobalt (Ranvah et al., 2008b).

Figure 4-51 shows the near zero Kelvin maximum magnetisation for aluminium substituted cobalt ferrite. Aluminium does not have a strong site preference for either of A-sites (tetrahedral) or B-sites (octahedral). This results in aluminium substituting in both the A and B sites for low amounts of aluminium and the net near zero Kelvin moment does not change significantly as can be observed in the figure. For higher amounts of aluminium substitution (x = 0.5), the net near zero Kelvin moment decreases in comparison to that of pure cobalt ferrite due to the magnetic dilution due to the processes described in Section 4.02.5.

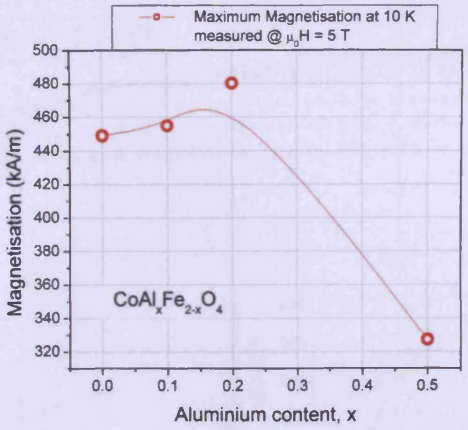

Figure 4-51 Near Zero Kelvin moment of aluminium-substituted cobalt ferrite.

4.04.4 Magnetisation loops at different temperatures for aluminium substituted cobalt ferrite

Magnetisation loops were measured for all the samples in the temperature range of 10 – 400 K. Figure 4-52 - Figure 4-54 show the magnetisation loops at temperatures: 10, 50, 100, 150, 200, 250, 300, 350, & 400 K, for samples with Al-content x = 0.1, 0.2, and 0.5 respectively.

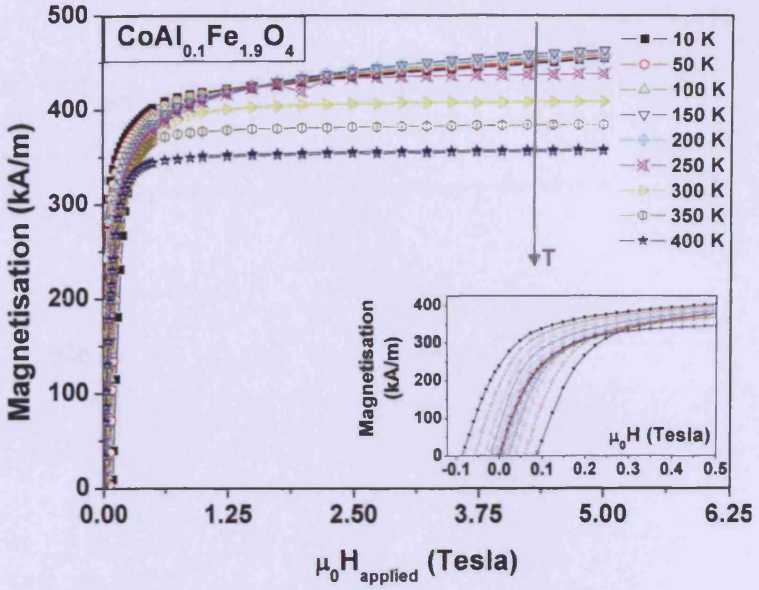

Figure 4-52 First quadrant of the magnetisation vs temperature curves for $CoAl_{0.1}Fe_{1.9}O_4$. Inset shows the low field regions of the magnetisation curves which were used for calculation of the coercive field.

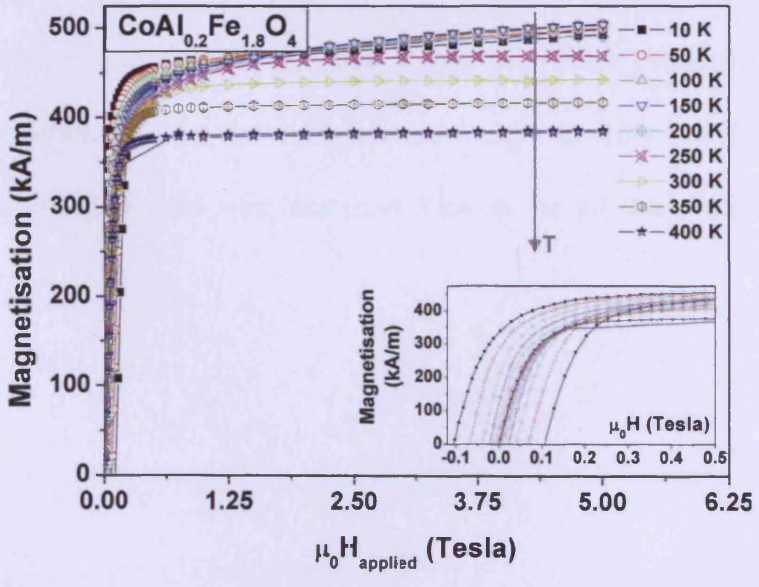

Figure 4-53 First quadrant of the magnetisation vs temperature curves for $CoAl_{0.2}Fe_{1.8}O_4$. Inset shows the low field regions of the magnetisation curves which were used for calculation of the coercive field.

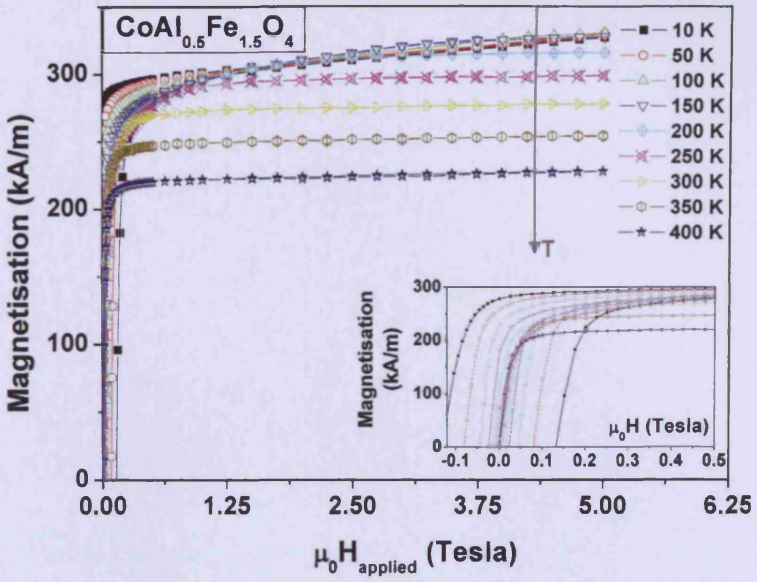

Figure 4-54 First quadrant of the magnetisation vs temperature curves for $CoAl_{0.5}Fe_{1.5}O_4$. Inset shows the low field regions of the magnetisation curves which were used for calculation of the coercive field.

The coercive field of aluminium substituted cobalt ferrite was calculated from the magnetisation loops. The coercive fields increased monotonically with decreasing temperature in the temperature range of 10 – 400 K for all the samples. The coercive field was less than 3 kA/m for all the samples at room temperature.

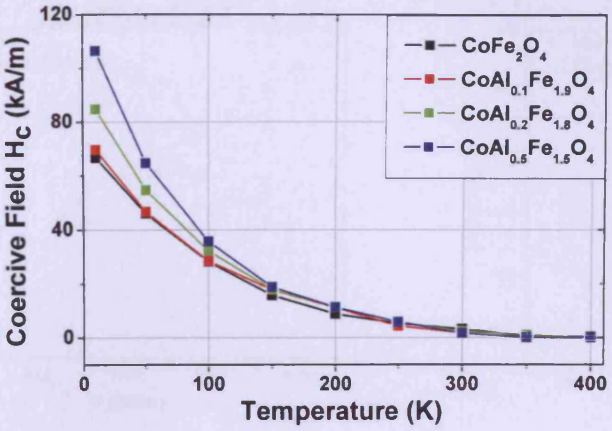

Figure 4-55 The variation of the coercive field of $CoAl_xFe_{2-x}O_4$ with temperature.

4.04.5 Anisotropy vs Temperature for aluminium substituted cobalt ferrite

The anisotropy of $CoAl_xFe_{2-x}O_4$ was calculated by fitting the high field regions of the M-H loops to the Law of Approach to Saturation. The fitting for compositions from x = 0.1 to x = 0.5 is shown in Figure 4-56 - Figure 4-58. Uncertainty in the values of K_1 that arose due to the fitting was calculated based on the values of M_s and κ using Equation 4-. Figure 4-59 shows the calculated anisotropy for different compositions of aluminium substituted cobalt ferrite. The diagram also shows the uncertainty arising in the value of K_1 due to the fitting.

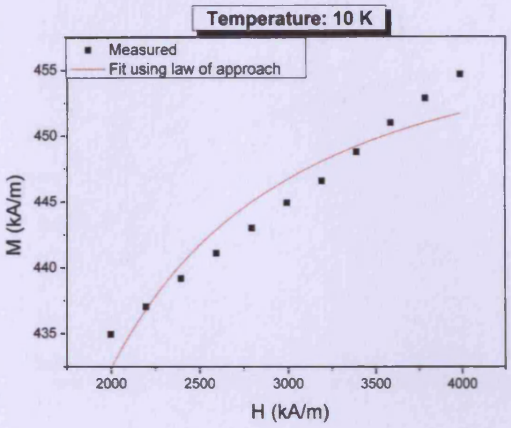
Temperature: 10 K
Measured
Fit using law of approach
M (kA/m)
H (kA/m)

(a)

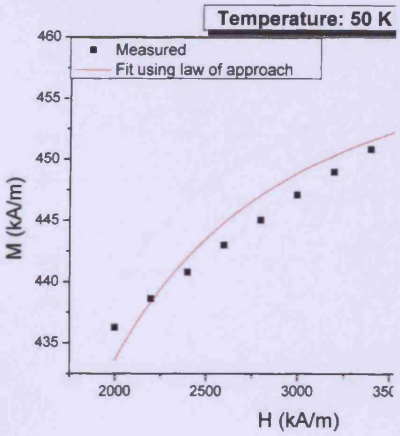
Temperature: 50 K
Measured
Fit using law of approach
M (kA/m)
H (kA/m)

(b)

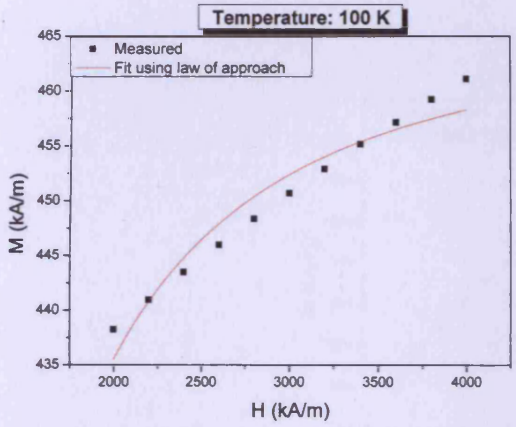
Temperature: 100 K
Measured
Fit using law of approach
M (kA/m)
H (kA/m)

(c)

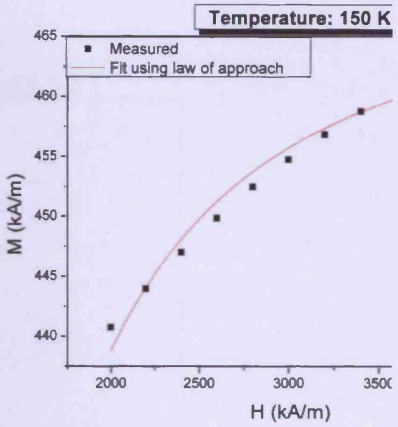
Temperature: 150 K
Measured
Fit using law of approach
M (kA/m)
H (kA/m)

(d)

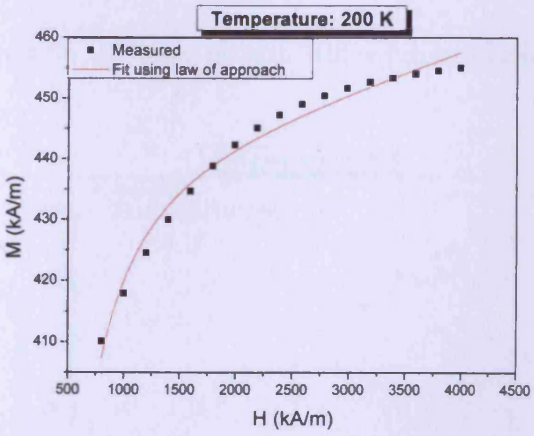
Temperature: 200 K
Measured
Fit using law of approach
M (kA/m)
H (kA/m)

(e)

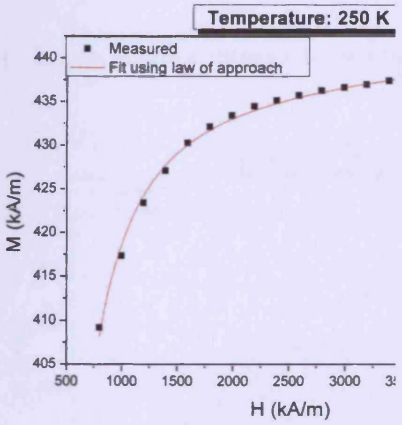
Temperature: 250 K
Measured
Fit using law of approach
M (kA/m)
H (kA/m)

(f)

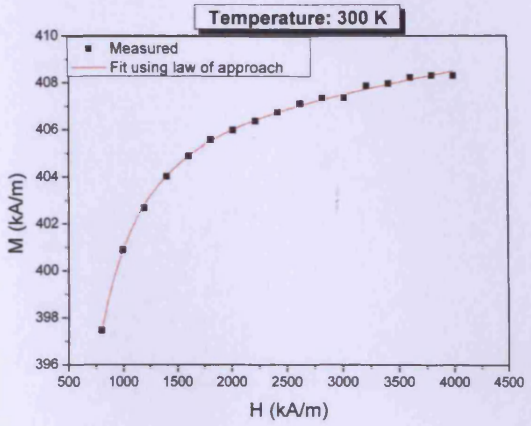

(g)

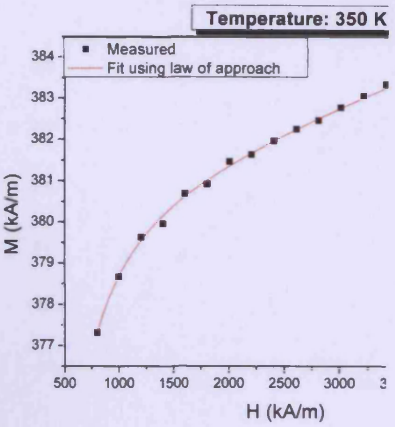

(h)

(i)

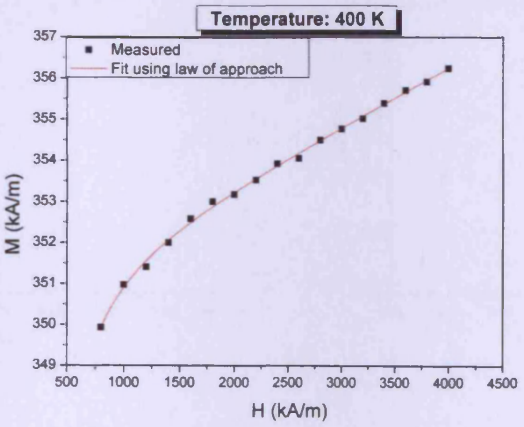

Figure 4-56 Fitting the high field region M-H data for $CoAl_{0.1}Fe_{1.9}O_4$ at temperatures in the range 10 - 400 K.

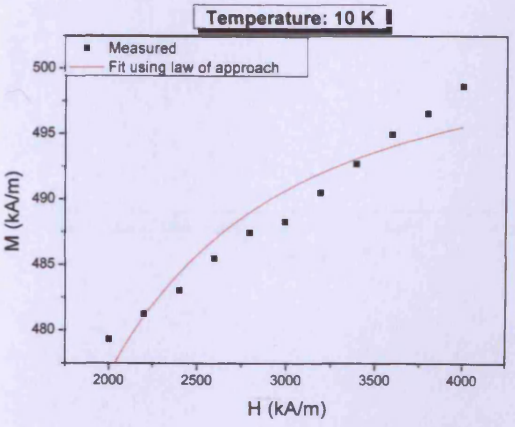

(a)

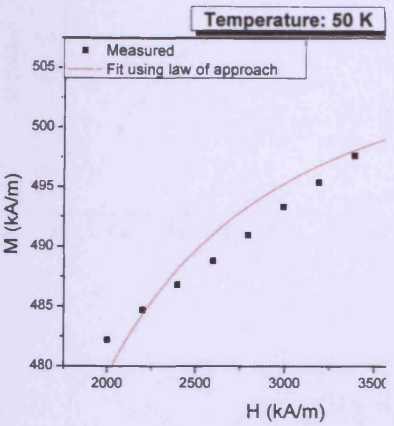

(b)

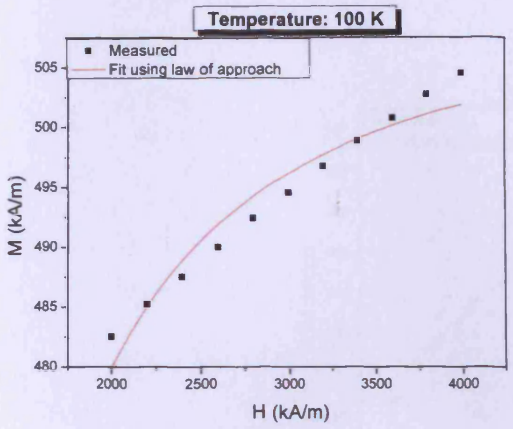
Temperature: 100 K
Measured
Fit using law of approach
M (kA/m)
H (kA/m)

(c)

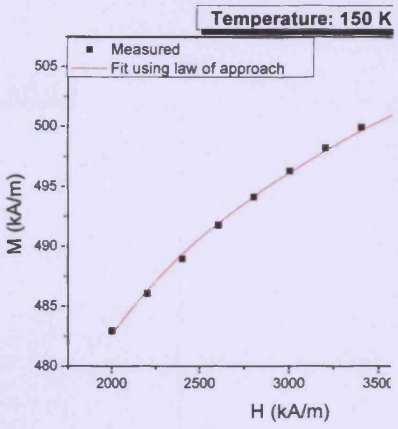
Temperature: 150 K
Measured
Fit using law of approach
M (kA/m)
H (kA/m)

(d)

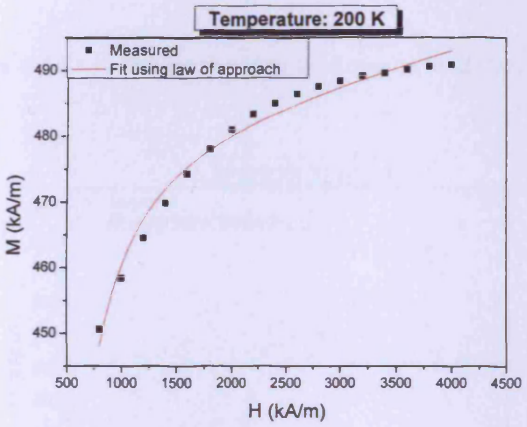
Temperature: 200 K
Measured
Fit using law of approach
M (kA/m)
H (kA/m)

(e)

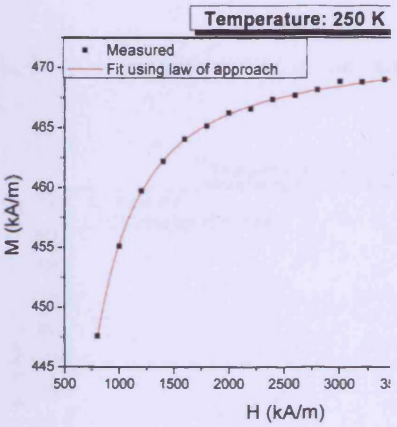
Temperature: 250 K
Measured
Fit using law of approach
M (kA/m)
H (kA/m)

(f)

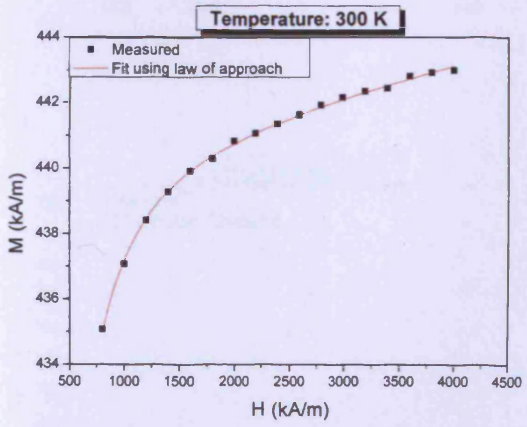
Temperature: 300 K
Measured
Fit using law of approach
M (kA/m)
H (kA/m)

(g)

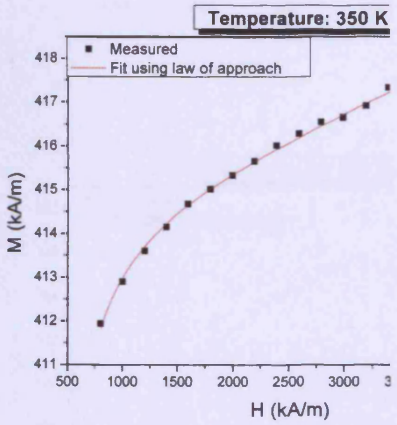
Temperature: 350 K
Measured
Fit using law of approach
M (kA/m)
H (kA/m)

(h)

(i)

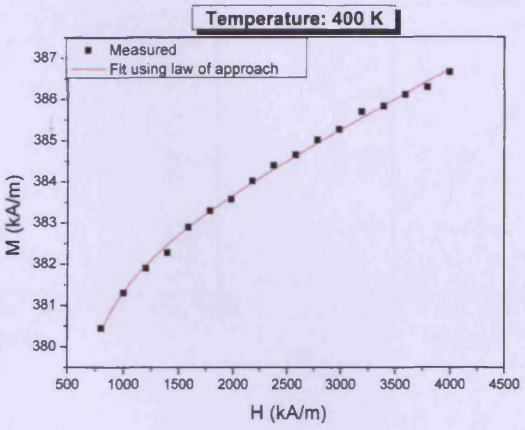

Figure 4-57 Fitting the high field region M-H data for $CoAl_{0.2}Fe_{1.8}O_4$ at temperatures in the range 10 - 400 K.

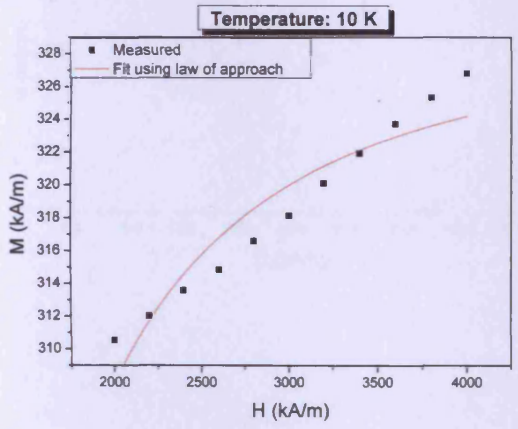

(a)

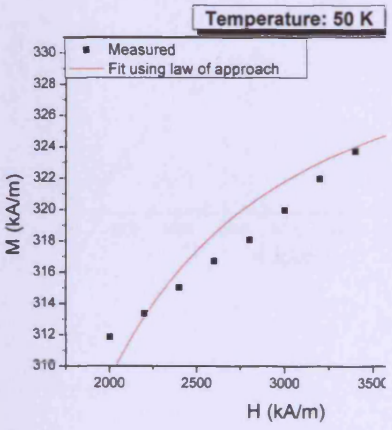

(b)

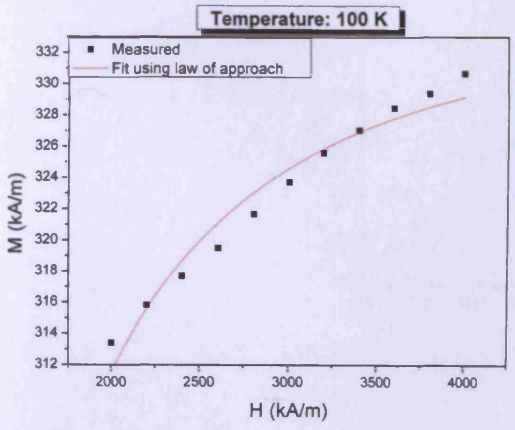

(c)

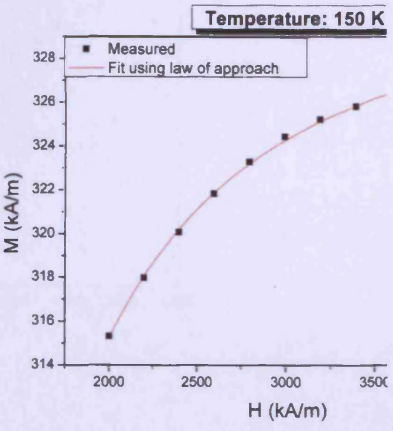

(d)

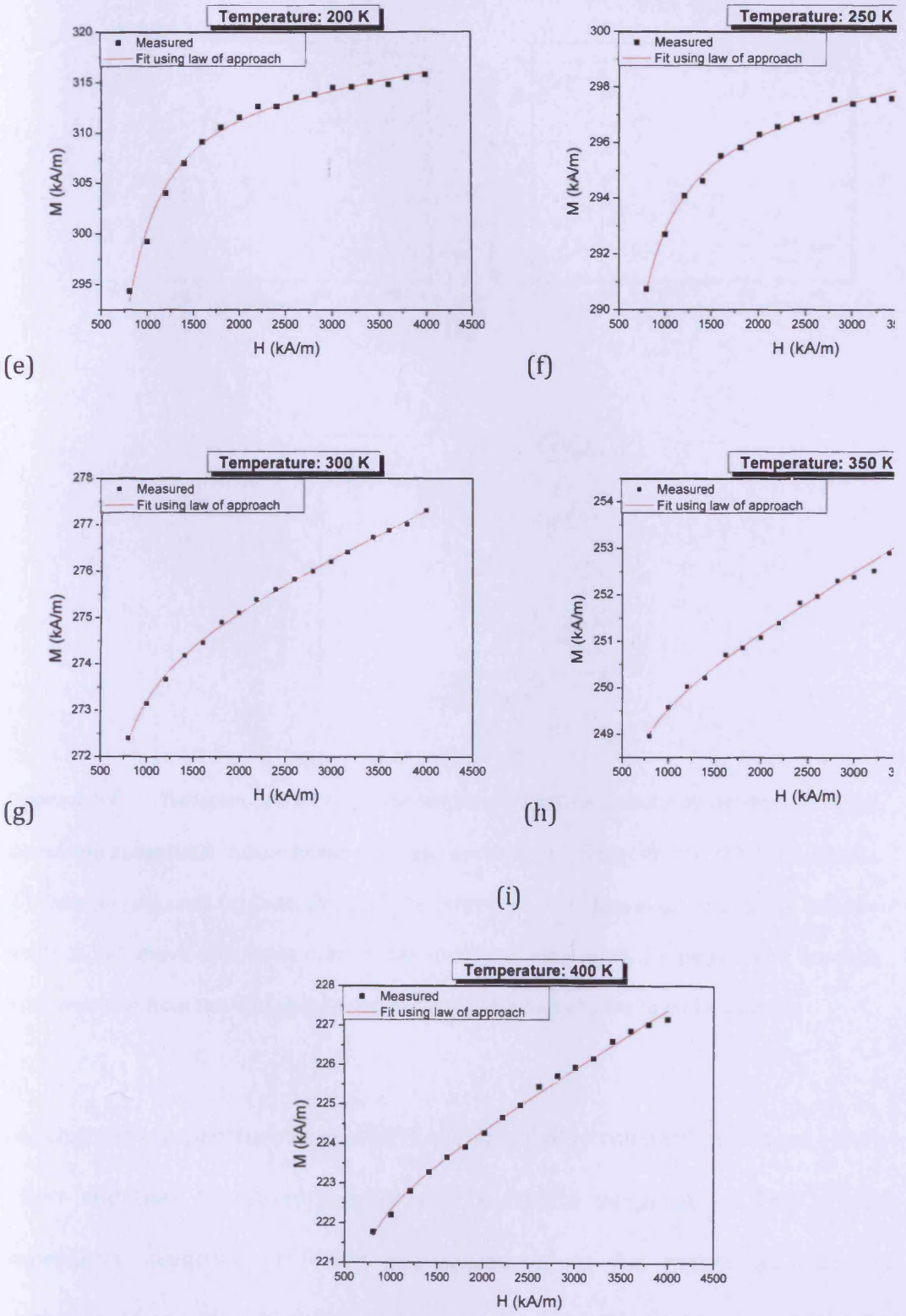

Figure 4-58 Fitting the high field region M-H data for $CoAl_{0.5}Fe_{1.5}O_4$ at temperatures in the range 10 - 400 K.

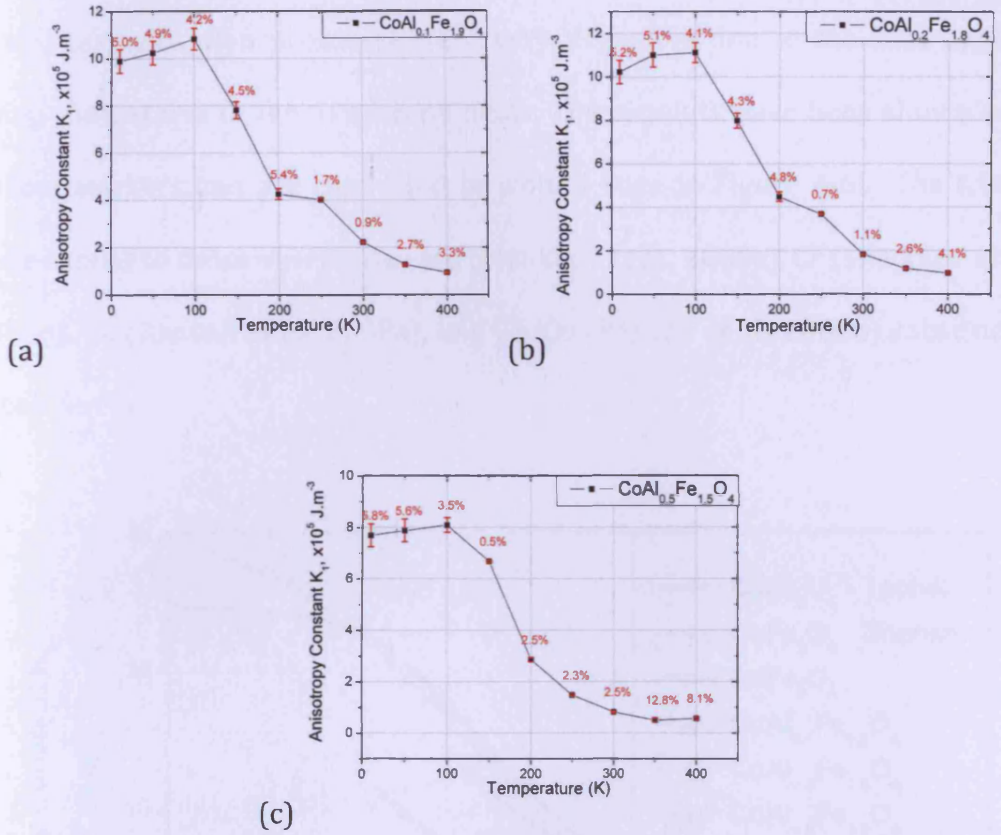

Figure 4-59 Variation of the first order magnetocrystalline anisotropy constant K_1 of the aluminium-substituted cobalt ferrite with temperature for compositions: (a) $CoAl_{0.1}Fe_{1.9}O_4$, (b) $CoAl_{0.2}Fe_{1.8}O_4$, and (c) $CoAl_{0.5}Fe_{1.5}O_4$. The error bars are shown for each point and the labels in red above each point indicate the estimated uncertainty (in percentage) for each point resulting from fitting high field regions of the M-H loops to the Law of Approach.

Reducing the temperature from 400 K, the anisotropy constant increased slowly at first and then increased rapidly after a critical temperature. This critical temperature occurred at lower and lower values for higher amounts of aluminium. It was observed that at low temperatures, the field was not able to cause complete rotation of the domain magnetisations from their local anisotropy directions towards the field direction. In such cases, the Law of

Approach was modified to fix the value of $\kappa = 0$ to represent the fact that the forced magnetisation processes were very negligible due to the field applied being comparable to the anisotropy fields. These points have been shown with hollow markers and are connected by dotted lines in Figure 4-60. The trends were similar to those observed in Mn (Melikhov et al., 2006a), Cr (Melikhov et al., 2006b), Ga (Ranvah et al., 2008a), and Ge/Co (Ranvah et al., 2008b) substituted cobalt ferrite.

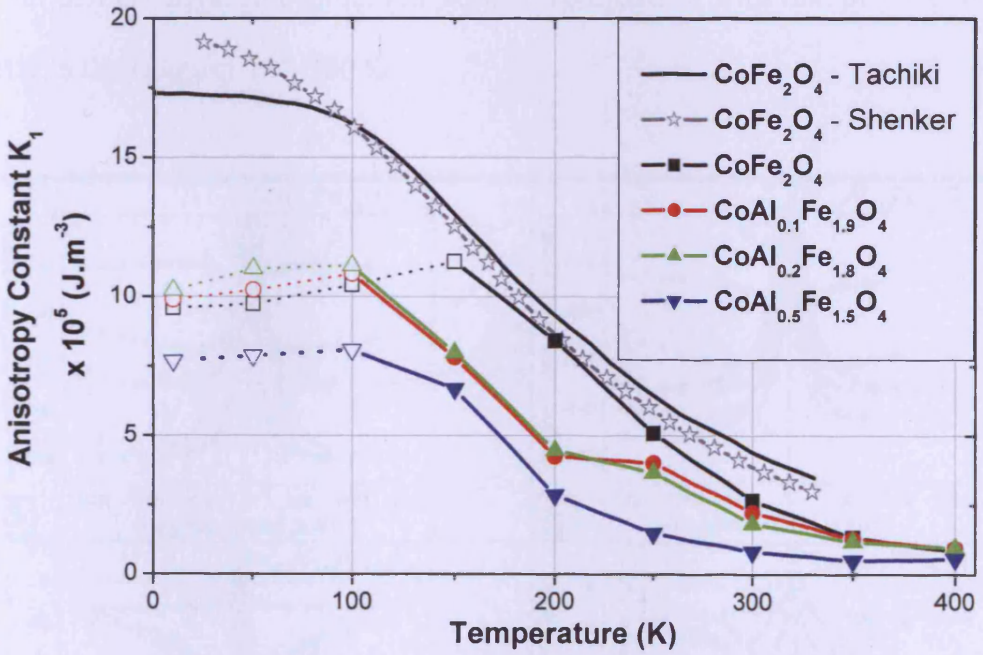

Figure 4-60 The first order magnetocrystalline cubic anisotropy constant K_1 for aluminium-substituted cobalt ferrite, calculated by fitting the experimental data to the Law of Approach to Saturation. The cases in which the forced magnetisation constant (κ) was assumed to be zero are shown as joined by dotted lines and with hollow markers. Experimentally measured data labelled as Shenker (Shenker, 1957) and theoretically predicted data marked as Tachiki (Tachiki, 1960) are shown for comparison.

4.04.6 Magnetostriction vs applied field for aluminium substituted cobalt ferrite

A study of the temperature dependence of the field induced magnetostriction of aluminium substituted cobalt ferrite prepared by ceramic methods has been performed by Ikenna (Nlebedim et al., 2010). The results are show for x = 0.0, 0.2, 0.5, and 0.7 in Figure 4-61. The maximum field induced magnetostriction was found to reduce with increasing temperature. $CoAl_{0.2}Fe_{1.8}O_4$ has a higher maximum field induced magnetostriction in comparison with that of pure cobalt ferrite in the range of 250-350 K.

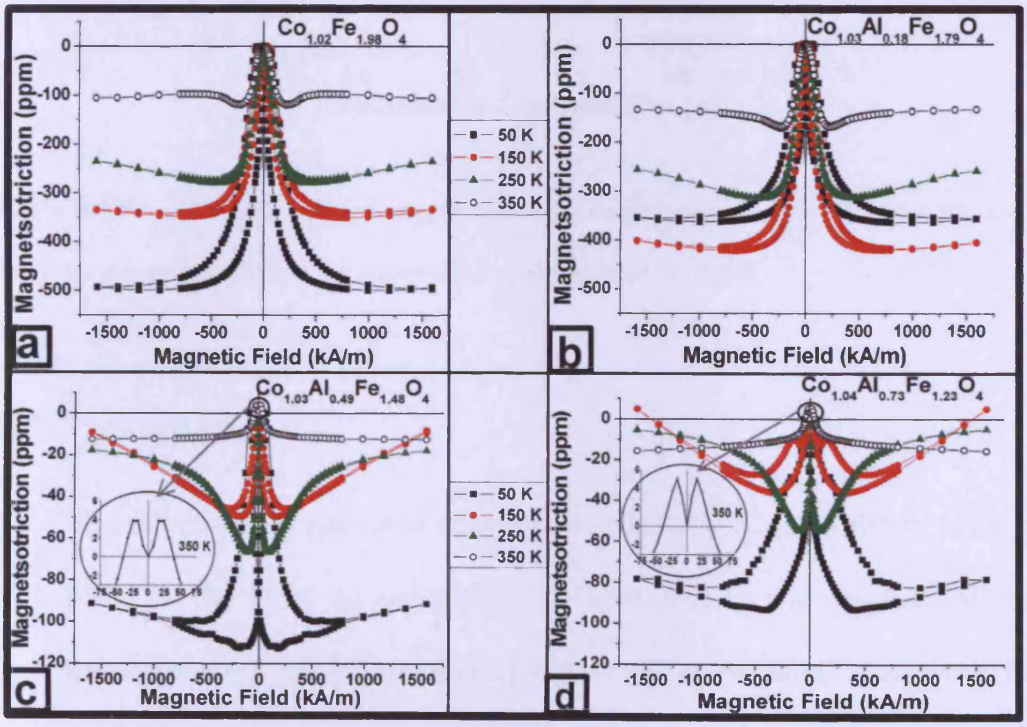

Figure 4-61 The field induced magnetostriction curves measured at 50, 150, 250, and 350 K for aluminium substituted cobalt ferrite (Nlebedim et al., 2010).

Figure 4-62 shows the variation of the strain derivative ($d\lambda/dH$) with aluminium content and temperature in the aluminium substituted cobalt ferrite. At 250 K, the strain derivative $d\lambda/dH$ is higher for $CoAl_{0.2}Fe_{1.8}O_4$ than that for pure cobalt ferrite. Similar trends were observed for low amounts of Ga (Ranvah *et al.*, 2007) and Ge/Co substitution (Ranvah et al., 2008c).

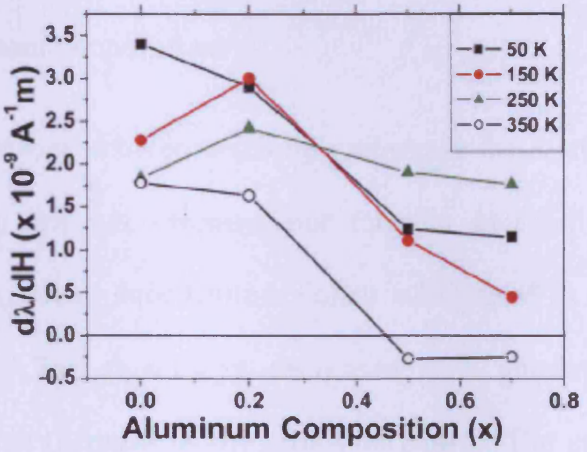

Figure 4-62 The field induced magnetostriction curves measured at 50, 150, 250, and 350 K for aluminium substituted cobalt ferrite (Nlebedim et al., 2010).

4.05 Summary

- The effect of the chemical substitution (Ga^{3+}, Ge^{4+}/Co^{2+}, Al^{3+} in place of some of the Fe^{3+}) on properties of cobalt ferrite was studied. All the measurements were done over a wide temperature range to ascertain the performance of these materials across these temperatures. These three substitutions were chosen to investigate the effect of substituting less magnetic ions into the A-sites, as opposed to the previously tried substitutions of manganese and chromium, which substitute into the B-sites.

- Gallium ions showed a preference for the A-sites resulting in an increase in the net moment per formula unit for low amounts of gallium substitution. The anisotropy decreased with gallium substitution leading to an increase in the strain derivative. The strain derivative of $CoGa_{0.2}Fe_{1.8}O_4$ was twice in comparison to that of pure cobalt ferrite and its maximum magnetostriction was about the same as that of pure cobalt ferrite at room temperature.

- Germanium ions showed a strong preference for A-sites resulting in an increase in the net moment per formula unit for low amounts of germanium/cobalt substitution. Cobalt substituted in place of iron into the B-sites. The anisotropy decreased with germanium substitution leading to an increase in the strain derivative. The strain derivative of $Co_{1.1}Ge_{0.1}Fe_{1.8}O_4$ was twice in comparison to that of pure cobalt ferrite and its maximum magnetostriction was 25% more than that of pure cobalt ferrite at room temperature.

- Aluminium ions exhibited no strong preference for any particular site in the cobalt ferrite lattice. The anisotropy decreased with aluminium substitution. The strain derivative of $CoAl_{0.2}Fe_{1.8}O_5$ was more than that of pure cobalt ferrite at 250 K, however it was lower than that of pure cobalt ferrite at 350 K.

- Chemical substitution of less magnetic ions into A-sites has been shown to be a useful method of adjusting the properties of cobalt ferrite. An understanding of the mechanisms that change the properties of cobalt

ferrite creates a scope for tailoring the materials to suit specific applications. An analysis of how different properties are interrelated was presented based on several compositions of three different substitutions into cobalt ferrite.

- The net moment per formula unit was observed to be sensitive to the site preference of the substituted ion. The anisotropy decreased with increasing amounts of substitution. A decrease in the anisotropy resulted in higher values of the strain derivative for low amounts of substitution. This behaviour was observed for all three substitutions.

- Substituting ions with a strong A-site preference can result in the dual property improvement of an increased maximum magnetostriction and an increased strain derivative. These improved properties of A-site substituted cobalt ferrite materials make them candidates for stress/torque sensor/actuator applications.

4.06 Bibliography

Al-Rawas, AD, Rais, A, Yousif, AA, Gismelseed, AM, Elzain, ME, Mazen, S, Al-Falaky, A. 2004. Magnetic properties of $Cu_{1+x}M_xFe_{2-2x}O_4$ mixed ferrites (M=Ge,Ti, $0 \leq x \leq 0.4$). *Journal of Magnetism and Magnetic Materials* **269:** 168-175.

Bozorth, RM, Tilden, EF, Williams, AJ. 1955. Anisotropy and Magnetostriction of Some Ferrites. *Phys. Rev.* **99:** 1788--1798.

Chen, Y, Jiles, DC. 2000. The Magnetomechanical Effect Under Torsional Stress in a Cobalt Ferrite Composite. *IEEE TRANSACTIONS ON MAGNETICS* **36:** 3244-3247.

Chen, Y, Kriegermeier-Sutton, BK, Snyder, JE, Dennis, KW, McCallum, RW, Jiles, DC. 2001. Magnetomechanical effects under torsional strain in iron, cobalt and nickel. *Journal of Magnetism and Magnetic Materials* **236:** 131-138.

Chen, Y, Snyder, JE, Dennis, KW, McCallum, RW, Jiles, DC. 2000. Temperature dependence of the magnetomechanical effect in metal-bonded cobalt ferrite composites under torsional strain. *J. Appl. Phys* **87:** 5798-5800.

Chen, Y, Snyder, JE, Schwichtenberg, CR, Callum, KW, Jiles, DC. 1999. Metal-bonded Co-ferrite composites for magnetostrictive torque sensor applications. *Magnetics, IEEE Transactions on* **35:** 3652.

Cullity, BD, Graham, CD 2009. *Introduction to Magnetic Materials*: John Willey & Sons.

Ito, T, Nakatsuka, A, Maekawa, H, Yoshiasa, A, Yamanaka, T. 2000. Site Preference of Cations and Structural Variation in $MgAl_{2-x}Ga_xO_4$ ($0 \leq x \leq 2$) Spinel Solid Solution. *Zeitschrift f¸r anorganische und allgemeine Chemie* **626:** 42-49.

Krieble, K, Devlin, M, Lee, SJ, Aldini, ST, Snyder, JE. 2008. Investigation of Ga substitution in cobalt ferrite ($CoGa_xFe_{2-x}O4$) using Mossbauer spectroscopy. *JOURNAL OF APPLIED PHYSICS* **103:** 07E508-503.

Kulkarni, JA, et al. 1985. Structural, magnetic and transport properties of the spinel ferrites Ga x Fe 1-x NiCrO 4. *Journal of Physics C: Solid State Physics* **18:** 2593.

Kulkarni, RG, Trivedi, BS, Joshi, HH, Baldha, GJ. 1996. Magnetic properties of copper ferrite aluminates. *Journal of Magnetism and Magnetic Materials* **159:** 375-380.

Lee, SJ, Lo, CCH, Matlage, PN, Song, SH, Melikhov, Y, Snyder, JE, Jiles, DC. 2007. Magnetic and magnetoelastic properties of Cr-substituted cobalt ferrite. *JOURNAL OF APPLIED PHYSICS* **102:** 073910.

Lo, CCH, Matlage, PN, Melikhov, Y, Snyder, JE, Song, SH, Jiles, DC. 2006. Magnetoelastic and Magnetic Properties of Chromium substituted Cobalt Ferrite.

Mahmoud, MH, Hamdeh, HH, Ho, JC, Abdalla, AM, Abdel-Mageed, AI. 2001. M^ssbauer studies on $MnGa_xFe_{2-x}O_4$. *Solid State Communications* **120:** 451-453.

Melikhov, Y, Snyder, JE, Jiles, DC, Ring, AP, Paulsen, JA, Lo, CCH, Dennis, KW. 2006a. Temperature dependence of magnetic anisotropy in Mn-substituted cobalt ferrite. *JOURNAL OF APPLIED PHYSICS* **99:** 08R102.

Melikhov, Y, Snyder, JE, Lo, CCH, Matlage, PN, Song, SH, Dennis, KW, Jiles, DC. 2006b. The Effect of Cr-Substitution on the Magnetic Anisotropy and Its Temperature Dependence in Cr-Substituted Cobalt Ferrite. *Magnetics, IEEE Transactions on* **42:** 2861-2863.

Nlebedim, IC, Ranvah, N, Melikhov, Y, Williams, PI, Snyder, JE, Moses, AJ, Jiles, DC. 2010. Effect of temperature variation on the magnetostrictive properties of $CoAl_xFe_{2-x}O_4$. *JOURNAL OF APPLIED PHYSICS* **107:** 09A936-909A936-933.

Paulsen, JA, .Ring, AP, Lo, CCH, Snyder, JE, Jiles, DC. 2005. Manganese-substituted cobalt ferrite magnetostrictive materials for magnetic stress sensor applications. *JOURNAL OF APPLIED PHYSICS* **97:** 044502.

Paulsen, JA, Snyder, JE, Ring, AP, Lieb, JS, Lo, CCH, Jiles, DC. 2003. Study of the Curie Temperature of Cobalt Ferrite Based Composites for Stress Sensor Applications. *IEEE TRANSACTIONS ON MAGNETICS* **39:** 3316-3318.

Ranvah, N, Melikhov, Y, Jiles, DC, Snyder, JE, Moses, AJ, Williams, PI, Song, SH. 2007. Variation of magnetoelastic properties of $CoGa_xFe_{2-x}O_4$ with temperature. *Magnetism and Magnetic Materials Conference.* 52 ed. Tampa, Florida, USA.

Ranvah, N, Melikhov, Y, Jiles, DC, Snyder, JE, Moses, AJ, Williams, PI, Song, SH. 2008a. Temperature dependence of magnetic anisotropy of Ga-substituted cobalt ferrite. *Journal of Applied Physics* **103:** 07E506.

Ranvah, N, Melikhov, Y, Nlebedim, IC, Jiles, DC, Snyder, JE, Moses, AJ, Williams, PI. 2008b. Temperature dependence of magnetic anisotropy of germanium/cobalt co-substituted cobalt ferrite. *JOURNAL OF APPLIED PHYSICS* **105:** 07A518.

Ranvah, N, Nlebedim, CI, Melikhov, Y, Snyder, JE, Williams, PI, Moses, AJ, Jiles, DC. 2009. Temperature dependence of magnetic properties of CoAlxFe2-xO4. *IEEE TRANSACTIONS ON MAGNETICS* **45:** 4261 - 4264

Ranvah, N, Nlebedim, IC, Melikhov, Y, Jiles, DC, Snyder, JE, Moses, AJ, Williams, PI, Song, SH. 2008c. Temperature dependence of magnetostriction of $Co_{1+x}Ge_xFe_{2-2x}O_4$ for magnetostrictive sensor and actuator applications. *IEEE TRANSACTIONS ON MAGNETICS* **44:** 3013-3016.

Sattar, AA, El-Sayed, HM, El-Shokrofy, KM, El-Tabey, MM. 2005. Improvement of the Magnetic Properties of Mn-Ni-Zn Ferrite by the Non-magnetic Al^{3+}-Ion Substitution. *Journal of Applied Sciences* **5:** 162-168.

Shenker, H. 1957. Magnetic Anisotropy of Cobalt Ferrite ($Co_{1.01}Fe_{2.00}O_{3.62}$) and Nickel Cobalt Ferrite ($Ni_{0.72}Fe_{0.20}Co_{0.08}Fe_2O_4$). *Physical Review* **107:** 1246.

Smit, J, Wijn, HJ 1959. *Ferrites*: N. V. Philips' Gloeilampenfabrieken, Eindhoven, Holland.

Song, SH. 2007. Magnetic and magnetoelastic properties of M-substituted cobalt ferrites (M=Mn, Cr, Ga, Ge). Iowa State University, Ames, Iowa.

Song, SH, Lo, CCH, Lee, SJ, Aldini, ST, Snyder, JE, Jiles, DC. 2007. Magnetic and Magnetoeleastic Properties of Ga-substituted Cobalt Ferrite. Joint Magnetism and Magnetic Materials/ InterMag Conference.

Tachiki, M. 1960. Origin of the Magnetic Anisotropy Energy of Cobalt Ferrite. *Progress of Theoretical Physics* **23:** 1055-1072.

Upadhyay, RV. 1990. YK type of magnetic ordering in $Co_{1+x}Ge_xFe_{2-2x}O_4$ spinel system. *Solid State Communications* **73:** 463-465.

Chapter 5. AC Magnetic Hysteresis of Cobalt Ferrite

5.01 Introduction

AC magnetic hysteresis loops were measured for pure cobalt ferrite to determine its suitability in AC applications. One of the important applications of magnetostrictive materials is in making magnetostrictive actuators working at a particular frequency. Some of the early research in magnetostrictive materials was focussed on their usage as sonar actuators at different frequencies (Claeyssen *et al.*, 1997). It is therefore important to ascertain the change in properties of magnetostrictive materials at different frequencies.

In the current study an AC B-H loop measurement system was built and the magnetic hysteresis of pure cobalt ferrite were studied at different frequencies between 10-100 Hz using a measurement system designed and assembled for this study. The description of the system and the experiments is given in the following sections. Due to limited availability of suitable samples, AC magnetic properties could only be measured for pure cobalt ferrite.

Three parameters were chosen to check the variation of B-H loops of cobalt ferrite in the linear region of its hysteresis curve: coercivity, differential permeability, and energy loss inside the hysteresis loop. Little variation in the magnetic hysteresis parameters would indicate that the usage of these materials in 10-100 Hz range applications would offer the possibility of choosing any

operational frequency in this range without much difference in magnetic performance.

5.02 Specifications of the AC magnetic property measurement system

The system was designed to provide reproducible standardised results within the frequency range of 10-100 Hz. Thus it was built with certain features and specifications in mind. These features and specifications are described below:

5.02.1 Schematic

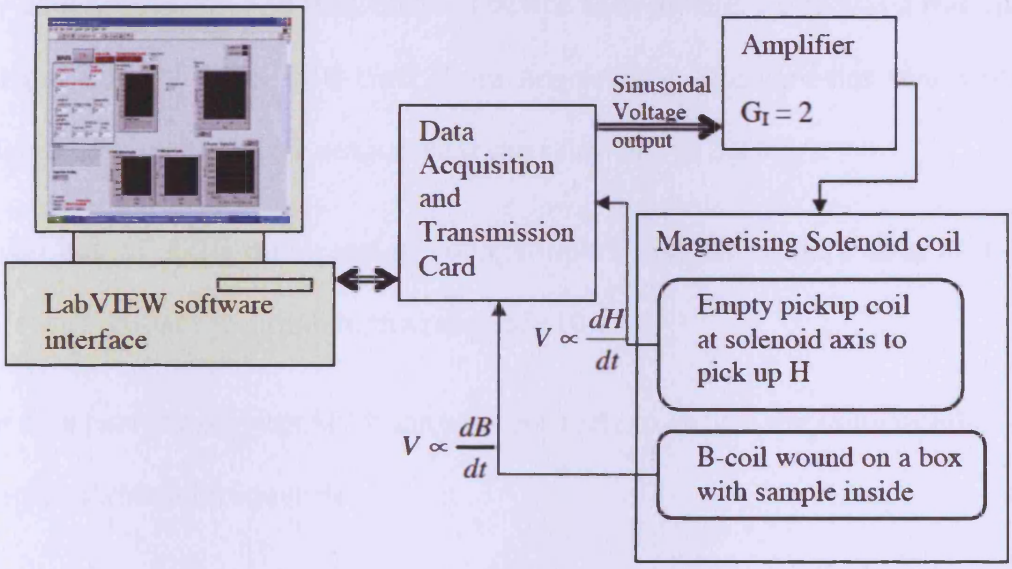

Figure 5-1 A schematic of the measurement system used to measure the AC magnetic hysteresis of pure cobalt ferrite.

Figure 5-1 shows a schematic of the system used to measure the AC magnetic hysteresis of pure cobalt ferrite.

5.02.2 Choice of computer interface

It was desired that the system should have an easy to use interface. Therefore, it was built such that control and measurement instrumentation can be linked to a computer using the National Instruments LabView interface. LabView provides a customisable, upgradable, easy to use intuitive graphical user interface front-end with the ability to perform fast and complex computations with the acquired data (National Instruments, 2010). LabView also provides the ability to acquire and send data using the LabView NI data acquisition devices (DAQ devices).

5.02.3 Data Acquisition

The data acquisition and transmission device used for this study was a National Instruments PCI-6255 DAQ card (Data Acquisition). The card has two 16-bit differential analog voltage outputs that can relay data at 2.8 MS/s.

It also has 40 differential analog voltage inputs that can acquire data at 1.25 MS/s with 16-bit resolution in the range of ±10 V.

The data rate chosen was 5000 samples per cycle to ensure the same number of samples across all frequencies.

5.02.4 Current to Voltage Amplifier

The data generated by the computer was transferred to the NI LabView DAQ card described in section below. The DAQ card provided a low power ±10 V signal. This signal was fed into a Voltage to Current Amplifier to produce a current waveform proportional to the input signal. The Voltage to Current Amplifier used was a Kepco BOP 50-20MG Power Supply (Kepco Inc., 2008). The

current required to drive fields of 40kA/m using the solenoid was in the range of 12-13 A. This power supply was chosen as it has the ability to supply high current (I_{max} = 20 A). It has a voltage to current gain G_I = 2 A/V. Thus it can be driven with a voltage signal between ±10 V, which was ideal as the DAQ card used also has the same voltage output range. The amplifier had the capability of being used in both current and voltage supply mode. It was used in the current supply mode. The input signal was fed between Pin-3 (IOUT_DMM) and PIN-4 (SGND) of the Analog I/O Port at the rear of the amplifier. The output was fed to the solenoid.

5.02.5 Experimental Setup

The magnetic measurement systems can suffer from vibrations due to Lorentz forces. Thus the system was made such that it avoids vibrations. Exact drawings are given in Appendix II.

5.02.5.1 Base

A 30 cm × 30 cm × 1 cm aluminium base was designed to mount the experimental setup. The depth of the base was chosen to be 1 cm for providing enough space to affix the experimental setup. The weight of the base reduces the vibrations in the experimental setup. A schematic of the base is shown in Figure 5-2.

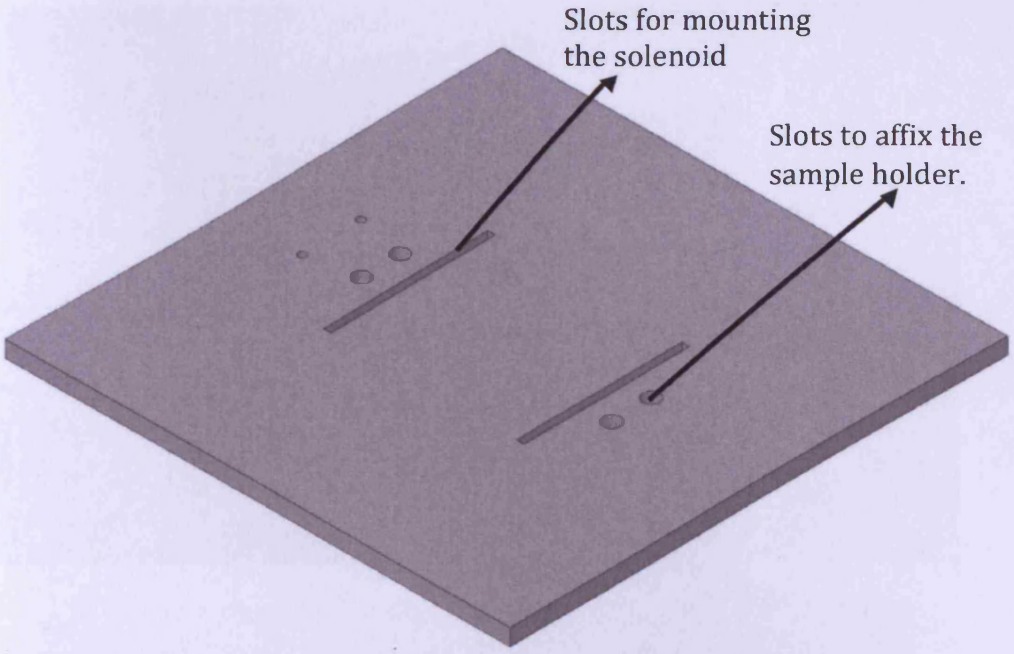

Figure 5-2 The aluminium base on which the experimental setup was mounted.

5.02.5.2 Experimental Setup

The experimental setup is shown in Figure 5-3.

Solenoid: An 80 turn solenoid was wound over a cylinder with a diameter of 60 mm and a length of 120 mm. The solenoid was mounted on the base using the square ends as are visible in Figure 5-3.

Sample Holder: A sample holder was designed such that it could be affixed to the base with rigidity and ensured that the sample could be mounted in exactly the same location every time.

Sample Cage: The sample was placed inside the sample cage, which was at the centre of the solenoid. The sample was secured inside the sample cage by securing it tightly using non-magnetic Teflon (PTFE) tape.

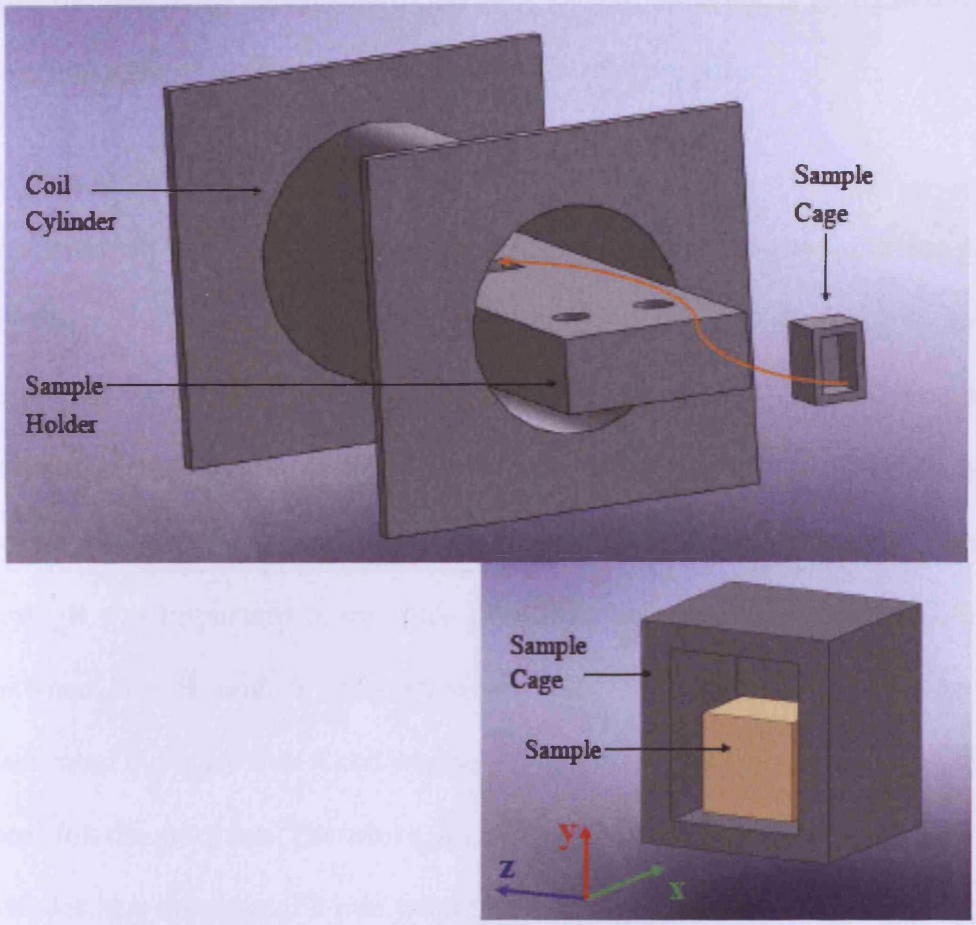

Figure 5-3 The experimental setup for AC magnetic hysteresis measurements. The magnetic field is generated by the coil wound over the coil cylinder in the X-direction.

5.02.6 Measurement Sensors

5.02.6.1 Magnetic induction (B) measurement

The magnetic induction was measured by measuring the voltage across a 30 turn secondary coil wound around the sample cage which measures a voltage proportional to $-\frac{dB}{dT}$. The coil was wound in the Y-Z plane such that it can measure the induction in the X-direction (same as the applied magnetic field).

The voltage measured was fed to the DAQ card in differential mode and the data was then relayed to the LabView software on the computer.

5.02.6.2 *Magnetic field (H) measurement*

The measurement system was designed to make measurements for the AC magnetic field excitations of 10-100 Hz frequencies. It was required that the magnetic field measurements should be synchronised with the magnetic induction measurements. Since the magnetic induction measurements were carried out by measuring the voltage across the secondary coil with negligible delay, it was important to measure H without delay as well. A phase difference between the H and B measurements can induce significant errors, as is illustrated in Figure 5-4. A coil wound around an empty cylinder was found to be ideal for the purpose. Therefore, an 80 turn coil was placed at the axis of the cylinder at a distance of 3 mm from the sample. H was calculated by integrating the voltage across this empty coil.

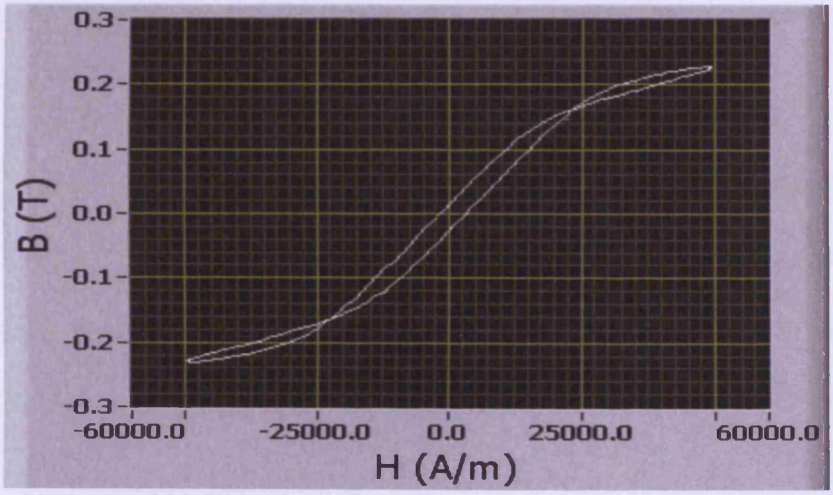

Figure 5-4 An example of the error introduced in B-H measurement due to phase lag.

5.03 Measurement of AC B-H characteristics of cobalt ferrite

5.03.1 Sample

A pure cobalt ferrite sample was cut into a cuboid with dimensions of 5.80 mm, 8.90 mm, and 6.85 mm along the X, Y, and Z directions respectively

5.03.2 Experimental conditions

Since high current was pumped through the solenoid in order to produce AC magnetic fields of amplitude 40 kA/m, the system was prone to heating caused due to increase in coil temperature. Three constant flow AC powered cooling fans were used to maintain the temperature within the range of 23-25 °C. A temperature sensor was placed inside the coil mounted on the sample holder at a distance of 7 mm from the sample to monitor the temperature during the experiment.

For the purpose of comparison across frequencies, a sinusoidal magnetic field with a peak magnitude of 40 kA/m was generated for experiments at all frequencies.

50 loops were measured in a batch and the voltage data were averaged over these 50 loops. The H calculated from the averaged data was used to calculate the feedback to achieve a desired H waveform that resulted in a subsequent batch of 50 B-H loops that met the following conditions:

- H_{peak} error < 2%. This condition was imposed to ensure a constant peak of the H-field stimulus.

- Total Harmonic Distortion in H < 2%. This condition was imposed to ensure the sinusoidal nature of the magnetic field.

- 23 °C < Temperature < 28 °C. This condition was imposed to ensure stable environmental conditions throughout the duration of the experiment.

- $\frac{\sigma_{H_c}}{\langle H_c \rangle} < 2\%$, where σ_{H_c} is the standard deviation in coercive field H_c measured over 50 cycles and $\langle H_c \rangle$ is the mean coercive field measured over 50 cycles. This condition was imposed to ensure repeatability of measurements.

5.04 Results of AC magnetic hysteresis measurements

A pure cobalt ferrite sample was tested at frequencies between 10 Hz and 100 Hz in steps of 10 Hz. The measurements were carried out in the linear regions of the B-H loop far away from saturation. An example of the B-H loops measured is given in Figure 5-5.

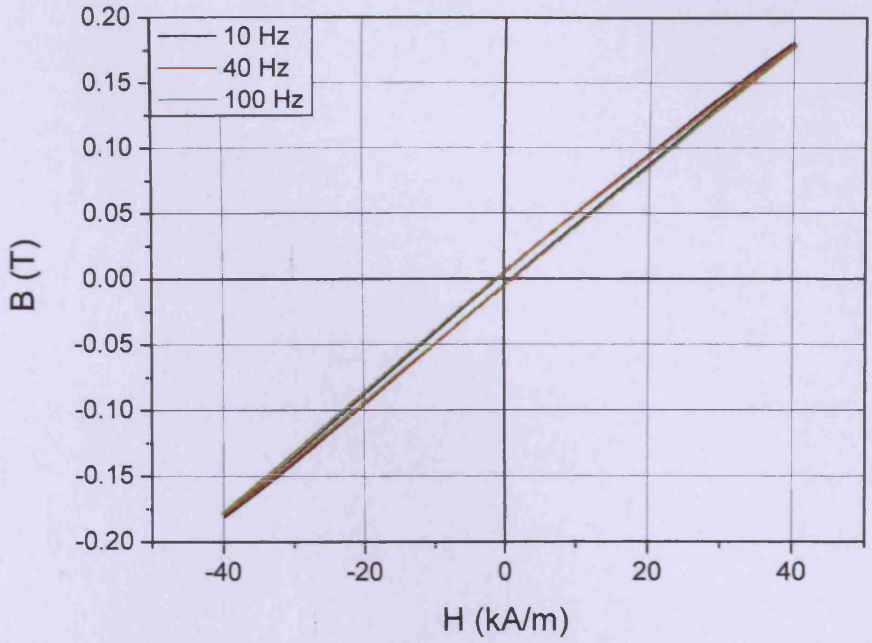

Figure 5-5 An example of the B-H curves measured in the linear regions of the cobalt ferrite's hysteresis loop. H was fixed to an amplitude of 40 kA/m. It was observed that B was also constant at around 0.18 T.

Since cobalt ferrite is a non-conducting ceramic, it does not show any effect of eddy currents. The differential susceptibility at zero crossings on the B-H loops (i.e. at B = 0) was seen to vary by less than 2% in the 10 – 100 Hz range as can be observed from Figure 5-6. Jiles had measured the frequency dependence of hysteresis curves in non-conducting magnetic materials for a zinc ferrite (Philip Series 3C81 ferrite material) material and the results are in agreement (Jiles, 1993, Phlips Co., 1989). The initial permeability measured did not vary between 10 and 100 Hz, although it reduced significantly as the frequency was increased beyond 500 Hz.

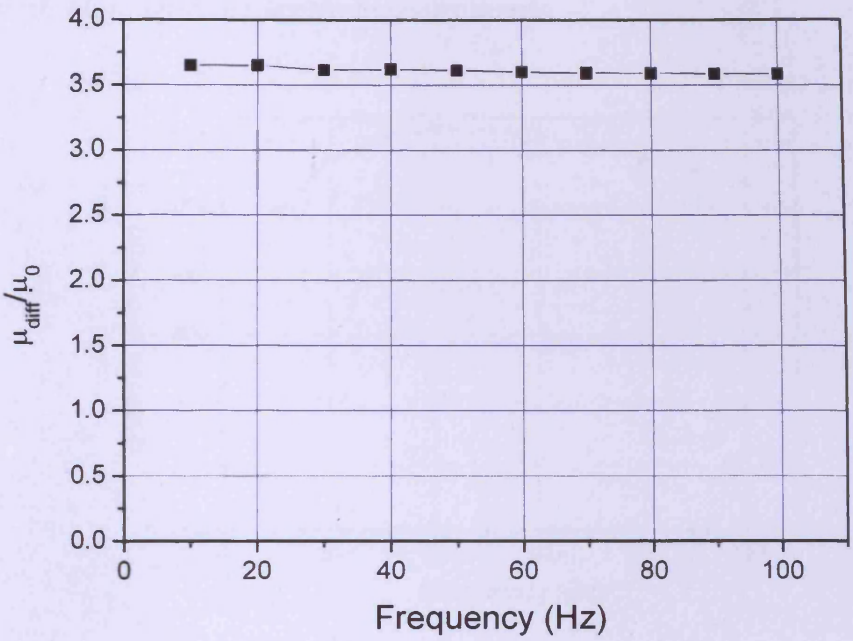

Figure 5-6 The frequency dependence of the relative differential permeability at B=0, averaged over 50 B-H loops.

The coercive field was calculated from the B-H loops measured in the frequency range of 10 – 100 Hz and it was less than 1600 A/m (20 Oe) for all frequencies in the range. This means that the material is a candidate for AC magnetic field applications. Figure 5-7 shows the variation of coercive field with the frequency of the applied magnetic field.

The energy loss in the B-H loop (area of the loop) was also calculated and its variation was measured with the frequency. Since the loops were in the linear region, and the shape of the loop and permeability did not change very much over the frequency range (see Figure 5-5), the energy loss results correlated with the coercive field values, as can be seen in Figure 5-8. The trends in energy loss

and the coercive field are new and need to be studied in detail in future work along with AC magnetostriction measurements.

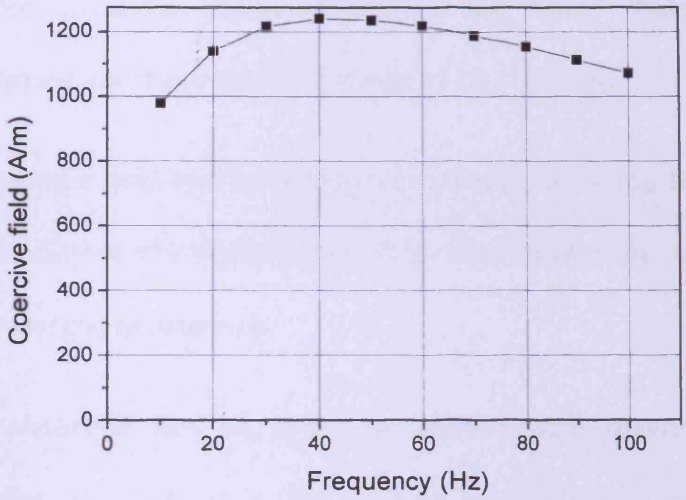

Figure 5-7 The frequency dependence of the coercive field of cobalt ferrite, averaged over 50 B-H loops.

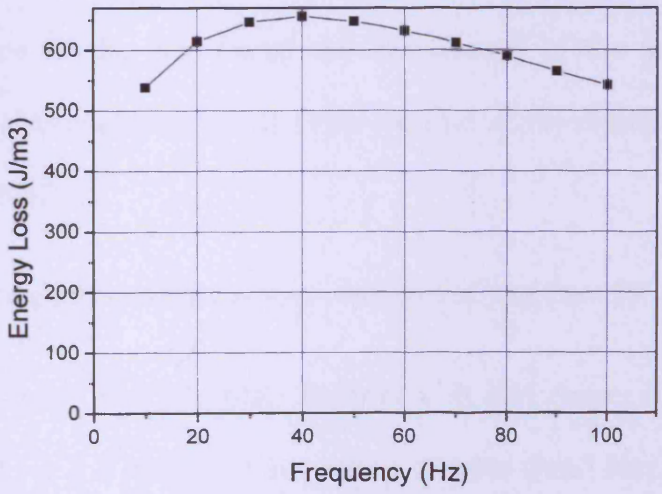

Figure 5-8 The frequency dependence of the energy loss (area inside B-H loop) for cobalt ferrite, averaged over 50 B-H loops.

5.05 Summary

- An AC B-H loop measurement system was built to measure the magnetic properties of pure cobalt ferrite in the linear region of its B-H characteristic for frequencies in range of 10 – 100 Hz.

- Both magnetic field and induction were measured using coils to eliminate the possibility of any phase delay. This ensured that the measurements of H and B were synchronised.

- It was observed that in order to achieve high magnetic fields with amplitudes of 40 kA/m, a high current needed to be circulated in the primary coil. A cooling and temperature monitoring system was added to the measurement system to keep in check any temperature change caused by heating of the primary coil.

- The shape of the B-H curve did not change in the 10-100 Hz range. Keeping H as constant, it was observed that B also remained constant at a value of 0.17 T.

- The relative differential permeability varied less than 2% in this range.

- The coercivity was less than 1600 A/m in this range. A new trend was observed for the change in coercivity. Similar trend was observed in the variation of Energy loss with frequency. It is suggested that this trend be studied further in future work.

- The non-conducting nature, low coercivity, and small variation in the sensitivity (dB/dH) make the material useful for AC magnetic field

environment applications. The lack of variation of magnetic hysteresis parameters in 10-100 Hz range indicated that cobalt ferrite could be a material of interest in AC magnetic field applications where the design demands a flexibility of operational frequency.

- It is suggested that the variation of AC magnetic properties of cobalt ferrite with chemical substitution be studied as a continuation of the present work. This work has looked at AC magnetic properties in the narrow frequency range of 10-100 Hz. It is suggested that future work be carried out in a larger range of frequencies.

5.06 Bibliography

Philips Co. 1989. Ferrite materials and components catalogue. Catalogue Number: PC052-1.

Kepco Inc. 2008. Operator's Manual: BOP 1000 W High Power Bipolar Power Supply. Flushing, NY.

Claeyssen, F, Lhermet, N, Le Letty, R, Bouchilloux, P. 1997. Actuators, transducers and motors based on giant magnetostrictive materials. *Journal of Alloys and Compounds* **258:** 61-73.

National Instruments. 2010. What is in NI LabView? (http://www.ni.com/labview/whatis/).

Jiles, DC. 1993. Frequency Dependence of Hysteresis Curves in Non-Conducting Magnetic Materials. *IEEE Trans. Mag.* **29:** 3490 - 3492.

Chapter 6. Conclusions and Future Work

6.01 Introduction

The effect of the chemical substitution on the magnetic and magnetostrictive properties of cobalt ferrite was investigated in the present study. Dopants with A-site preference were chosen and it was aimed to increase both the maximum magnetostriction and strain derivative. Three different cation substitutions (Ga^{3+}, Ge^{4+}/Co^{2+}, Al^{3+}) were used to replace some of the Fe^{3+} ions in the cobalt ferrite lattice. The samples tested for magnetic and magnetostrictive properties were:

- $CoGa_xFe_{2-x}O_4$ with x = 0.0, 0.2, 0.4, 0.6, and 0.8
- $Co_{1+x}Ge_xFe_{2-2x}O_4$ with x = 0.0, 0.1, 0.2, 0.4, and 0.6
- $CoAl_xFe_{2-x}O_4$ with x = 0.0, 0.1, 0.2, and 0.5

The following measurements were made:

- Maximum magnetisation (at $\mu_0 H = 5$ T) vs Temperature between 10 – 400 K
- Magnetisation loops measured at temperatures between 10 and 400 K in the magnetic field range $\mu_0 H = \pm 5$ T
- Magnetostriction loops measured between 250 and 400 K in the field range $\mu_0 H = \pm 2$ T

- B-H loops for pure cobalt ferrite in the frequency range of 10 – 100 Hz for sinusoidal AC magnetic field excitation with a peak magnetic field of $H = \pm 40 kA/m$

The first order cubic magnetocrystalline anisotropy constant for a randomly oriented polycrystalline material was calculated by fitting the high field regions of M-H loops to the Law of Approach to Saturation. The strain derivative and maximum magnetostriction in the linear region of magnetostriction curves were calculated from the magnetostriction loops.

6.02 Conclusions

The main conclusions of this study are:

- It was observed that the addition of small amounts (less than 20% stoichiometric) of ions with lower atomic magnetic moment (Ga^{3+}, Ge^{4+}, Al^{3+}) in place of an ion with a large net atomic magnetic moment (Fe^{3+}) resulted in higher net magnetic moment per formula unit. This is because of the cations with lower magnetic moment are replacing iron with higher magnetic moment in the A-sites which are anti parallel to the moments in the B-sites.

- Chemical substitution can be used to adjust the properties of cobalt ferrite. The properties of the resulting substituted cobalt ferrite depend on site preference of the substituted ion, the size of the ion, the net magnetic moment contribution of the ion and the exchange interaction.

- Substitution of cations with lower net atomic magnetic moment in place of iron ions with higher moment caused a reduction in the magnetocrystalline anisotropy by a reduction in the A-B superexchange coupling. This was the primary mechanism of reduction in anisotropy for low amounts of substitution. At higher amounts of substitution (more than 50% stoichiometry), the splitting of the B-lattice into two sub-lattices, with moments at acute angles to each other, causes the anisotropy to reduce even further.

- The field induced magnetostriction of cobalt ferrite is dominated by the contribution from two magnetostriction constants, λ_{100} and λ_{111}. The maximum magnetostriction in the linear region of the magnetostriction curve ($\lambda_{max,\ linear\ region}$) was observed to be highest for the composition $Co_{1.1}Ge_{0.1}Fe_{1.8}O_4$.

- In general, the strain derivative was observed to increase when a small amounts of chemical substitution was employed. The decrease in the anisotropy caused an increase in the strain derivative. The decrease in strain derivative has huge implications on the power required to magnetise the magnetostrictive material, as this power reduces as the square of the strain derivative.

- The new substitutions investigated in this study demonstrated better properties for magnetostrictive sensor and actuator applications than previous studies on manganese and chromium substitution. The study highlighted how individual properties can be tailored by substituting ions

with different site preferences. The strain derivative increase more than two times for several substitutions along with a 25% increase in maximum magnetostriction. The strain derivative was higher than that of manganese and chromium substitution for gallium and germanium/cobalt co-substituted cobalt ferrite.

- AC magnetic hysteresis loops were measured for pure cobalt ferrite in the linear region of its B-H characteristics. The coercivity of the material remained below 1600 A/m (20 Oe). The lack of eddy currents meant that there was little variation in the 10 – 100 Hz range. The coercivity was not a monotonically increasing function of frequency of the magnetic field, which is a new trend. The variation of energy loss (area inside the B-H loop) with frequency was correlated to the coercivity within this range. The relative differential permeability at B = 0 varied by less than 2% in the frequency range of 10-100 Hz range. This little variation of the AC magnetic properties in the 10-100 Hz range makes cobalt ferrite a useful magnetic material in applications where there is a need for flexibility in operational frequency without change in magnetic performance.

- The newly substituted cobalt ferrite materials investigated in this study are chemically stable, mechanically strong, sensitive to field and have a range of response ($\lambda_{max,\ linear\ region}$) which makes them good candidate materials for magnetostrictive sensor and actuator applications. The absence of eddy currents and negligible change in magnetic hysteresis over 10-100 Hz range makes these materials fit for use in applications with AC magnetic fields.

- This study contributes scientific data and analysis on the properties of A-site substituted cobalt ferrite, which enables future application designers to reference this work to choose a material with desirable properties. The study has also proposed the mechanisms by which different properties of cobalt ferrite can be changed in order to suit an application. An analysis is also presented to enhance the understanding of correlation of different magnetic properties of cobalt ferrite based materials.

6.03 Future work

The following proposed future work leads on naturally from this study and would contribute significantly towards furthering the progress of research in this area:

- A new study to determine the exact site occupancy data for cations in substituted cobalt ferrite would be highly desirable. This would validate the findings of this study and form the basis for a mathematical model which can calculate the contribution of the site occupancy of cations to the macroscopic properties of these materials. Neutron diffraction and X-ray diffraction are suggested as possible routes for determination of exact site occupancy of the different ions in cobalt ferrite's lattice.

- There should be a study on the temperature dependence of λ_{100} and λ_{111} and their contribution to the field induced magnetostriction. Single crystal cobalt ferrite could be used for this study, as it is easier to study the directional contributions in single crystal materials. This study can

then be used to predict the temperature dependent magnetostrictive properties of polycrystalline cobalt ferrite.

- AC magnetic and magnetostrictive properties of substituted cobalt ferrite should be studied with an eye on the applications of these materials with AC magnetic field excitation. Further work needs to be done on the measurement system to include AC magnetostriction measurement capability. This would enable researchers to validate the usability of this material in AC stress/torque sensor/actuator applications.

- More chemical substitutions need to be studied to examine the effects of the presence of different cations in the cobalt ferrite lattice on its macroscopic properties. Substitution of Sn in place of Fe is suggested as a promising candidate since the Ge subsitution provided encouraging results in the present study and both elements occupy adjacent positions in the same group in the periodic table. The analysis of site occupancy of Sn would be easier as its Mossbauer signature is distinguishable from that of iron. It was also observed that the Curie temperature was a linear function of the dopant concentration. This result could be used to empirically estimate the Curie temperature of different substitutions at material design stages.

- It is recommended that prototype stress/torque sensor and actuators be built using cobalt ferrite based materials and further research in the area be done with a focus on challenges of developing a reliable device.

Appendices

Appendix 1: Magnetic properties of $Co_{1.6}Ge_{1.6}Fe_{0.8}O_4$

The properties of cobalt/germanium co-substituted cobalt ferrite were discussed in Chapter 4. The analysis of the magnetic properties of $Co_{1.6}Ge_{1.6}Fe_{0.8}O_4$ is discussed here. The magnetic properties of this substitution are out of the trend with the rest of the series of germanium/cobalt co-substituted samples.

Figure A1- 1 shows the variation of the maximum magnetisation of Ge/Co co-substituted cobalt ferrite with temperature in the range 10 - 400 K. As can be observed from the figure the sample with x = 0.6 has a characteristic which is different from the rest of the series of samples. This could be because the sample has more Ge/Co than Fe and the structure and properties of the sample could be of a very different nature than the rest of the substituted cobalt ferrite samples with Fe^{3+} as the majority cation.

Figure A1-2 shows the variation of the first order cubic magnetocrystalline anisotropy constant with temperature. As can be observed from the figure, the sample with x=0.6 is out of the trend for rest of the samples. The sample's anisotropy at low temperatures (below 150 K) is between samples with x=0.3 and x=0.4. At higher temperatures (above 200 K), the anisotropy constant for the sample with x=0.6 increases slightly to values above even pure cobalt ferrite. The reasons for this behaviour were not studied as a part of this study as the magnetostriction of this material is low and is outside the range which makes these materials useful for magnetostrictive stress/torque sensor/actuator applications.

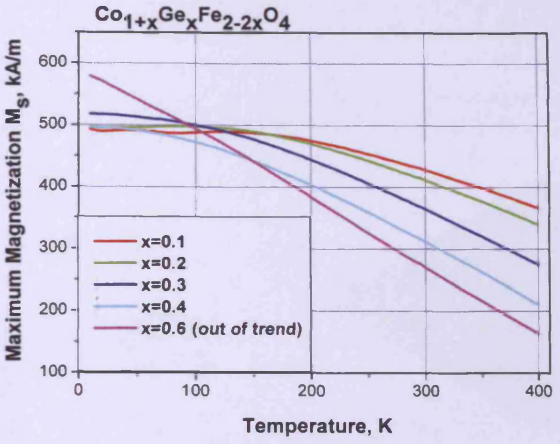

Figure A1- 1 The variation of the maximum magnetisation of germanium/cobalt co-substituted cobalt ferrite with temperature. The maximum magnetisation was measured at an applied field of $\mu_0 H$ = 5 T. The sample with x=0.6 is out of trend.

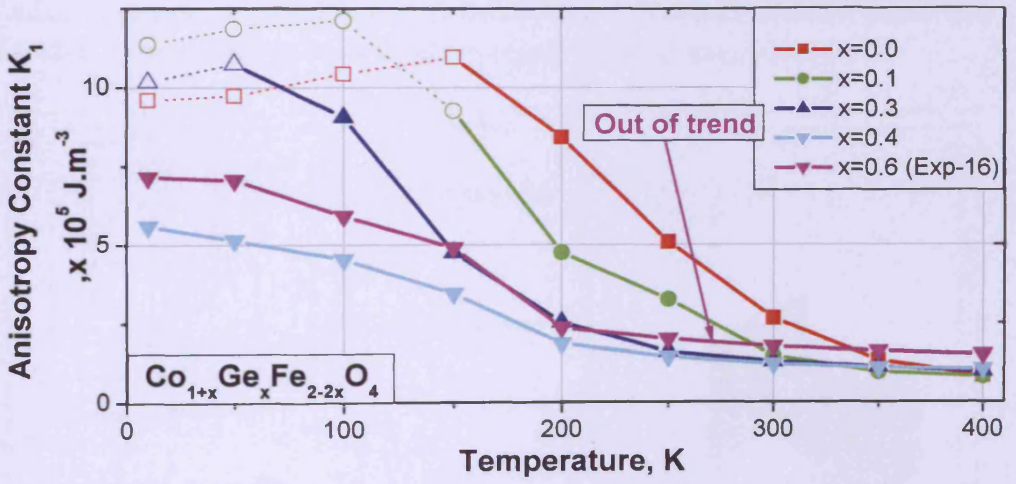

Figure A1- 2 The variation of the first order magnetocrystalline cubic anisotropy constant K_1 of germanium/cobalt co-substituted cobalt ferrite with temperature. The sample with x=0.6 is out of the trend.

Appendix 2: Drawings for AC Measurement System

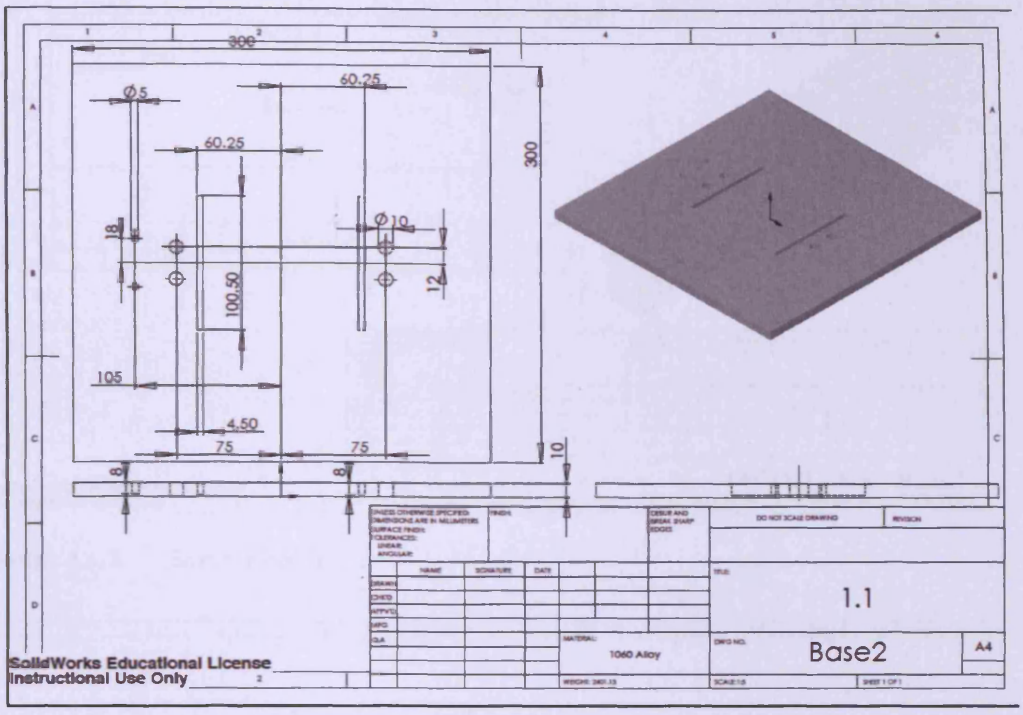

Figure A2-1 Aluminium base on which the rest of the setup was mounted.

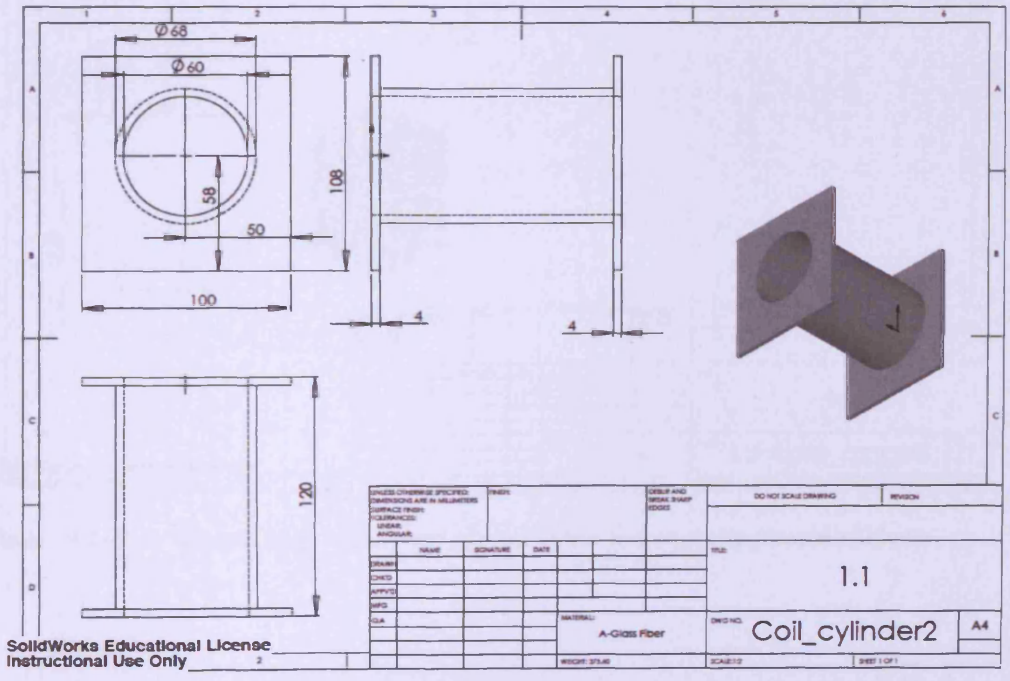

Figure A2-2 Coil cylinder on which the solenoid was wound.

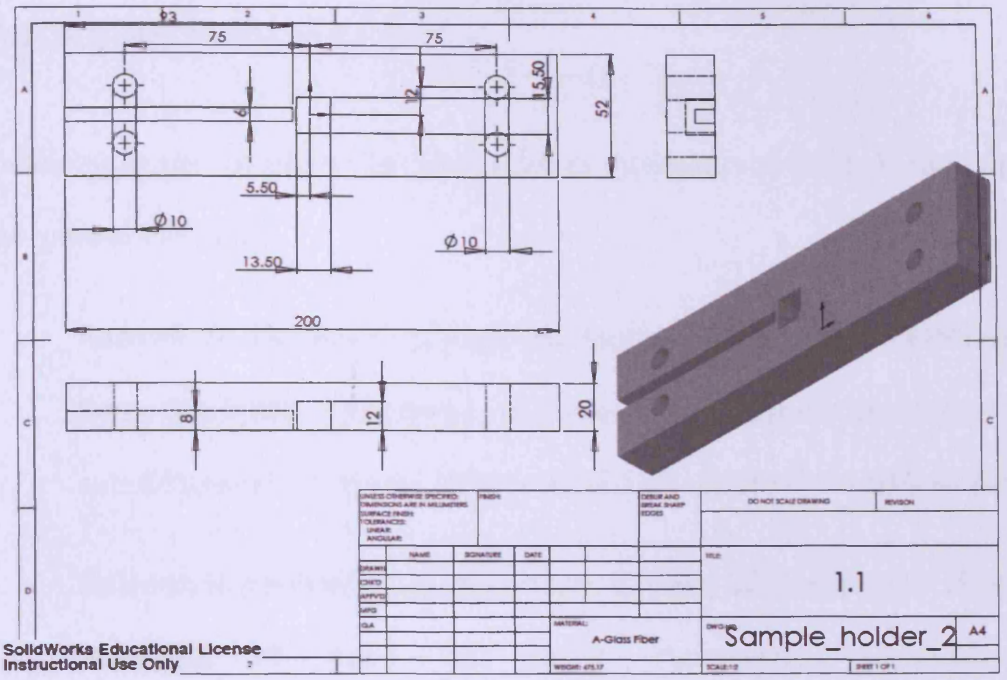

Figure A2-3 Sample holder.

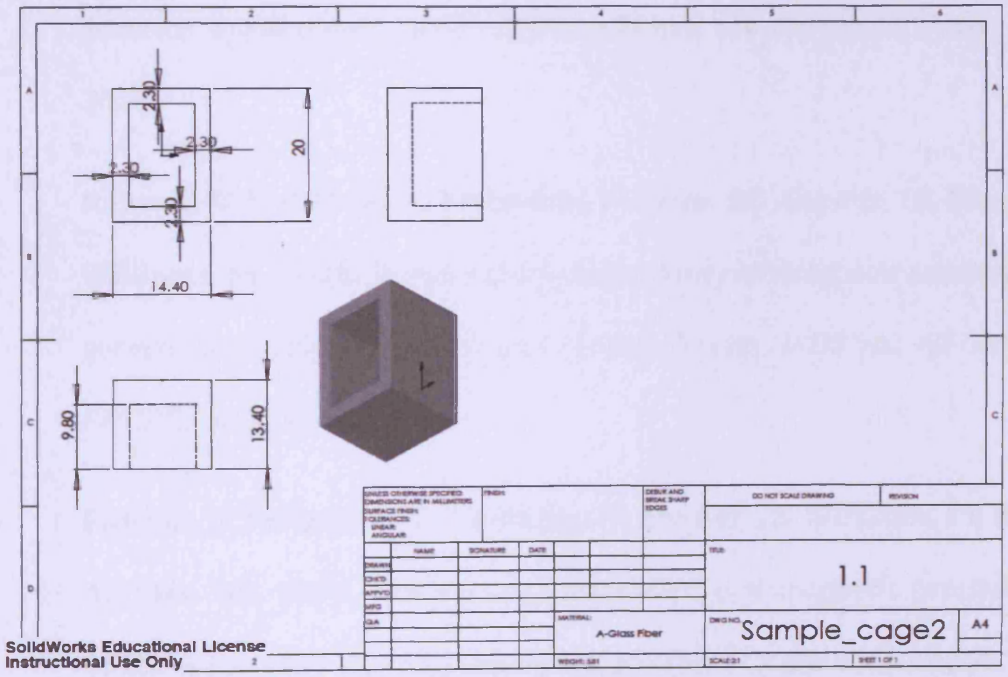

Figure A2-4 Sample cage which was placed at the centre of the sample holder.

Appendix 3: Publications

Following is the list of articles published in international journals that were an outcome of this study:

- **Ranvah, N, Melikhov, Y, Jiles, DC, Snyder, JE, Moses, AJ, Williams, PI, Song, SH. 2008.** Temperature dependence of magnetic anisotropy of Ga-substituted cobalt ferrite. *JOURNAL OF APPLIED PHYSICS* **103:** 07E506.

- **Ranvah, N, Nlebedim, IC, Melikhov, Y, Jiles, DC, Snyder, JE, Moses, AJ, Williams, PI, Song, SH. 2008.** Temperature dependence of magnetostriction of $Co_{1+x}Ge_xFe_{2-2x}O_4$ for magnetostrictive sensor and actuator applications. *IEEE TRANSACTIONS ON MAGNETICS* **44:** 3013-3016.

- **Ranvah, N, Melikhov, Y, Nlebedim, IC, Jiles, DC, Snyder, JE, Moses, AJ, Williams, PI. 2009.** Temperature dependence of magnetic anisotropy of germanium/cobalt co-substituted cobalt ferrite. *JOURNAL OF APPLIED PHYSICS* **105:** 07A518.

- **Ranvah, N, Nlebedim, CI, Melikhov, Y, Snyder, JE, Williams, PI, Moses, AJ, Jiles, DC. 2009.** Temperature dependence of magnetic properties of $CoAl_xFe_{2-x}O_4$. *IEEE TRANSACTIONS ON MAGNETICS* **45:** 4261 - 4264

Following are the awards that were earned by presentation of this study at various events:

- First position in Wales (zonal level) at Young Person's Lecture Competition, 2009
- First position in South-West UK (regional level) at Young Person's Lecture Competition, 2009
- Among the 7 finalist at National level of Young Person's Lecture Competition, UK
- First position among student presenters at IEEE Magnetics, UKRI Chapter Meeting in Cardiff, 2009

A copy of journal publications follows.

Temperature dependence of magnetic anisotropy of Ga-substituted cobalt ferrite

N. Ranvah,[1,a)] Y. Melikhov,[1] D. C. Jiles,[1] J. E. Snyder,[1] A. J. Moses,[1] P. I. Williams,[1] and S. H. Song[2]
[1]*Wolfson Centre for Magnetics, Cardiff University, Cardiff CF24 3AA, United Kingdom*
[2]*Materials Science and Engineering Department, Iowa State University, Ames, Iowa 50011, USA*

(Presented on 6 November 2007; received 5 October 2007; accepted 23 October 2007; published online 14 February 2008)

The temperature dependence of magnetization, magnetic anisotropy, and coercive field of gallium-substituted cobalt ferrite was investigated for a series of compositions of $CoGa_xFe_{2-x}O_4$ ($0 \leq x \leq 0.8$). Hysteresis loops were measured for each sample over the range of $-5\ T \leq \mu_0 H \leq 5\ T$ for selected temperatures between 10 and 400 K. The magnetization at 5 T and low temperatures was found to increase for the lower Ga contents ($x=0.2$ and 0.4) compared to pure $CoFe_2O_4$, indicating that at least initially, Ga^{3+} substitutes predominantly into the tetrahedral sites of the spinel structure. The high field regions of these loops were modeled using the law of approach to saturation, which represents the rotational process, together with an additional linear forced magnetization term. The first order cubic magnetocrystalline anisotropy coefficient K_1 was calculated from curve fitting to these data. It was found that K_1 decreased with increasing Ga content at all temperatures. Both anisotropy and coercivity increased substantially as temperature decreased. Below 150 K, for certain compositions ($x=0$, 0.2, 0.4), the maximum applied field of $\mu_0 H=5$ T was less than the anisotropy field and, therefore, insufficient to saturate the magnetization. In these cases, the use of the law of approach method can lead to calculated values of K_1 which are lower than the correct value. © *2008 American Institute of Physics*. [DOI: 10.1063/1.2832503]

INTRODUCTION

There has been much interest recently in the properties of magnetoelastic cobalt ferrite and cobalt ferrite composites.[1–4] These materials exhibit high levels of magnetostriction λ and high sensitivity to field $d\lambda/dH$, which make them candidate materials for stress and torque sensor, and actuator applications. Substitution of a cation M for Fe in $CoM_xFe_{2-x}O_4$ reduces the Curie temperature and improves magnetic and magnetoelastic properties in the cases of M =Mn or Cr.[3,4] To fully control the magnetomechanical response of these materials, more needs to be known about their magnetic properties and their temperature dependences, especially the magnetic anisotropy. In the present work, the effect of gallium substitution on the temperature dependence of magnetization, magnetocrystalline anisotropy, and coercivity of $CoGa_xFe_{2-x}O_4$ ($0 \leq x \leq 0.8$) was investigated over the temperature range of 10–400 K.

EXPERIMENT AND RESULTS

A series of gallium-substituted cobalt ferrite samples was prepared by standard ceramic techniques[1,2] with a final sintering at a temperature of 1350 °C for 24 h, followed by furnace cooling to room temperature. Energy dispersive x-ray spectroscopy (EDS) was used to determine the actual final compositions of the samples, which were found to be close to the target compositions. Table I shows the comparison of target and actual compositions.

Dependence of technical saturation magnetization on temperature was measured using a superconducting quantum interference device (SQUID) magnetometer under an applied field of 5 T, as shown in Fig. 1. It was observed that magnetization monotonically increased as temperature decreased from 400 to 160 K for all samples. Below 160 K, magnetization increased slowly with decreasing temperature for most samples but decreased for pure $CoFe_2O_4$ (from 160 K) and $CoGa_{0.2}Fe_{1.8}O_4$ (from 100 K). This apparent decrease can be explained by the presence of high anisotropy fields at low temperatures for these samples, which prevented complete saturation of magnetization under the field strengths used.

Symmetric magnetic hysteresis loops were measured over temperatures ranging from 10 to 400 K using a SQUID magnetometer, with a maximum applied field of 5 T. An example of the temperature dependence of the first quadrant of the hysteresis curves is given in Fig. 2 for $CoGa_{0.4}Fe_{1.6}O_4$. The coercive fields for each sample at different temperatures are shown in Fig. 3.

For the calculation of anisotropy, it was assumed that

TABLE I. Comparison of target and actual compositions in $CoGa_xFe_{2-x}O_4$.

Target composition	Composition by EDS		
	Co	Fe	Ga
$CoFe_2O_4$	0.95	2.05	···
$CoGa_{0.2}Fe_{1.8}O_4$	1.00	1.81	0.19
$CoGa_{0.4}Fe_{1.6}O_4$	1.04	1.55	0.41
$CoGa_{0.6}Fe_{1.4}O_4$	0.98	1.33	0.69
$CoGa_{0.8}Fe_{1.2}O_4$	1.04	1.15	0.81

a)Electronic mail: ranvahn@cardiff.ac.uk.

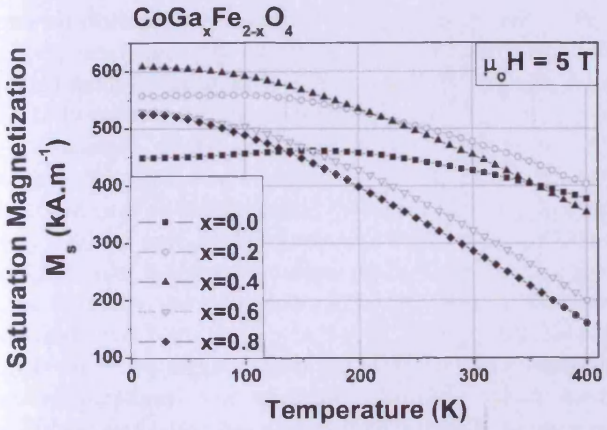

FIG. 1. Temperature dependence of magnetization of Ga-substituted cobalt ferrite at an applied field of 5 T.

after the closing of the hysteresis loops, all the irreversible processes were finished. The high field regions represent the processes of rotation against anisotropy and at the higher temperatures, forced magnetization. According to the law of approach (LA) to saturation,[5] the effect of these processes on magnetization, for $H \gg H_C$, can be modeled by the equation

$$M = M_s\left[1 - \frac{8}{105}\frac{K_1^2}{\mu_0^2 M_s^2}\frac{1}{H^2}\right] + \kappa H, \tag{1}$$

where M is magnetization, M_s is saturation magnetization, K_1 is first order cubic anisotropy coefficient, H is magnetic field, and κ is the forced magnetization coefficient representing the linear increase in spontaneous magnetization at high applied field values. The constant 8/105 applies to first order cubic anisotropy of random polycrystalline samples.

The data from high field regimes were fitted to Eq. (1). To extract the most appropriate values of K_1, M_s, and κ, only data at applied fields above 1 T were used to fit to the LA for temperatures above 150 K. For temperatures below 150 K, only data at applied fields higher than 2.5 T were fitted to the LA. The values of anisotropy coefficient K_1 computed using this procedure are shown in Fig. 4. For low Ga content (x =0, 0.2, 0.4) and low temperatures (T=100, 50, and 10 K), it was observed that the value of kappa, calculated directly from the fits, increased with decreasing temperature, which is

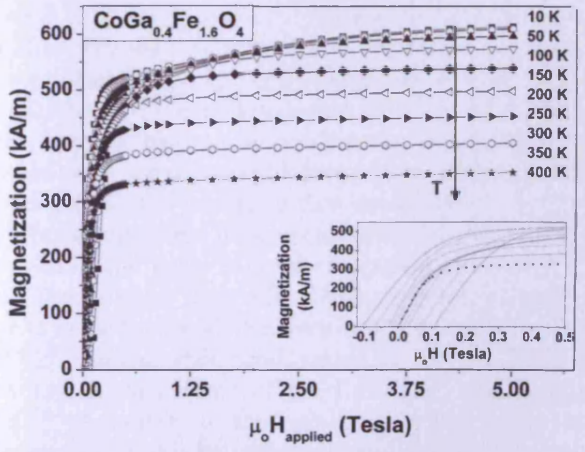

FIG. 2. First quadrant of hysteresis loops for $CoGa_{0.4}Fe_{1.6}O_4$. The inset shows the low field regions of hysteresis loops used to calculate coercivity.

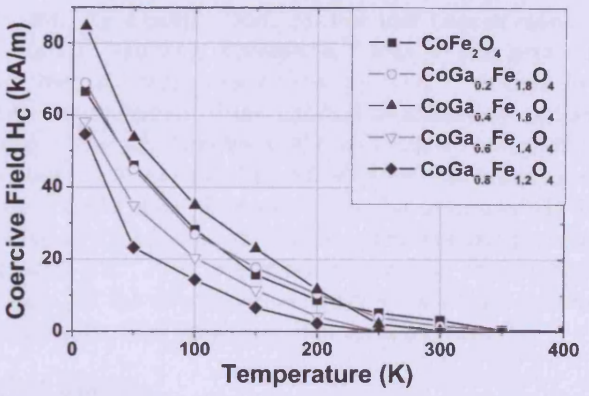

FIG. 3. Temperature dependence of coercive fields for $CoGa_xFe_{2-x}O_4$.

an artefact. In these cases, the estimated anisotropy fields were greater than the maximum applied field, thus indicating that anisotropy dominated over forced magnetization (see Conclusion and Refs. 3 and 4). Forced magnetization was assumed to be negligible at these temperatures and the experimental data were refitted to the LA with κ=0 for these points so that M_s and K_1 were the only fitting parameters for these calculations. These points are connected with a dotted line in Fig. 4. The values of M_s obtained by fitting the experimental data to Eq. (1) were in agreement with the magnetization measured at an applied field of 5 T, except for the samples with $x \leq 0.2$ for temperatures below 150 K. In these cases, the values obtained from the calculations were slightly above the measured values, which is consistent with the idea that the anisotropy field is greater than the maximum applied field.

DISCUSSION

Starting from 400 K, the anisotropy coefficient K_1 is observed to increase with decreasing temperature for all compositions, with the region of steepest increase coming at progressively lower temperatures for increasing Ga content until x=0.6, then the x=0.8 sample was essentially the same as the x=0.6 sample. However, for the low Ga contents (x=0, 0.2, or 0.4) and lower temperatures, K_1 calculated from the LA fits was observed to peak and decrease or level off. This

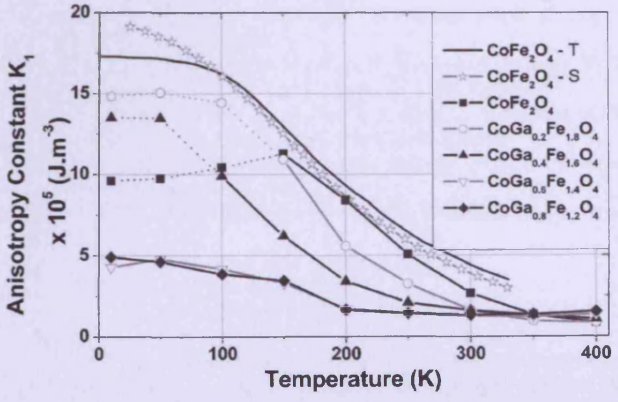

FIG. 4. Temperature dependence of cubic anisotropy constant K_1, calculated by fitting experimental data to LA, for $CoGa_xFe_{2-x}O_4$. Experimental data (Ref. 8) marked as $CoFe_2O_4$—S and theoretically calculated data (Ref. 9) marked as $CoFe_2O_4$—T are presented for comparison.

apparent decrease was because the anisotropy fields of these samples reach such high levels at low temperatures that the applied fields of up to $\mu_0 H=5$ T (maximum available) were unable to saturate the magnetization.

Estimation of the anisotropy fields for these samples supports this idea. For a cubic crystal with the ⟨100⟩ easy directions such as cobalt ferrite, $H_K=2K_1/\mu_0 M_s$.[6] The anisotropy field for pure cobalt ferrite at 150 K was estimated to be 4.8 T, and it should increase further at lower temperatures. Similarly, the estimated anisotropy field for the specimen with $x=0.2$ at 100 K was 5.16 T. These ideas are also supported by the magnetization data for low Ga contents and low temperatures. For example, for pure cobalt ferrite ($x=0$), magnetization has a maximum at 160 K for pure cobalt ferrite and for the gallium-substituted sample with $x=0.2$, magnetization has a maximum at 100 K (see Fig. 1). Therefore, the anisotropy prevents a complete approach to saturation in these cases and, hence, the values of K_1 calculated from fitting the experimental data to the LA equation are unreliable.

The LA gives the absolute value of the cubic anisotropy coefficient K_1. To second order, the numerical expression is the same for cubic anisotropy with the ⟨100⟩ and ⟨111⟩ easy axes. Pure cobalt ferrite has been reported to have the ⟨100⟩ easy axis directions, with K_1 values that are positive and range from 2.1×10^5 to 3.9×10^5 J/m^3 at 300 K, with variation caused by heat treatment and stoichiometry of the material.[7] The value of K_1 for pure cobalt ferrite at 300 K, in the present study, is 2.66×10^5 J/m^3. This is consistent with the results of Shenker,[8] who measured anisotropy for single-crystal pure cobalt ferrite and also with the theoretical work of Tachiki for pure cobalt ferrite[9] (see Fig. 4).

Despite the fact that the 5 T applied field cannot entirely saturate the lower Ga-content samples at the lower temperatures, magnetization at 10 K is clearly observed to increase for the $x=0.2$ and $x=0.4$ samples compared to pure $CoFe_2O_4$ (see Fig. 1). This indicates that initially, at least, the Ga^{3+} ions substitute into the tetrahedral sites in the inverse spinel structure. Ga^{3+} has ten $3d$ electrons and, thus, no magnetic moment. The net moment of ferrimagnetic spinels is determined by the difference of the octahedral moments M_B minus the tetrahedral moments M_A. Thus, the only way that substituting nonmagnetic ions can make the magnetization increase, is if they substitute onto the tetrahedral sites. It is not clear why the low temperature magnetization decreases for the higher Ga contents ($x=0.6$ and 0.8). It could be due to the additional Ga substituting into the octahedral sites for these compositions, or to noncollinear spin arrangements brought on by the decreased tetrahedral-octahedral exchange coupling. This will require further investigation.

The assertion that for low concentrations, Ga^{3+} ions occupy tetrahedral sites, is further supported by recent Mössbauer spectroscopy data, which indicate that Ga^{3+} ions appear to favor the tetrahedral sites in $CoGa_xFe_{2-x}O_4$.[10] Mn^{3+} and Cr^{3+}, on the other hand, substitute into the octahedral sites and displace some of the Co^{2+} onto the tetrahedral sites.[11,12] According to the one-ion anisotropy model, the high anisotropy of cobalt ferrite is primarily due to the presence of Co^{2+} ions on the octahedral sites of the spinel structure (see, for example, Ref. 5). For low concentrations of Ga^{3+} ($x=0.2$ and 0.4), although Ga^{3+} ions go into tetrahedral sites, they still reduce the anisotropy. This is thought to be due to the reduction of the tetrahedral-octahedral exchange coupling. For the samples $x=0.6$ and 0.8, however, the K_1 reduction could be caused by either of two mechanisms. Anisotropy could either decrease due to the additional Ga substituting into the octahedral sites for these compositions (and displacing Co^{2+} ions to tetrahedral sites), or due to further decrease of the tetrahedral-octahedral exchange coupling, which brings on noncollinear spin arrangements.

CONCLUSION

The effect of Ga substitution on the temperature dependence of the magnetic anisotropy, magnetization, and coercivity of polycrystalline cobalt ferrite $CoGa_xFe_{2-x}O_4$ ($0\leqslant x\leqslant 0.8$) was investigated over the temperature range of 10–400 K. The first order cubic anisotropy coefficient K_1 was estimated by fitting the high field region of the hysteresis loops to the law of approach to saturation. It was found that anisotropy of all Ga-substituted cobalt ferrite samples increased with decreasing temperature. It was also found that the anisotropy of gallium-substituted cobalt ferrite decreased with increasing gallium content at all temperatures. It was observed that the magnetization at 10 K increased for lower Ga contents ($x=0.2$ and 0.4) compared to pure cobalt ferrite. The results indicate that Ga ions preferentially substitute into the tetrahedral sites. It was concluded that the anisotropy of $CoGa_xFe_{2-x}O_4$ for low Ga content ($x=0$, 0.2, and 0.4) was so high at low temperatures that it prevented complete approach to saturation, similar to what had been observed with Mn or Cr substitution.[3,4] Thus, it is not possible to reliably calculate the values of K_1 at these low temperatures using the law of approach method.

ACKNOWLEDGMENTS

This research was supported by the U.K. Engineering and Physical Sciences Research Council under Grant No. EP/D057094 and by the U.S. National Science Foundation under Grant No. DMR-0402716.

[1] Y. Chen, J. E. Snyder, C. R. Schwichtenberg, K. W. Callum, and D. C. Jiles, IEEE Trans. Magn. **35**, 3652 (1999).
[2] J. A. Paulsen, A. P. Ring, C. C. H. Lo, J. E. Snyder, and D. C. Jiles, J. Appl. Phys. **97**, 044502 (2005).
[3] Y. Melikhov, J. E. Snyder, C. C. H. Lo, P. N. Matlage, S. H. Song, K. W. Dennis, and D. C. Jiles, IEEE Trans. Magn. **42**, 2861 (2006).
[4] Y. Melikhov, J. E. Snyder, C. C. H. Lo, A. P. Ring, J. A. Paulsen, K. W. Dennis, and D. C. Jiles, J. Appl. Phys. **99**, 08R102 (2006).
[5] S. Chikazumi, *Physics of Ferromagnetism*, 2nd ed. (Oxford University Press, Oxford, 1997), pp. 503–508.
[6] B. D. Cullity, *Introduction to Magnetic Materials* (Addison-Wesley, Reading, MA, 1972), p. 233.
[7] J. Smit, *Ferrites* (Wiley, New York, 1959), p. 163.
[8] H. Shenker, Phys. Rev. **107**, 1246 (1957).
[9] M. Tachiki, Prog. Theor. Phys. **23**, 1055 (1960).
[10] K. Krieble, M. Devlin, S. J. Lee, S. T. Aldini, and J. E. Snyder, "Investigation of Ga substitution in Cobalt-Ferrite ($CoGa_xFe_{2-x}O_4$) using Mossbauer spectroscopy," J. Appl. Phys. (these proceedings), Abstract No. BH-15.
[11] K. Krieble, C. C. H. Lo, Y. Melikhov, and J. E. Snyder, J. Appl. Phys. **99**, 08M812 (2006).
[12] K. Krieble *et al.*, J. Appl. Phys. **97**, 10F101 (2005).

Temperature Dependence of Magnetostriction of $Co_{1+x}Ge_xFe_{2-2x}O_4$ for Magnetostrictive Sensor and Actuator Applications

Naresh Ranvah[1], I. C. Nlebedim[1], Y. Melikhov[1], J. E. Snyder[1], D. C. Jiles[1], *Fellow, IEEE*, A. J. Moses[1], P. I. Williams[1], F. Anayi[1], and Sang-Hoon Song[2]

[1]Wolfson Centre for Magnetics, Cardiff University, Wales CF24 3AA, U.K.
[2]Materials Science Engineering Department, Iowa State University, Ames, IA 50010 USA

The temperature dependence of the magnetoelastic properties of a series of germanium/cobalt co-substituted cobalt ferrite samples has been measured. Magnetostriction loops of the compositions $Co_{1+x}Ge_xFe_{2-2x}O_4$ ($x = 0.1$, 0.3, and 0.6) were measured over a temperature range of 250–400 K. Germanium/cobalt co-substitution was found to change the Curie temperature, anisotropy, and the magnetostriction coefficients in the crystal directions of [100] and [111]. Both magnetostriction and strain sensitivity were seen to decrease in magnitude with increasing temperature. $Co_{1.1}Ge_{0.1}Fe_{1.8}O_4$ was found to have a maximum sensitivity $(d\lambda/dH)_\sigma$ of 2.6×10^{-9} $A^{-1}.m$, which is twice the value obtained for pure cobalt ferrite, without any decrease in maximum magnetostriction in the linear region.

Index Terms—**Cobalt ferrite, germanium substitution, magnetostriction, stress sensor.**

I. Introduction

COBALT ferrite based materials have generated considerable interest for applications in magnetostrictive torque and stress sensor and actuator applications [1]–[4]. Magnetoelastic stress sensors work on the principle that basic magnetic properties such as permeability and magnetization are altered in the presence of stress due to the magnetoelastic coupling which results in a stress dependent contribution to the anisotropy that alters the permeability of the material. This contribution is sometimes represented as an equivalent field H_σ although the analogy with magnetic field is not exact. Thus, stress can be detected by using a non-contact magnetic field sensor to measure the altered magnetic properties of a magnetoelastic material [1].

An ideal non-contact magnetoelastic sensor material will have a high sensitivity of magnetic flux density to applied stress $(dB/d\sigma)_H$ (where B is the magnetic flux density and σ is the stress, λ is the magnetostrictive strain, and H is the magnetic field) and negligible hysteresis. The relationship between strain derivative and the sensitivity of magnetization to applied stress can be expressed as [5]

$$\left(\frac{d\lambda}{dH}\right)_\sigma = \mu_0 \left(\frac{dB}{d\sigma}\right)_H \tag{1}$$

where μ_0 is the permeability of free space. Thus, a high strain derivative is indicative of promising characteristics for both a magnetoelastic sensor and an actuator material.

Giant magnetostrictive materials such as Terfenol have high magnetostriction coefficients, but not a very high sensitivity of magnetic flux density to stress for a stress sensor material [1]. Cobalt ferrite-based materials have a high sensitivity of magnetization to applied stress and an excellent chemical stability, which indicate their potential for non-contact magnetostrictive sensor and actuator applications [1], [6], [7]. The niche area of application of these materials is in situations with low strain requiring high sensitivity [1]. Chemical substitutions have been used to selectively tailor the properties of these materials. Substitution for Fe^{3+}-cations with trivalent M^{3+}-cations (M = Mn, Cr, and Ga), to obtain $CoM_xFe_{2-x}O_4$, produces lower Curie temperature and improved magnetic and magnetoelastic properties [3], [4], [8]. Cobalt ferrite has a cubic spinel-type structure in which the O^{2-} ions form an fcc-like lattice. The Co^{2+} and Fe^{3+} ions occupy either of the two interstitial sites—tetrahedral (A sites) or octahedral (B sites). Magnetic and magnetoelastic properties of cobalt ferrite-based materials depend on the exchange interactions, which in turn depends on the cation distribution in the lattice. The cobalt ions in cobalt ferrite have a preference for the octahedral (B) sites and the actual distribution depends on how close to equilibrium these distributions get, and that in turn depends on the thermal treatment during processing [9]. In the present work, the effect of germanium/cobalt-substitution on the temperature dependence of the magnetoelastic properties of $Co_{1+x}Ge_xFe_{2-2x}O_4$ has been studied over a temperature range of 250–400 K for $x = 0.1, 0.3$, and 0.6. The substitution of a tetravalent Ge^{4+}-ion and divalent Co^{2+}-ion for two trivalent Fe^{3+} ions was expected to produce a cation distribution that is different from that of previously tested trivalent substitutions and hence the material was expected to exhibit different properties from those of the previous materials.

II. Sample Preparation

A series of polycrystalline Ge/Co-substituted cobalt ferrite samples, $Co_{1+x}Ge_xFe_{2-2x}O_4$, was prepared by standard powder ceramic techniques using a final sintering at a temperature of 1623 K for 24 hours, followed by furnace cooling to room temperature [1], [2]. Energy dispersive x-ray spectroscopy (EDS/EDX) was used to determine the actual chemical compositions, which were found to be close to the target compositions (see Table I) [10].

Digital Object Identifier 10.1109/TMAG.2008.2004535

TABLE I
COMPOSITION OF $Co_{1+x}Ge_xFe_{2-2x}O_4$ DETERMINED BY EDS [10]

Target compositions	Composition by EDS		
	Fe	Co	Ge
Co1.1Ge0.1Fe1.8O4	1.77	1.11	0.12
Co1.3Ge0.3Fe1.4O4	1.29	1.33	0.38
Co1.6Ge0.6Fe0.8O4	0.70	1.63	0.67

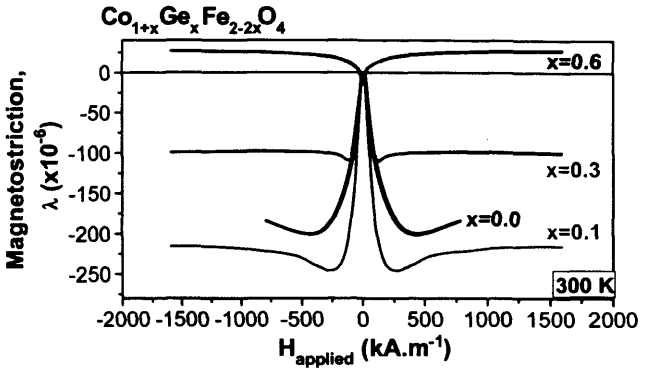

Fig. 1. Field induced magnetostriction of $Co_{1+x}Ge_xFe_{2-2x}O_4$ ($x = 0.0$ from [2]) at 300 K.

III. EXPERIMENTAL DETAILS

The Curie temperatures were determined by vibrating sample magnetometry and they were found to decrease with increasing Ge-content. Curie temperatures of samples with Ge-content of $x = 0.1$, 0.3, and 0.6 were measured to be 715 K, 558 K and 407 K respectively. The Curie temperature of pure cobalt ferrite prepared by the same process was 784 K [3]. The field-induced magnetostriction was measured with a strain gauge setup. 350 Ω strain gauges and M-Bond 610 strain gauge adhesive from Vishay Micromeasurements were used; both function over the entire temperature range of the experiment. Magnetostriction loops ($\lambda - H$) were measured over a field range of $-2\ \mathrm{T} \leq \mu_0 H \leq 2\ \mathrm{T}$ within a temperature range of 250–400 K.

IV. RESULTS AND DISCUSSION

The magnetostriction curves at room temperature of all the measured compositions are shown in Fig. 1. Fig. 2 shows the variation of the sensitivity parameter $d\lambda/dH$ with field and composition.

A. Shapes of the Curves

Over the temperature range of 250–400 K, three different shapes of magnetostriction curves were observed and classified as shown in Fig. 3(a) and (b). Cobalt ferrite has two independent magnetostriction coefficients, λ_{100} and λ_{111}, along the two crystal directions of [100] and [111] respectively. At 300 K, it is known that $\lambda_{100} < 0$, $\lambda_{111} > 0$, and $|\lambda_{100}| > (3/2)|\lambda_{111}|$ in pure cobalt ferrite. Furthermore, the first order cubic anisotropy constant K_1 for pure cobalt ferrite is positive at all temperatures, making [100] the easy-direction. At low field values, the field-induced strain $\lambda(H)$ has a large negative slope due to a dominant contribution from λ_{100}. After the alignment of domain magnetizations with the local easy axes, a further increase

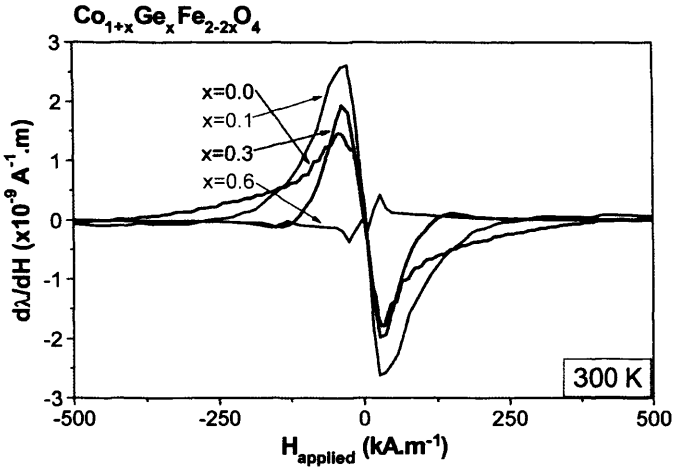

Fig. 2. Strain derivative ($d\lambda/dH$) of $Co_{1+x}Ge_xFe_{2-2x}O_4$ ($x = 0.0$ from [2]) at 300 K.

in field causes $\lambda(H)$ to increase slowly with a positive slope because of the contribution from λ_{111} as some magnetization vectors are forced away from the easy axes towards the hard axes in order to align with the magnetic field. These variations and the contributions of the two magnetostriction coefficients to the shape of the field-induced magnetostriction curve of pure cobalt ferrite under different conditions have been discussed by others [11].

The three shapes found in the magnetostriction curves of germanium/cobalt substituted cobalt ferrite are due to the changes in K_1, λ_{100} and λ_{111} with temperature and composition. Shape-A was obtained when the contribution of λ_{100} to strain increased faster with increasing field than the λ_{111} contribution, at low fields. This initial high negative slope continued until complete alignment of domains with the easy [100] axes. An increase in field beyond this point results in λ_{111} making a contribution to the positive slope of $\lambda(H)$ at these fields. The positive slope at high fields is much less than the negative slope at low fields. Shape-A was observed for samples with Ge-content of $x = 0.1$ at all observed temperatures, and for $x = 0.3$ at 250 and 300 K.

Shape-B was observed when the contribution of λ_{100} to $\lambda(H)$ was dominant at all fields. At high field values, the contribution of λ_{111} was either negligible or small and negative. Shape-B was observed for samples with Ge-content of $x = 0.3$ at 350 and 400 K.

Shape-C is an inverted form of Shape-B. Such characteristic shape of $\lambda(H)$ curve can be obtained when either the contribution of λ_{100} to the field induced magnetostriction becomes negligible, or when λ_{100} or K_1 switches sign. Shape C was observed for $Co_{1.6}Ge_{0.6}Fe_{0.8}O_4$ over the entire temperature range of the experiment.

B. Strain Amplitude and Strain Derivative

The field-induced magnetostrictive strain amplitude $\lambda_{\mathrm{max,linear}}$, for the initial high-sensitivity "linear" region of the λ(H) characteristic, was determined. For Shape-A, the maximum of λ(H) at the end of the linear region was chosen as the value of $\lambda_{\mathrm{max,linear}}$. For Shape-B and C, the end of "linear"

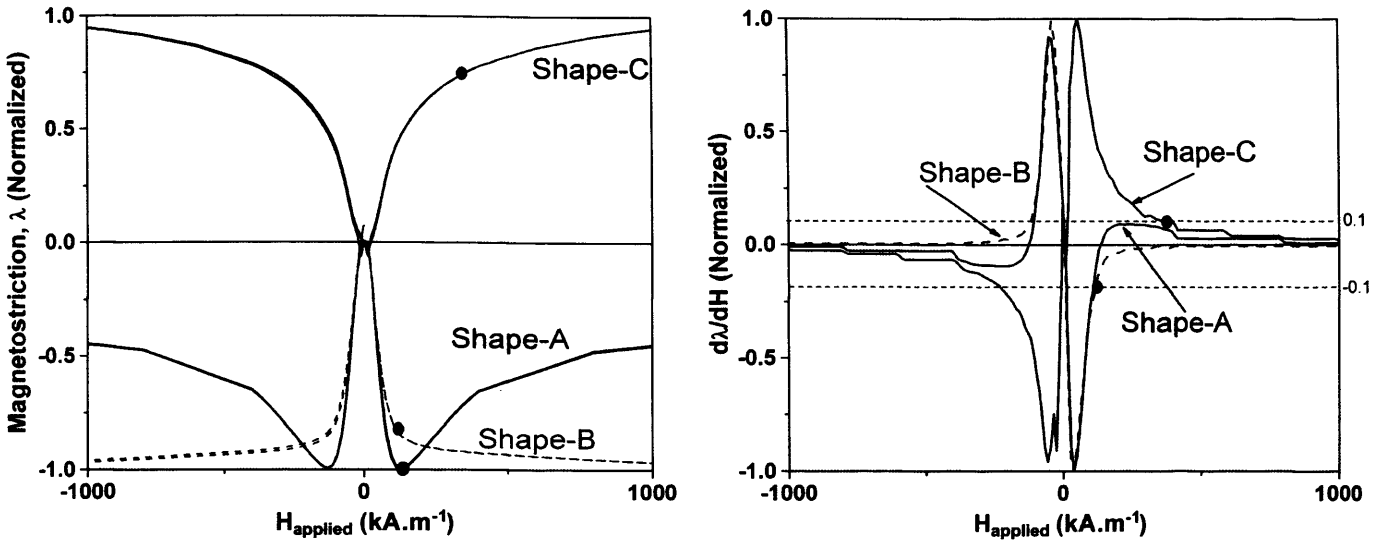

Fig. 3. (a) Classification of different shapes of magnetostriction $\lambda - H$ curves. (b) Corresponding $d\lambda/dH - H$ curves. Field induced magnetostrictive strain amplitude is marked with filled dots onto both the curves. For Shape-B and Shape-C, the value of magnetostrictive strain amplitude was chosen as the point where the value of $d\lambda/dH$ is 10% of the $(d\lambda/dH)_{max}$ for that sample. Such points have been marked with filled dots on curves corresponding for Shape-B and Shape-C.

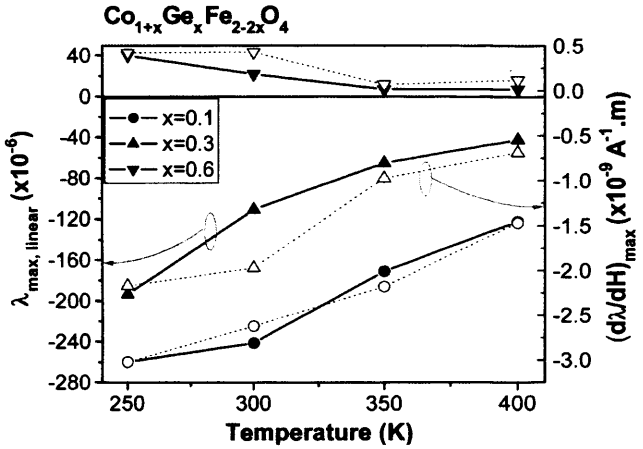

Fig. 4. Solid lines and solid symbols show the field induced magnetostrictive stain amplitude $\lambda_{max,linear}$. Dotted lines and hollow symbols show amplitude of field-induced strain derivative $(d\lambda/dH)_{max}$. Note that the sample with Ge-content of $x = 0.6$ had a positive magnetostriction, whereas all other samples had negative magnetostriction. For pure cobalt ferrite, the value of $\lambda_{max,linear}$ is -225×10^{-6} and the value of $(d\lambda/dH)_{max}$. is -1.3×10^{-9} A^{-1}.m [1].

region was chosen as the point where $(d\lambda/dH)$ has decreased to 10% of $(d\lambda/dH)_{max}$ [see Fig. 3(a) and (b)]. Fig. 4 shows the temperature dependence of $\lambda_{max,linear}$ and $(d\lambda/dH)_{max}$ for the various measured compositions. Please note that the sign of magnetostriction is also shown in the figure.

$|\lambda_{max,linear}|$ decreased for all samples with temperature increasing towards the Curie temperature T_C. $|d\lambda/dH|_{max}$, also followed the same trend with temperature. At room temperature, for the $Co_{1.1}Ge_{0.1}Fe_{1.8}O_4$ sample, the value of $\lambda_{max,linear}$ is -241×10^{-6}, which is 7% higher than for pure cobalt ferrite (-225×10^{-6}). Also the value of $(d\lambda/dH)_{max}$ for the sample with Ge-content of $x = 0.1$ was 102% higher (-2.6×10^{-9} A^{-1}.m vs. -1.3×10^{-9} A^{-1}.m) than the value for pure cobalt ferrite [1]. Thus the sample with Ge-content of $x = 0.1$ achieved a value of $\lambda_{max,linear}$ comparable to that of pure cobalt ferrite at less than half (27%) of the field needed by pure cobalt ferrite to achieve its maximum magnetostriction. In design of a sensor, this would translate to 93% less power consumption in comparison to pure cobalt ferrite.

In comparison to results of previous studies, the amplitude of strain derivative $(d\lambda/dH)_{max}$ of $Co_{1.1}Ge_{0.1}Fe_{1.8}O_4$ is comparable to that of $CoMn_{0.2}Fe_{1.8}O_4$ and $CoCr_{0.2}Fe_{1.8}O_4$ and less than that of $CoGa_{0.2}Fe_{1.8}O_4$ ($(d\lambda/dH)_{max} = -3.2 \times 10^{-9}$ A^{-1}.m) [8], [12]. However, its amplitude of field induced magnetostriction $\lambda_{max,linear}$ is more than that of $CoGa_{0.2}Fe_{1.8}O_4$ ($\lambda_{max,linear} = -192 \times 10^{-6}$), $CoCr_{0.2}Fe_{1.8}O_4$ ($\lambda_{max,linear} = -78 \times 10^{-6}$), and $CoMn_{0.2}Fe_{1.8}O_4$ ($\lambda_{max,linear} = -184 \times 10^{-6}$) [8], [13].

C. *Effect of Anisotropy*

The field induced strain derivative is an important characteristic of a magnetoelastic sensor/actuator material and it has been suggested that the strain derivative of a material depends on both magnetostriction and magnetic anisotropy. Anisotropy can be considered as the spring constant against which the field is producing a strain in the material [14]. The high sensitivity region of magnetostriction characteristics is obtained as a result of the domain magnetization processes caused by applied field or stress. These processes occur more readily in a material with a lower anisotropy. A lower polycrystalline magnetic anisotropy therefore should result in a higher sensitivity of strain to applied field. Previously, it was found that the randomly oriented magnetocrystalline anisotropy for polycrystalline materials reduces with increasing substitution of M = Cr, Mn, and Ga for Fe [3], [4], [15]. The anisotropy in cubic spinel materials, which is dependent on the exchange interaction, can be reduced due to the weakening of $A - B$ exchange interaction on substitution of other cations for Fe [13]. It is probable that such a process is responsible for the high strain derivatives observed in chemically substituted cobalt ferrite-based materials. Ge tends to have tetrahedral coordination in solid structures due

to its four unpaired electrons, and tendency towards sp^3 hybridization. Indeed, Ge^{4+}-ion has shown a preference for the tetrahedral A-sites in copper ferrite [16]. Thus, it is possible that the Ge^{4+} ions introduced into the cobalt ferrite crystal displace Co^{2+} ions into the B-sites along with the additionally substituted cobalt ions. Magnetostriction of cobalt ferrite is enhanced by the presence of cobalt in B-sites. Thus, the Ge/Co-substitution into cobalt ferrite works towards increasing both magnetostriction and sensitivity of strain to the field.

V. Conclusion

Temperature dependences of magnetoelastic properties of polycrystalline Ge/Co-substituted cobalt ferrite, $Co_{1+x}Ge_xFe_{2-2x}O_4$ with ($x = 0.1$, 0.3, and 0.6), were measured over a temperature range of 250–400 K. It was found that the contributions of the two magnetostriction coefficients, λ_{100} and λ_{111}, to field-induced strain $\lambda(H)$ changed with chemical composition and temperature. The field-induced strain amplitude $\lambda_{max,linear}$ and strain derivative $(d\lambda/dH)_{max}$ were observed to decrease in magnitude with increasing temperature. These two parameters were also seen to decrease at all temperatures as Ge-content increased from $x = 0.1$ to $x = 0.6$. However, $\lambda_{max,linear}$ for $x = 0.1$ was 7% greater than for pure cobalt ferrite, and $(d\lambda/dH)_{max}$ for $x = 0.1$ was -2.6×10^{-9} $A^{-1}.m$, which is double that of pure cobalt ferrite under the same conditions. This represents a significant improvement given that the Curie temperature of $Co_{1.1}Ge_{0.1}Fe_{1.8}O_4$ is also about 65°C less than that of pure cobalt ferrite indicating the likelihood of less magnetomechanical hysteresis for sensor applications at room temperature. The higher strain derivative of $Co_{1.1}Ge_{0.1}Fe_{1.8}O_4$ also ensures lower power consumption in a sensor or actuator device. The understanding of effect of chemical substitution on temperature dependence of magnetoelastic properties of novel Ge/Co co-substituted cobalt ferrite has therefore provided an increased understanding of the potential of cobalt ferrite based materials for sensor and actuator applications over a range of temperature.

Acknowledgment

This research was supported in part by the UK Engineering and Physical Sciences Research Council under Grant EP/D057094 and in part by the US National Science Foundation under Grant DMR-0402716.

References

[1] Y. Chen, J. E. Snyder, C. R. Schwichtenberg, K. W. Callum, and D. C. Jiles, "Metal-bonded Co-ferrite composites for magnetostrictive torque sensor applications," *IEEE Trans. Magn.*, vol. 35, no. 5, p. 3652, 1999.

[2] J. A. Paulsen, A. P. Ring, C. C. H. Lo, J. E. Snyder, and D. C. Jiles, "Manganese-substituted cobalt ferrite magnetostrictive materials for magnetic stress sensor applications," *J. Appl. Phys.*, vol. 97, p. 044502, 2005.

[3] Y. Melikhov and J. E. Snyder *et al.*, "Temperature dependence of magnetic anisotropy in Mn-substituted cobalt ferrite," *J. Appl. Phys.*, vol. 99, p. 08R102, 2006.

[4] Y. Melikhov and J. E. Snyder *et al.*, "The effect of Cr-substitution on the magnetic anisotropy and its temperature dependence in Cr-substituted cobalt ferrite," *IEEE Trans. Magn.*, vol. 42, no. 10, pp. 2861–2863, 2006.

[5] R. M. Bozorth, *Ferromagnetism*. Princeton, NJ: D. Van Nostrand, 1951.

[6] Y. Chen, J. E. Snyder, K. W. Dennis, R. W. McCallum, and D. C. Jiles, "Temperature dependence of the magnetomechanical effect in metal-bonded cobalt ferrite composites under torsional strain," *J. Appl. Phys.*, vol. 87, no. 9, pp. 5798–5800, 2000.

[7] B. Zhou and Y.-W. Zhang *et al.*, "Enhanced magnetooptical Kerr effects and decreased Curie temperature in Co-Mn ferrite thin films," *Appl. Phys. Lett.*, vol. 79, no. 12, pp. 1849–1851, 2001.

[8] N. Ranvah and Y. Melikhov *et al.*, "Variation of magnetoelastic properties of $CoGa_xFe_{2-x}O_4$ with temperature," in *Presentation HG-08 52nd Conf. Magnetism and Mag. Mater.*, Tampa, FL, 5–9, 2007.

[9] G. A. Sawatzky, F. Van Der Woude, and A. H. Morrish, "Mössbauer study of several ferrimagnetic spinels," *Phys. Rev.*, vol. 187, no. 2, pp. 747–757, Nov. 1969.

[10] S. H. Song, "Magnetic and magnetoelastic properties of M-substituted cobalt ferrites (M = Mn, Cr, Ga, Ge)," Ph.D. dissertation, Iowa State Univ., Ames, IA, 2007.

[11] R. M. Bozorth, E. F. Tilden, and A. J. Williams, "Anisotropy and magnetostriction of some ferrites," *Phys. Rev.*, vol. 99, no. 6, pp. 1788–1798, Sep. 1955.

[12] C. C. H. Lo, "Compositional dependence of the magnetomechanical effect in substituted cobalt ferrite for magnetoelastic stress sensors," *IEEE Trans. Magn.*, vol. 43, no. 6, 2007.

[13] S. J. Lee and C. C. H. Lo *et al.*, "Magnetic and magnetoelastic properties of Cr-substituted cobalt ferrite," *J. Appl. Phys.*, vol. 102, no. 7, p. 073910, 2007.

[14] Y. Chen, B. K. Kriegermeier-Sutton, J. E. Snyder, K. W. Dennis, R. W. McCallum, and D. C. Jiles, "Magnetomechanical effects under torsional strain in iron, cobalt and nickel," *J. Magnetism Magn. Mater.*, vol. 236, no. 1–2, pp. 131–138, Oct. 2001.

[15] N. Ranvah and Y. Melikhov *et al.*, "Temperature dependence of magnetic anisotropy of Ga-substituted cobalt ferrite," *J. Appl. Phys.* vol. 103, no. 7, p. 07E506, 2008. [Online]. Available: http://link.aip.org/link/?JAP/103/07E506/1

[16] A. D. Al-Rawas and A. Rais *et al.*, "Magnetic properties of $Cu_{1+x}M_xFe_{2-2x}O_4$ mixed ferrites (M = Ge, Ti, $0 \leq x \leq 0.4$)," *J. Magnetism Magn. Mater.*, vol. 269, no. 2, pp. 168–175, 2004.

Manuscript received March 03, 2008. Current version published December 17, 2008. Corresponding author: N. Ranvah (e-mail: RanvahN@cf.ac.uk; RanvahN@cardiff.ac.uk).

Temperature dependence of magnetic anisotropy of germanium/cobalt cosubstituted cobalt ferrite

N. Ranvah,[a] Y. Melikhov, I. C. Nlebedim, D. C. Jiles, J. E. Snyder, A. J. Moses, and P. I. Williams
Wolfson Centre for Magnetics, Cardiff University, Cardiff CF24 3AA, United Kingdom

(Presented 14 November 2008; received 22 September 2008; accepted 4 January 2009; published online 9 March 2009)

The variations in magnetization and magnetic anisotropy of Ge^{4+}/Co^{2+} cosubstituted cobalt ferrite with temperature were investigated for a series of compositions $Co_{1+x}Ge_xFe_{2-2x}O_4$ ($0 \leq x \leq 0.4$). The magnetization at 5 T and low temperature were observed to increase for all Ge/Co cosubstituted samples compared to pure $CoFe_2O_4$. Hysteresis loops were measured for each sample over the magnetic field range of −5 T to +5 T for temperatures in the range of 10–400 K. The high field regions of these loops were modeled using Law of Approach to saturation, which represents the rotational and forced magnetization processes. The first order cubic magnetocrystalline anisotropy coefficient K_1 was calculated from these fits. K_1 decreased with increasing Ge content at all temperatures. Anisotropy increased substantially as temperature decreased. Below 150 K, for certain compositions ($x=0$, 0.1, 0.2, and 0.3), the maximum applied field of $\mu_0 H=5$ T was less than the anisotropy field and therefore insufficient to saturate the magnetization. In these cases, the use of the Law of Approach model can give values of K_1 that are lower than the correct values and this method cannot be used to estimate anisotropy accurately under these conditions. © *2009 American Institute of Physics*. [DOI: 10.1063/1.3077201]

I. INTRODUCTION

There has been a recent interest in cobalt ferrite based materials because of their high magnetostrictive strain amplitude, high magnetostrictive strain derivative (rate of change in magnetostrictive strain with applied field), and low hysteresis, which makes them a candidate material for high performance stress/torque sensor and actuator applications.[1–6] Chemical substitution can enhance the properties of cobalt ferrite by altering the cation distribution in the cubic spinel structure, therefore, influencing the magnetoelastic properties of these materials. Previous studies have shown that the substitution of M^{3+} (Mn^{3+}, Cr^{3+}, and Ga^{3+})[2,3,7] in place of some of Fe^{3+} reduces the hysteresis and increases the strain derivative of cobalt ferrite for certain compositions with, however, a decline or no improvement in the magnitude of magnetostrictive strain amplitude. The change in magnetoelastic properties of these materials can be explained in terms of the change in important magnetic properties such as the magnetization characteristics and magnetocrystalline anisotropy.

In the present study, we have investigated a new cosubstitution of Ge^{4+}/Co^{2+} in place of some of Fe^{3+} in cobalt ferrite. The high tetrahedral site preference of Ge^{4+} in the cubic spinel lattice of cobalt ferrite and the additional substitution of Co^{2+} produced a more favorable change in properties in comparison to previously tried substitutions.

II. EXPERIMENT AND RESULTS

A series of randomly oriented polycrystalline Ge^{4+}/Co^{2+} cosubstituted cobalt ferrite samples with general composition of $Co_{1+x}Ge_xFe_{2-2x}O_4$ was made by standard powder ceramic techniques with a final sintering at 1350 °C for 24 h, followed by furnace cooling to room temperature.[1,3] The target compositions had a germanium content of $x=0$, 0.1, 0.2, 0.3, and 0.4. The actual compositions were determined using energy dispersive x-ray spectroscopy (EDS) in a scanning electron microscope (SEM) and were found to be close to the target compositions, as shown in Table I. The Curie temperatures of Ge/Co cosubstituted cobalt ferrite have been found to decrease with increasing x.[8]

The variation in technical saturation of magnetization with temperature was measured using a superconducting quantum interference device (SQUID) magnetometer at an applied field of $\mu_0 H=5$ T. As can be seen in Fig. 1, the magnetization increased monotonically with decreasing temperature over the range of 400–160 K for all samples. The apparent saturation magnetization decreased for $CoFe_2O_4$ below 160 K, for $Co_{1.1}Ge_{0.1}Fe_{1.8}O_4$ below 128 K, and for $Co_{1.2}Ge_{0.2}Fe_{1.6}O_4$ below 78 K. For all other samples, saturation magnetization was observed to increase with decreasing temperature throughout the entire temperature range.

TABLE I. Comparison of target and actual compositions in $CoGe_xFe_{2-2x}O_4$.

	Composition by EDS		
Target compositions	Fe	Co	Ge
$CoFe_2O_4$	2.05	0.95	···
$Co_{1.1}Ge_{0.1}Fe_{1.8}O_4$	1.77	1.11	0.12
$Co_{1.2}Ge_{0.2}Fe_{1.6}O_4$	1.57	1.21	0.22
$Co_{1.3}Ge_{0.3}Fe_{1.4}O_4$	1.29	1.33	0.38
$Co_{1.4}Ge_{0.4}Fe_{1.2}O_4$	1.10	1.43	0.47

[a]Electronic mail: ranvahn@cf.ac.uk.

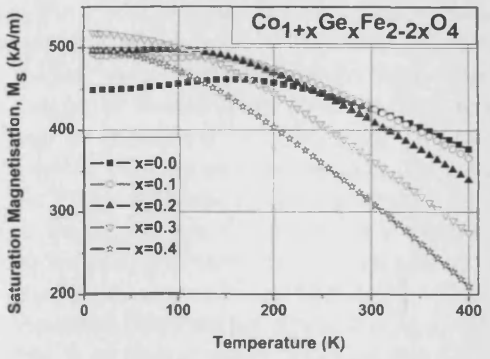

FIG. 1. The variation in technical saturation magnetization with temperature.

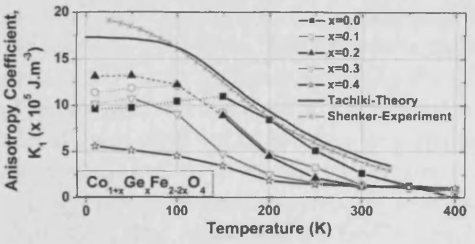

FIG. 2. Temperature dependence of cubic anisotropy coefficient K_1 calculated by fitting the experimental data to Law of Approach for $Co_{1+x}Ge_xFe_{2-2x}O_4$. Experimental data (Ref. 11) marked as Shenker experiment and theoretically calculated data (Ref. 12) marked as Tachiki theory are presented for comparison.

Symmetric magnetic hysteresis loops were measured with a SQUID magnetometer for temperatures 10, 50, 100, 150, 200, 250, 300, 350, and 400 K using a maximum applied field of $\mu_0 H = 5$ T.

For calculation of anisotropy, the high field regions of the *M-H* loops were fitted to the *Law of Approach* to saturation.[9] The underlying assumption is that this high field regime represents the processes of reversible rotation of magnetization against anisotropy and forced magnetization. According to the Law of Approach, the high field regions ($H \gg H_{\text{coercivity}}$) of *M-H* loops can be described by

$$M = M_s\left[1 - \frac{8}{105}\frac{K_1^2}{\mu_0 M_s^2}\frac{1}{H^2}\right] + \kappa H, \tag{1}$$

where M is the magnetization, M_s is the saturation magnetization, H is the applied field, κ is the forced magnetization coefficient that describes the linear increase in spontaneous magnetization at high fields, and K_1 is the first order cubic anisotropy coefficient. The constant 8/105 is specific to cubic anisotropy of randomly oriented polycrystalline materials. At temperatures above 150 K, data from the field region $\mu_0 H \geq 1$ T were fitted to Eq. (1) to determine the values of parameters M_s, K_1, and κ. At temperatures below 150 K, the field range for fitting was restricted to $\mu_0 H \geq 2$ T, and, in some cases, the forced magnetization term was set to zero, i.e., $\kappa = 0$, with M_S and K_1 being the only fitting parameters (see discussion below).

III. DISCUSSION

The analysis of temperature dependence of cubic anisotropy of germanium/cobalt cosubstituted cobalt ferrite can be divided into two temperature zones, above and below 150 K. Above 150 K, the maximum applied field is sufficiently large compared to the anisotropy field so as to give good approach to saturation and good fits. The anisotropy of all samples was observed to increase as the temperature decreased. This is so because during cooling, as we move further away from the Curie temperature of these samples, the ratio of exchange interaction to thermal energy increases, which contributes to the increase in anisotropy. As the temperature was reduced from 400 K, the cubic anisotropy for every sample increased slowly at first and steeply below a certain temperature. As can be seen in Fig. 2, the region of steep increase in K_1 moved to lower temperatures as the Ge/Co ratio increased from $x = 0.0$ to $x = 0.4$. It is possible that this effect is correlated with the decrease in Curie temperature of Ge/Co cosubstituted cobalt ferrite with increasing germanium/cobalt ratio.

Below 150 K, the first order magnetocrystalline cubic anisotropy coefficient K_1 appears to decrease with decreasing temperature for $CoFe_2O_4$ below 150 K, for $Co_{1.1}Ge_{0.1}Fe_{1.8}O_4$ below 100 K, and for $Co_{1.2}Ge_{0.2}Fe_{1.6}O_4$ and $Co_{1.3}Ge_{0.3}Fe_{1.4}O_4$ below 50 K. This apparent decrease can be explained by the presence of anisotropy fields higher than the applied field of $\mu_0 H = 5$ T. This high anisotropy prevents the rotation against it, therefore, causing the apparent saturation magnetization to decrease for $CoFe_2O_4$ below 160 K, for $Co_{1.1}Ge_{0.1}Fe_{1.8}O_4$ below 128 K, and for $Co_{1.2}Ge_{0.2}Fe_{1.6}O_4$ below 78 K, and preventing from complete saturation being reached in these cases (see Fig. 1). The estimated value of anisotropy field $H_k = 2K_1/(\mu_0 M)$ (Ref. 10) for pure cobalt ferrite at 150 K is 4.8 T and is expected to rise above the maximum applied field of 5 T at temperatures below 150 K. Therefore, in these cases, the anisotropy coefficient could not be calculated accurately by fitting the data available to the Law of Approach even using special adjustment procedures.[6] As anisotropy field increased significantly close to 150 K, the region of hysteresis loop where rotation of magnetization against anisotropy takes place shifts to higher field values; therefore, the field range for fitting was restricted to $\mu_0 H \geq 2$ T. Additionally, the force magnetization coefficient was set to zero, i.e., $\kappa = 0$, as in the presence of such high anisotropy fields, the maximum applied field of $\mu_0 H = 5$ T was not sufficient to cause forced magnetization, but rather is still rotating magnetization against the high anisotropy field. Despite these adjustment procedures the values of anisotropy coefficient K_1, calculated with $\kappa = 0$, are suspect and are connected with dotted lines in Fig. 2. The results from Shenker,[11] who determined cubic anisotropy of $CoFe_2O_4$ using single crystals and torque measurements near their easy axes, support our hypothesis of high anisotropy fields. Additionally, the room temperature value of K_1 for $CoFe_2O_4$ we determined ($K_1 = 2.66 \times 10^5$ J m^{-3}) is consistent with the theoretical predictions made by Tachiki.[12]

As can be seen from Fig. 1, the sample with Ge concentration of $x = 0.1$ has higher technical saturation magnetization than pure cobalt ferrite at room temperature. Furthermore, the extrapolated 0 K saturation magnetization $M(0\ \text{K})$ appears to increase initially as we substitute Ge/Co into co-

balt ferrite (for $x=0.1$, 0.2, and 0.3) and then it reduces with high concentration of Ge ($x=0.4$). This indicates that at least initially, the Ge^{4+} ions substitute predominantly into the tetrahedral sites in the inverse spinel structure. This increase in $M(0\ K)$ can be understood by considering the structure of the ferrimagnetic cubic spinels and the fact that at least initially the Ge^{4+} ions substitute predominantly into the tetrahedral sites in the inverse spinel structure. In a spinel structure, there are twice as many octahedral sites as tetrahedral sites, and the moments on the octahedral sites and tetrahedral sites couple antiparallel. Thus the net moment is $M_{oct}-M_{tet}$. Pure cobalt ferrite is an inverse spinel, meaning that Co^{2+} has an energetic preference for the octahedral sites; however, it tends not to be 100% inverse, meaning that some smaller amount of Co does reside on the tetrahedral sites. Ge^{4+}, on the other hand, is expected to have a natural preference for the tetrahedral sites due to its tetravalence and tendency toward sp^3 hybridization.[13] So although in Ge^{4+}/Co^{2+} cosubstitution for Fe^{3+} much of the Co^{2+} might be substituting into the octahedral sites and decreasing M_{oct} by a little, most of the Ge^{4+} indeed appears to be substituting into the tetrahedral sites, decreasing M_{tet} by much more (since Ge^{4+} has no magnetic moment). Thus the net moment goes up. For high content of Ge ($x=0.4$), $M(0\ K)$ appears to decrease again. This could be due to either some of the additional Ge^{4+} substituting into the octahedral sites or due to decrease in the tetrahedral-octahedral exchange coupling to the point that a noncollinear spin arrangement occurs.[14]

The substitution of Ge^{4+} reduces the exchange coupling between the octahedral and tetrahedral sites, as can be seen from the steep decrease in Curie temperature with Ge content.[8] It is probable that this reduction in exchange coupling is responsible for the reduction in the magnitude of magnetic anisotropy, despite the fact that upon Ge/Co cosubstitution, the amount of Co in the octahedral sites most likely increases. The crystalline anisotropy in cobalt ferrite acts like the spring constant against which applied field is acting while producing magnetostriction. Thus, with reduction in anisotropy, the strain derivative (i.e., rate of change in magnetostrictive strain with applied field) increases.[15] This has been indeed observed in the case of Ge/Co cosubstitution.[8]

As opposed to all our previously investigated substitutions of Mn^{3+},[3] Cr^{3+},[4] and Ga^{3+} (Ref. 7) for Fe^{3+} in cobalt ferrite, for small amounts of Ge/Co cosubstitution ($x=0.1$), the maximum magnetostriction actually increases, rather than decreasing, and then falls off initially more slowly.[8] This is likely due to increased amount of Co^{2+} in the octahedral sites. This combination of both increasing strain derivative and increasing magnetostriction amplitude with small amounts of Ge/Co cosubstitution makes this material series favorable out of those we have investigated for stress sensor and actuator applications.

IV. SUMMARY AND CONCLUSION

The temperature dependence of magnetic properties of a series of Ge/Co cosubstituted cobalt ferrite with a general formula of $Co_{1+x}Ge_xFe_{2-2x}O_4$ has been measured within a temperature range of 10–400 K. The first order cubic anisotropy coefficient K_1 was calculated by fitting the high field regimes of the magnetization curves to the Law of Approach to saturation. K_1 was observed to increase in magnitude with decrease in temperature with the region of steep increase coming at progressively lower temperatures with increasing Ge/Co substitution. The anisotropy of Ge/Co cosubstituted cobalt ferrite was seen to decrease with increasing germanium concentration at all temperatures. The saturation magnetization at 10 K was seen to increase with germanium concentration for $0\leq x\leq 0.3$, indicating that for these compositions, Ge^{4+} substitutes predominantly into the tetrahedral sites. It was found that in certain cases of low temperature, the anisotropy of samples with germanium concentration of $x=0$, 0.1, 0.2, and 0.3 was so high that it prevents complete approach to saturation in the presence of maximum applied field of 5 T. For Ge/Co cosubstituted compositions in the region of $Co_{1.1}Ge_{0.1}Fe_{1.8}O_4$, the combination of higher magnetostrictive strain derivative brought about by lower anisotropy than pure cobalt ferrite and the increased maximum magnetostriction make this material a favorable candidate for stress sensor and actuator applications.

ACKNOWLEDGMENTS

This research was supported by the UK Engineering and Physical Sciences Research Council under Grant No. EP/D057094 and by the U.S. National Science Foundation under Grant No. DMR-0402716.

[1] Y. Chen, J. E. Snyder, C. R. Schwichtenberg, K. W. Callum, and D. C. Jiles, IEEE Trans. Magn. **35**, 3652 (1999).
[2] S. J. Lee, C. C. H. Lo, P. N. Matlage, S. H. Song, Y. Melikhov, J. E. Snyder, and D. C. Jiles, J. Appl. Phys. **102**, 073910 (2007).
[3] J. A. Paulsen, A. P. Ring, C. C. H. Lo, J. E. Snyder, and D. C. Jiles, J. Appl. Phys. **97**, 044502 (2005).
[4] Y. Melikhov, J. E. Snyder, C. C. H. Lo, P. N. Matlage, S. H. Song, K. W. Dennis, and D. C. Jiles, IEEE Trans. Magn. **42**, 2861 (2006).
[5] Y. Melikhov, J. E. Snyder, C. C. H. Lo, A. P. Ring, J. A. Paulsen, K. W. Dennis, and D. C. Jiles, J. Appl. Phys. **99**, 08R102 (2006).
[6] N. Ranvah, Y. Melikhov, D. C. Jiles, J. E. Snyder, A. J. Moses, P. I. Williams, and S. H. Song, J. Appl. Phys. **103**, 07E506 (2008).
[7] N. Ranvah, Y. Melikhov, J. E. Snyder, S. H. Song, D. C. Jiles, A. J. Moses, and P. I. Williams, 52nd Conference on Magnetism and Magnetic Materials, Tampa, Florida, 2007 (unpublished).
[8] N. Ranvah, I. C. Nlebedim, Y. Melikhov, J. E. Snyder, D. C. Jiles, A. J. Moses, P. I. Williams, F. Anayi, and S.-H. Song, IEEE Trans. Magn. **44**, 3013 (2008).
[9] S. Chikazumi, *Physics of Ferromagnetism*, 2nd ed. (Oxford University Press, New York, 1997), pp. 503–508.
[10] B. D. Cullity, *Introduction to Magnetic Materials* (Addison-Wesley, Reading, MA, 1972), p. 233.
[11] H. Shenker, Phys. Rev. **107**, 1246 (1957).
[12] M. Tachiki, Prog. Theor. Phys. **23**, 1055 (1960).
[13] A. D. Al-Rawas, A. Rais, A. A. Yousif, A. M. Gismelseed, M. E. Elzain, S. Mazen, and A. Al-Falaky, J. Magn. Magn. Mater. **269**, 168 (2004).
[14] J. Smit and H. P. J. Wijn, *Ferrites* (N.V. Philips, Eindhoven, Holland, 1959), p. 163.
[15] D. C. Jiles, J. B. Thoelke, and M. K. Devine, IEEE Trans. Magn. **28**, 27 (1992).

Temperature Dependence of Magnetic Properties of $CoAl_xFe_{2-x}O_4$

N. Ranvah, I. C. Nlebedim, Y. Melikhov, J. E. Snyder, P. I. Williams, A. J. Moses, and D. C. Jiles

Wolfson Centre for Magnetics, School of Engineering, Cardiff University, Cardiff CF24 3AA, U.K.

The temperature dependence of magnetic properties of a series of aluminium-substituted cobalt ferrite, with the general composition of $CoAl_xFe_{2-x}O_4$ ($x = 0, 0.1, 0.2, 0.5$), has been studied. It was observed that the magnetization, at an applied field of $\mu_0 H = 5$ T and a temperature of 10 K, does not change significantly for small amounts of Al, then reduces sharply for larger amounts of Al. Magnetic hysteresis loops were measured over a field range of $-5\ \text{T} \leq \mu_0 H \leq 5$ T at temperatures between 10 and 400 K. The high field regions of these loops were modelled using the Law of Approach to saturation, which can be used to calculate the magnetocrystalline anisotropy using its description of the processes of rotation of domain magnetizations against anisotropy and forced magnetization. It was found that the first-order cubic anisotropy of these materials decreased with increasing temperature. It was also observed that the anisotropy of these materials decreased with increasing Al-content at a given temperature.

Index Terms—**Aluminium substitution, cobalt ferrite, magnetic anisotropy, magnetization, site occupancy, spinel structure.**

I. Introduction

HIGHLY magnetostrictive cobalt ferrite materials have generated recent interest as candidate materials for torque/stress sensor and actuator applications [1]–[4]. The materials have attractive properties of high magnetostriction (λ), low hysteresis, high chemical stability, mechanical strength and above all high magnetostrictive strain sensitivity ($d\lambda/dH$). The high magnetostrictive strain sensitivity implies that these materials can produce high magnetostriction at low fields, which points towards a lower magnetizing current requirement in actuator applications [5]. The magnetoelastic properties of these materials are related to their magnetic properties. It has been found that a lower anisotropy leads to higher magnetostrictive stain sensitivity. In the past, several substitutions of Mn^{3+} [3], Cr^{3+} [4], Ga^{3+} [6] and Ge^{4+}/Co^{2+} [7] for some of the Fe^{3+} have been found to improve their magnetic and consequently magnetoelastic properties.

In the present work, we have investigated a new Al^{3+} substitution in the place of some of the Fe^{3+} in cobalt ferrite.

II. Sample Preparation and Experimental Details

A series of randomly oriented polycrystalline Al-substituted cobalt ferrite samples with the general formula of $CoAl_xFe_{2-x}O_4$ were prepared using standard powder ceramic techniques with a final sintering of 1300°C for 24 hours, followed by furnace cooling to room temperature [1], [2]. The target compositions were $x = 0.0, 0.1, 0.2$ and 0.5. The actual compositions were determined using energy dispersive X-ray spectroscopy (EDS) in a scanning electron microscope (SEM), and were found to be close to the target compositions (see Table I).

The temperature dependence of magnetization was measured at an applied field of $\mu_0 H = 5$ T within a temperature range of 10 K to 400 K. The magnetic hysteresis loops were measured over a field range of -5 T to $+5$ T at several temperatures between 10 K and 400 K. The high field regions of these loops were modelled using the *Law of Approach* (LA) to saturation to extract anisotropy information. The LA method accounts for the two dominant processes at high fields—rotation of domain magnetizations against anisotropy and the linearly increasing forced magnetization. These two processes have been described in the LA as [8]

$$M = M_s\left[1 - \frac{8}{105}\frac{K_1^2}{\mu_0^2 M_s^2}\frac{1}{H^2}\right] + \kappa H \qquad (1)$$

where M is the magnetization, H is the magnetic field, M_s is the saturation magnetization, K_1 is the first-order cubic anisotropy constant and the term κ is the forced magnetization coefficient that describes the linear increase in spontaneous magnetization at high fields. The constant 8/105 is relevant to the calculations for randomly oriented polycrystalline cubic materials. At temperatures above 150 K, the M-H data above $\mu_0 H = 1$ T was fitted to the LA method as described in (1) to calculate K_1. Close to 150 K, the anisotropy fields rise rapidly and hence a higher field is needed to cause rotation against anisotropy. Therefore, at these temperatures, only M-H data above $\mu_0 H = 2$ T was fitted to (1) to calculate K_1.

TABLE I
Composition of $CoAl_xFe_{2-x}O_4$ Determined by EDS

Target compositions	Composition by EDS		
	Co	Al	Fe
$CoFe_2O_4$	1.02	-	1.98
$CoAl_{0.1}Fe_{1.9}O_4$	1.03	0.08	1.89
$CoAl_{0.2}Fe_{1.8}O_4$	1.03	0.18	1.79
$CoAl_{0.5}Fe_{1.5}O_4$	1.03	0.49	1.48

III. Results and Discussions

The study of the temperature dependence of magnetic properties of aluminium-substituted cobalt ferrite can be broken down into two temperature ranges:—above and below 150 K.

Fig. 1 shows the variation of magnetization (measured at $\mu_0 H = 5$ T) with temperature. Above 150 K, the magnetization increases monotonically with decreasing temperature for all compositions. Below 150 K, the applied field of $\mu_0 H = 5$

Manuscript received March 06, 2009; revised May 24, 2009. Current version published September 18, 2009. Corresponding author: N. Ranvah (e-mail: nranvah@gmail.com).

Color versions of one or more of the figures in this paper are available online at http://ieeexplore.ieee.org.

Digital Object Identifier 10.1109/TMAG.2009.2024767

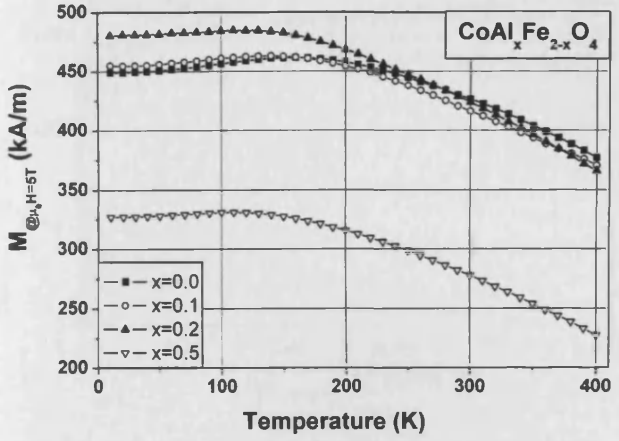

Fig. 1. Variation of magnetization of $CoAl_xFe_{2-x}O_4$ at an applied field of $\mu_0 H = 5$ T. There is a 5% error bar on all points on this graph.

T was not enough to saturate the domain magnetization and its rotation against high anisotropy fields at low temperatures. Thus, the slight decrease observed in magnetization below 150 K was not indicative of saturation magnetization. However, the magnetization at these low temperatures is still a good indicator of the trends in near zero Kelvin saturation magnetization.

The magnetic properties of cobalt ferrite based materials are heavily dependent on the site occupancy of different ions in its lattice. The spinel structure of cobalt ferrite based materials has half the number of tetrahedral sites (A) in comparison to octahedral sites (B). In a pure inverse spinel, all the divalent M^{2+} cations and half of the Fe^{3+} go into the B-sites. In reality, cobalt ferrite has Co^{2+} residing in both A and B sites and the structure is a mixed spinel.

The strongest exchange coupling is the antiparallel coupling between the A and B sites keeping the moments in them aligned antiparallel to each other. The net magnetization comes from subtracting the net moment on A-sites from the net moment on B-sites. The study of near zero Kelvin saturation magnetization is useful in this case because the magnetic moments are predominantly aligned either parallel or antiparallel to each other due to the lack of thermal disorder. Since the change in near zero Kelvin magnetization due to change in composition depends on the site occupancy and the magnetic moment contribution of the dopant ion, its analysis can be used to deduce trends in site occupancy with substitution.

It has been reported that aluminium does not have a strong preference for either of the sites in the cobalt ferrite lattice [9]. The observation that with low amounts of aluminium ($x = 0.1$ and 0.2), the saturation magnetization does not change significantly in comparison to cobalt ferrite, leads us to believe that initially aluminium ions substitute into both the sites in approximately equal numbers reducing their moments in approximately equal amounts and hence keeping the net moment at the same level as pure cobalt ferrite ($x = 0$). With higher amounts of Al, the net magnetization decreases. This could be due to the additional Al substituting increasingly into B-sites or it could be due to non-collinear spin arrangement caused by greatly decreased tetrahedral-octahedral exchange coupling.

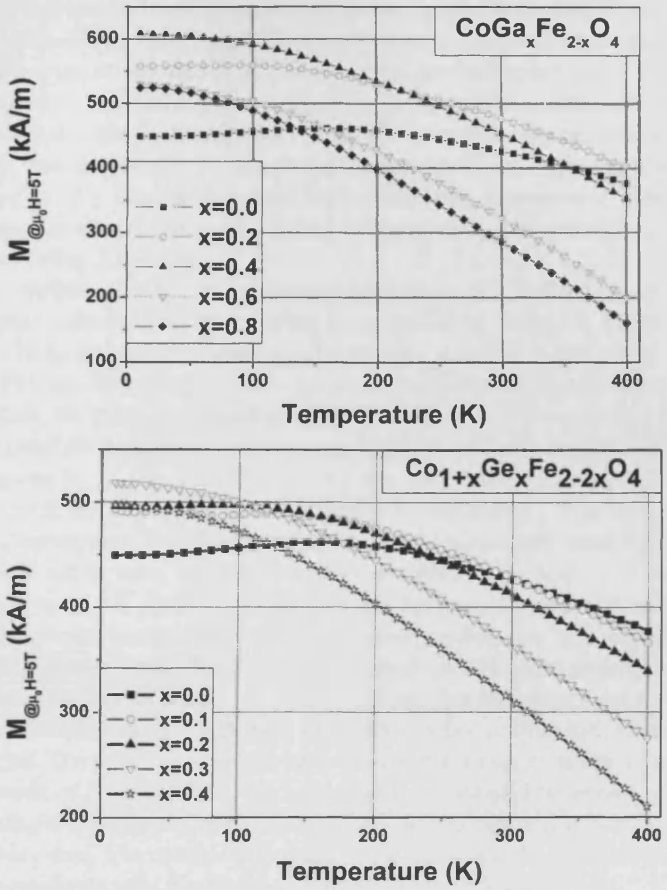

Fig. 2. Variation of magnetization of Ga-substituted [6] and Ge/Co-cosubstituted [7] cobalt ferrite at an applied field of $\mu_0 H = 5$ T.

The model outlined above can be supported by analysing the near zero Kelvin saturation magnetization in Ga-substituted and Ge/Co-cosubstituted cobalt ferrite materials (see Fig. 2). Ga^{3+} ions have a preference for A-sites [10]. Therefore, initially, for low amounts of gallium, Ga^{3+} ions substitute into the A-sites in place of Fe^{3+}. Since the Ga^{3+} ions do not contribute to the magnetic moment, the net moment in A-sites decreases, leading to an increase in the net magnetization of the material. However, for higher amounts of gallium, the net magnetization decreases. This could be due to the additional Ga substituting increasingly into B-sites, or it could be due to non-collinear spin arrangements brought on by the decreased A-B exchange coupling.

In the case of germanium substitution, Ge^{4+} ions have a very strong A-site (tetrahedral) preference because of their valence state and tendency to form four bonds with tetrahedral coordination. Therefore, for almost all compositions, the Ge^{4+} ions go into the A-sites reducing their moment and hence increasing the net magnetization [7]. The near zero Kelvin saturation magnetization observations for all the three substitutions are in agreement with the hypothesised site occupancy predictions.

An example of the M-H loops measured for calculation of the anisotropy coefficient and coercive field is shown in Fig. 3. The temperature dependence of anisotropy coefficient K_1 is shown in Fig. 4. Like the analysis of magnetization of aluminium-substituted cobalt ferrite, the analysis of anisotropy

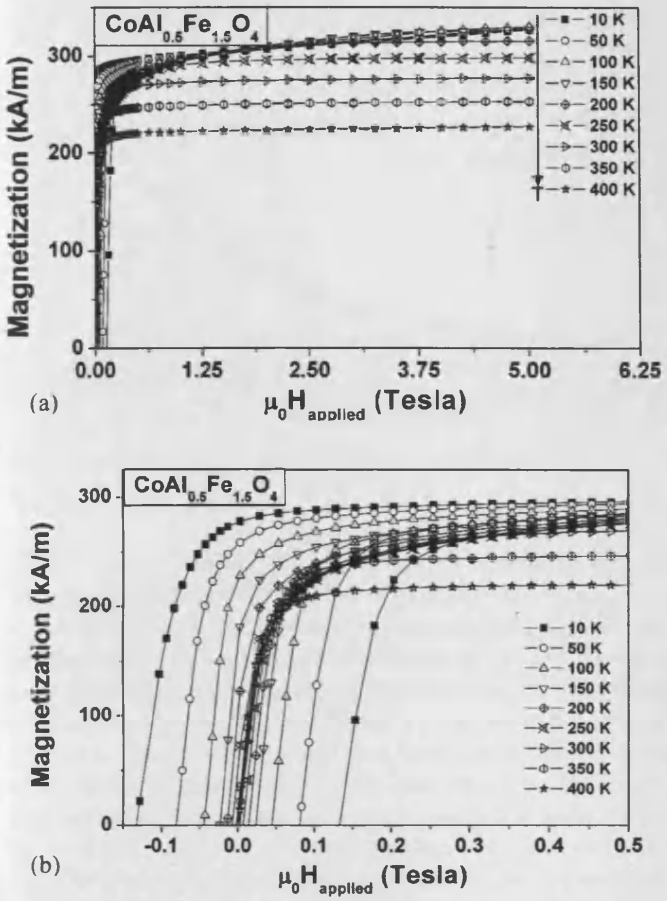

Fig. 3. First quadrant of hysteresis loop of $CoAl_{0.5}Fe_{1.5}O_4$. (a) Shows the high field regions that were used for the calculation of anisotropy. (b) Low field regions of these loops, which were used for calculation of coercive field.

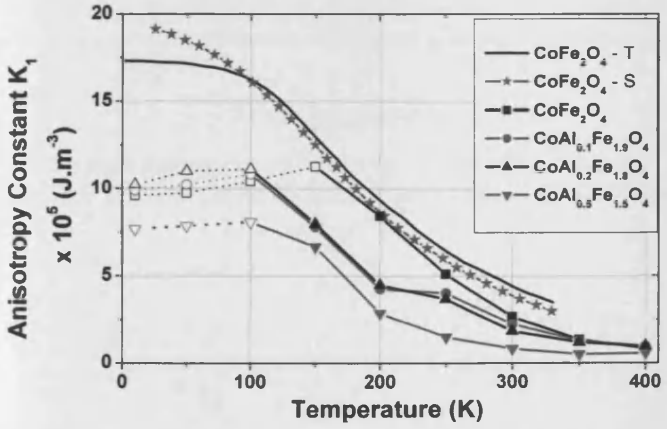

Fig. 4. First order cubic anisotropy constant of Al-substituted cobalt ferrite. The hollow markers indicate temperatures at which the anisotropy field value is more than the maximum applied field in the experiment ($\mu_0 H = 5$ T). The data is in agreement with the theoretical calculations of Tachiki [13] and experimental observations of Shenker [12], shown here as $CoFe_2O_4$-T and $CoFe_2O_4$-S respectively.

of these materials can also be broken down into two regions:- below and above 150 K.

Above 150 K, the applied fields were high enough to overcome anisotropy, and cause the rotation of the domain magnetizations against anisotropy, hence causing a complete approach to saturation. The first-order cubic anisotropy coefficient K_1 increased with decreasing temperature for all compositions of aluminium-substituted cobalt ferrite. This can be explained by exchange interactions, unchanged with temperature, dominating over thermal agitations that reduce when temperature decreases. It was also observed that, as we cooled down, beyond a certain point, K_1 increased rapidly with decreasing temperature. The region of steep increase shifted to lower temperatures with increasing Al-content.

Below 150 K, the anisotropy coefficient K_1 showed an apparent decrease with reducing temperature for $CoFe_2O_4$ below 150 K, and for all aluminium-substituted samples below 100 K. This can be explained by the presence of anisotropy fields higher than the maximum applied field of $\mu_0 H = 5$ T that prevent a complete approach to saturation. The value of anisotropy field given by $\mu_0 H_k = 2K_1/M$ [11] was calculated to be 4.8 T at 150 K for $CoFe_2O_4$ and is expected to rise above 5 T at lower temperatures. For these cases, the forced magnetization constant was set to zero, i.e., the calculations were made with $\kappa = 0$ and with M_s and K_1 being the only fitting parameters. These points are shown in Fig. 4 with hollow markers and are joined with dotted lines. Since, the assumption of complete approach to saturation of the LA method is not fulfilled in these cases, the calculation of K_1, although indicative, is not considered accurate. The anisotropy results are consistent with the experimental work of Shenker [12], who measured the cubic anisotropy of single crystals of $CoFe_2O_4$ using torque measurements near an easy axis. The calculated values of K_1 for $CoFe_2O_4$ are also in agreement with the theoretical predictions of Tachiki [13].

Magnetocrystalline anisotropy is an important metric of performance in evaluating magnetoelastic materials for use in stress sensor and actuator applications. The magnetoelastic properties of magnetic materials are coupled to their magnetic properties. An understanding of how chemical substitution changes magnetic properties helps in understanding its effect on the magnetoelastic properties which are crucial to the potential stress sensor and actuator applications. It has been observed in the case of Mn, Cr, Ga and Ge/Co substitution that with lower cubic anisotropy, the magnetostrictive strain sensitivity increases. Although the magnetostriction amplitude was seen to reduce by a small amount, the magnetostrictive strain sensitivity was observed to increase by 112% for Al-substituted cobalt ferrite [14].

Another important metric of performance for a sensor or actuator material is hysteresis. While the magnetostrictive strain sensitivity improved with addition of aluminium, the coercivity was seen to not change significantly with aluminium addition at temperatures in the potential operational range around 300 K for the proposed devices. Two important factors determining the coercivity are the anisotropy field and domain wall pinning. Although anisotropy reduced with increasing Al content, a seemingly insignificant change in coercivity points towards the fact that the anisotropy is not the dominating factor deciding coercivity in these materials. The temperature dependence of the coercive field is show in Fig. 5.

IV. Conclusion

The magnetic properties of aluminium-substituted cobalt ferrite with the general composition of $CoAl_xFe_{2-x}O_4$

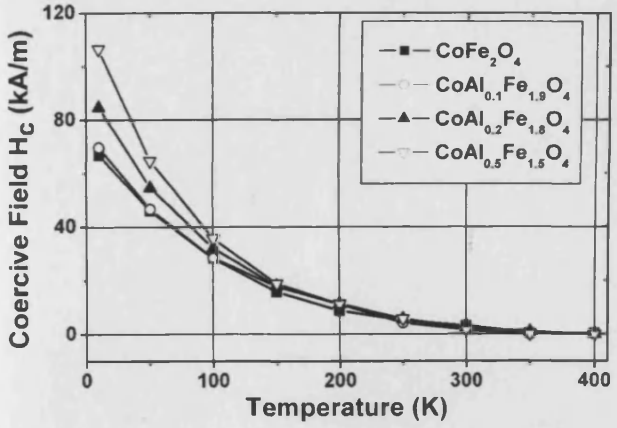

Fig. 5. Variation of coercive field of $CoAl_xFe_{2-x}O_4$ with temperature.

($x = 0.0, 0.1, 0.2$ and 0.5) were measured within the temperature range of 10 to 400 K. The magnetization at $\mu_0 H = 5$ T was observed to increase with decreasing temperature. The addition of small amounts of aluminium ($x = 0.1$ and 0.2) did not change the magnetization significantly. Large amounts of aluminium ($x = 0.5$) resulted in a rapid decrease in magnetization. These observations have been explained in terms of the site preference of Al^{3+} ions that substitute Fe^{3+} ions. Further support to this site occupancy model has been gained by a similar analysis of magnetization for Ga-substituted and Ge/Co-cosubstituted cobalt ferrite. The first-order cubic anisotropy coefficient for Al-substituted cobalt ferrite was calculated using the LA method. The cubic anisotropy of cobalt ferrite was seen to decrease with substitution of aluminium in place of some of the iron. This caused an increase in the magnetostrictive strain sensitivity, a crucial metric of performance for a magnetostrictive stress sensor and actuator material.

ACKNOWLEDGMENT

This work was supported in part by the U.K. Engineering and Physical Sciences Research Council under Grant EP/D057094 and by the US National Science Foundation under Grant DMR-0402716.

REFERENCES

[1] Y. Chen, J. E. Snyder, C. R. Schwichtenberg, K. W. Callum, and D. C. Jiles, "Metal-bonded Co-ferrite composites for magnetostrictive torque sensor applications," *IEEE Trans. Magn.*, vol. 35, no. 5, p. 3652, Oct. 1999.

[2] J. A. Paulsen, A. P. Ring, C. C. H. Lo, J. E. Snyder, and D. C. Jiles, "Manganese-substituted cobalt ferrite magnetostrictive materials for magnetic stress sensor applications," *J. Appl. Phys.*, vol. 97, p. 044502, 1999.

[3] Y. Melikhov *et al.*, "Temperature dependence of magnetic anisotropy in Mn-substituted cobalt ferrite," *J. Appl. Phys.*, vol. 99, p. 08R102, 2006.

[4] Y. Melikhov *et al.*, "The effect of Cr-substitution on the magnetic anisotropy and its temperature dependence in Cr-substituted cobalt ferrite," *IEEE Trans. Magn.*, vol. 42, no. 10, pp. 2861–2863, 2006.

[5] N. Ranvah, I. C. Nlebedim, Y. Melikhov, J. E. Snyder, D. C. Jiles, A. J. Moses, and P. I. Williams, "Temperature dependence of magnetostriction of $Co_{1+x}Ge_xFe_{2-2x}O_4$ for magnetostrictive sensor and actuator applications," *IEEE Trans. Magn.*, vol. 44, no. 11, pp. 3013–3016, 2008.

[6] N. Ranvah, Y. Melikhov, D. C. Jiles, J. E. Snyder, A. J. Moses, P. I. Williams, and S. H. Song, "Temperature dependence of magnetic anisotropy of Ga-substituted cobalt ferrite," *J. Appl Phys.*, vol. 103, no. 7, p. 07E506, 2008.

[7] N. Ranvah, Y. Melikhov, I. C. Nlebedim, D. C. Jiles, J. E. Snyder, A. J. Moses, and P. I. Williams, "Temperature dependence of magnetic anisotropy of germanium/cobalt co-substituted cobalt ferrite," in *53rd MMM Conf.*, Austin, Nov. 10–14, 2009.

[8] S. Chikazumi. *Physics of Ferromagnetism*. Oxford, U.K.: Oxford University Press, 1997, pp. 502–504.

[9] A. Sattar, H. El-Sayed, K. El-Shokrofy, and M. El-Tabey, "Improvement of the magnetic properties of Mn-Ni-Zn ferrite by the non-magnetic Al^{3+}-ion substitution," *J. Appl. Sci.*, vol. 5, no. 1, pp. 162–168, 2005.

[10] K. Krieble, M. Devlin, S. J. Lee, S. T. Aldini, and J. E. Snyder, "Investigation of gas-substitution in cobalt ferrite ($CoGa_xFe_{2-x}O_4$) using Mossbauer spectroscopy," *J. Appl. Phys.*, vol. 103, p. 07E508, 2008.

[11] B. D. Cullity, *Introduction to Magnetic Materials*. Reading, MA: Addison-Wesley, 1972, p. 233.

[12] H. Shenker, "Magnetic anisotropy of cobalt ferrite ($Co_{1.01}Fe_{2.00}O_{3.62}$) and nickel cobalt ferrite ($Ni_{0.72}Fe_{0.20}Co_{0.08}Fe_2O_4$)," *Phys. Rev.*, vol. 107, p. 1246, 1957.

[13] M. Tachiki, "Origin of the magnetic anisotropy energy of cobalt ferrite," *Prog. Theor. Phys.*, vol. 23, p. 1055, 1960.

[14] C. I. Nlebedim, N. Ranvah, Y. Melikhov, P. I. Williams, J. E. Snyder, A. J. Moses, and D. C. Jiles, "Magnetic and magnetomechanical properties of $CoAl_xFe_{2-x}O_4$ for stress sensor application," in *INTERMAG*, Sacramento, CA, May 4–8, 2009, Digest ID: 606241.